The application of Ag/AgCl electrodes as chloride sensors in cementitious materials

Pargar, Farhad

DOI
10.4233/uuid:935b7fbf-3b06-468b-92cc-722943f8b3ba

Publication date
2018

Document Version
Final published version

Citation (APA)
Pargar, F. (2018). *The application of Ag/AgCl electrodes as chloride sensors in cementitious materials*. [Dissertation (TU Delft), Delft University of Technology]. https://doi.org/10.4233/uuid:935b7fbf-3b06-468b-92cc-722943f8b3ba

The application of Ag/AgCl electrodes as chloride sensors in cementitious materials

Proefschrift

ter verkrijging van de graad van doctor
aan de Technische Universiteit Delft,
op gezag van de Rector Magnificus Prof.dr.ir. T.H.J.J. van der Hagen

voorzitter van het College voor Promoties,
in het openbaar te verdedigen op
Vrijdag 16 November, 2018 om 10:00 uur

door

Farhad PARGAR

Master of Science in Civil engineering, University of Tehran, Iran
geboren te Astaneh ashrafieh, Iran

Dit proefschrift is goedgekeurd door de:

Promotor: Prof. dr. ir. K. van Breugel

Copromotor: Dr. ir. D.A. Koleva

Samenstelling promotiecommissie:

Rector Magnificus,	Voorzitter
Prof. dr. ir. K. van Breugel,	Delft University of Technology, promotor
Dr. ir. D.A. Koleva,	Delft University of Technology, copromotor

Onafhankelijke leden:

Prof. dr. ir. J.M.C. Mol	Delft University of Technology
Prof. dr. C. Andrade	International Centre for Numerical Methods in Engineering
Prof. dr. M. Shekarchi Zadeh	University of Tehran
Dr. ir. W. Olthuis	University of Twente
Dr. ir. A. Homborg	Netherlands Defence Academy

Overrig lid:

Prof. dr. ir. H.E.J.G. Schlangen	Delft University of Technology

ISBN: 978-94-6186-972-2

Keywords: Ag/AgCl electrode, chloride sensor, anodization, open circuit potential, stability, alkalinity, interference, hydration product, corrosion of steel.

Printing: Glideprint

Cover design: Farhad Pargar

Printed in The Netherlands.

Acknowledgments

I greatly acknowledge the financial support of this research project by STW (Dutch science foundation) in the framework of IS2C (Integral Solutions for Sustainable Construction) program.

I would like to thank my promoter Prof. Klaas van Breugel, who gave me the opportunity to work on this project in Microlab. My thesis could not be accomplished without his constructive advice and support. His guidance not only helped me in this work but also trained me for my future career and life.

I would like to sincerely thank my co-promotor Dr. Dessi Koleva for supervision, guidance and support during my PhD study. This research study could go nowhere unless I had her experience and expertise on my side. Thank you Dessi for all the discussion and support during the past years.

I am very thankful to the members of my doctoral committee for their valuable comments on the current work. I would like to specifically thank the committee member "Dr Shekarchi" for his support during my master study and work in Construction Materials Institute at the University of Tehran.

I would like to thank Dr. Oguzhan Copuroglu, Dr. Peyman Taheri and Dr. Hristo Kolev for constructive comments in very specialized areas of work. I also would like to thank Mr. Arjan Thijssen and Mr. Kees van Beek for sharing great ideas in experimental work. Many thanks to Ms. Jeanette van den Bos for translating my thesis summary into the Dutch language.

I would like to express my gratitude to the head of Microlab Prof. Erik Schlangen for all the support throughout these years. Many thanks to administrative staff (Claire, Claudia and Nynke) and technicians of Section of Materials and Environment (Arjan, John, Maiko and Gerrit) for assistance and help on daily issues.

I would like to thank all the colleagues in the Section of Materials and Environment for creating a nice working environment and the friendship. It was a great pleasure to work with all of you. I would like to specifically thank Aug Susanto, Zhipei Cheng, Amir Zommorodian, Hitham Amin, Nader Sadeghi and Davoud Tavakoli for all the great moments we have experienced together.

I am very thankful to my family members in Iran for their invaluable encouragement. My sincere gratitude goes to my parents and my brothers who always have been supportive. Mom, dad words cannot express how I am indebted to you. Thank you so much for the endless support you have given me.

Finally, I would like to convey my special appreciation and gratitude to my wife Hamideh for her emotional support, encouragement, giving hope and, most of all, her patience during these years.

Farhad Pargar
Delft, 2018

Table of Contents

List of Figures

List of Tables

List of Abbreviations

Ag°	metalic silver
AFm	monosulfate aluminate hydrate
AFt	ettringite
AgCl	silver chloride
Ag_2O	silver (I) oxide
AgO	silver (II) oxide
Ag_2S	silver sulfide
BSE	backscattered electron
C_3A	tricalcium aluminate
C_3S	tricalcium silicate
CH	calcium hydroxide
CV	cyclic voltammetry
C-S-H	calcium silicate hydrate
EDS	energy dispersive spectroscopy
EIS	electrochemical impedance spectroscopy
ESEM	environmental scanning electron microscope
HCl	hydrochloric acid
NaCl	sodium chloride
OCP	open circuit potential
PDP	potentio-dynamic polarization
SCE	saturated calomel electrode
SE	secondary electron
XPS	X-ray photoelectron spectroscopy
XRD	X-ray diffraction
w/c	water to cement ratio
w/p	water to powder ratio

Chapter 1

Introduction

Reinforced concrete (RC) is one of the most widely used construction materials worldwide. The broad application of RC follows its relatively low cost, high loading capacity and generally good resistance in different environmental condition. Common knowledge is that the extension of the service life of RC structures directly reduces the ecological impact of the construction industry. Therefore, enhancing the service life of RC has always been targeted in both research and innovative engineering approaches.

Chloride-induced corrosion of the steel reinforcement in concrete structures is among the major durability-related challenges for the engineering practice. The premature deterioration of RC structures, due to corrosion of embedded steel, is increasingly demanding optimum solutions for assessing the reinforcement corrosion. The limitations of conventional methods for corrosion monitoring ask for novel and reliable techniques for better service life prediction, planning of repairs and resource allocation.

The modern way of managing infrastructural assets (e.g. RC structures) is based on life-cycle assessment and health monitoring. Understanding of degradation processes and failure mechanisms of RC structures are the key input of asset management systems. This information allows owners to operate their structures, to control maintenance expenses, to find the optimum repair solution and to minimize or avoid future risks. Managers often have only limited time and limited resources for their decision-making process. Therefore, the typical approach to durability assessment narrows down to just on-site inspection, which is initially or subsequently linked to service-life models.

- **Traditional inspection**

In a chloride-rich environment, visual inspection and determination of electrical properties of concrete are among the first evaluation steps. These are usually followed by destructive chemical analysis and electrochemical techniques for corrosion monitoring of the steel reinforcement. The appearance of damage would be the signal for taking action in the right place, but not necessarily at the right time. Nowadays, there is an increasing demand for more accuracy in monitoring and inspection of RC structures. This is in addition to the limitations of the traditional approach. Therefore, efforts are being made to reduce the direct and indirect costs for maintenance and repair expenses, cost efficiency, e.g. through innovative and reliable structural health monitoring systems.

- **Service life prediction models**

Service life models are used to predict the long-term durability of structures. The two main input parameters for calibration and validation of these models are: (i) chloride content in the concrete cover, and (ii) the time to initiation of chloride-induced corrosion of the reinforcing steel, linked to the chloride threshold value. Determination of chloride diffusion coefficients does not necessarily mean deriving the right and relevant chloride threshold value. The rate of

chloride penetration and the chloride diffusion coefficient, respectively, depend on the microstructure and transport properties of the bulk material. The chloride threshold value depends on many parameters, such as the steel surface condition and the steel-concrete interface. For a better estimation of the time to chloride-induced corrosion information is needed about the *free chloride content* in both the concrete cover and in the vicinity of the steel reinforcement. Practical approaches are needed to satisfy this requirement, e.g. by using a non-destructive chloride monitoring system.

1.1 Motivation and scope of this work

A system for continuous monitoring of the chloride ions content in RC structures would be valuable for the calibration/validation of service life prediction models. The obtained information can foster a better understanding and prediction of a degradation process, e.g. chloride-induced corrosion.

For the past decades attempts have been made to develop a reliable chloride monitoring system, replacing the destructive methods for chloride measurement in cement-based materials. A new sensor technology should be superior in terms of efficiency and effectiveness. It should also be more accurate compared to that of traditional ways of powder drilling and wet chemical analysis of the chloride content. This line of considerations forms the background of this thesis.

Embedded chloride sensors at certain depths in a concrete structure respond to the local chloride ions activity and chloride concentration, respectively. Currently, the state-of-the-art reports focus on two main types of in-situ chloride sensors for concrete applications: chloride ion-selective electrodes, e.g. Ag/AgCl electrodes (Fig. 1.1), and fiber optic sensors. The focus of this thesis is on the potentiometric determination of chloride ions using Ag/AgCl electrodes as chloride sensors in cementitious materials. Two main benefits of these sensors are: (i) non-destructive measurement of the chloride ions concentration in the concrete bulk and in the vicinity of the reinforcing steel, (ii) the inexpensive/simple instrumentation.

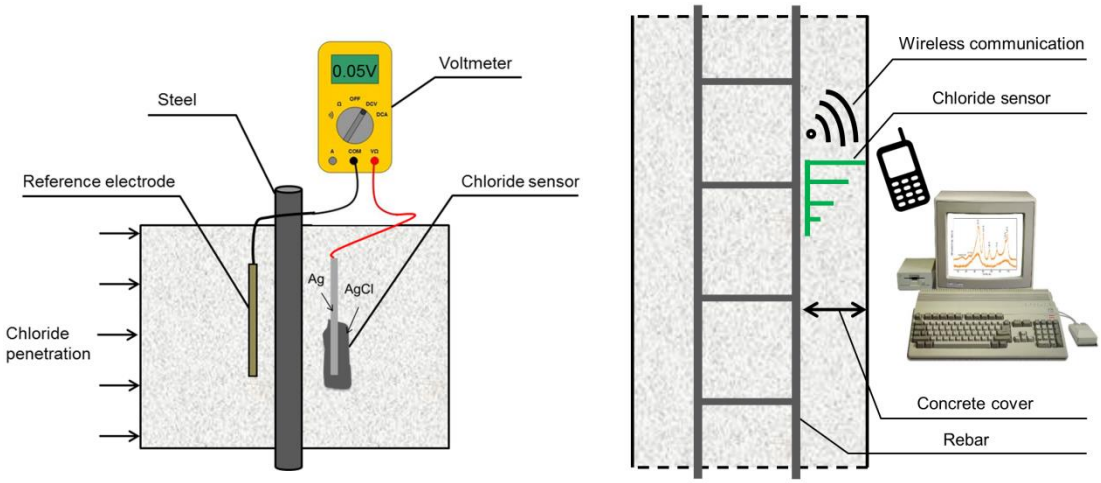

Figure 1.1: Schematic illustration of the instrumentation for chloride sensor readings in reinforced cement-based material.

The instrumentation used to perform potentiometry consists of a chloride sensor, a reference electrode, and a potential (voltage) measuring device, e.g. a voltmeter (Fig. 1.1). Despite the simplicity of this set-up, there are certain drawbacks of the sensor measurement in alkaline medium. The important factors affecting the reliability of the Ag/AgCl sensors' response need to be carefully assessed. For instance, the electrochemical response of the sensor is considerably sensitive to chemical species, other than chloride ions, e.g. hydroxide ions. Therefore, the applicability of the sensor in a concrete environment can be impaired by the influence of hydroxide ions in the medium. Hence, research on sensors' optimization for reinforced concrete applications is continuously on-going.

1.2 Main objectives of this thesis

Science-based information on the performance of chloride sensors in the highly alkaline environment, like concrete, is scarce. The available studies about stability, reliability and durability of chloride sensors in such an alkaline medium are quite limited and insufficiently justified. The performance of a chloride sensor is determined by the sensor's properties (thickness, morphology and microstructure of the AgCl layer) and the environment to which the sensor is exposed (interfering ions, hydration products of cementitious materials). In this thesis, the contribution of the aforementioned factors to the possible deviation from an expected sensor's response is discussed in cementitious materials. Three factors for the deviation of a sensor's response from the expected value are considered:

1) The contribution of the sensor preparation method (regime) to the sensor's response is a factor, which, although of high significance, is so far not described in the present state-of-the-art. This aspect is the starting point of the research focus of this thesis.
2) The influence of cementitious mix design and cement composition on the stability of the sensor's response has not been investigated. Hence, the sensor's reading in a cement-based matrix of varying w/c ratio and cement composition will be studied.
3) The interference of hydroxide and sulfide ions (as present in the pore solution of cementitious materials) with the sensor's response has already been reported. However, the level of this interference is still under debate. The interference of sulfide ions with the sensor was identified, while no experimental evidence in cementitious materials to confirm the effect of sulfide ions has been found.

This thesis is one of the three interconnected parts of the research project, "An integral in-situ chloride sensing and monitoring system for concrete structures" (code: No. 10968) (Fig. 1.2). The project was funded by the Dutch National Science Foundation (STW) as a research campaign on Integral Solutions for Sustainable Concrete (IS2C). The obtained knowledge contributes to the chloride sensor's technology for non-destructive monitoring of chloride ions in RC structures. As shown in Fig. 1.2, this thesis (Ph.D. 2) is a transition from the study on the sensor development (Ph.D. 1) to the study on chloride ion's transport in cementitious materials (Ph.D. 3).

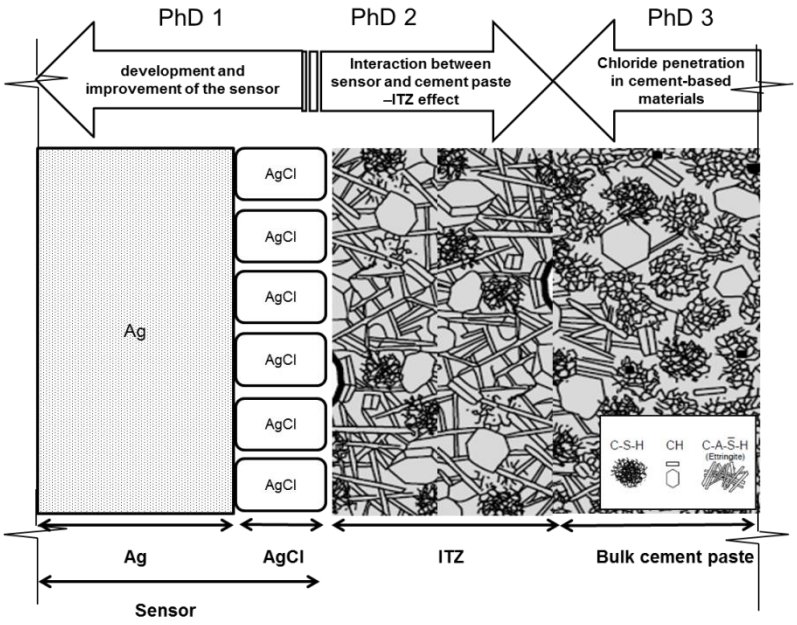

Figure 1.2: Interaction between the three parts of the STW project on "An integral in-situ chloride sensing and monitoring system for concrete structures".

The focus of this thesis is on the interaction between the chloride sensor and the surrounding medium. In this regard, the main research tasks are as follows:

- *Determination of the chloride sensors' performance in simulated pore water (aqueous medium) and cement-based environment*. The stability, reliability, reproducibility and reversibility of the sensor's response are explained through plausible electrochemical reactions at the sensor's surface.
- *Evaluation of the relation between non-destructive and destructive chloride determination techniques*. The limitations of these techniques for quantification of the free chloride ions concentration are discussed.
- *Correlation of the sensor's response to the corrosion activity on the steel surface.* According to the sensor's response, the chloride content in the vicinity of the reinforcing steel at the time of corrosion initiation is determined. Hence, an attempt for a non-destructive determination of the chloride threshold value is made.

In light of the above research tasks, this work contributes to clarification of some main practical challenges for the field of civil engineering, where debates are still ongoing, namely:

- Can sensors be used for accurate determination of the chloride ions concentration, irrespective of the concrete mixture? What are the factors affecting the sensor's reading, i.e. which factors determine stability of these sensors?
- How accurate is the measured chloride threshold value, determined by using chloride sensors? In other words, which factors affect the chloride threshold value.

1.3 Layout of the thesis

The results of this work are presented in seven chapters, in accordance to the flowchart in Fig. 1.3. In Chapters 1 and 2, the motivation for this research is introduced, and the relevant theoretical/technical background is discussed.

Chapter 1 is the current chapter, which is a general introduction, providing the background of this thesis and motivation for research.

Chapter 2 addresses the basic principles of a Ag/AgCl sensor for monitoring of the chloride ions concentration in cementitious materials and in the vicinity of the reinforcing steel. As the chloride sensor is in contact with a cementitious material, main aspects on the pore solution composition and the hydration products of the cementitious material at the interface with the sensor are reviewed. The fundamental aspects and technical background related to the chloride sensors are described, and the influence of cementitious materials on the reliability of the sensors' response is discussed.

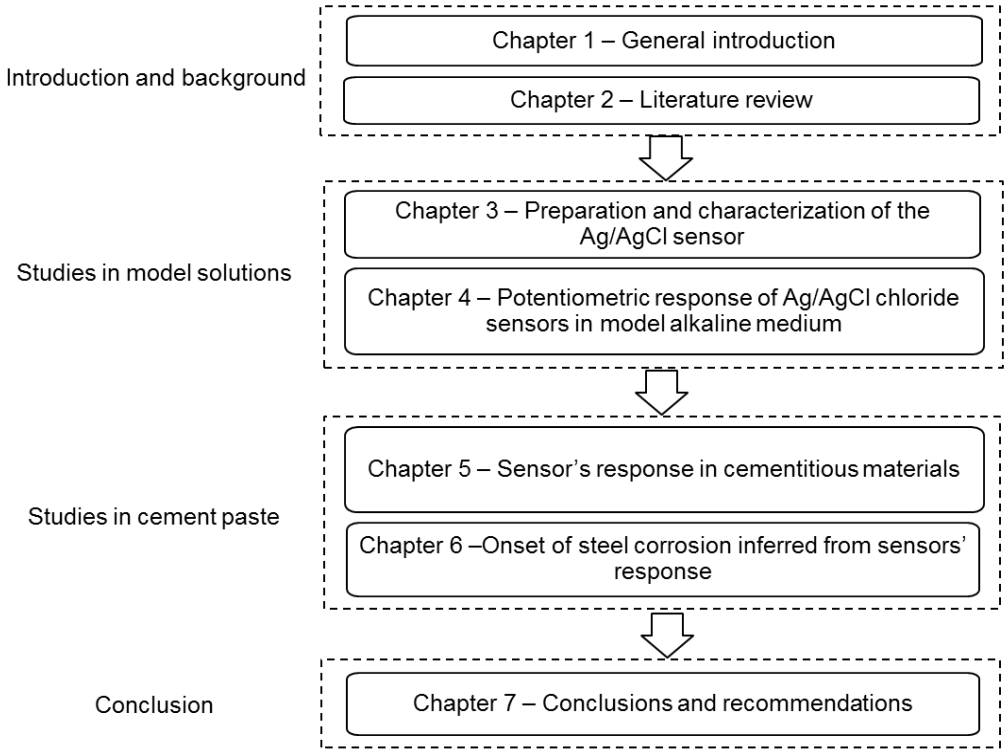

Figure 1.3: Outline of the thesis.

In Chapters 3 and 4, the mechanisms related to the electrochemical response of the chloride sensor in alkaline solutions, resembling the concrete environment, are presented. These chapters deal with the sensors' preparation, characterization, calibration and performance in different aqueous environments. The sensors' response is correlated to overall thermodynamics and kinetics of the electrochemical reactions at the sensors' surface. The stability, reliability, reproducibility and reversibility of sensors' response in model solutions are assessed. The obtained information links these aspects to the chloride and hydroxide content in the solution, as well as the AgCl layer properties (thickness, morphology, microstructure and composition). The cementitious mix design and composition are also important for the electrochemical reactions, relevant to the sensor's response. Therefore, in

Chapters 5 and 6, the gained knowledge from Chapters 3 and 4 is used to interpret the response of sensors, embedded in a cementitious matrix.

Chapter 5 deals with the chloride sensor's response in cementitious materials of different mix design, cement composition and chloride concentration. The chloride content based on the sensor's response is also compared to that obtained by destructive test methods. The results give an insight into how a cementitious mix design and cement composition are important for the measured chloride content based on the sensor's response and the one obtained from the destructive test methods.

In Chapter 6, the onset of chloride-induced corrosion of embedded steel is separately recorded via electrochemical monitoring and inferred from the chloride sensors' response. With this approach, the applicability of the chloride sensor for determination of the critical chloride content for corrosion initiation of reinforcing steel is evaluated. The possible deviation among the measured and expected chloride contents is also discussed.

In Chapter 7, the main results of this thesis are summarized and recommendations for future research are given.

Chapter 2

Determination of chloride content in cementitious materials: from fundamental aspects to application of Ag/AgCl chloride sensors

Abstract

This chapter reports about the advantages and drawbacks of available test methods for determination of the chloride content in cementitious materials in general, and the application of Ag/AgCl chloride sensors in particular. The main factors that affect the reliability of a chloride sensor are presented. The thermodynamic behaviour of silver in the presence or absence of chloride ions is described and kinetic restrictions are addressed. The parameters that can affect the activity of chloride ions in the medium and/or the rate of ion exchange and dissolution/precipitation processes at the sensor's surface are also considered. In this regard, the contribution of morphology and microstructure of the AgCl layer, binding of chloride ions and the compactness of hydration products around the chloride sensor are highlighted. The important parameters for a reliable sensor's response are discussed and the possible causes of inaccuracies are evaluated.

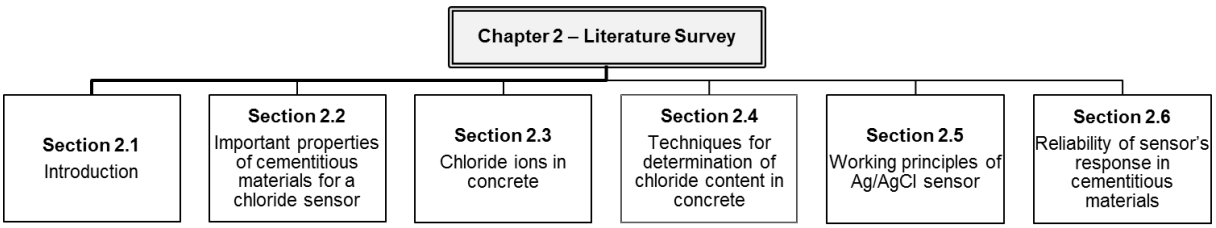

Structure of this chapter

This Chapter 2 is based on the paper:

Pargar, F., Koleva, D. A., & van Breugel, K. (2017). Determination of Chloride Content in Cementitious Materials: From Fundamental Aspects to Application of Ag/AgCl Chloride Sensors. Sensors, 17(11), 2482.

2.1 Introduction

Chloride ions are among the primary causes of steel corrosion in reinforced concrete structures. Determination of the chloride content in the concrete cover and near the steel reinforcement is needed for evaluating the risk of corrosion. The drawbacks of conventional techniques for determination of the chloride content call for novel and reliable techniques. One of the first documented attempts for non-destructive determination of the chloride content in cementitious materials was reported in the early 1990s. In those years Ag/AgCl sensors were used in cementitious materials [Molina, 1993]. However, the literature on the performance of chloride sensors in cementitious materials is still scarce and the interpretation of sensors' readings is far from straightforward.

The performance of a chloride sensor in cementitious materials depends on the physico-chemical condition of the interfaces (Ag/AgCl/cement paste) at the sensor's surface as well as the pore solution composition. A schematic presentation of the Ag/AgCl sensor in cement paste is depicted in Fig. 2.1. This figure illustrates some morphological and microstructural features of the AgCl layer and the adjacent cementitious material, both important for the sensor's response. The pores at the surface of the AgCl layer provide a pathway for penetration of ions into the layer (Fig 2.1a). The presence of different ions in the pore channels of this layer (Fig. 2.1b) subsequently affects the sensor's response. When the chloride sensor is embedded in cementitious materials (Fig. 2.1c), the microstructure of these cementitious materials (Figs. 2.1d,e) is also important for the electrochemical reactions, relevant to the sensor's response. In this regard, the influence of pore solution composition and compactness of the hydration products at the sensor's surface on the sensor's response should be considered.

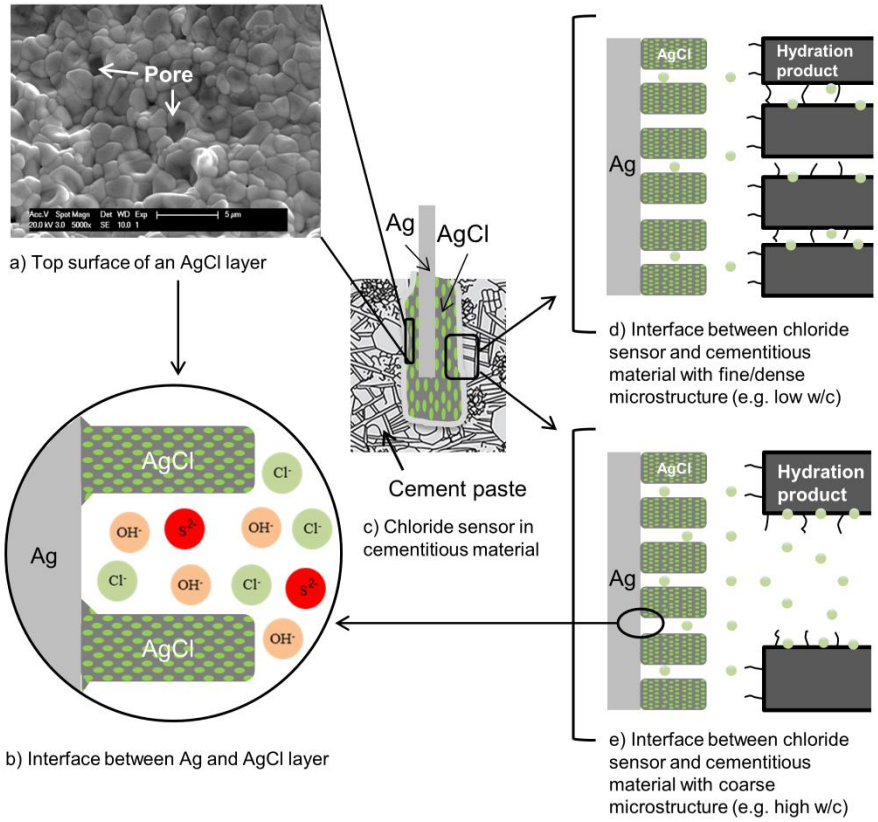

Figure 2.1: Schematic representation of a chloride sensor embedded in a cementitious matrix.

An electrode potential develops on a metal/electrolyte interface after immersion of that metal in a solution, called an open circuit potential (OCP). The (electrochemical) response of a chloride sensor is a function of the surface characteristics of the sensor and the rate of electron/ion transfer at the sensor's surface [Bard and Rubinstein, 1996]. In this regard, the surrounding medium can affect the thermodynamically plausible reactions at the chloride sensor's surface. For example, binding of chloride ions to the hydration products, together with distribution and compactness of hydration products around the sensor, make the chloride ions less mobile in the pore solution than expected based on their concentration. Moreover, the sensitivity of a chloride sensor to the chloride ions depends on the concentration of interfering species, such as hydroxide and sulfide ions in the medium. These processes subsequently limit the rate of reactions at the sensor's surface. Therefore, the cement chemistry and composition of cementitious materials are also reviewed in the following sections.

In view of the above-outlined factors, this chapter follows a sequence of steps to determine the chloride ions content and sensor's response in a concrete environment. Figure 2.1 can be considered as a schematic presentation of the different influential parameters, interfaces and points of interest with regard to a Ag/AgCl sensor performance. This chapter encompasses five main sections, structured as follows:

1) In Section 2.2 the main hydration products of cement paste in the bulk matrix and at the sensor-cement paste interface are described. The composition of the pore solution in the pore system of the paste, the various ions being in contact with the sensor's surface, hence, of importance for sensors' readings are also assessed.

2) Next, the binding of chloride ions in cementitious materials are reviewed and the importance of chloride sensors for local chloride measurements, specifically, at the level of the reinforcement, is discussed.

3) Section 2.4 presents different techniques for the determination of the chloride content in concrete and the advantages of chloride sensors' application, in particular for free chloride determination.

4, 5) Sections 2.5 and 2.6 bridge fundamental considerations and technical background, both related to the performance, characterization and application of Ag/AgCl sensors. The advantages and drawbacks of the chloride sensors are described. The thermodynamic behaviour of silver and the electrochemical kinetics of AgCl formation are discussed and the relevance of these parameters to the reliability of the sensors' response in cementitious materials is evaluated. The above framework outlines the structure of this chapter, highlighting the principles, related mechanisms and determining factors for the monitoring of chloride ions in cementitious materials.

2.2 Important properties of cementitious materials in view of chloride measurements via Ag/AgCl sensors

A cementitious paste is a heterogeneous material with high alkalinity, a pore solution with different composition, and a pore system with different porosity and pore size distribution (see also Figs. 2.1d,e) [Hewlett, 2003]. In the following, some properties of cementitious materials that are important for the response of a chloride sensor are highlighted. The main hydration products and microstructure of cementitious materials are described (Section 2.2.1). The presence of interfering ions, i.e. hydroxide and sulfide ions (Fig. 2.1b) in the pore solution of Portland cement paste and blast furnace slag cement paste is reviewed (Section 2.2.2). Slag

cement paste is also considered because it contains a high amount of water-soluble sulfates and sulfide ions [Vollpracht et al., 2016].

2.2.1 Hydration products and microstructure of cement paste

Hardened Portland cement paste is a porous material containing calcium hydroxide ($Ca(OH)_2$, Portlandite), aluminate compounds, such as monosulfate, hydroxyl-AFm, ettringite (AFt) and unhydrated cement particles, surrounded by an amorphous hydration product, known as C-S-H (calcium silicate hydrate) [Mehta and Monterio, 2006].

The heterogeneity of hydration products and the microstructure of cementitious materials are important factors in view of the reliability and reproducibility of the sensor's response (Figs. 2.1d,e). These factors can be assessed from the available studies on the interfacial properties between the cement paste and the aggregate. The microstructure and hydration products of cement paste in the vicinity of an aggregate differ from those in the bulk matrix. This distinctive region is termed interfacial transition zone (ITZ). When the cement grains encounter the "wall" of the aggregate, a region of a higher porosity and different composition near the aggregate surface appears [van Breugel, 1991]. The porosity of ITZ is two to three times higher than the porosity in the bulk [Ollivier et al., 1995]. The wall effect creates a water concentration gradient around the aggregate. A locally higher w/c ratio with fewer nucleation sites forms larger crystals in contact with aggregates [Ollivier et al., 1995]. In this region, the ettringite and calcium hydroxide tend to form larger crystals [Mehta and Monterio, 2006]. A rim of massive calcium hydroxide can often be observed around the aggregates. This information implies that the ITZ properties at the interface between the sensor and cementitious materials are the principal factor influencing the performance of the chloride sensor.

2.2.2 Ions in pore solution

As shown in Fig. 2.1b, the composition of the pore solution of cementitious materials determines the ions that can come in contact with the sensor. Hydroxide and sulfide ions are the two main ions of cement paste which can interfere with the chloride sensor's response. In the following, main aspects in view of the presence of these ions in the pore solution of Portland cement and slag cement is reviewed.

2.2.2.1 Portland cement

The aqueous electrolyte in the spaces not filled by solid hydration products is known as the pore solution [Swamy, 1992]. The embedded chloride sensor in cementitious material, similar to embedded reinforcement, is in contact with the pore solution. The composition of the pore solution depends on the hydration of different cement phases and the solubility of these products. Once the cement is mixed with water and starts to dissolve, every element that is present in the cement can also be found in the form of dissolved ions in the pore solution.

The pore solution of Portland cement paste is mainly composed of alkaline hydroxides (mainly KOH and NaOH). Other species, such as SO_4^{2-} and Ca^{2+}, are present in much lower concentrations [Elakneswaran et al., 2009]. The change in alkalinity of the pore solution during cement hydration depends on the w/c ratio and the cement type [Lothenbach and Winnefeld, 2006]. Alkalis in Portland cement (K_2O and Na_2O) are mainly responsible for the high pH range of the pore solution [Diamond, 1989]. The hydroxide concentration in cement paste with CEM I 42.5N and w/c=0.5 increases from 150 mM at 7 h to 540 mM after 29 days [Lothenbach and Winnefeld, 2006]. The concentration of hydroxide ions is important for the performance of a Ag/AgCl chloride sensor (Fig. 2.1b), as will be discussed in section 2.6.

2.2.2.2 Blast furnace slag cement

The alkalinity of the pore solution in slag cement paste (CEM III/B, w/c=0.5, pH~13, sealed and cured for 6 months) is lower than that in Portland cement paste (CEM I, w/c=0.5, pH>13.5, sealed and cured for 6 months) [Hewlett, 2003]. For slag cement the concentration of alkaline ions (Na^+ and K^+) and hydroxide ions decreases during the slag hydration process. This results in a pH reduction of the pore solution for slag cement paste to a value lower than that of Portland cement paste [Hewlett, 2003].

The pore solution composition of slag cement paste is to a large extent similar to that of Portland cement paste. The difference is a remarkable amount of sulfide ions (S^{2-}) in slag cement paste [Vollpracht et al., 2016]. The sulfide content in slag is about 1%, while in Portland cement it is lower than 0.1% [Garcia et al., 2014]. After 10 h of hydration, sulfide ions were detected in the pore solution of blended cement paste containing slag (CEM III/B 42.5 L) [Lothenbach et al., 2012]. The concentration of sulfide ions increased to 5 mM after seven days, and then stabilized at 8-11 mM [Lothenbach et al., 2012]. The concentration of sulfide ions, similar to hydroxide ions, is important for the performance of a Ag/AgCl chloride sensor (Fig. 2.1b). This will be discussed in section 2.6.

2.3 Chloride in cement-based materials

The ingress of chloride ions in concrete takes place via the pore system and can be affected by binding of chloride ions to the hydration products. The chloride in cement-based materials is present as free, physically bound and chemically bound chlorides. The chloride ions can be bound chemically in compounds like Friedel's salt (calcium chloroaluminate hydrate) or adsorbed physically at the surface of cement hydration products, such as C-S-H, Friedel's salt and Portlandite. The chloride ions in the bulk pore solution are called free chloride (Fig. 2.2). The binding of chloride ions to the cement hydration products continues up to a level at which an equilibrium between bound (chemically and physically) and free chlorides is reached.

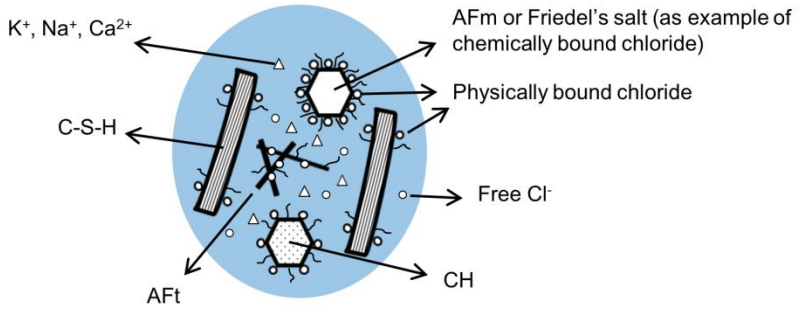

Figure 2.2: Schematic of main hydration products of cement paste and their contribution to the binding of chloride ions.

Glass et al. [1996] classified the chloride in cementitious materials into four categories – free, loosely bound, bound and strongly bound chlorides. The amount of free chloride can be measured by the "equilibrium method". In this method, concrete samples are stored in a solution of known chloride concentration until equilibrium is reached between the external solution and the concrete pore solution. For example, the time required for a cement paste sample with 1 cm thickness to reach equilibrium can extend up to one year. In equilibrium condition, the free chloride in the concrete sample is equal to the chloride concentration in the external solution. The chloride is "loosely bound", when it can be extracted from the concrete samples under high pressure (in the range of hundreds of MPa). The physically bound chloride can be considered as loosely bound chloride. The term "bound chloride" refers to the chloride that cannot be extracted from the concrete samples under pressure. This holds for the chemically bound chloride. The traditional method for determination of total chloride content in a concrete sample is "acid-soluble chloride extraction" [RILEM TC 178-TMC, 2002; ASTM C1152, 2003; NT Build 208, 1996]. Extraction of total chloride content using this method may not end with release of all the bound chlorides. Therefore, the total chloride content of the sample can be underestimated [Dhir et al., 1990]. The part of bound chloride that is not released by the acid-soluble extraction method is known as "strongly bound chloride". Although most of the phases containing chloride compounds dissolve in the acidic medium of the test [RILEM TC 178-TMC, 2002; ASTM C1152, 2003; NT Build 208, 1996], the release of "strongly bound" chloride may require a higher acidity.

2.3.1 Free chloride

There are several techniques for evaluation of the free chloride content. Different test procedures, applied in these techniques, result in different outcomes for the free chloride content. For instance, chemical extraction of chloride ions from a concrete sample gives a significantly higher amount of chloride than extraction under high pressure [Arya, 1989]. Determination of free chloride content is discussed in Section 2.4.2 with respect to the chloride sensors' response.

Section 2.3.2 reviews main aspects of classification of bound chlorides in a cementitious matrix. These are important in view of the general debates about the determination of chloride content and the application of sensors. The available techniques for determination of the chloride content in cementitious materials are described in section 2.4.

2.3.2 Bound chloride

2.3.2.1 Chemical binding of chloride

Friedel's salt is the main reaction product that binds chloride ions chemically in concrete. It forms due to the reaction between chloride ions and hydration products of C_3A, e.g. hydroxyl-AFm, monosulfate and AFt phases [Birnin-Yauri and Glasser, 1998]. It is assumed that all aluminate hydrates transform to Friedel's salt with increasing chloride concentration in the pore solution [Birnin-Yauri and Glasser, 1998]. In general, the tendency of sulfate ions (SO_4^{2-}) to bind in hydration products is higher than that of chloride and hydroxide ions, i.e. $SO_4^{2-} > Cl^- >> OH^-$ [Maslehuddin et al., 1997]. However, the concentration of sulfate ions (SO_4^{2-}) in the pore solution of mature (28 days) cement paste is low (Table 2.1). Therefore, chloride ions can react with the AFm phases to form Friedel's salt. Even the sulfate-containing hydration products (monosulfate and Aft) convert into Friedel's salt if the chloride concentration in the pore solution is sufficiently high [Zibara, 2001].

Table 2.1. Concentration of ions in the pore solution of hydrated Portland cement paste (w/c=0.5) after a 28 days curing period [Elakneswaran et al., 2009].

	Concentration (mmol/l)					
	Na^+	K^+	Ca^{2+}	Cl^-	SO_4^{2-}	Ionic strength (mmol/l)
Hydrated cement paste	88.9	74.8	4.8	1.4	0.2	178.3

2.3.2.2 Physical binding of chloride

Similar to most other materials, the surface of hydration products becomes electrically charged when in contact with a polar solution, such as water. The ionic binding properties of hydration products govern the dissolution of surface species or adsorption of ions from the solution. This process electrically charges the surface of the hydrated phases.

If we look at the interface of a hydration product, we see an accumulation of chloride ions and a depletion of cations near the charged surface of hydration products and in the vicinity of an adsorbed layer of cations (Fig. 2.3) [Elakneswaran, 2009]. In the bulk solution, electroneutrality prevails (Fig. 2.3). Although the layer of physically bound chloride is not more than a few nm, it can comprise a considerable amount of chloride ions [Elakneswaran, 2009]. The thickness of this layer decreases with increasing chloride concentration in the solution [Yuan et al., 2011; Hu et al., 2015; He et al., 2016]. This subsequently lowers the physical chloride binding capacity of cement hydration products.

As mentioned in Section 2.3.1, the physically bound chloride (Fig 2.3) can be "squeezed out" when the cement paste is subjected to high pressure and/or thermal loads [Glass et al., 1996]. Therefore, the physically bound chloride has been classified as loosely bound chloride [Glass et al., 1996]. The erratic random movement of physically bound chloride is continuously affected by the surrounding molecules [Birdi, 2015]. In this condition, the activity of chloride ions increases with increasing distance from the surface of hydration product (Fig. 2.3) [Birdi, 2015]. Therefore, physically bound chloride can be considered as free chloride ions, but with low activity.

The chloride binding mechanisms and microstructure of cementitious materials are also important for determination of the so-called chloride threshold value. The threshold value, i.e. the value of the critical chloride content for corrosion initiation of reinforcing steel, is still under debate. In the next section, several aspects on the determination of the chloride threshold value are presented.

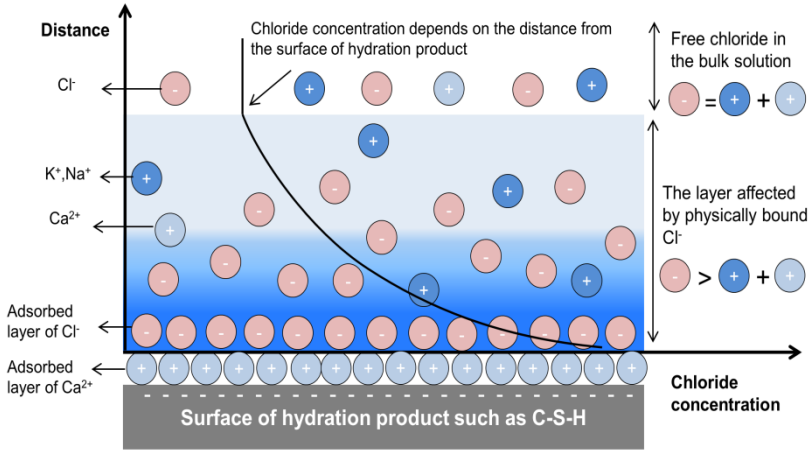

Figure 2.3: Schematic diagram of physical binding of chloride ions to the cement hydration product exposed to chloride environment. The adsorption of chloride ions subsequently induces a chloride concentration gradient between the bulk solution and the surface of a hydration product.

2.3.3 Chloride threshold value

The process of steel corrosion in reinforced concrete can be divided into two phases; initiation and propagation [Hausmann, 1967]. The first stage, i.e. initiation phase, is generally related to the time needed for chloride ions to penetrate into the concrete and reach a critical chloride concentration at the steel bar to initiate corrosion. The subsequent propagation stage extends up to the time when the corrosion damage is beyond the acceptable limits and cracks due to the expansion of corrosion products appear on the concrete surface.

An impressive number of studies on the chloride threshold value has been published since the 1960s [Melchers, 2016]. As shown in Table 2.2, a unique chloride threshold value does not exist. Similarly, a generally accepted or standardized method for determination of the critical chloride content does not exist as well. Even, the concept of chloride threshold value has been questioned [Alonso et al., 2000]. This controversy is mainly due to the variety of influential factors, such as concrete mixture, environmental factors and surface condition of the embedded reinforcing steel. Apart from these factors, different techniques and criteria have been used for both the detection of the time to steel depassivation and measuring the chloride content close to the reinforcement. The measured chloride content is presented in different units and related to the concrete or binder weight (Table 2.2). As the binder content is not always known, it is sometimes preferred to present the total chloride content as percentage of the weight of concrete. The free chloride content is presented in different ways: as percentage of the binder or concrete weight, mole per liter of concrete pore solution (mol/l) and the ratio of chloride to hydroxide ions ($[Cl^-]/[OH^-]$) in the pore solution (Table 2.2).

Table 2.2: Different expression forms of the critical chloride content and the range of reported chloride threshold values for steel, embedded in cement-based materials.

Aggressive species	Expressed as	Reported Chloride threshold value	References
Total chloride (including free chloride)	% by weight of binder	(1.24-3.08)[a], (1–8.34)[b] (0.68-0.97)[c]	a: Alonso et al., 2000 b: Alonso et al., 2002 c: Oh et al., 2003
	% by weight of concrete	(0.03-0.07)[a] (0.03-0.2)[b] (0.06-0.2)[c] (0.06-0.37)[d]	a: Anon, 2002 b: Stratfull et al., 1975 c: Ferreira, 2004 d: Maes et al., 2013
Free chloride	% by weight of binder	(0.39–1.16)[a], (1-4)[b], (0.5-2)[c]	a: Alonso et al., 2000 b: Alonso et al., 2002 c: Schiessl and Raupach, 1990
	% by weight of concrete*	0.026	Daily, 1999
	mol/l	(0.36-3.22)[a], (0.44-0.65)[b], (0.045-0.55)[c]	a: Pettersson, 1992 b: Elsener et al., 1995 c: Zimmermann et al., 1999
	$[Cl^-]/[OH^-]$	(1.17-3.98)[a],(1.7-20)[b] (3-20)[c]	a: Alonso et al., 2000 b: Alonso et al., 2002 c: Lambert et al., 1991

[1] Expression of critical free chloride content by weight of concrete is scarcely available in the literature.

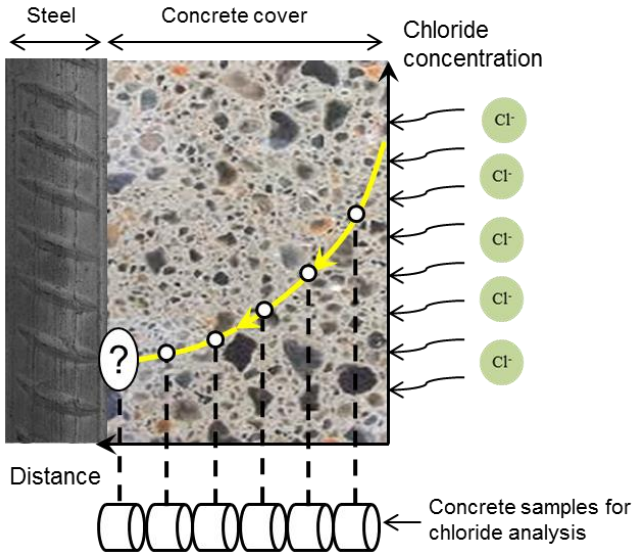

Figure 2.4: Chloride profile in concrete and determination of chloride threshold value.

Some researchers proposed that the *total* chloride content is responsible for corrosion initiation of steel rods [Stratfull et al., 1975]. Many authors believe, however, that bound chloride does not impose any risk for corrosion initiation [Mohammed and Hamada, 2003]. Still, the chloride threshold value is quantified in terms of either total or free chloride content (Table 2.2).

Actually, measuring the free chloride content in the cement paste, mortar or concrete is complicated. This is mainly due to the limitations of the available techniques for extraction of free chloride ions from the cementitious materials. As a result, the total chloride content is generally considered as the criteria for the chloride threshold value.

The different methods for determination of the chloride content also result in a variation in the reported chloride threshold values. Traditionally, one or more cores from the concrete cover are taken at the time when corrosion starts (Fig. 2.4). The sliced cores are analyzed for chloride at different depths from the concrete surface. The chloride content in the slice near the rebar depth is compared with the chloride threshold value. The measured chloride content in this relatively large sample is not exactly representative for the local amount of chloride close to reinforcement. The chloride content in the sample along the rebar–concrete interface is the average amount of chloride over the rebar surface. To determine the deviation from the average value, it is reasonable to measure the chloride content in local points at the steel-concrete interface [Silva et al., 2013]. In this regard, non-destructive in situ techniques have been developed for the determination of the local chloride content at different places close to the reinforcement. In the next section, available techniques and main limitations for measuring the local chloride content are discussed and the significance of developing a chloride sensor for chloride measurement is explained.

2.4 Techniques for determination of chloride content in concrete

2.4.1 Lab techniques

The techniques for determination of the chloride content in concrete can be classified into lab techniques and non-destructive in situ techniques. Figure 2.5 gives an overview of these

techniques. In lab techniques, the concrete samples/cores are taken from the structure for further analysis in the laboratory. Generally, the lab techniques are time-consuming, expensive and cannot be used for continuous monitoring of the chloride content in a concrete structure.

The most popular and traditional lab technique for chloride determination in cementitious materials is the leaching method. In this method, acid-soluble chloride and water-soluble chloride are extracted from the powdered concrete samples into the solution. The extracted solution is further analyzed for chloride content using different methods, such as Volhard titration [Maierhofer et al., 2010]. In most cases, the acid-soluble chloride is considered equivalent to the total chloride [RILEM TC 178-TMC, 2002].

Water-soluble chloride does not necessarily represent the free chloride only, as it is sensitive to the test condition. The extracted chloride content depends on the fineness of sample powder, the amount of water added to the powder (powder/water ratio), the contact time and the temperature of the suspension [Haque and Kayali, 1995; Glass et al., 1996; Silva et al., 2013]. As a result, the different values of water-soluble chloride in a concrete sample can partly be attributed to the different test procedures used [RILEM TC 178-TMC, 2002a; ASTM C1218, 2015].

The traditional method for determination of the free chloride content in concrete specimens in the lab is extraction of pore water under pressure. The concrete specimens are pressed to extract the pore water. A few milliliters of pore water are needed for chloride analysis [Tritthart, 1989]. To obtain the minimum volume of pore water, a large volume of concrete sample with high w/c ratio, low content of aggregate and wet moisture state was suggested [Arya and Newman, 1990]. This technique is not practical for field application. Moreover, local chloride gradients cannot be determined with this technique.

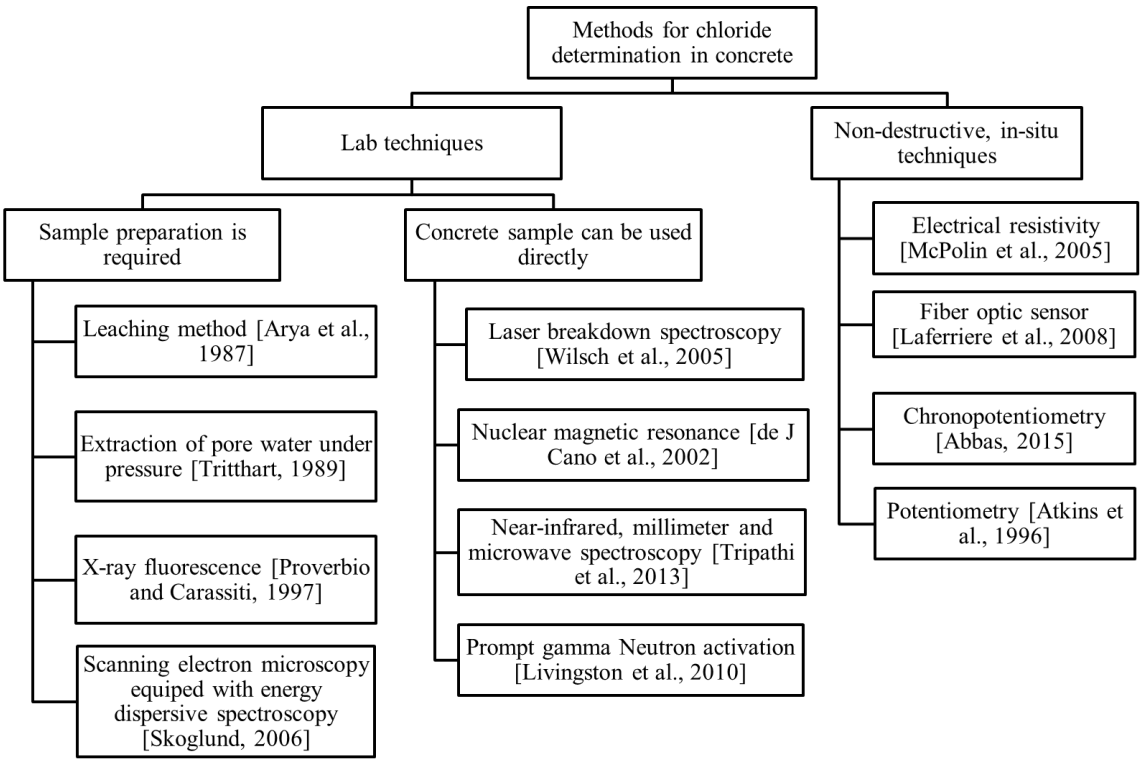

Figure 2.5: An overview of the available techniques for measuring the chloride content in concrete.

The total chloride content can also be measured by X-ray fluorescence, scanning electron microscopy equipped with energy dispersive spectroscopy and laser breakdown spectroscopy. The first two techniques need preparation of the concrete sample/core before chloride measurement. The advantage of chloride determination using laser breakdown spectroscopy is the possibility for on-site application and no need for sample preparation.

Other lab techniques are nuclear magnetic resonance (NMR), prompt gamma neutron activation analysis and near-infrared, millimeter and micro-wave spectroscopy. These techniques are expensive and labour-intensive, so their use is limited to appropriately equipped laboratories.

2.4.2 Non-destructive in-situ techniques

In the past decades attempts were made to develop non-destructive devices for in situ monitoring of the free chloride ions and chloride profiles in concrete structures. The many influencing factors, however, make the application of in situ techniques complex and difficult.

In situ techniques for measuring, or indicating, the chloride concentration are: electrical resistivity, fiber optic sensors, chronopotentiometry and potentiometry methods. The electrical resistivity can be used not only in field structures, but also in the laboratory on samples taken from the structure [Mc-Polin et al., 2005]. However, resistivity measurements for a cement-based material are very sensitive to moisture content, while not as sensitive to the chloride content. Therefore, alterations in the concrete resistivity measurements cannot simply be correlated to the chloride content in the pore water.

A fiber optic sensor consists of a fiber with an optical transducer, sensitive to chloride ions. The lifetime of optical transducers, protection of fibers and the bulky measurement setup are the limitations of this technique [Laferriere et al., 2008].

Chronopotentiometry is a dynamic electrochemical method used for an indicative determination of the chloride content at the surface of a working electrode. The current stimulus is applied to the working electrode and the potential response is measured against a pseudo-reference electrode. The use of this method for chloride measurement in concrete was recently hypothesized [Abbas, 2015].

The potentiometry technique is a measurement of open circuit potential (OCP) of an embedded Ag/AgCl electrode (chloride sensor) against a reference electrode (Figs. 2.6a,b). This method is considered the most practical approach for continuous monitoring of chloride content in the concrete environment. Interpretation of the measured OCP requires detailed information of the environment at the sensor-concrete interface (Figs. 2.1d,e and 2.6c,d) and knowledge of characteristics of the chloride sensor (Figs. 2.1a,b). In this regard, the composition of the pore solution is important for the OCP response of the chloride sensor (Fig. 2.6). For example, the concentration of hydroxide ions can affect the stability of the chloride sensor. The chloride sensor is typically not stable in alkaline medium with low chloride concentration [Jin et al., 2017] (Fig. 2.6d). The stability of the chloride sensor increases, when chloride ions are present in the pore solution, and/or when the alkalinity of the medium is low (Fig. 2.6c) [De Vera et al., 2010].

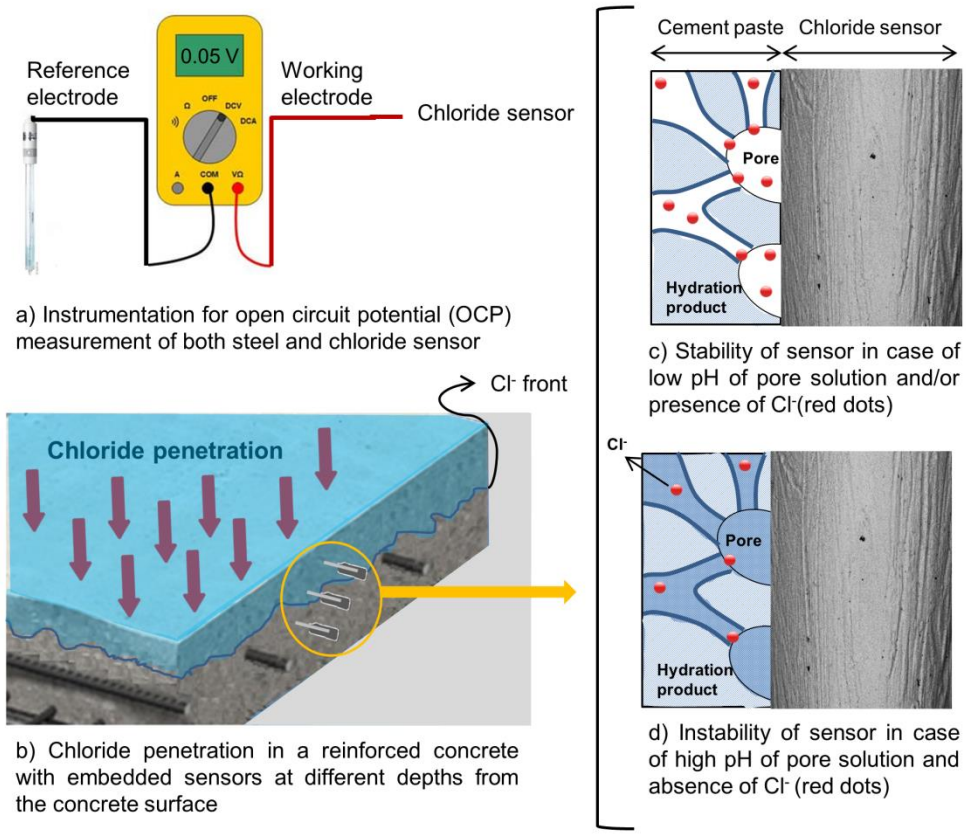

Figure 2.6: Schematic representation of chloride sensor and steel rods in cementitious materials. The open circuit potential (OCP) of chloride sensor can be related to the chloride content in the medium, while the OCP of steel rod represents the electrochemical state of the steel in concrete.

In the previous sections (2.1, 2.2 and 2.3) the main properties of cementitious materials for the sensor's response were discussed. The obtained information revealed the importance of the microstructure of cementitious materials at the interface with the sensor for a reliable sensor reading (Figs. 2.1d,e). In the next section the importance of the characteristics of the chloride sensor in the presence of interfering ions is discussed (Figs. 2.1a,b).

2.5 Ag/AgCl chloride sensor

2.5.1 Working principles of the Ag/AgCl electrode

Although the instrumentation for the Ag/AgCl chloride sensor seems simple (Figs. 2.1c, 2.6c), the interpretation of the measurements requires knowledge of the electrochemical state of the chloride sensor itself and the interaction of the sensor with the environment.

Similar to all electrochemical phenomena, the response of a Ag/AgCl chloride sensor follows the laws of thermodynamics. Therefore, an overview of the thermodynamically plausible reactions and different oxidation states of Ag in highly alkaline solutions need to be considered. A clear understanding of the sensor's response requires knowledge of the kinetics of the reactions at the sensor's surface. Kinetic parameters and relevant constraints will also be discussed in the next section.

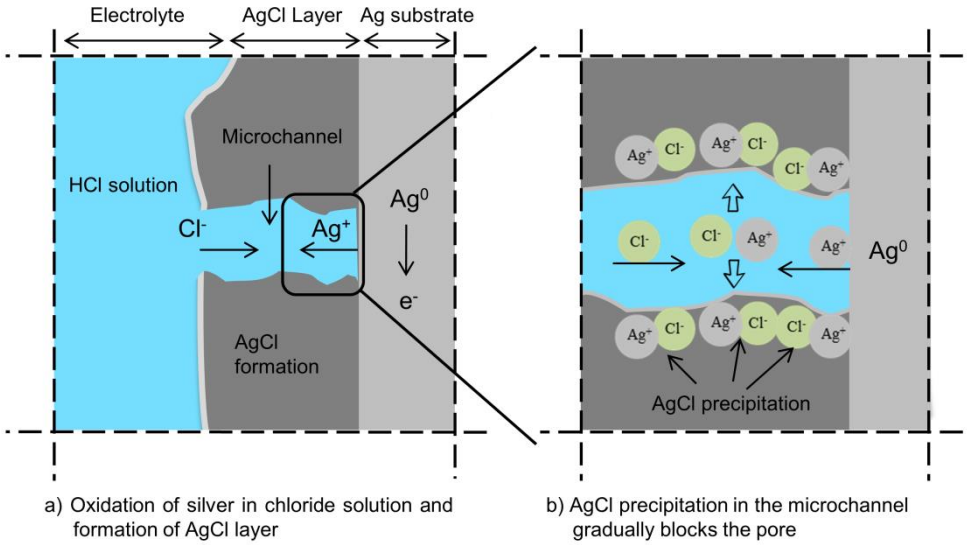

Figure 2.7: The electrochemical oxidation of Ag in HCl solution.

Silver in the form of a Ag/AgCl electrode is widely used in industrial technologies, medical instruments and as a reference electrode in electrochemistry. Some state-of-the-art reports on Ag/AgCl electrodes date back to early 1900 [Carmody, 1929]. However, the relation between the AgCl structure, the resistivity of the AgCl layer and the transport process of silver and chloride ions in that layer has not been sufficiently described [Ha and Payer, 2011]. Consequently, debates are still going on as to how to interpret the sensor readings.

One of the characteristics of a Ag/AgCl electrode is its (supposedly) rapid response. When no kinetic restrictions apply, the dynamic equilibrium between metallic silver (Ag°) and Ag^{+} can be established in a short period. This feature makes the noble Ag metal prone to "corrosion" in environments with aggressive ions, such as chloride ions. The reaction rate depends on the electrochemical state of the electrode in the aqueous medium. The electrochemical oxidation of silver in chloride containing solutions, e.g. HCl solution, results in the formation of a silver chloride layer on the silver substrate [Ha and Payer, 2011]. The mechanism of silver chloride formation is schematized in Fig. 2.7 and discussed in Section 2.5.2.

The electrochemical response of the Ag/AgCl electrode in a certain environment is different from the Ag metal alone. The change in activity of chloride ions (concentration) in the medium affects the equilibrium at the Ag/AgCl interface. However, the electrode returns rapidly to the equilibrium potential after a small transient perturbation. When a metal is in contact with an (external) solution, the metal begins to oxidize (loosing electrons, transported along the metallic conductive path) and forming positive ions, which are transported into the electrolyte. This results in a potential difference between the metal piece and the electrolyte. This potential difference is the electrode potential of the metal in that solution. An equilibrium electrode potential is the electrode potential of the metal when in equilibrium with its own ions in the solution. The electrode potential can be affected by kinetics of all electrochemical reactions, simultaneously occurring on a metal surface. In (dynamic) equilibrium conditions, the rate of all oxidation reactions equals the rate of all reduction reactions. A mixed equilibrium potential (corrosion potential) is developed, also called open circuit potential (OCP). The principle of Ag/AgCl electrode response is based on two equilibriums: the electrochemical equilibrium involving the formation of interfacial potential, and the solubility equilibrium between the Ag cation and its sparsely soluble salt (AgCl) [Janata, 2009]. This is further explained in the following.

The electrochemical equilibrium at the silver surface can be described with Eq. 2.1:

$$Ag \leftrightarrow Ag^{+} + e^{-} \quad (2.1)$$

At 25°C, the solubility product (K_{sp}) of AgCl is $K_{sp}=1.8\times10^{-10}$ [Polk et al., 2006].
The solubility equilibrium is represented by Eq. 2.2:

$$AgCl \leftrightarrow Ag^{+} + Cl^{-} \quad (2.2)$$

Combining the above two reactions, the oxidation-reduction equilibrium reaction can be written as (Eq. 2.3):

$$AgCl + e^{-} \leftrightarrow Ag + Cl^{-} \quad (2.3)$$

in which solid AgCl deposits at a potential near the thermodynamic reversible potential for the Ag/AgCl electrode in the chloride-containing medium. In this description, the silver chloride is the "core" of the Ag/AgCl electrode (chloride sensor), controlling its selectivity for chloride ions. The relation between the electrode potential (or OCP) of the chloride sensor and the chloride ions activity is expressed by the Nernst equation (Eq. 2.4) [Orna and Stock, 1989]:

$$E_{Ag/AgCl} = E^{0}_{Ag/AgCl} - 2.303\frac{RT}{nF}\lg[a_{Cl^-}] \quad (2.4)$$

where $E_{Ag/AgCl}$ is the measured electrode potential [V], $E^{\circ}_{Ag/AgCl}$ is the standard electrode potential of the Ag/AgCl electrode [V], a_{Cl^-} is the activity of the chloride ions [mol·dm^{-3}] in the vicinity of the electrode, R is the gas constant [J·mol^{-1}·K^{-1}], F is the Faraday constant [C·mol^{-1}] and T is the absolute temperature (K).

The chloride ions activity is linked to the chloride ions concentration by the activity coefficient (γ) (Eq. 2.5) [Dobos,1975]:

$$a_{cl^-} = C_{Cl^-}.\gamma_{Cl^-} \quad (2.5)$$

Therefore, by measuring the OCP of the Ag/AgCl electrode and using Eq. 2.4, the chloride activity, and subsequently the chloride concentration in the solution, can be calculated.

2.5.2 Electrochemical kinetics of AgCl layer formation

In most studies of Ag/AgCl production, anodization (galvanostatic regime) of silver in chloride-containing solutions was the method used for oxidation of silver and formation of AgCl on the silver substrate [Jaya et al., 1987]. The main differences among the anodization regimes are the current density and the duration of anodization. In some cases, the anodized AgCl layer was additionally dipped in AgCl melt to achieve a more stable AgCl layer.

It has been reported that after nucleation, the growth of a AgCl layer on the silver substrate proceeds with the formation of small patches of rounded and smooth surface with no sign of crystal orientation [Katan et al., 1974]. At this stage, the size of the AgCl particles is less than 0.5 μm [Jin et al., 2003]. However, transition to a multilayer brings dense and fine AgCl particles to the surface (Fig. 2.8a). Anodization at high current density changes the surface morphology of the AgCl layer to the so-called mosaic appearance (Fig. 2.8b).

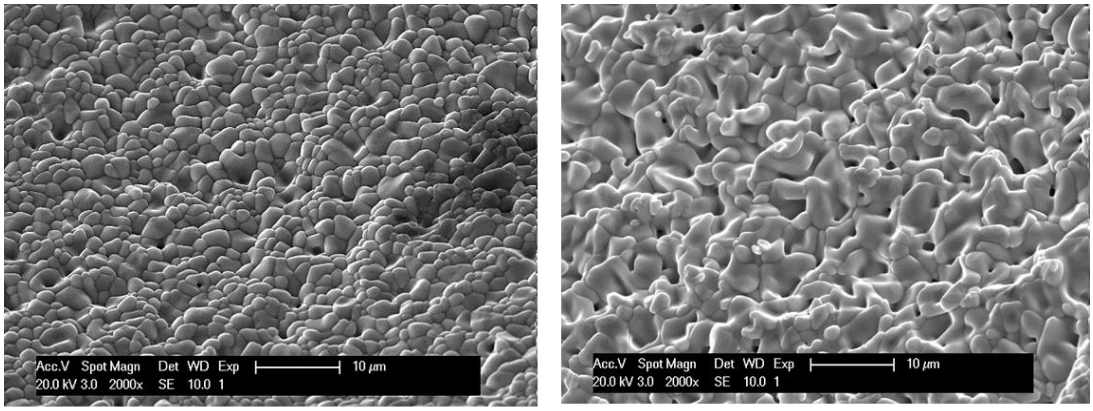

a) Anodization at 0.5 mA/cm^2 b) Anodization at 4 mA/cm^2

Figure 2.8: Surface morphology of AgCl layer prepared by one-hour anodization at different current densities.

The galvanostatic growth of a AgCl multilayer is accompanied by an increase in the overpotential due to the ohmic resistance of the AgCl layer itself [Lal et al., 1951]. The AgCl itself is non-conductive, so the effective ionic conductivity of such a layer depends on the pores (microchannels) between the AgCl grains (Fig. 2.7a). The growth of the AgCl layer is a function of the ionic conductivity of the microchannels [Stoica et al., 2011].

The observed potential difference among different Ag/AgCl chloride sensors in an alkaline medium with the same chloride concentration was attributed to the sensor preparation method [Elsener et al., 2003; Duffo et al., 2009]. However, no evidence in support of this assertion was provided. For instance, the OCPs of two differently prepared Ag/AgCl chloride sensors were measured in $Ca(OH)_2$ solution with 0.002 M to 0.86 M NaCl. The observed OCP of the sensors were different in the entire range of the chloride concentrations. The effect was higher at lower chloride concentration, e.g. 60 mV was recorded at 0.002 M chloride concentration versus 40 mV at 0.86 M chloride concentration was reported [Montemor et al., 2006]. In a similar study, two differently prepared chloride sensors were embedded in mortar samples. A difference of 100 mV in the initial OCP of the chloride sensors was reported [Elsener et al., 2003]. These studies did not provide further evidence for the observed discrepancies between the sensor readings. The influence of AgCl layer properties on the reproducibility and reliability of the sensor's response was not further discussed. Within anodization, the mechanism of ionic conductivity governs the kinetics for silver dissolution and AgCl formation. The change in conductivity of the layer can subsequently affect the AgCl layer morphology and microstructure. The alteration in the physical properties of the AgCl layer (porosity, thickness, morphology, etc.) can affect the stability and reliability of the sensor readings in cementitious materials.

2.5.3 Thermodynamic behaviour of silver

AgCl is a "corrosion product" of silver in a chloride-containing environment. The electrochemical state of silver, similar to all electrochemical phenomena, follows laws of thermodynamics. Hence, a full understanding and prediction of a corrosion process undoubtedly require consideration of thermodynamic principles. Following these principles, the standard Gibbs free energy (ΔG) for a given compound is the energy for the formation of 1 mole of that compound from its constituents. A negative ΔG is an indication of a spontaneous reaction.

Table 2.3 gives the standard Gibbs energies of formation of the species and phases in the silver-chloride-water system [Bard et al., 1985]. The positive Gibbs energy of silver ions (Ag^+) and AgO is an indication of non-spontaneous reactions. The Gibbs energy of the ionic silver compounds, such as $Ag(OH)_2^-$, $AgCl_2^-$ and $AgCl_4^{3-}$ is more negative than the crystalline phases (c), such as AgCl(c) and Ag_2O(c). Consequently, the formation of the former compounds is more product-favoured than the latter ones. The spontaneous corrosion product of silver in a chloride-containing medium is AgCl (e.g. AgCl with Gibbs energy= -110 KJ/mol), rather than silver oxide (e.g. Ag_2O with Gibbs energy= -11 KJ/mol).

Table 2.3: Gibbs free energies for the formation of species in silver-halide-water systems at 25 °C [Bard et al., 1985].

Species	Gibbs free energy (KJ/mol)	Species	Gibbs free energy (KJ/mol)
Ag^+	77	AgCl (c)	-110
Cl^-	-131	AgCl (aq)	-54
Ag_2O (c)	-11	$AgCl_2^-$	-216
AgO (c)	15	$AgCl_4^{3-}$	-478
AgOH	-80	Ag_2S	-41
$Ag(OH)_2^-$	-260	---	---

(aq): aqueous phase – (c): crystalline phase

Kinetic restrictions exist in all thermodynamically possible reactions. The actual occurrence, direction and rate of thermodynamically possible reactions are governed by electrochemical kinetics. For example, the thermodynamic data indicates the formation of ionic silver compounds or AgCl as the favoured reaction product on silver. However, the rate of formation of these compounds depends on the concentration of chloride and hydroxide ions in the medium. This process is also reflected in the response of Ag/AgCl sensor in an alkaline medium with low chloride content. In this condition, the alkalinity of the medium and transformation rate of silver chloride to silver oxide at the sensor's surface governs the sensor's response. The influence of this transformation rate on the sensor's response is generally not discussed in the reported studies.

The Pourbaix diagram (potential-pH) is derived from the Nernst equation. It is based on thermodynamics, so it can only "map out" thermodynamic stability of metal species and compounds at various combinations of equilibrium potential and pH in an aqueous medium under standard conditions. For instance, the Pourbaix diagram for the silver–chloride-water system (Fig. 2.9a) in comparison to silver–water system (Fig. 2.9a) shows that the chloride ion is a strong oxidizing agent for Ag(s) and crystalline AgCl (AgCl(c)) is the thermodynamically favourable oxidation product. It is reported that the increase in the concentration of chloride ions causes dissolution of AgCl(c) and formation of ionic silver chloride, such as $AgCl_2^-$ or $AgCl_4^{3-}$ [Giles, 1970]. Fig. 2.9b shows the Pourbaix diagram for the silver-water system. The Ag^+ ions are formed at low pH values and high overpotentials. The oxidation of silver in an alkaline environment (Figs. 2.9a,b) results in formation of different silver compounds, such as Ag_2O, Ag_2O_2 (AgO). In chloride-containing system (Figs. 2.9a), the silver oxide compounds (e.g. Ag_2O_2) can also exist but in higher pH value than that in chloride-free system (Figs. 2.9a,b). The AgCl can counterbalance the silver oxides formation, depending on the chloride concentration and pH of the environment (Fig. 2.9a). All these processes can be related to the performance of the Ag/AgCl chloride sensor in

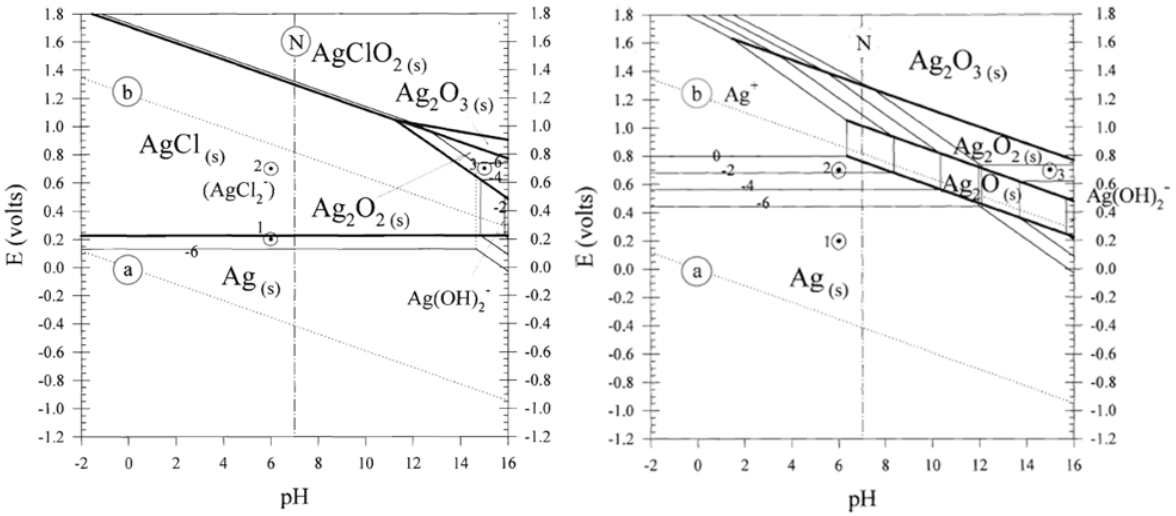

a) Pourbaix diagram for a silver-chloride-water system b) Pourbaix diagram for a silver-water system

Figure 2.9: a) Pourbaix diagram for a silver-chloride-water system at 25 °C with 1 m chloride concentration and different concentrations of silver ions (10^{-6}, 10^{-4}, 10^{-2} m), b) Pourbaix diagram for a Ag-water system at 25°C with different concentration of silver ions from 1 to 10^{-6} m. The potentials are vs. SHE reference electrode [Winston, 2000].

cementitious materials. The dissolution of AgCl(c) and formation of silver chloride complexes ($AgCl_n^{(1-n)}$), or formation of silver oxide, may deviate the response of the chloride sensor as determined by Eq. 2.4. In other words, the OCP measured as $E_{Ag/AgCl}$ will no longer satisfy Eq. 2.4 or be valid for a Ag/AgCl interface.

2.6 Reliability of sensor's response in cementitious materials

The performance of a chloride sensor in cementitious materials depends on the thermodynamic stability of the AgCl layer at the sensor's surface. In the presence of chloride ions in the solution, AgCl is the dominant reaction product (Figs. 2.10). The increase in the

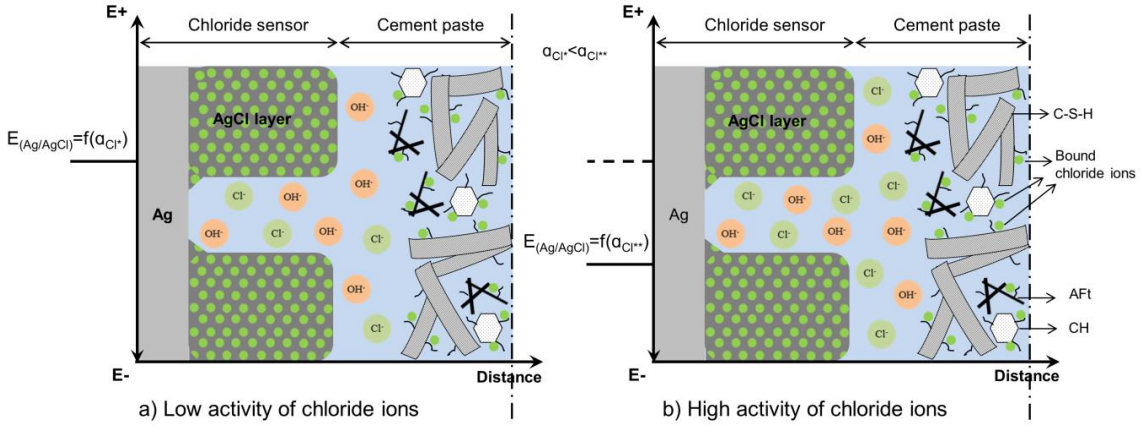

Figure 2.10: Schematic of Ag/AgCl/pore solution interface in chloride-containing cementitious materials, a) low activity of chloride ions, b) high activity of chloride ions. In the presence of chloride ions, the surface of the sensor mainly consists of AgCl particles. The binding of chloride ions to the hydration products together with the microstructure of cementitious materials affect the activity of the chloride ions at the sensor's surface.

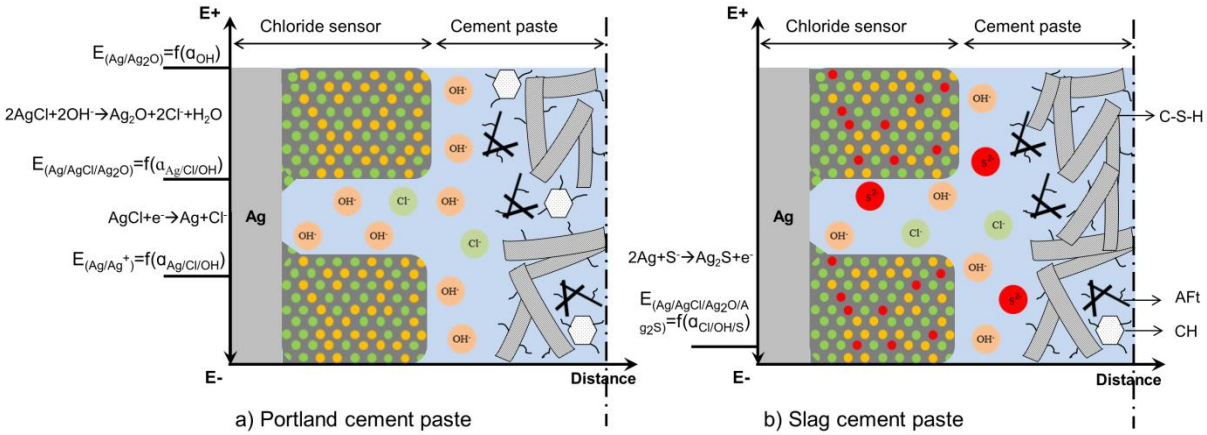

Figure 2.11: Schematic of Ag/AgCl/pore solution interface in chloride-free cementitious materials, a) Portland cement paste, b) slag cement paste. In the absence of chloride ions, a gradual dissolution of the AgCl layer is accompanied by the formation of Ag_2O, Ag° or Ag_2S (in case of slag cement concrete) [Graedel, 1992; Femenias et al., 2015]. The formation of these products depends on the concentration of hydroxide and sulfide ions in the medium and the microstructure of cementitious materials at the interfacial zone with the sensor.

activity of chloride ions shifts the sensor's OCP to more negative potentials (Figs. 2.10, as indicated on the vertical axes). However, the interference of hydroxide and sulfide ions in the solution can limit the otherwise plausible reaction of AgCl formation on the sensor's surface (Fig. 2.11). Therefore, the rate of AgCl transformation into Ag_2O or Ag_2S controls the variation in the sensor's OCP. This process essentially makes the OCP of the Ag/AgCl sensor deviating from the expected response for a Ag/AgCl electrode (Eq. 2.4).

In solutions with high pH values and low chloride concentration (Fig. 2.11a), AgCl can be partly or entirely converted into silver oxide compounds (Ag_2O, AgO, AgOH, etc.). In those cases, the sensor gradually acts as a pH sensor rather than a chloride sensor. In this condition, the activity of silver ions in the vicinity of the sensor is determined by exchange equilibrium and formation of Ag_2O, as indicated in Fig. 2.11a. However, the dissolved silver chloride ($K_{sp}AgCl=1.8\times10^{-10}$ at 25°C) and/or the formed silver oxide ions ($K_{sp}(AgOH)=2\times10^{-8}$ at 25°C [Moody et al., 1981]) do not necessarily adhere to the sensor's surface [Angst et al., 2010]. These ions can leave the sensor's surface and diffuse into the cementitious material.

Thermodynamically, the formation of Ag_2S with lower solubility ($K_{sp}(Ag_2S)=1.6x10^{-49}$ at 25°C) [Raynauld and Laviolette, 1987] is favored when a sufficient amount of sulfide ions is present in the medium, e.g. in concrete with slag cement. It has been stated that a sulfide content of higher than 6 mM can affect the chloride sensor's response in a sulfide-containing solution [Femenias et al., 2015]. The extent to which Ag_2S forms on the sensor's surface determines the shift to cathodic OCP response of the chloride sensor (Fig. 2.11b) [Suzuki et al., 1998]. The lower solubility product of Ag_2S than those of AgCl and Ag_2O is the main reason for the lack of the sensor's sensitivity to chloride ions in a sulfide-containing medium [Raynauld and Laviolette, 1987; Graedel, 1992; Altunbulduk et al., 1995]. Hence, the presence of sulfide ions in the pore solution of slag cement can affect the chloride sensor's response [Femenias et al., 2015]. The extent of such an influence depends on the kinetics of reactions of sulfide ions with the AgCl layer at the sensor's surface.

The AgCl layer gradually dissolves in chloride-free solutions even in the absence of interfering ions (hydroxide and sulfide ions). The gradual dissolution of the AgCl layer can be fatal for the sensor performance [Raynauld and Laviolette, 1987]. The dissolved ions can

gradually diffuse in the medium, exposing the Ag substrate to direct contact with the environment. In this condition, the OCP of the Ag metal depends on adventitious impurities in the medium (Fig. 2.11a). The measured OCP is a "mixed potential" which is unstable, irreproducible and cannot be described by Eq. 2.4 [Janz and Ives, 1968].

All above considerations with regards to (electro)chemical reactions and actual sensors' response depend on the availability of ions (chloride ions and interfering ones) and ion transport, or limitations in the surrounding medium, i.e. pore water and pore network. The importance of the microstructure of cementitious materials involves the influence of different hydration products and their compactness at the sensor's surface. In the presence of large pores at the sensor–cement paste interface (Figs. 2.1d,e), a considerable number of chloride ions are free. Ongoing hydration of cement densifies the interface between the sensor and the cementitious material. Densification of the interface results in the formation of finer pores of nm size between the sensor and hydration products. Finer pores promote physical binding of chloride ions. The physical binding of chloride ions to the surface of hydration products lowers the activity of chloride ions at the sensor's surface. This will be reflected in the sensor's response. The presence of crystalline phases of cement pastes at the interface (Section 2.2.1) limits the dissolution/precipitation processes at the sensor's surface. This will also be reflected in the sensor's response. Consequently, the properties of the sensor and the surrounding cementitious material can affect (or redirect) the thermodynamically plausible reactions at the sensor's surface. This is due to the limitations of electron/ion transport at the sensor surface and/or limitations caused by the resistive properties of the surrounding medium. The AgCl layer properties, different cement hydration products and their compactness at the interface between sensor and bulk matrix are the major factors that affect the sensor performance. Therefore, recognition of the imposed limitations from these factors is important for interpretation of the chloride sensor measurement.

2.7 Conclusion

A reliable and reproducible chloride sensor measurement and correct interpretation of this measurement require knowledge of the inherent properties of the sensor and adjacent matrix in which the sensor is embedded. In this regard, the following should be considered:

1) The interfacial properties between the silver substrate and the AgCl layer, i.e. morphology of the AgCl particles and the conductivity of the layer.
2) The presence of interfering hydroxide and sulfide ions, i.e. the pore water composition.
3) The relative distribution and compactness of cement hydration products at the sensor's surface.

The physical properties of the AgCl layer (porosity, thickness, morphology, etc.) affect the rate of ion exchange and dissolution/precipitation processes at the sensor's surface. Instability of a Ag/AgCl chloride sensor is attributed to dissolution of the AgCl layer and/or the formation of other silver compounds. As a result, a mixed potential subsequently develops at the sensor's surface. The AgCl layer is more stable when the chloride concentration is high, while at low concentrations, products other than silver chloride form. The presence of other silver compounds obviously affects the performance of the sensor. If the aim is to determine the chloride content close to the reinforcement at the time of corrosion of reinforcement with high accuracy, the sensor's response should be reliable in a wide range of chloride concentration, i.e., 0.045–3.22 mol/l (Table 2.2). As the source of chloride ions is mainly from the external

environment, the time required for chloride ions to penetrate into the concrete and reach at least 0.045 mol/l at the sensor surface can be very long. Consequently, the sensor will be exposed to an alkaline medium free of chloride ions (or with a very low chloride content) for a relatively long period of time. In such a case, the accuracy of the chloride sensor cannot be simply judged from the viewpoint of thermodynamic principles, but will depend on the reaction kinetics on the sensor's surface. For this reason, the influence of the microstructure of surrounding cement-based materials on the lifetime of the chloride sensor should be taken into account.

In a cement-based system the hydration products are the resistive component that can limit ion transport at the sensor's surface and affect the response of the chloride sensor. The hydration products also cover the sensor's surface, slowing down the rate of AgCl dissolution. This feature can be beneficial for the long-term performance of the chloride sensor, since the dissolution of the AgCl layer can be fatal for the sensor performance. The dissolved AgCl particles can gradually diffuse into the medium, while the Ag substrate becomes in direct contact with the medium. Moreover, the presence of hydroxide and/or sulfide ions in the pore solution can interfere with the sensors' response. The different cement hydration products and their compactness around the sensor will subsequently influence the activity of chloride ions. The alteration in chloride ions activity, however, will be reflected in the sensor's response. Hence, the morphology and microstructure of the AgCl layer, binding of chloride ions to the hydration products and the pore size distribution around the sensor should be considered for interpretation of the sensor's response.

2.8 References

Abbas, Y. (2015). *In-situ measurement of chloride ion concentration in concrete*, Ph.D. thesis, University of Twente, Netherlands.

Alonso, C., Andrade, C., Castellote, M. and Castro, P. (2000). Chloride threshold values to depassivate reinforcing bars embedded in a standardized OPC mortar, *Cement and Concrete Research*, Vol. 30(7), p. 1047–1055.

Alonso, C., Castellote, M. and Andrade, C. (2002). Chloride threshold dependence of pitting potential of reinforcements, *Electrochimica Acta*, Vol. 47(21), p. 3469-3481.

Altunbulduk, T., Kocker, H. M. and Frenzel, W. (1995). Studies on the elimination of sulfide interference in the potentiometric determination of chloride using ion-selective electrodes in a flow injection system, *Fresenius' Journal of Analytical Chemistry*, Vol. 351(7), p. 593-598.

Angst, U., Elsener, B., Larsen, C. K. and Vennesland, O. (2010). Potentiometric determination of the chloride ion activity in cement-based materials, *Journal of Applied Electrochemistry*, Vol. 40(3), p. 561–573.

Anon. (2002). *Condition investigation manual for concrete facade panels:* BY 42. Concrete Association of Finland, Helsinki, p. 178 (in Finnish).

Arya, C. (1989). *Assessment of chlorides in concrete*, University of London, Ph.D. thesis.

Arya, C. and Newman, J. B. (1990). An Assessment of Four Methods of Determining the Free Chloride Content of Concrete, *Materials and Structures*, Vol. 23(5), p. 319-330.

Arya, C., Buenfeld, N. R. and Newman, J. B. (1987). Assessment of simple methods of determining the free chloride ion content of cement paste, *Cement and Concrete Research*, Vol. 17(6), p. 907-918.

ASTM C114. (2000). *Standard Test Methods for Chemical Analysis of Hydraulic Cement*, American Society for Testing and Materials (ASTM) Philadelphia, PA.

ASTM C1152. (2003). *Standard Test Method for Acid-Soluble Chloride in Mortar and Concrete*, American Society for Testing and Materials (ASTM) Philadelphia, PA.

ASTM C1218. (2015). *Standard Test Method for Water-Soluble Chloride in Mortar and Concrete*,

American Society for Testing and Materials (ASTM) Philadelphia, PA.
Bard, A. J. and Rubinstein, I. (1996). *Electroanalytical Chemistry: A Series of Advances*, Vol. 22, Marcel Dekker, Inc. USA.
Bard, A.J., Parsons, R. and Jordan, J. (1985). *Standard Potentials in Aqueous Solution*, Marcel Dekker, New York, p. 294-312. change the place
Beck, T.R. and Rice, D.E. (1984). Conductivity of anodic silver chloride during formation, *Journal of the Electrochemical Society*, Vol. 131(1), p. 89-93.
Birdi, K. A. S. (2015). *Handbook of surface and colloid chemistry*, CRC Press.
Birnin-Yauri, U.A. and Glasser, F.P. (1998). Friedel's salt, $Ca_2Al(OH)_6(Cl,OH).2H_2O$: its solid solutions and their role in chloride binding, *Cement and Concrete Research*, Vol. 28(12), p. 1713-1723.
Carmody, W. R. (1929). A study of the silver chloride electrode, *Journal of the American Chemical Society*, Vol. 51(10), p. 2901–2904.
Daily, S. F. (1999). *Understanding corrosion and cathodic protection of reinforced concrete structures*, Corrpro Companies, Incorporated.
De J Cano, F., Bremner, T. W., McGregor, R. P. and Balcom, B. J. (2002). Magnetic resonance imaging of 1 H, 23 Na, and 35 Cl penetration in Portland cement mortar, *Cement and Concrete Research*, Vol. 32(7), p. 1067-1070.
De Vera, G., Climent, M. A., Anton, C., Hidalgo, A. and Andrade, C. (2010). Determination of the selectivity coefficient of a chloride ion selective electrode in alkaline media simulating the cement paste pore solution, *Journal of Electroanalytical Chemistry*, Vol. 639(1), p. 43-49.
Dhir, R.K.; Jones, M.R.; Ahmed, H.E.H. (1990). Determination of total and soluble chlorides in concrete, *Cement and Concrete Research*, 20, p. 579–590.
Diamond, S. (1989). ASR-Another Look at Mechanisms, *Proceedings of the Eighth International Conference on Alkali-Aggregate Reaction in Concrete*, Kyoto, Japan, p. 83–94.
Dobos, D. (1975). *Electrochemical data: a handbook for electrochemists in industry and universities*, Elsevier Science and Technology.
Duffo, G. S., Farina, S. B. and Giordano, C. M. (2009). Characterization of solid embeddable reference electrodes for corrosion monitoring in reinforced concrete structures, *Electrochimica Acta*, Vol. 54(3), p. 2010–2020.
Elakneswaran, Y. (2009). *Multi-ionic transport in cementitious materials with ion-cement hydrates interactions*, Doctoral dissertation, Ph.D. thesis, Hokkaido University, Solid Waste, Resources and Geoenviromental Engineering.
Elakneswaran, Y., Nawa, T. and Kurumisawa, K. (2009). Electrokinetic potential of hydrated cement in relation to adsorption of chlorides, *Cement and Concrete Research*, Vol. 39(4), p.340-344.
Elsener, B., Zimmermann, L. and Bohni, H. (2003). Non-destructive determination of the free chloride content in cement-based materials, *Materials and Corrosion*, Vol. 54 (6), p. 440–446.
Elsener, B., Zimmermann, L., Fluckiger, D., Burchler, D. and Bohni, H. (1995). Chloride penetration-non-destructive determination of the free chloride content in mortar and concrete, *Proc. RILEM Int. Workshop "Chloride penetration into concrete"*, Paris.
Femenias, Y. S. Angst, U., Caruso, F. and Elsener, B. (2015). Ag/AgCl ion-selective electrodes in neutral and alkaline environments containing interfering ions, *Materials and Structures*, p. 1-15.
Ferreira, R. M. (2004). *Probability-based durability analysis of concrete structures in marine environment*, Ph.D. thesis, University of Minho, Portugal.
Gao, P. (2018). *Simulation of hydration and microstructure development of blended cement*, Ph.D. thesis, Department of Materials and Environment, Delft University of Technology, The Netherlands.
Garcia, V., Francois, R., Carcasses, M. and Gegout, P. (2014). Potential measurement to determine the chloride threshold concentration that initiates corrosion of reinforcing steel bar in slag concretes, *Materials and Structures*, Vol. 47(9), p. 1483-1499.
Giles, R.D. (1970). The anodic behaviour of silver single crystal electrodes in concentrated chloride solutions, *Journal of Electroanalytical Chemistry and Interfacial Electrochemistry*, Vol. 27(1), p. 11-19.

Glass, G. K., Wang, Y. and Buenfeld, N. R., (1996). An investigation of experimental methods used to determine free and total chloride contents, *Cement and Concrete Research*, Vol. 26(9), p. 1443-1449.

Graedel, T. E. (1992). Corrosion mechanisms for silver exposed to the atmosphere, *Journal of the Electrochemical Society*, Vol. 139(7), p. 1963-1970.

Ha, H. and Payer, J. (2011). The effect of silver chloride formation on the kinetics of silver dissolution in chloride solution, *Electrochimica Acta*, Vol. 56(7), p. 2781–2791.

Haque, M.N. and Kayali, O. A. (1995). Free and water-soluble chloride in concrete, *Cement and Concrete Research*, Vol. 25 (3), p. 531-542.

Hausmann, D.A. (1967). Steel corrosion in concrete. How does it occur?, *Materials Protection*, Vol. 6, p. 19–23.

He, F., Shi, C., Hu, X., Wang, R., Shi, Z., Li, Q. and An, X. (2016). Calculation of chloride ion concentration in expressed pore solution of cement-based materials exposed to a chloride salt solution, *Cement and Concrete Research*, Vol. 89, p. 168-176.

Hewlett, P. C. (2003). *Lea's Chemistry of Cement and Concrete (Fourth Edition)*, Butterworth Heinemann, Elsevier Ltd.

Hu, X., Shi, C. and De Schutter, G. (2015). Influences of chloride immersion on zeta potential and chloride in concentration of cement-based materials, *14th International Congress on the Chemistry of Cement*, p. 1-15.

Janata, J. (2009). *Principles of Chemical Sensors*, Springer Book, New York.

Janz, G. J. and Ives, D. J. (1968). *Silver, silver chloride electrodes*. Annals of the New York Academy of Sciences, Vol. 148(1), p. 210-221.

Jaya, S. Rao, T.P. and Rao, G.P. (1987). Mono- and multilayer formation studied of silver chloride on silver electrodes from chloride-containing solutions, *Journal of Applied Electrochemistry*, Vol. 17(3), p. 635-640.

Jin, M., Jiang, L. and Zhu, Q. (2017). Monitoring chloride ion penetration in concrete with different mineral admixtures based on embedded chloride ion-selective electrodes, *Construction and Building Materials*, Vol. 143, p. 1-15.

Jin, X., Lu, J., Liu, P. and Tong, H. (2003). The electrochemical formation and reduction of a thick AgCl deposition layer on a silver substrate, *Journal of Electroanalytical Chemistry*, Vol. 542, p. 85-96.

Katan, T., Szpak, S. and Douglas, N.B. (1974). Silver/silver chloride electrodes: surface morphology on charging and discharging, *Journal of the Electrochemical Society*, Vol. 121 (6), p. 757-764.

Laferriere, F., Inaudi, D., Kronenberg, P. and Smith, I. F. (2008). A new system for early chloride detection in concrete, *Smart Materials and Structures*, Vol. 17(4), 045017.

Lal, H., Thirsk, H.R. and Jones, W.F.K.W. (1951). A study of the behavior of polarized electrodes, Part I – the silver/silver halide system, *Transactions of the Faraday Society*, Vol. 47, p. 70-77.

Lambert, P., Page, C. L. and Vassie, P. R. (1991). Investigations of reinforcement corrosion. 2. Electrochemical monitoring of steel in chloride-contaminated concrete, *Materials and Structures*, Vol. 24(5), p. 351-358.

Livingston, R. A., Al-Sheikhly, M. and Mohamed, A. B. (2010). Numerical simulation of the PGNA signal from chlorine diffusion gradients in concrete, *Applied Radiation and Isotopes*, Vol. 68(4), p. 679-682.

Lothenbach, B. and Winnefeld, F. (2006). Thermodynamic modelling of the hydration of Portland cement, *Cement and Concrete Research*, Vol. 36(2), p. 209–226.

Lothenbach, B., Le Saout, G., Haha, M. B., Figi, R. and Wieland, E. (2012). Hydration of a low-alkali CEM III/B–SiO 2 cement (LAC), *Cement and Concrete Research*, 42(2), 410-423.

Maes, M., Gruyaert, E. and De Belie, N. (2013). Resistance of concrete with blast-furnace slag against chlorides, investigated by comparing chloride profiles after migration and diffusion, *Materials and structures*, Vol. 46(1-2), p. 89-103.

Maierhofer, C., Reinhardt, H. W. and Dobmann, G. (Eds.). (2010). *Non-Destructive Evaluation of Reinforced Concrete Structures: Non-Destructive Testing Methods*, Elsevier.

Maslehuddin, M., Page, C. L. and Rasheeduzzafar (1997). Temperature effect on the pore solution

chemistry in contaminated cements, *Magazine of Concrete Research*, Vol. 49(178), p. 5-14.
McPolin, D., Basheer, P. A. M., Long, A. E., Grattan, K. T. V. and Sun, T. (2005). Obtaining progressive chloride profiles in cementitious materials, *Construction and Building Materials*, Vol. 19(9), p. 666-673.
Mehta, P. K. and Monterio P. J. M. (2006). *Concrete, microstructure, properties and materials*, third edition, McGraw-Hill Companies.
Melchers, R. E. (2016). *Developing realistic deterioration models. In Life-Cycle of Engineering Systems: Emphasis on Sustainable Civil Infrastructure*, p. 28-32, CRC Press.
Mohammed, T. U. and Hamada, H. (2003). Relationship between free chloride and total chloride contents in concrete, *Cement and Concrete Research*, Vol. 33(9), p. 1487-1490.
Molina, M. (1993). Zerstörungsfreie Erfassung der gelösten Chloride im Beton, Diss. ETH, Nr. 10315, ETH Zurich.
Montemor, M. F., Alves, J. H., Simoes, A. M., Fernandes, J. C. S., Lourenço, Z., Costa, A. J. S., Appleton, A.J. and Ferreira, M. G. S. (2006). Multiprobe chloride sensor for in situ monitoring of reinforced concrete structures, *Cement and Concrete Composites*, Vol. 28(3), p. 233-236.
Moody, G. J., Rigdon, L. P., Meisenheimer, R. G. and Frazer, J. W. (1981). Selectivity Parameters of Homogeneous Solid –state Chloride ion-selective Electrodes and the Surface, Morphology of Silver Chloride - Silver Sulphide Discs under Simulated Interference Conditions, *The Analyst*, Vol. 106(1262), p. 547-556.
Mundra, S., Criado, M., Bernal, S. A. and Provis, J. L. (2017). Chloride-induced corrosion of steel rebars in simulated pore solutions of alkali-activated concretes, *Cement and Concrete Research*, Vol. 100, p. 385-397.
NT Build 208. (1996). *Concrete, Hardened: Chloride content by Volhard Titration*, Nordtest.
Oh, B. H., Jang, S. Y. and Shin, Y. S. (2003). Experimental investigation of the threshold chloride concentration for corrosion initiation in reinforced concrete structures, *Magazine of Concrete Research*, Vol. 55(2), p. 117-124.
Ollivier, J. P., Maso, J. C., and Bourdette, B. (1995). Interfacial transition zone in concrete, *Advanced Cement Based Materials*, Vol. 2(1), p. 30–38.
Orna, M.V. and Stock, J. (1989). *Electrochemistry, past and present*. American Chemical Society.
Pettersson, K. (1992). *Corrosion threshold value and corrosion rate in reinforced concrete*, CBI REPORT 2.
Polk, B. J., Stelzenmuller, A., Mijares, G., MacCrehan, W. and Gaitan, M. (2006). Ag/AgCl microelectrodes with improved stability for microfluidics, *Sensors and Actuators*, Vol. 114(1), p. 239–247.
Proverbio, E. and Carassiti, F. (1997). Evaluation of chloride content in concrete by X-ray fluorescence, *Cement and Concrete Research*, Vol. 27(8), p. 1213-1223.
Raynauld, J. P. and Laviolette, J. R. (1987). The silver-silver chloride electrode: a possible generator of offset voltages and currents, *Journal of neuroscience methods*, Vol. 19(3), p. 249-255.
RILEM TC 178-TMC. (2002). Analysis of total chloride in concrete, *Material and Structures*, 35, p. 583-585.
RILEM TC 178-TMC. (2002a). Analysis of water-soluble chloride content in concrete, Recommendation, *Materials and Structures*, Vol. 35, p. 586-588.
Schiessl P. and Raupach, M. (1990). *Corrosion of Reinforcement in Concrete*, Elsevier Applied Science, London.
Silva, N., Tang, L., Lindqvist, J. E. and Boubitsas, D. (2013). Chloride profiles along the concrete-steel interface, *International Journal of Structural Engineering*, Vol. 4(1-2), p. 100-112.
Skoglund, P. (2006). *Chloride Transport and Reinforcement Corrosion in the Vicinity of the Transition Zone between Substrate and Repair Concrete*, Licentiate Thesis, TRITA-BKN, Bulletin 89, Stockholm, Sweden.
Stoica, D., Brewer, P. J., Brown, R. J. and Fisicaro, P. (2011). Influence of fabrication procedure on the electrochemical performance of Ag/AgCl reference electrodes, *Electrochimica Acta*, Vol. 56(27), p. 10009-10015.
Stratfull, R. F., Jurkovich, and W.J., Spellman, D.L. (1975). *Corrosion Testing of Bridge Decks*,

Highway Research Record 539, Washington, DC. Transportation Research Board.

Suzuki, H., Hiratsuka, A., Sasaki, S. and Karube, I. (1998). Problems associated with the thin-film Ag/AgCl reference electrode and a novel structure with improved durability, *Sensors and Actuators B: Chemical*, Vol. 46(2), p. 104-113.

Swamy, R. N. (1992). *The alkali-silica reaction in concrete*, The Blackie Publishing Group, Glasgow, Scotland.

Tripathi, S. R., Inoue, H., Hasegawa, T. and Kawase, K. (2013). Non-destructive Inspection of Chloride Ion in Concrete Structures Using Attenuated Total Reflection of Millimeter Waves. *Journal of Infrared, Millimeter, and Terahertz Waves*, Vol. 34(2), p. 181-186.

Tritthart, J. (1989). Chloride binding in Cement II. The influence of the hydroxide concentration in the pore solution of hardened cement paste on chloride binding, *Cement and Concrete Research*, Vol. 19(5), p. 683-691.

Van Breugel, K. (1991). *Simulation of hydration and formation of structure in hardening cement-based materials*, Ph.D. thesis, Delft University of Technology, The Netherlands.

Vollpracht, A., Lothenbach, B., Snellings, R. and Haufe, J. (2016). The pore solution of blended cements: a review, *Materials and Structures*, Vol. 49(8), p. 3341-3367.

Wilsch, G., Weritz, F., Schaurich, D. and Wiggenhauser, H. (2005). Determination of chloride content in concrete structures with laser-induced breakdown spectroscopy, *Construction and Building Materials*, Vol. 19(10), p. 724-730.

Winston, R. (2011). *Uhlig's corrosion handbook, Part 1, Pourbaix diagrams for multielement systems*, Chapter 8, p. 103.

Yuan, Q., Deng, D., Shi, C. and De Schutter, G., Deng，D. and He, F. (2011). Chloride ion concentration on the surface of cement-based materials in chloride solutions, *Journal of the Chinese ceramic society*, Vol. 39(3), p. 544-549.

Zibara, H. (2001). *Binding of external chloride by cement pastes*, Ph.D. thesis, Department of Building Materials, University of Toronto, Canada.

Zimmermann, L., Elsener, B. and Bohni, H. (1999). Critical factors for the initiation of rebar corrosion, *Proc. EUROCORR '99, European Federation of Corrosion*, Aachen, Germany.

Chapter 3

Preparation and characterization of the Ag/AgCl chloride sensor

Abstract

Characterization of the Ag/AgCl electrode is a necessary step towards its application as a chloride sensor in a highly alkaline medium, such as concrete. The nucleation and growth of AgCl on Ag in 0.1 M HCl was verified by cyclic voltammetry. Ag anodization was performed at current densities, determined by potentiodynamic polarization in the same (0.1 M HCl) medium. The morphology and microstructure of the AgCl layers were evaluated via electron microscopy, while surface chemistry was studied by energy dispersive spectroscopy (EDS) and X-ray photoelectron spectroscopy (XPS). At a current density above 2 mA/cm^2, the thickness and ionic resistivity of the AgCl layer increased. In this condition, small AgCl particles formed in the immediate vicinity of the Ag substrate, subsequently weakening the bond strength of the Ag/AgCl interface. During production of the sensor, silver oxide-based or carbon-based impurities were formed on the sensor surface in amounts proportional to the thickness as well as the morphology and microstructure of the AgCl layer.

It is concluded that a well-defined link exists between the properties of the AgCl layer, the applied current density and the recorded overpotential during Ag anodization. The results can be used as a recommendation for preparation of chloride sensors with stable performance in cementitious materials.

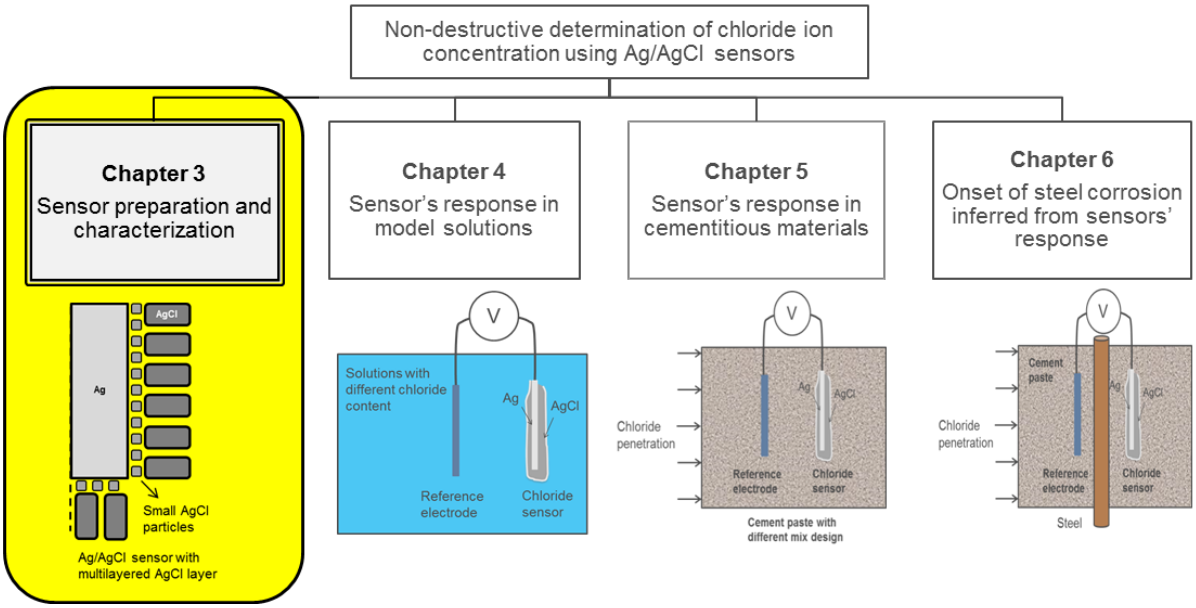

Structure of research process and sequence of chapters in the thesis.

This Chapter 3 is based on the paper:

Pargar, F., Kolev, H., Koleva, D. A. & van Breugel, K.. (2018). Microstructure, surface chemistry and altered response of Ag|AgCl sensors in alkaline media, Journal of Materials Science, Vol. 53(10), p. 7527–7550 .

3.1 Introduction

The thermodynamic considerations and the kinetics of AgCl formation on a Ag substrate were subject to numerous works in the fields of electrochemistry and crystal growth since the early 1950s [Lal et al., 1951; Katan and Bennion, 1976; Burstein and Misra, 1983; Beck et al., 1984; Jaya et al., 1987; Birss and Smith, 1987; Jin et al., 2003]. Despite the results in these thoroughly elaborated works, the properties and performance of Ag/AgCl electrodes in an alkaline medium are yet to be affirmed, especially in view of their application as chloride sensors for reinforced concrete structures. One of the reasons for a limited number of reports on the correlation between the properties of the AgCl layer and the response of the sensor in alkaline medium is related to unsuccessful attempts of observing the inner morphology of the AgCl layer. For instance, as reported in [Jin et al., 2003; Bozzini et al., 2007; Ha and Payer, 2011]: microscopic observations of the Ag/AgCl interface was problematic. The attempts to stiffen the sample by Cu and Ni–P plating or liquid N_2 (low temperature of approx. -190°C) was not successful, since the soft AgCl particles spread over the entire surface of the samples and mask the interface. Sample preparation to address the above challenges is discussed in this chapter and is part of in-depth investigation of the Ag/AgCl sensors' performance in alkaline medium.

Different techniques are available for the AgCl formation on a Ag substrate [Polk et al., 2006]. One of the most frequently used methods is anodization of Ag in a HCl solution [Climent-Llorca et al., 1996; Vera et al., 2000; Atkins et al., 2001; Montemor et al., 2006; Duffo et al., 2009; Jin et al., 2017]. The Ag/AgCl sensor preparation by Ag anodization in HCl solution is schematically shown in Fig. 3.1. The low pH of a HCl solution (Fig. 3.1a) would limit the possible Ag_2O formation [Stoica et al., 2011; Brewer et al., 2015] and would result in AgCl formation on the Ag substrate (Fig. 3.1b). A layer of AgCl with sufficient thickness was considered to be of ca. tens of the micrometer range [Ha and Payer, 2011]. With anodization, the rate of AgCl formation depends on the applied current density and the time of the anodization (Fig. 3.1b) [Briggs and Thirsk, 1952; Suzuki et al., 1998]. Different current density and anodizing time have been reported for the preparation of sensors, e.g. 0.4 mA/cm^2 for 30 minutes [Climent-Llorca et al., 1996; Atkins et al., 2001], 2 mA/cm^2 for 30 minutes [Montemor et al., 2006], 0.2 mA/cm^2 for 1h [Jin et al., 2017], 0.4 mA/cm^2 for 2h [Gao et al., 2011]. Logically, as with each electrochemical process of this kind, the anodization regime will affect the produced layer thickness, surface morphology and ionic/electron conductivity, respectively (Fig. 3.1c) [Lal et al., 1951; Birss and Smith, 1987]. These features of the AgCl layer may subsequently be reflected in the electrochemical response of the sensor, especially in alkaline medium. Considering the aforementioned, the focus of this chapter is to characterize the Ag/AgCl sensors, produced at various anodization regimes, and link the current density levels during Ag anodization to the AgCl properties and microstructure. The importance of this correlation is in view of the research question: how different morphology, microstructure and composition of the AgCl layer affect the accuracy of a chloride sensor and determination of the chloride content in a relevant medium.

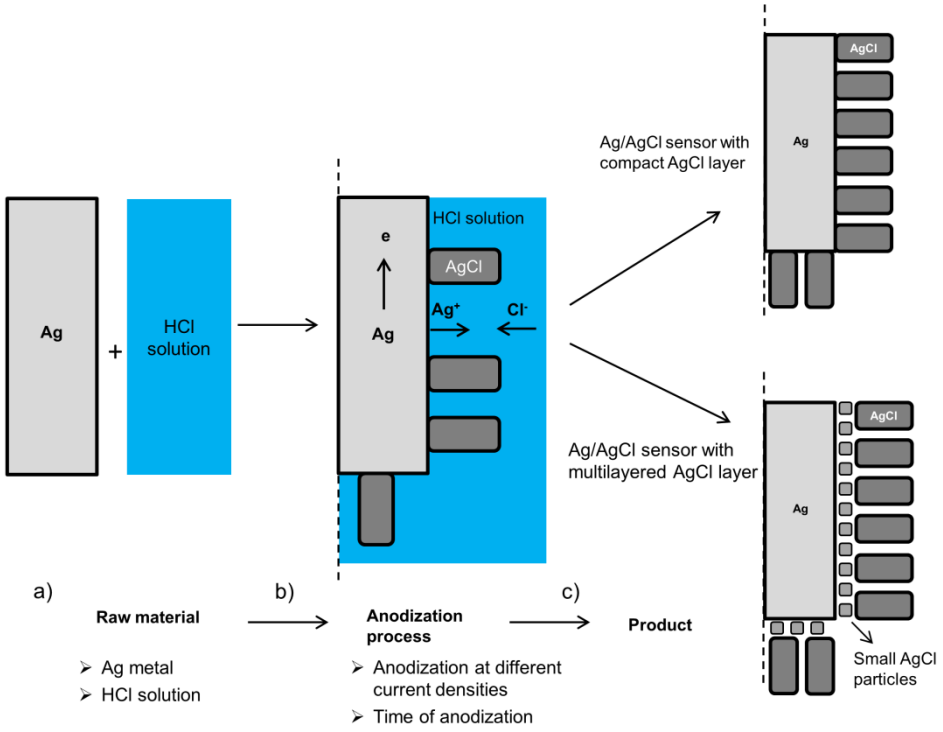

Figure 3.1: Schematic representation of chloride sensor preparation.

3.2 Experimental materials, methods and technical background

3.2.1 Electrochemical tests on Ag in 0.1 M HCl solution

Linear sweep cyclic voltammetry (CV) and potentio-dynamic polarization (PDP) were employed as screening techniques to derive information about AgCl formation on the Ag substrate. Ag wires of 99.5% purity, 1 mm diameter, were supplied by Salomon's Metalen B.V. Netherlands. The CV and PDP tests were carried out in 0.1 M HCl solution (pH~1.4) in a conventional three-electrode cell arrangement, where the Ag wire (1 cm length) was the working electrode, a Pt mesh was the counter electrode and a saturated calomel electrode (SCE) was the reference electrode. The CV scans were performed from -400 mV to +150 mV (versus OCP) at a scan rate of 100 mV/s with the aim to verify AgCl nucleation and growth in the chosen medium. PDP was performed in the range of −200 mV to +1600 mV versus OCP at a scan rate of 0.5 mV/s. The PDP test results determined the range of current densities, potentially suitable for anodizing Ag in the chosen medium. A PGSTAT 302N potentiostat (Metrohm Autolab B.V., The Netherlands) was used for all electrochemical tests.

3.2.2 Ag anodization - preparation of Ag/AgCl sensors

The Ag wires were cleaned for two hours in concentrated ammonia, then immersed in demineralized water overnight, prior to anodization in 0.1 M HCl solution. Anodization was carried out for equal time duration of 1h, but at four different current density levels, i.e. 0.5 mA/cm^2 (regime A), 1 mA/cm^2 (regime B), 2 mA/cm^2 (regime C) and 4 mA/cm^2 (regime D). A regime of maximum current density (4 mA/cm^2) but varying anodization time from 900s to 1h, was also considered as a supportive investigation, results of which are presented as additional information in Annex A of this thesis.

The experimental setup and instrumentation for sensor preparation were identical to the one for the CV and PDP tests. The current regimes were chosen based on the PDP screening test as specified in Section 3.2.1. The thickness of the AgCl layer was both experimentally determined (Section 3.2.3) and theoretically approximated by employing Eq. 3.1, which essentially is a modification of the Faraday's law:

$$X = \frac{i.M.t}{F.d} \tag{3.1}$$

where X is the thickness of the AgCl layer (cm); i is the applied current density (A/cm^2); M is the molecular weight of AgCl, 143.5 g/mol; t is the duration of anodization; F is the Faraday's constant (F=96500 C/mol/equiv); d is the density of the AgCl layer, 5.56 g/cm^3. The theoretical approximation of a AgCl layer after Ag anodization is also reported in the literature [Lal et al., 1951].

3.2.3 Morphology, microstructure and surface chemistry of the AgCl layer

The following procedure sequence (Fig. 3.2) was employed prior to microscopic observations of the Ag/AgCl interface: i) a portion of the Ag wire was narrowed prior to anodization; ii) the narrowed portion was stretched from the two sides of the notch; iii) this allowed investigation of a "cross section", i.e. the parallel growth of the AgCl layer on the Ag substrate.

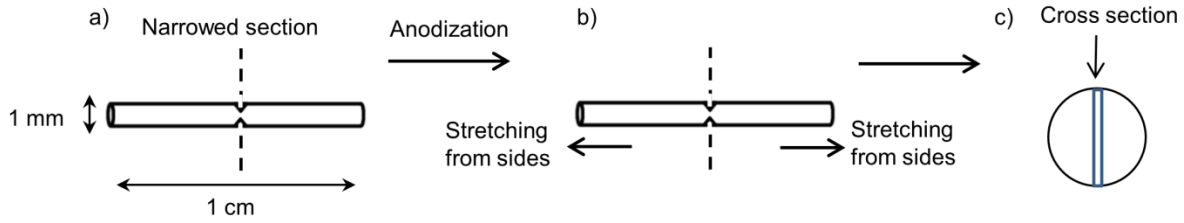

Figure 3.2: Procedure sequence for the preparation of a cross section of the Ag/AgCl sensor: a) narrowing the Ag wire before anodization; b) stretching from both sides after anodization; c) as prepared cross section for ESEM observations.

The obtained cross section resembled a fracture surface. This enabled the inner morphology of the AgCl layer to be well observed. This procedure and sequence were specifically chosen for clear differentiation of the AgCl layers' formation on identically handled Ag substrates, but in conditions of different anodization regime (various current density, Section 3.2.2). This approach was chosen as the only suitable one to address the objectives of this work and to overcome the challenges with Ag/AgCl sample preparation for microscopy purposes, as specifically outlined in the introduction section.

The AgCl layers were analyzed, using Environmental Scanning Electron Microscopy (ESEM), Philips-XL30 equipped with an energy dispersive spectrometer (EDS). The samples were examined under accelerating voltage of 20 kV in high vacuum mode. Surface chemistry was evaluated by X-ray photoelectron spectroscopy (XPS). The measurements were taken using an ESCALAB MkII (VG Scientific) electron spectrometer at a base pressure in the analysis chamber of 5×10^{-10} mbar using twin anode MgKα/AlKα X-ray source with excitation energies of 1253.6 and 1486.6 eV, respectively. The XPS spectra were recorded at the total instrumental resolution (as it was measured with the FWHM of Ag3d5/2 photoelectron line)

of 1.06eV and 1.18eV for MgKα and AlKα excitation sources. The processing of the measured spectra included a subtraction of X-ray satellites and Shirley-type background [Shirley, 1972]. The peak positions and peak areas were evaluated by a symmetrical Gaussian-Lorentzian curve fitting. The relative concentrations of various chemical species were determined by normalization of the peak areas to their photoionization cross sections, calculated by Scofield [Scofield, 1976].

3.3 Results and discussion

3.3.1 AgCl nucleation and growth

When a phase nucleation on a metal surface is involved (as AgCl on Ag), the CV curve (Fig. 3.3) will reflect a number of characteristic features: i) an enhanced anodic and cathodic peak currents, in contrast to the generally observed narrow response for a general mass transport controlled CV; ii) a characteristic cross-over in the reverse branch of the CV scan will be observed (Fig. 3.3, point at E = 40 mV); along with iii) the presence of a current maxima in the reversed scan (peak C2 in Fig. 3.3), caused by the phase nucleation in the forward scan.

The theory and observable characteristic features in a CV scan were formulated for both interfacial and diffusion control of the crystal growth kinetics [Fletcher et al., 1983] and are well seen in Fig. 3.3. These characteristic features are: the hysteresis loop, forming in the reverse scan of the recorded CV for Ag in 0.1 M HCl solution, the cross-over point at ca. 40 mV and the peak C2, which all define the nucleation of AgCl on the Ag substrate. Next, the cross-over point remains constant with subsequent scans (Fig. 3.3, inlet), which proves an interfacial control of the AgCl growth kinetics.

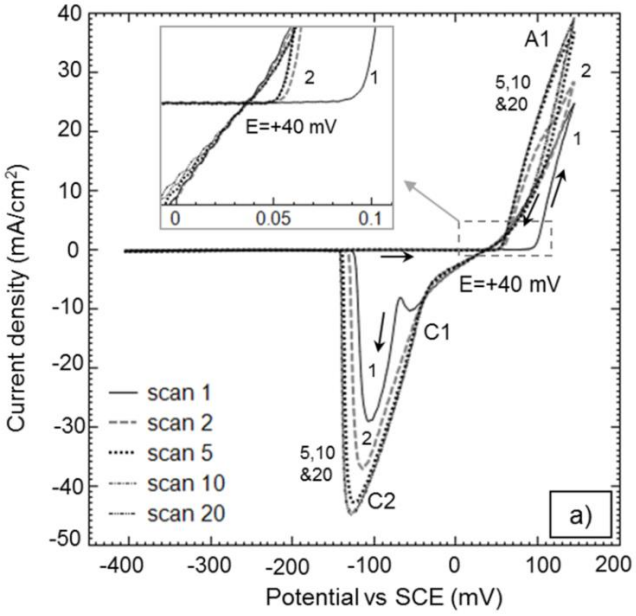

Figure 3.3: An overlay of the 1st, 2nd, 5th, 10th and 20th CV scan for Ag in 0.1 M HCl solution.

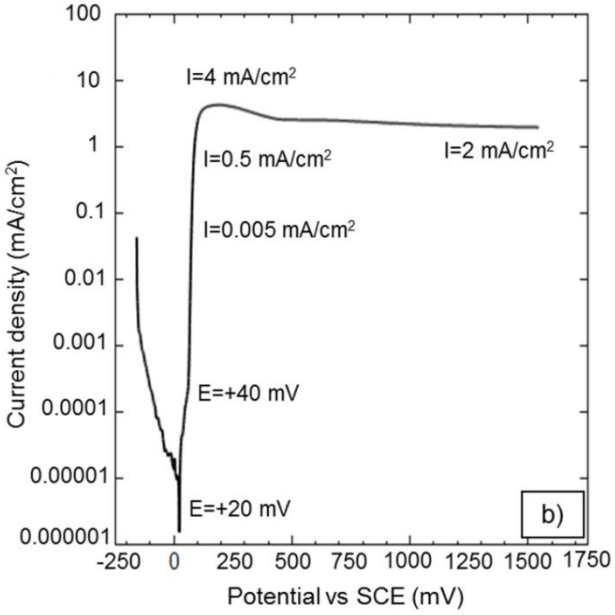

Figure 3.4: Potentio-dynamic polarization curve for Ag in 0.1 M HCl solution.

The cathodic peak C1 (-55 mV), was recorded only in the 1st scan and can be associated with: i) the very first stage of deposition (initiation) of AgCl nuclei [Birss and Smith, 1987]; ii) the increased Ag^+ concentration, following the first anodic current increase [Boxall et al., 1974]; iii) the contribution of an initially smaller size AgCl nuclei on the Ag substrate. Similar variation in cathodic peaks potential and currents within AgCl formation on a Ag substrate was reported in all scans and linked to the contribution of large (e.g. peak C2) or smaller (e.g. peak C1) AgCl nuclei [Birss and Smith, 1987]. The mechanism here is obviously different, since a re-occurrence of the peak C1 with subsequent scans was not recorded (Fig. 3.3).

With scanning, both anodic and cathodic peak currents initially increased, Fig. 3.3), as expected, while the cross-over point remained at the same current-potential location, irrespective of the scan number (Fig. 3.3 and inlet). A constancy of the cross-over point would mean the formation of crystals of a large size, while in contrast, a cathodic shift of this point would be denoted to diffusion-controlled crystal growth and will also imply a decreasing crystal size [Fletcher et al., 1983]. A cathodic shift of the cross-over point (Fig. 3.3) was not observed. Therefore, the peak C1 most likely reflects an increased Ag^+ concentration during the initial Ag dissolution, followed by initiation of AgCl nuclei formation.

The interfacial controlled crystal growth of AgCl nuclei of sufficiently large size is reflected by the shape of the CVs with subsequent scans, where stabilization in both anodic and cathodic currents was observed between the 5th and 20th cycles (Fig. 3.3), attributable to the coverage of the Ag substrate by a AgCl layer. The actual morphology and microstructure of AgCl, grown on the Ag substrate, will be discussed in detail in Section 3.3.2.

The PDP test (Fig. 3.4) was performed to determine the range of suitable current densities for AgCl formation. At potentials more noble than the corrosion potential (E_{corr} = 20mV vs. SCE), the PDP curve shows a sharp increase in anodic current, Fig. 3.4. This increase in current with anodic polarization was almost potential independent until ca. 150 mV, corresponding to an anodic current maximum of 4 mA/cm^2.

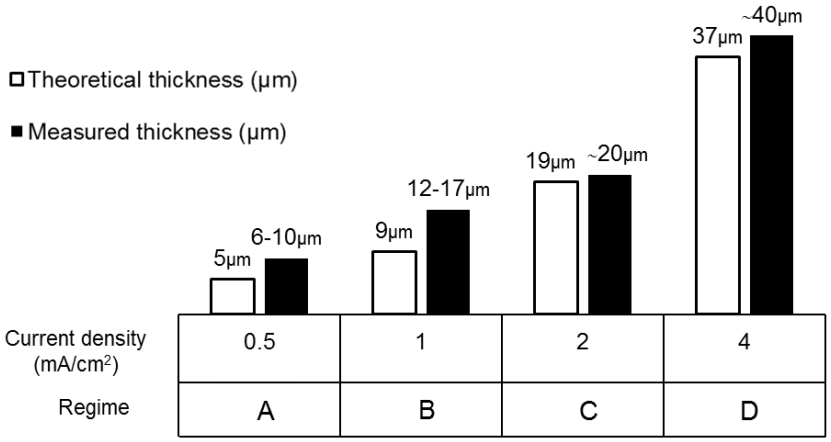

Figure 3.5: One-hour anodization regimes used for sensor preparation and AgCl layer thickness.

Stabilization followed after this point and independence of current from potential with further polarization was observed. At potential values more anodic than 300 mV, a limitation of anodic current was relevant with a current stabilization at approx. 2 mA/cm^2. This limitation in the current density can be interpreted as a coverage of the Ag surface by a AgCl layer. Based on the PDP test result (Fig. 3.4), the current density range for AgCl layer formation is between ca. 0.05 mA/cm^2 and 4 mA/cm^2, with 4 mA/cm^2 as a maximum and 0.5 mA/cm^2 to 2 mA/cm^2 as an average range, where the Ag substrate is supposedly uniformly covered by AgCl. Therefore, for the Ag anodization process in 0.1 M HCl and Ag/AgCl sensor preparation, respectively, four current densities in the range of 0.5 mA/cm^2 to 4 mA/cm^2 were employed for 1 hour and represented by regimes A to D, summarized in Fig. 3.5. The current densities of 2 mA/cm^2 and 4 mA/cm^2 can be referred to as high current densities, while 0.5 mA/cm^2 and 1 mA/cm^2 are considered as average to low current densities.

The anodization regimes A to D in Fig. 3.5, are from this point forward used as sensors' designation, i.e. sensors A, B, C and D are discussed in the following sections. Figure 3.5 also gives the theoretically approximated thickness of the AgCl layer in each regime, together with the experimentally derived one. The former was calculated using the previously introduced Eq. 3.1, the latter is subject to discussion in Section 3.3.2.

3.3.2 Surface morphology and microstructure of the AgCl layer

Figure 3.6 depicts ESEM micrographs from the top surface of the sensors, visualizing the AgCl layers, as obtained in each anodization regime. As can be observed, the morphological features and packing of the AgCl layer are different in each case. For sensors A and B (Figs. 3.6a,b), "packed-piled" AgCl particles were well observed on the Ag substrate. Additionally, the AgCl layer appears to be relatively uniform, presenting rounded shape AgCl particles, 1 to 2 µm in surface size, and distinct boundary between these particles. Along with clearly observable boundaries, specifically for sensor A (Fig. 3.6a), well-defined are the surface openings of micro-channels. Although these features for sensor B (Fig. 3.6b) became slightly distorted, the surface morphology was still similar to that of sensor A.

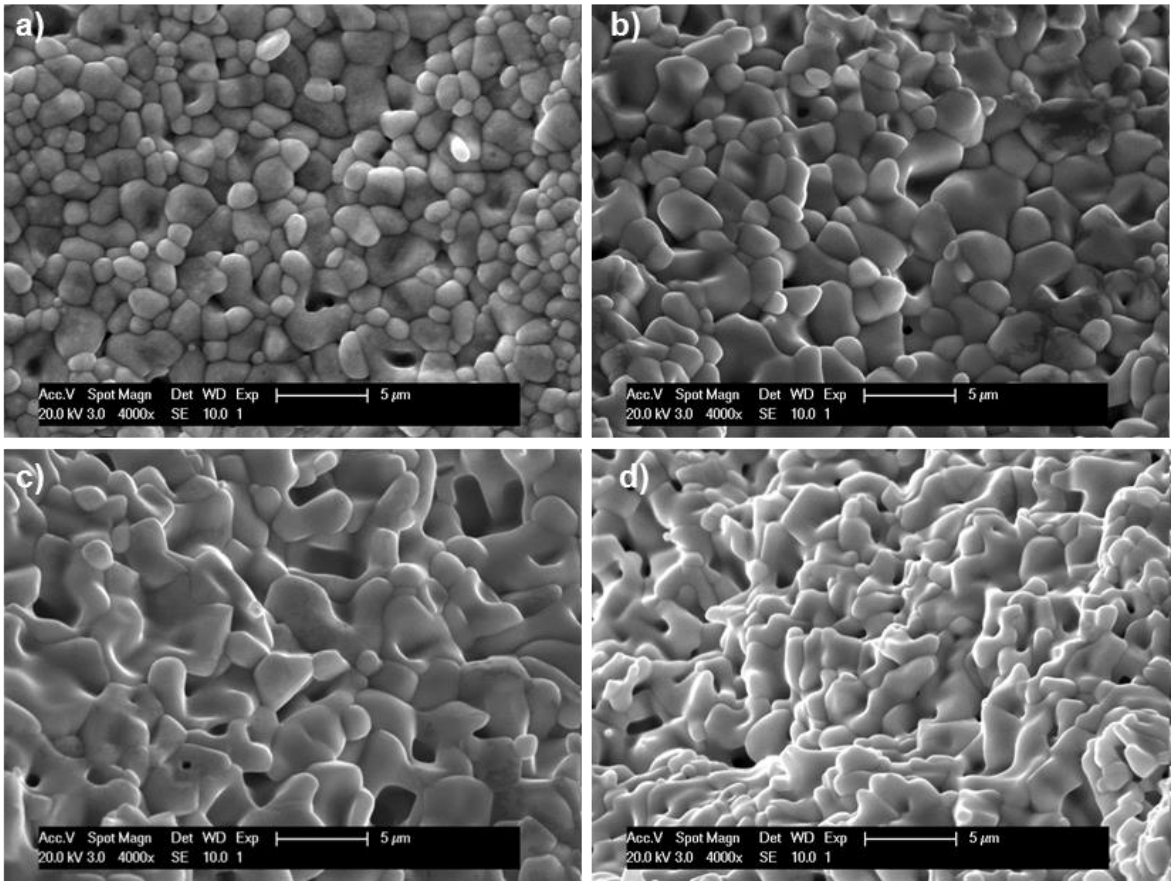

Figure 3.6: ESEM images of the AgCl layer on the surface of (a) sensor A at 0.5 mA/cm^2, (b) sensor B at 1 mA/cm^2, (c) sensor C at 2 mA/cm^2 and (d) sensor D at 4 mA/cm^2.

In contrast, the AgCl layer for sensors C and D became a mosaic of complex patterns (Figs. 3.6c,d). The high current densities, as employed for 1h in the production of sensors C and D (2 mA/cm^2 and 4 mA/cm^2), apparently induced the formation of elongated and discontinuous, "twisted" AgCl particles.

The "inner" microstructure of the AgCl layer cannot be judged from surface observations only, but can be clearly visualized on a cross section of the Ag/AgCl interface. Figure 3.7 presents the cross sections for sensors A and D, together with relevant EDS analysis in depth of the sections, towards the Ag substrate (the results for sensors A and B were similar, as well as for sensors C and D, micrographs of the cross section for B and C sensors are, therefore, not presented). The EDS analysis (in Fig. 3.7) of the cross section of the AgCl layer of sensors A and D depicts the presence of Ag and Cl in this layer, while only Ag for the Ag substrate. This is the expected qualitative outcome for a Ag/AgCl interface.

For sensor A, Fig. 3.7a, a well-adhered and homogeneous AgCl layer on the silver substrate can be observed. The grain boundaries in depth of the layer can be well seen, showing a well-packed and almost perpendicular orientation towards the Ag substrate. This upright particles' orientation would account for lower tortuosity of the micro-channel network in depth of the layer. The contribution of such a morphology and microstructure to the performance of the sensor would be reflected in a rapid response to the environment. This is because (vertically) open micro-channels would facilitate the ion transport in the AgCl layer. These microstructural features versus the ohmic (incl. ionic) resistance of the AgCl layer will be discussed in Section 3.3.4.

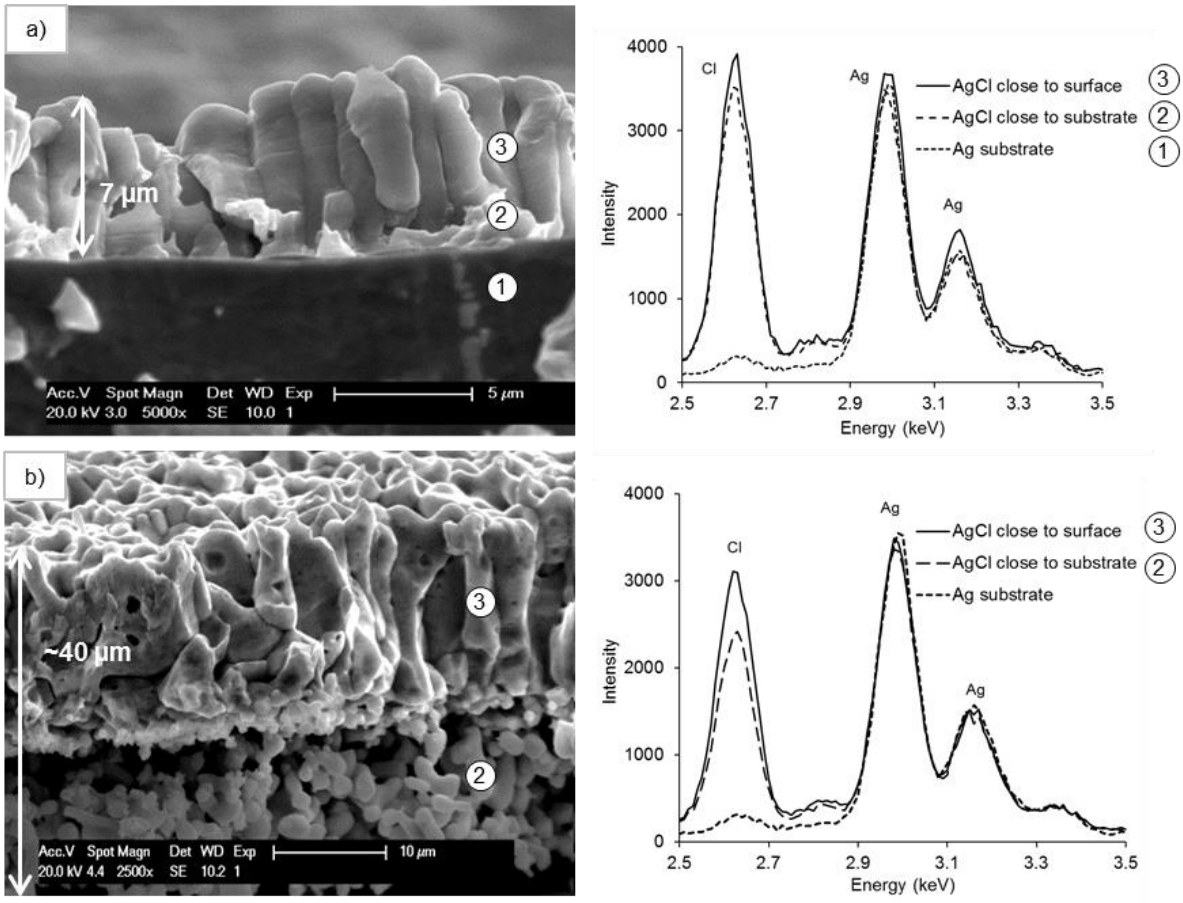

Figure 3.7: Cross section and EDS spectra of the Ag/AgCl interface in (a) sensor A at 0.5 mA/cm^2 and (b) sensor D at 4 mA/cm^2.

Note: Ag substrate in Fig. 3.7b is not seen at this 2500x magnification, which is chosen to allow visibility of the bi-layer structure in sensor D, together with the full AgCl layer thickness.

As shown in Fig. 3.7, increasing the current density from 0.5 mA/cm^2 (sensor A, Fig. 3.7a) to 4 mA/cm^2 (sensor D, Fig. 3.7b) results in a thicker AgCl layer. The experimentally determined AgCl thickness for each sensor was well in line with the theoretically approximated value (from Faraday's law, Eq. 3.1) (Fig. 3.5). The higher current density increased the thickness of the AgCl layer and resulted in the formation of an additional inner-layer of smaller AgCl grains close to the Ag substrate (Fig. 3.7b). For sensor D, Fig. 3.7b, a bi-layer appearance is obvious with an increased level of tortuosity, visually not as uniform and well adhered to the Ag substrate, as in sensor A (Fig. 3.7a). What can also be observed are a large number of occluded pores in the top (surface) portion of the AgCl layer (Fig. 3.7b). The small AgCl grains can also be found randomly in the bulk top layer (Fig. 3.6d). These features together with the "twisted" morphology of the ca. 20 µm top (surface) portion would account for an increased ohmic and ionic resistances of the total (40 µm-thick) AgCl layer. Additionally, an increased tortuosity of the micro-channel network would be relevant. All these features limit the ions transport in the AgCl layer which would affect the sensor's performance in cementitious materials. The reproducibility and stability of the sensors' OCP in different solutions are discussed in detail in Chapter 4.

Next to the above, the appearance of the small AgCl grains close to the Ag substrate in sensor D resembles the morphological features of the AgCl layer after reduction cycles [Jin et

al., 2003]. This indicates the possibility of altered AgCl layer formation and reduction on the surface of the sensor D due to the high current density during anodization. The appearance of an inner layer of small AgCl grains, with open inter-grain pore spaces, can be an indication of weak adhesion of the AgCl layer to the Ag substrate. This is important because the layer of smaller (AgCl) grains accounts for ca. 50% of the total thickness of AgCl layer on the surface of D sensor (Fig. 3.7b).

The microscopy studies showed that 1h anodization of Ag wire at the highest current density regime (sensor D) causes a high level of complexity, variation in morphological features and a distinct bi-layer structure of AgCl on the Ag substrate. Hence, it is possible that a different mechanism is responsible for the AgCl formation at high current densities. Annex A contains more evidence for the properties of the AgCl layer, produced at high current density levels and varying anodization time. The morphology and microstructure of the AgCl layers are further discussed in Section 3.3.4.1 with respect to the ohmic resistance of the AgCl layer and the actual charge during anodization.

3.3.3 Surface chemistry and composition of the AgCl layer

The XPS analysis on the sensor's surface provides information about the surface composition. The test results confirm AgCl formation and also give information about possible impurities. The recorded XPS survey-scans for sensors A (0.5 mA/cm^2 regime) and D (4 mA/cm^2 regime) with lowest and highest thickness of the AgCl layer are depicted in Fig. 3.8. The survey-scans show dominant peaks for Ag3p, Ag3d and Cl2p, along with peaks for oxygen (O1s) and carbon (C1s) impurities. The peaks of the relevant elements have different intensities for sensors A and D (Fig. 3.8). While the presence of Ag and Cl was as expected, the presence of oxygen and carbon can be denoted as contamination or impurities. The adsorption of substances (oxygen and carbon), during anodization, from the environment at the sensor's surface was larger for the thicker AgCl layer (i.e. sensor D). This is evident by the significantly higher peaks for C1s and O1s for sensor D, if compared to sensor A (Fig. 3.8). In other words, the presence of O_2, CO_2 and humidity in the environment affects more significantly the composition of sensors with a thicker AgCl layer. The higher amount of impurities in a thicker AgCl layer would also be related to the bi-layer structure of the AgCl (as observed, Fig. 3.6), that results in a larger "active" surface area for adsorption of impurities.

Additionally, it is possible that adsorption of impurities occurred in depth of the AgCl layers, but this cannot be judged from XPS surface analysis only. The results, however, clearly support the adsorption of impurities in the thicker AgCl layers. The possible effect of surface morphology and composition of AgCl layer on chloride content determination (i.e. sensors' response) will be discussed in Chapter 4.

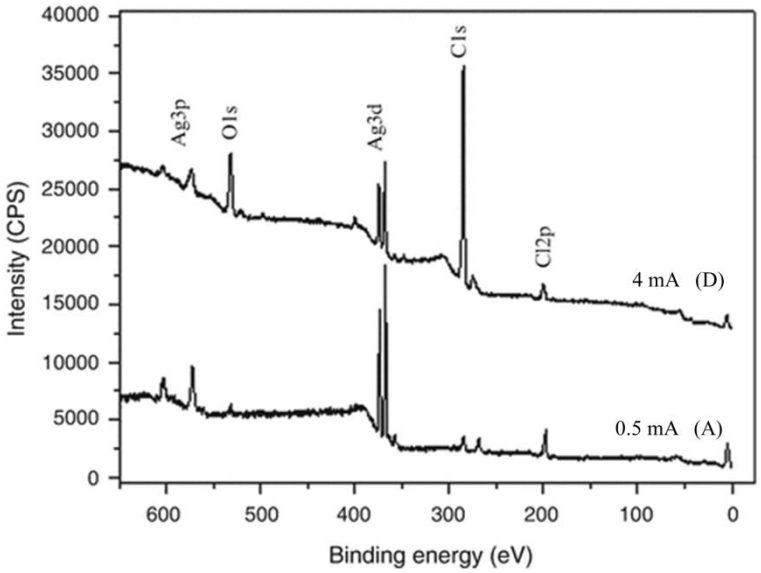

Figure 3.8: Survey XPS spectra for sensors A at 0.5 mA/cm^2 and sensor D at 4 mA/cm^2.

To this end, the increasing thickness, roughness and bi-layer structure of the AgCl for the cases of B, C and D sensors (as observed, Fig. 3.6) would account for a more pronounced adsorption of impurities (as recorded, Fig. 3.8), if compared to the case of A sensors. The surface XPS analysis of sensors A to D, including the high-resolution Ag3d, O1s and AgMNN Auger spectra are presented in Annex B.

3.3.4 Sensors' surface properties and ohmic resistance of the AgCl layer

As discussed in the previous sections, the process of Ag anodization involved the application of a constant current at a chosen current density level. In the medium of 0.1 M HCl, this results in the formation of a AgCl layer with a certain thickness, morphology and compactness. Figure 3.9 schematically presents a AgCl layer, formed on the surface of a Ag wire. The boundaries between the AgCl particles and the pore channels through the layer, known as micro-channels, are also indicated. These micro-channels are the main pathways for the transport of ions within the AgCl layer [Gu and Bennio, 1977; Pemberton and Girand, 1987] and develop differently at different anodization regime (Fig. 3.7). As the AgCl layer thickens, ion transport becomes limited due to microchannels confinement. This will be reflected by changes in the electrochemical response of the Ag/AgCl interface during anodization, and will be recorded as overpotential changes. In other words, while the applied current is maintained constant, the potential will reflect the above limitations and the electrochemical interface will respond by an increase in overpotential.

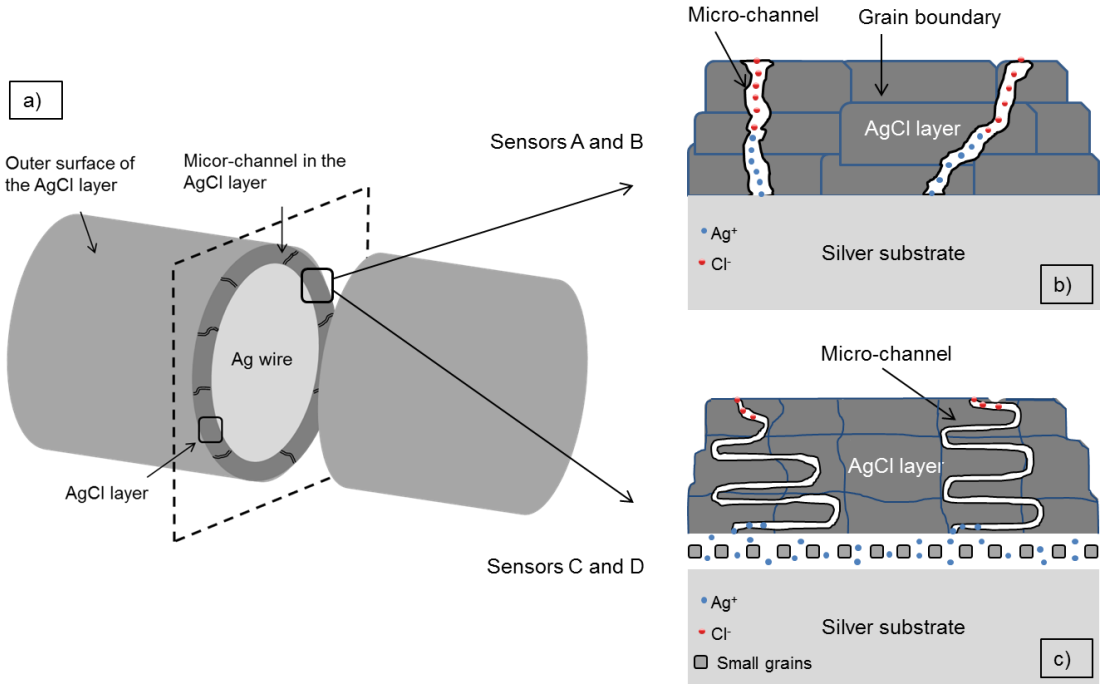

Figure 3.9: Schematic of a Ag/AgCl sensor: a) AgCl layer on the surface of a Ag wire; b) AgCl layer as produced at lower current density regimes of 0.5 and 1 mA/cm^2 (sensors A and B); and c) AgCl layer as produced at higher current density regimes of 2 and 4 mA/cm^2 (sensors C and D).

Fig. 3.10 depicts the experimentally derived overpotential increase during 1h anodization in the previously discussed regimes A, B, C and D (Fig. 3.5), i.e. during the production of sensors A to D, respectively. Figure 3.11 presents the relation of overpotential increase versus the actual charge density during anodization for all sensors. Both potential versus time (Fig. 3.10) and potential versus charge (Fig. 3.11) curves provide information, linked to the physical properties of the AgCl layer during anodization and are related to the layers' formation, possible re-structuring, surface roughness and/or limitations to further growth. The inflection points in the curves indicate the point(s) of AgCl layer alterations during anodization. Consequently, a linear relationship, as in regimes A and B (Fig. 3.10), accounts for a uniform and continuous AgCl formation – as in fact observed for sensors A and B. The overpotential response for the low current density regimes A and B is well in line with the actual morphological, microstructural and surface chemistry results (Sections 3.3.2 and 3.3.3).

A semi-linear relationship, as in regime C (non-linearity between 900s and 1200s, Fig. 3.10), indicates re-structuring and increased tortuosity of the layer. This is in line with the surface analysis for sensor C, resembling features and surface chemistry close to these for sensor D. The most significant non-linear response in Fig. 3.10 was for regime D with highest level of tortuosity of the AgCl layer, the presence of small AgCl grains close to the silver substrate and inter-grain voids and cavities in the layer (Figs. 3.6d, 3.7b, 3.9c).

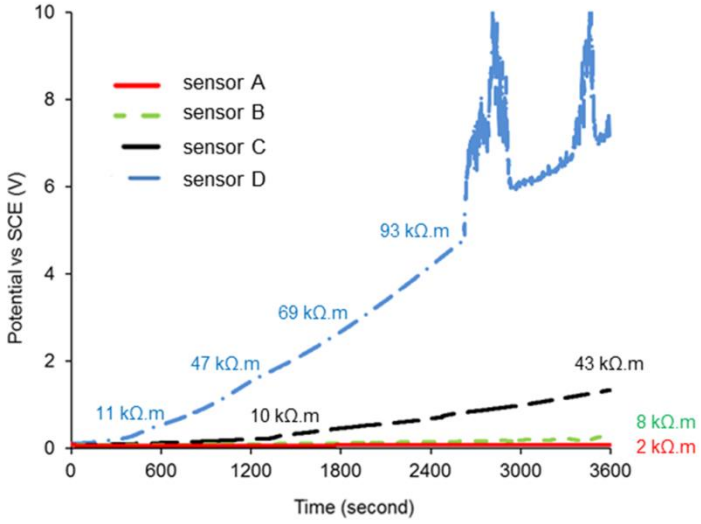

Figure 3.10: Overpotential vs. time during anodic formation of AgCl on a Ag wire in 0.1 M HCl in different current density regimes of 0.5 mA/cm^2 (sensor A), 1 mA/cm^2 (sensor B), 2 mA/cm^2 (sensor AC) and 4 mA/cm^2 (sensor D).

3.3.4.1 Overpotentials in high current densities regimes – sensors D

As can be seen in both Figs. 3.10 and 3.11, the nonlinear response of sensor D can be segmented as follows: an increase in overpotential was recorded starting after ca. 300s, significantly more pronounced after 900s (Fig. 3.11); followed by further increase after 1500s and an abrupt rise of overpotential after 2500s, together with intensive fluctuations at the end of the test. At values above 4.5V, the overpotential for regime D showed an abnormal fluctuation, related to passivation-like behavior or significant increase in surface roughness.

Such fluctuations (erratic polarization response), as in the 4 mA/cm^2 regime for sensor D, were reported to result in evolution of oxygen and chlorine on the surface of the substrate [Katan and Bennion, 1976], which would (at the very least) cause surface heterogeneity and change in surface chemistry. The surface heterogeneity was reflected in a "twisted" AgCl layer morphology (Fig. 3.6d), and a bi-layer structure of the AgCl on the Ag surface (Figs. 3.7b and 3.9c). The change in surface chemistry was reflected in a more significant contribution of AgO and Ag-C-H-O-based compounds to the AgCl layer of sensors D, as derived by XPS analysis (Fig. 3.8).

In fact, well known is that high overpotential and oxygen evolution will be relevant during anodization at high current densities (as in the case of sensor D, Figs. 3.10, 3.11). The result for the metal electrode (Ag in this case) is a non-stable and non-reproducible potential. This is in addition to the fact that an anodic oxygen evolution in low pH medium can only occur at potentials significantly more positive than 1.299V. Additionally, at significantly positive potentials (Figs. 3.10, 3.11) the metal surface will be electrochemically altered, e.g. enhanced dissolution of the substrate or passivation will be relevant. In both cases, a substantial surface modification of the original metal substrate will be at hand. The above considerations and electrochemical aspects/phenomena are directly applicable to the sensor D, where surface modification and overpotential evolution during the anodization process were observed (Fig. 3.11). The microstructural studies and surface chemistry analysis confirmed the electrochemically induced change in the AgCl layer of sensor D. This might affect the performance of the sensor D in the model medium (presented in the next Chapter 4).

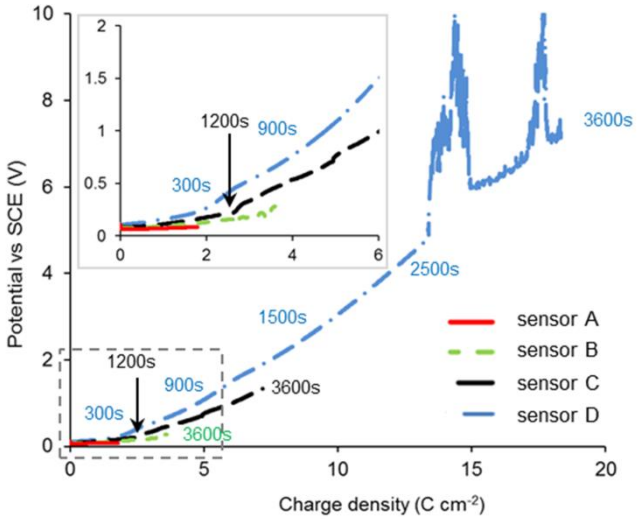

Figure 3.11: Overpotential vs. charge density during anodic formation of AgCl on a Ag wire in 0.1 M HCl in different current density regimes of 0.5 mA/cm^2 (sensor A), 1 mA/cm^2 (sensor B), 2 mA/cm^2 (sensor C) and 4 mA/cm^2 (sensor D).

3.3.4.2 Surface chemistry, microstructure and ohmic resistance of the AgCl layer

Except the above-discussed aspects about overpotential and surface of the sensors, abnormal overpotential evolution (as recorded for sensor D, Fig. 3.11) would be attributable to an increase in thickness and ohmic resistance of the surface layer [Beck and Rice, 1987]. The ohmic resistance, however, is a combination of both ionic and electron resistance. In the case of a Ag/AgCl interface, where the AgCl layer contains non-conductive solid AgCl particles, the effective conductivity of the surface (AgCl) layer depends on the presence of micro-channels (as schematically shown in Figs. 3.9b,c and the resulting ionic conductivity). In other words, the ionic resistance (and ionic conductance respectively) of the AgCl layer will be a dominating factor for ion transport, surface changes and ultimately the sensor's response in the model medium.

The ionic resistance (resistivity respectively) of the AgCl layer during anodization can be analytically derived by employing the results in Fig. 3.11 and Eq. 3.2. The linear increase in overpotential (ΔE) with charge density (ΔQ) is presented as follows, [Jin et al., 2003]:

$$\frac{\Delta E}{\Delta Q} = \rho J V_0 / F \qquad (3.2)$$

where ρ is the ionic resistivity, J is the current density, V_0 is the molar volume of the AgCl (25.8 cm^3 mol^{-1}) and F is the Faraday constant (96485.33 s A/mol).

To determine the ionic resistivity, a linear regression of the potential vs. charge curves in Fig. 3.11 was performed with an accuracy for the A and B sensors of R^2>0.99. For sensors C and D, a non-linear relation was recorded. Hence, the curves in Fig. 3.11 were segmented into linear portions with R^2>0.99 for each portion.

Table 3.1: Ionic resistivity of the AgCl layer at different current densities and anodization time.

Regime	Current density (mA/cm^2)	Measured thickness (μm)	Anodization time (s)	Charge density ($C.cm^{-2}$)	Ionic resistivity (kΩ.m)
A	0.5	6~10	0-3600	< 1.8	2
B	1	12~17	0-3600	< 3.6	8
C	2	–	0-1200	< 2.4	10
		~20	1200-3600	2.4-7.2	43
D	4	–	0-300	< 1.6	11
		~10	300-900	1.6-4.8	47
		~15	900-1500	4.8-8.6	69
		~30	1500-2500	8.6-13	93
		~40	2500-3600	N/A	N/A

Table 3.1 presents the measured thickness of the AgCl layer of sensor D (Figs. 3.7b and 3.9c), together with the calculated ionic resistivity per linear segment of the response in Fig. 3.11. As shown, the increase of the thickness of the AgCl layer is not proportional to the increase in ionic resistivity. For instance, if the rapid increase to ca. 70 kΩ.m upon thickness increase to 15 μm (Table 3.1) is considered, a layer thickness of 30 μm (after 2500 s anodization) would be expected to present an ionic resistivity in the range of 140 kΩ.m instead of the recorded 93 kΩ.m. This non-proportionality is attributable to: the actual morphology and microstructure of the AgCl layer in sensors D; the possibly high tortuosity of the micro-channel network (Fig. 3.9c); the occluded pores and the gaps and voids in the bi-layer structure (Figs. 3.7b, 3.9c). These features account for a limited ion transport, reflected by the increased ionic resistivity of the AgCl layer in sensor D.

3.3.4.3 Intrinsic and extrinsic conductivity of the AgCl layer

In conditions where the transport of ions in the AgCl layer is limited, due to concentration and/or resistance polarization (as in sensor D, schematically shown in Fig. 3.9c), the rate of overpotential increase (Fig. 3.11) is controlled by two processes: (i) migration/diffusion of Ag^+ ions away from the Ag substrate into the bulk solution and, conversely, (ii) chloride ions from the bulk solution towards the Ag substrate (Fig. 3.9c). The continuous formation of AgCl blocks the micro-channels, and decreases their radii with time. Eventually, the blockage and reduced number of micro-channels will increase the tortuosity and the transport distance of ions within the layer. At this stage, a sequence of incipient "crack" formation and "healing" of the already available cracks occurs [Beck and Rice, 1987]. The cracks are actually a slight broadening of the micro-channels, already existing in the layer. In this case, the AgCl growth follows the so-called low field conduction mechanism [Ha and Payer, 2011].

The decrease in the number of open micro-channels and the decrease in conductivity of the layer may lead to a reversal of the conduction mechanism from micro-channel–controlled (extrinsic conductivity) to AgCl solid phase–controlled (intrinsic conductivity) [Lal et al., 1951]. This is known as high field conduction. AgCl is a poorly conducting solid (1.2×10^{-7} S/cm) with large concentrations of ionic defects (Ag^+) that range up to 0.7% of the lattice ions [Baetzold and Eachus, 1995]. The contribution of interstitial Ag^+ to the migration of ions through the AgCl solid results in intrinsic conductivity of the AgCl layer [Cain and Slifkin, 1980]. The aforementioned mechanisms explain the different morphology, microstructure and

surface chemistry of the AgCl layer, obtained at different current densities, but equal anodization time (1h duration) (sensors A to D in Figs. 3.6 and 3.7 and 3.8). Considering the results in this chapter, fabrication of Ag/AgCl sensors needs careful considerations, specifically with respect to sensor's application in cement-based materials.

3.4 Conclusions

In this chapter the formation of a AgCl layer on a Ag substrate and the development of the sensors' surface morphology and surface chemistry were discussed. A correlation was made on the results for the sensors' microstructural properties and ohmic resistance of the obtained AgCl layers. The following main conclusions can be drawn:

- The AgCl layer morphology, microstructure and surface chemistry depend on the anodization regime. Current density above 2 mA/cm^2 was found to increase the thickness and the ionic resistivity of the AgCl layer. Silver oxide-based or carbon-based impurities were present on the surface of the sensor in amounts proportional to the thickness as well as the morphology and microstructure of the AgCl layer.
- Small (Ag)AgCl grains seemed to be embedded in the AgCl layer, judged from the microstructural analysis, the surface chemistry results and the mechanisms involved during anodization (altered electrochemical state of the Ag substrate in conditions of recorded overpotential, higher than 2V). These inclusions lead to an increase in ionic resistivity, non-proportional to the AgCl layer thickness, together with a weak adhesion of the AgCl layer to the Ag substrate.
- The results in this chapter can be used as a recommendation for preparing the sensors with stable performance in cementitious materials. The produced AgCl layer at low current density is more uniform, homogeneous and compact. Hence, preparing Ag/AgCl sensors at low current densities (e.g. 0.5 mA/cm^2) is favorable to high current densities (e.g. 4 mA/cm^2).

3.5 References

Atkins, C. P., Carter, M. A. and Scantlebury, J. D. (2001). Sources of error in using silver/silver chloride electrodes to monitor chloride activity in concrete, *Cement and Concrete Research*, Vol. 31(8), p. 1207-1211.

Baetzold, R. C. and Eachus, R S (1995). The possibility of a split interstitial silver ion in AgCl, *Journal of Physics: Condensed Matter*, Vol. 7(21). p. 3991-3999.

Birss, V. I. and Smith, C. K. (1987). The anodic behavior of silver in chloride solutions—I. The formation and reduction of thin silver chloride films, *Electrochimica Acta*, Vol. 32(2), p. 259-268.

Boxall, L. G., Jones, H. L. and Osteryoung, R. A. (1974). Electrochemical Studies on Ag, Fe, and Cu Species in AlCl3 - NaCl Melts, *Journal of the Electrochemical Society*, Vol. 121(2), p. 212-219.

Bozzini, B., Giovannelli, G. and Mele, C. (2007). Electrochemical dynamics and structure of the Ag/AgCl interface in chloride-containing aqueous solutions, *Surface and Coatings Technology*, Vol. 201(8), p. 4619-4627.

Brewer, P.J., Leach, A.S., Brown, R.J.C. (2015). The Role of the Electrolyte in the Fabrication of Ag| AgCl Reference Electrodes for pH Measurement, *Electrochimica Acta*, Vol. 161, p. 80-83.

Briggs, G. W. D. and Thirsk, H. R. (1952). A study of the behaviour of polarized electrodes. Part 3.—The behaviour of the silver/silver chloride system during electrolytic reduction. *Transactions of the Faraday Society*, Vol. 48, p. 1171-1178.

Burstein, G. T. and Misra, R. D. K. (1983). Electrochemistry of scratched silver electrodes in chloride solutions, *Electrochimica Acta*, Vol. 28(3), p. 363-369.

Cain, L.S. and Slifkin, L.M. (1980). Ionic conductivity of mixed silver halide crystals, *Journal of Physics and Chemistry of Solids*, Vol. 41(2), p. 173-178.

Climent-Llorca, M. A., Viqueira-Perez, E. and Lopez-Atalaya, M. M. (1996). Embeddable Ag/AgCl sensors for in-situ monitoring chloride contents in concrete, *Cement and Concrete Research*, Vol. 26(8), 1157-1161.

Duffo, G. S., Farina, S. B. and Giordano, C. M. (2009). Characterization of solid embeddable reference electrodes for corrosion monitoring in reinforced concrete structures, *Electrochimica Acta*, Vol. 54(3), p. 1010-1020.

Gao, X., ZhanG. J., YanG, Y. and Lu, S. (2011). Preparation of chloride ion selective electrode and its potential response to different chloride solutions representing concrete environments, *Materials science forum (Zürich-Stafa : Trans Tech Publ)*, Vol. 1206(675), p. 537-541.

Ha, H. and Payer, J. (2011). The effect of silver chloride formation on the kinetics of silver dissolution in chloride solution, *Electrochimica Acta*, Vol. 56(7), p. 2781–2791.

Jin, M., Jiang, L. and Zhu, Q. (2017). Monitoring chloride ion penetration in concrete with different mineral admixtures based on embedded chloride ion-selective electrodes, *Construction and Building Materials*, Vol. 143, p. 1-15.

Jin, X., Lu, J., Liu, P. and Tong, H. (2003). The electrochemical formation and reduction of a thick AgCl deposition layer on a silver substrate, *Journal of Electroanalytical Chemistry*, Vol. 542, p. 85-96.

Katan, T., Gu, H. and Bennion, D.N. (1976). Analysis of porous electrodes with sparingly soluble reactants IV. Application to Particulate Bed Electrode: Ag/AgCl System, *Journal Electrochemical Society*, Vol. 123(9), p. 1370-1376.

Lal, H., Thirsk, H. R. and Wynne-Jones, W. F. K. (1951). A study of the behaviour of polarized electrodes. Part I. The silver/silver halide system, *Transactions of the Faraday Society*, Vol. 47, p. 70-77.

Montemor, M. F., Alves, J. H., Simoes, A. M., Fernandes, J. C. S., Lourenço, Z., Costa, A. J. S., Appleton, A.J. and Ferreira, M. G. S. (2006). Multiprobe chloride sensor for in situ monitoring of reinforced concrete structures, *Cement and Concrete Composites*, Vol. 28(3), p. 233-236.

Pemberton, J.E. and Girand, M. M. (1987). Electrochemical and SEM characterization of Ag electrodes roughened by potential sweep and potential step processes in aqueous chloride and chloride+pyridine media, *Journal of Electroanalytical Chemistry and Interfacial Electrochemistry*, Vol. 217(1), p. 79-92.

Polk, B. J., Stelzenmuller, A., Mijares, G., MacCrehan, W. and Gaitan, M. (2006). Ag/AgCl microelectrodes with improved stability for microfluidics, *Sensors and Actuators B: Chemical*, Vol. 114(1), p. 239-247.

Scofield, J. H. (1976). Hartree-Slater subshell photoionization cross-sections at 1254 and 1487 eV, *Journal of Electron Spectroscopy and Related Phenomena*, Vol. 8(2), p. 129-137.

Shirley, D. A. (1972). High-resolution X-ray photoemission spectrum of the valence bands of gold, *Physical Review B*, Vol. 5(12), p. 4709-4714.

Stoica, D., Brewer, P. J., Brown, R. J. and Fisicaro, P. (2011). Influence of fabrication procedure on the electrochemical performance of Ag/AgCl reference electrodes, *Electrochimica Acta*, Vol. 56(27), p. 10009-10015.

Suzuki, H., Hiratsuka, A., Sasaki, S. and Karube, I. (1998). Problems associated with the thin-film Ag/AgCl reference electrode and a novel structure with improved durability. *Sensors and Actuators B: Chemical*, Vol. 46(2), p. 104-113.

Vera, G., Hidalgo, A., Climent, M. A., Andrade, C. and Alonso, C. (2000). Chloride ‐ Ion Activities in Simplified Synthetic Concrete Pore Solutions: The Effect of the Accompanying Ions, *Journal of the American Ceramic Society*, Vol. 83(3), p. 640-644.

Chapter 4

Potentiometric response of Ag/AgCl chloride sensors in model alkaline medium

Abstract

The stability and reproducibility of the Ag/AgCl sensors' response in an alkaline medium are important for the application of these sensors in cementitious materials. The sensors' response, or their open circuit potential (OCP), reflects a dynamic equilibrium at the sensor/environment interface. The OCP in an alkaline medium is affected by the presence of hydroxide ions. The interference of hydroxide ions leads to in-accuracies or a delay in the sensors' response to a certain chloride content. In this chapter, the potentiometric response (or OCP evolution) of the chloride sensors is measured in model solutions, resembling the concrete pore water. The scatter of the sensors' OCP is discussed with respect to the interference of hydroxide ions at varying chloride concentration in the medium. The deviation of the sensor's performance from the one determined by the Nernst law for a Ag/AgCl interface is attributed to de-chlorination of the AgCl layer and the formation of silver oxides on the sensor's surface. Results from XPS analysis of the AgCl layer before and after treatment in alkaline solution confirm these observations in view of chemical transformation of AgCl to Ag_2O.

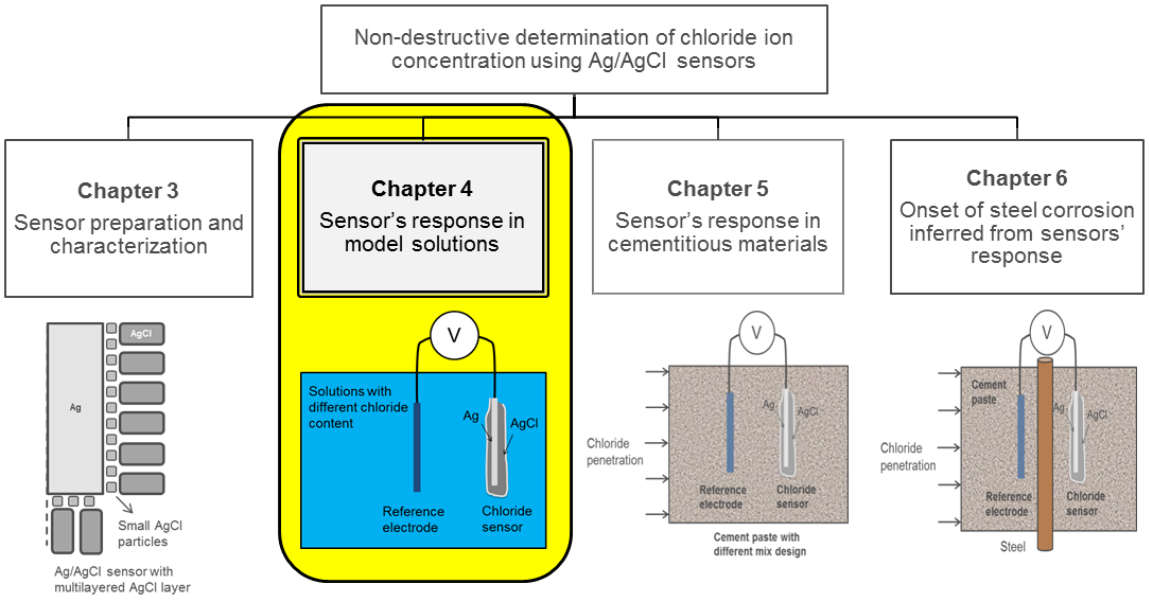

Structure of research process and sequence of chapters in the thesis.

This Chapter is based on the paper:

Pargar, F., Kolev, H., Koleva, D. A. & van Breugel, K. (2018). Potentiometric response of Ag/AgCl chloride sensors in model alkaline medium, Advances in Materials Science and Engineering, Vol. 2018, 8135492.

4.1 Introduction

In Chapter 2, Ag/AgCl electrodes were introduced as "chloride sensors" in cementitious materials for non-destructive and continuous monitoring of the free chloride concentration. It was mentioned that the stability and reproducibility of the sensors' response in alkaline medium, e.g. cementitious materials, have not been sufficiently addressed. For instance, the observed difference between the responses of identically prepared chloride sensors in an environment with a pre-defined chloride content is still a subject of discussion. Therefore, the performance of Ag/AgCl electrodes in alkaline medium needs further investigation.

While the sensor's response is just a common open circuit potential (OCP), the possible discrepancies reflect the time needed for establishment of a dynamic equilibrium at the sensor/environment interface. In an alkaline medium, like the pore water in cementitious materials, with zero or low chloride content, the OCP response of a sensor deviates from the one according to the Nernst equation for a Ag/AgCl interface. The interference of hydroxide ions determines an OCP response, not proportional to the activity of chloride ions only. Hence, the sensor's OCP is associated with the ratio of chloride to hydroxide ions at the sensor's surface [Jin et al., 2015; Femenias et al., 2016]. In such cases, the measured OCP does not present the Ag/AgCl equilibrium only (Eq. 4.1), but also reflects a mixed potential described by the Ag/AgCl/Ag_2O equilibrium (Eq. 4.2).

$$Ag + Cl^- \leftrightarrow AgCl + e^- \quad (4.1)$$

$$2AgCl + 2OH^- \leftrightarrow Ag_2O + 2Cl^- + H_2O \quad (4.2)$$

Consequently, with the gradual transformation from silver chloride to silver oxide, the sensor's OCP is no longer proportional to the activity of chloride ions in the medium. Hence, the stability and reliability of the sensor's response are largely affected and/or limited. The possible change in the sensor's OCP in an alkaline solution, e.g. due to silver oxide formation on the sensor's surface, and the reversibility of the sensor is schematically shown in Fig. 4.1. This subject is not sufficiently addressed in the current state-of-the-art [Duffo et al., 2009; Jin et al., 2015], although it is of significant importance for the practical application of a chloride sensor of this type.

Additionally, the physical properties of the AgCl layer would determine the interaction of sensor/medium and the OCP response of the sensors, respectively. The surface properties (morphology and microstructure) of the AgCl layer will affect the surface chemistry of the sensors. In Chapter 3, the surface chemistry of the AgCl layer was linked to the thickness, morphology and microstructure of this layer. These features were found to be also dependent on the anodization regime, as used for the sensor preparation. For instance, chemical recombination and the presence of oxygen or carbon-based compounds on the sensors' surface (discussed in Chapter 3) would be responsible for a deviation of the sensors' response from the one expected for a purely Ag/AgCl interface. Therefore, the surface properties of a AgCl layer would be important for the stability of the sensor's OCP, when the sensor is in contact with a chloride-free or a chloride-containing alkaline medium.

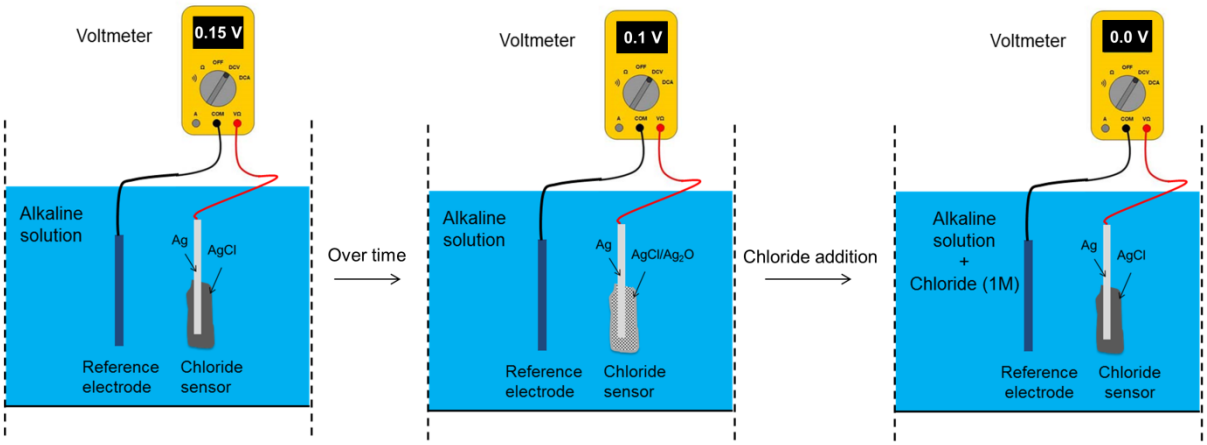

Figure 4.1: Schematic representation of the OCP changes of a chloride sensor in an alkaline medium. Left: initial OCP; Middle: Ag_2O formation on the sensor's surface changes the OCP over time; Right: reversibltiy of the chloride sensor upon addition of chloride.

This chapter presents the OCP evaluation of Ag/AgCl sensors in model alkaline environment. Sensitivity, stability and reproducibility of the chloride sensors in different solutions were assessed. Calibration of the sensors was performed and compared to available literature data. The potentiometric response of the sensors was recorded in conditions when the chloride concentration in the aqueous medium was either constant or varying. Hence, the reversibility of the sensors was also evaluated. This chapter concludes with the experimental evidence for the chemical transformation of the AgCl layer in contact with an alkaline medium, and also defines the chloride ions detection limits in such a medium.

4.2 Experimental materials and methods

4.2.1 Ag/AgCl sensors

The Ag/AgCl sensors, as produced at various anodization regimes (presented in detail in Chapter 3), were subject to electrochemical tests and calibration in various solutions. The assigned codes for sensors were based on the anodization regime used for sensor preparation, i.e. 0.5 mA/cm^2 (sensor A), 1 mA/cm^2 (sensor B), 2 mA/cm^2 (sensor C) and 4 mA/cm^2 (sensor D). The anodized Ag wires (i.e. the sensors as produced) were soldered to a copper wire and the junction was protected with an epoxy resin (Fig. 4.2). The final exposed length of the sensors was 1 cm. The sensors were stored out of direct sunlight until the moment of testing.

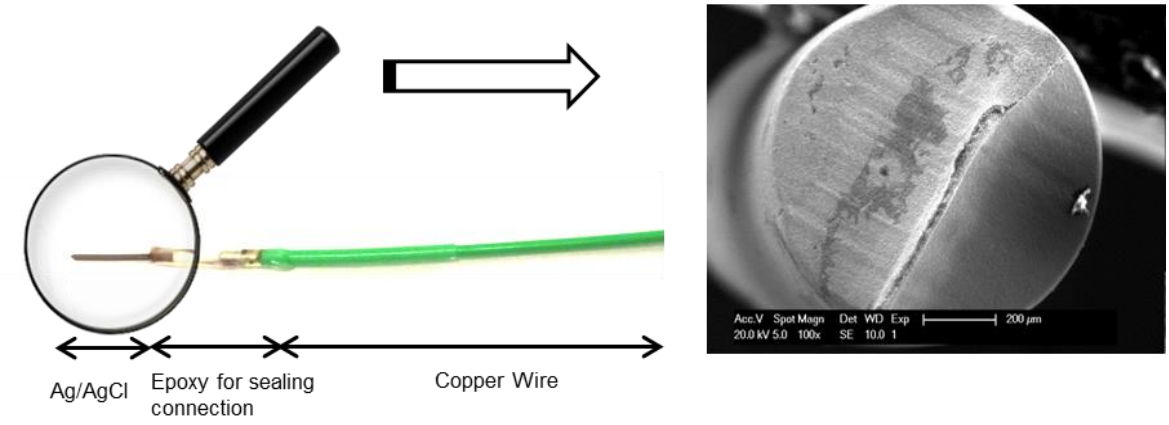

Figure 4.2: The as produced Ag/AgCl chloride sensor.

4.2.2 Model media

Different model solutions used in this study were: demineralized water (DW) of pH ~ 6; simulated concrete pore solution (SPS) (0.05 M NaOH + 0.63 M KOH + Sat. $Ca(OH)_2$, of pH~13.6; and cement extract (CE). The cement extract (CE), of pH ca. 12.8, was obtained by mixing cement powder (CEM I 42.5N) and tap water at the ratio of 1:1 in a bottle. The bottle was rotated for 24 hours, followed by filtration for obtaining the extract. The chemical composition of CE is as follows: Ca – 201 mg/l; K – 3.85 mg/l; Na – 1.33 mg/l; Al – 4 mg/l and Fe < 1 mg/l. The model solutions were chloride-free or chloride-contaminated (with a pre-defined chloride content), using NaCl additions.

Tables 4.1 and 4.2 present all model solutions and their composition. The sensor's OCP was measured in the so-called "calibration" solutions (Table 4.1). The criteria for the performance of a good sensor were evaluated by studying stability, reproducibility, sensitivity, reliability and reversibility of the sensor in these solutions (Table 4.2).

Table 4.1: Solutions for calibration of the chloride sensors.

No.	Solution	pH	Chloride concentration (mM)
1	Demineralized water	6	1, 2, 4, 8, 16, 31, 64, 125, 250, 500, 1000
2	Cement extract solution[1]	12.8	12, 14, 16, 20, 27, 44, 77, 142, 260, 513, 1008
3	Simulated pore solution	13.6	1, 2, 4, 8, 16, 31, 64, 125, 250, 500, 1000

[1] *CE solution is supposed to be chloride-free, chemical analysis of the solution, however, showed about 12 mM chloride content, due to the mixing water and chloride at levels of < 0.03 % in the original cement (ENCI, NL specifications).*

Table 4.2: Model solutions and criteria for sensors' performance.

Test series	Used medium	pH	Chloride concentration (mM)	Purpose of the OCP measurement in this environment (criteria for sensors performance)[2]
1	Simulated pore solution (SPS)	13.6	0	**Stability**: OCP variation in chloride-free alkaline solution (Fig. 4.3)
2	Cement extract solution (CE)	12.8	20, 260	**Stability & reproducibility**: dependence on different properties of the AgCl layer (Figs. 4.4 and 4.5)
3	Simulated pore solution (SPS)	7, 9, 12.8, 13.6	1, 2, 4, 16, 62, 250	**Reliability:** interference of hydroxide ions and chloride detection limits (Fig. 4.7)
4	Cement extract solution (CE)	12.8	12, 14, 16, 20, 27, 44, 77, 142, 260, 513, 1008	**Reversibility**: response to continuous addition of chloride (Figs. 4.8 and 4.9)
5	Simulated pore solution (SPS)	13.6	0, 125, 1000	

4.2.3 Open circuit potential (OCP) measurements

The records of OCP versus time were used to evaluate the sensor's performance in different solutions (Tables 4.1 and 4.2) The motivation behind OCP measurement and the evaluation criteria in each environment and test series are listed in Table 4.2. The set-up used to perform these potentiometric measurements comprised a chloride sensor (working electrode) and a reference electrode (Saturated Calomel Electrode, SCE), using a PGSTAT 302N potentiostat (Metrohm Autolab B.V., The Netherlands) and a common three-electrode cell arrangement. Although the counter electrode was not used for the tests in this chapter, the cell volumes and geometrical configuration were maintained identical to those used for the tests in Chapter 3.

4.2.4 X-ray photoelectron spectroscopy (XPS) analysis

XPS analysis was performed on Ag foil with a surface area of 2.4 cm^2 per sample (1 cm width, 2 cm length and 0.005 cm thickness). The Ag foil was anodized in regimes, identical to those used for the production of sensors A and sensors C (as representative cases for all sensors A to D), i.e. the Ag foil was anodized for one hour at 0.5 mA/cm^2 and 2 mA/cm^2 in 0.1 M HCl solution. The flat Ag/AgCl sensors were immersed in chloride-free NaOH solution (pH=13.7) and their OCP was measured continuously, reaching a stable value around 100 mV after 8 days of treatment. The composition of the AgCl layers of the "treated" sensors was determined by XPS and the results were compared to those for identically produced, untreated sensors.

The XPS measurements were carried out in AXIS Supra electron spectrometer (Kratos

[2] *To be noted is that the response of all types of sensors (A to D) was recorded in chloride-free and chloride-containing alkaline medium (CE), while calibration and evaluation for reproducibility, reliability and reversibility was tested for sensors A only. This was based on the decision made for sensor A as the most suitable choice for application in alkaline medium, and after considering various points, incl.: surface morphology, composition, possible limitations towards ion transport and electrochemical state in aqueous medium for sensors A, compared to all other sensors.*

Analytical Ltd.) using monochromatic AlKa radiation with a photon energy of 1486.6 eV. The samples were mounted with metal clips on the sample holder. The samples and the sample holder were grounded and neutralizer was used to compensate the charge on the surface. The high-resolution scans have been recorded with 20 eV pass energy. The energy calibration was performed by referencing the carbon (C1s) line of adsorbed adventitious hydrocarbons to 285.0 eV. The binding energies (BE) were determined with an accuracy of ±0.1 eV. Processing of the measured spectra includes a subtraction of Shirley-type background [Shirley, 1972]. The peak positions and areas were evaluated by a symmetrical Gaussian-Lorentzian curve fitting. The relative concentrations of the different chemical species were determined based on normalization of the peak areas to their photoionization cross-sections, calculated by Scofield [Scofield, 1976].

4.3 Results and discussion

4.3.1 OCP response of sensors in alkaline solutions

The sensors' OCP shifts in cathodic direction with increasing the chloride concentration in the medium (Chapter 2, Eq. 2.4). For instance, the OCP response of a chloride sensor in 250 mM and 500 mM chloride contents is 6 mV and 23 mV vs SCE, respectively [de Vera et al., 2010]. In a chloride-free environment, the sensors' OCP reflects a mixed potential described by a dynamic exchange equilibrium, similar to Eq. 4.2. In this condition, the OCP value is expected to be more anodic (ca. 100 mV to 150 mV vs SCE, [Polk et al., 2006; Svegl et al., 2006; de Vera et al., 2010]), due to a mixed potential, arising from OH^- ions interference [Elsener et al., 2003]. The level of OH^- ions interference depends on the chloride ions concentration (i.e. the OH^-/Cl^- ratio). In this regard, a chloride detection limit of 10 mM chloride content was reported [de Vera et al., 2010].

The OCP of all sensors in a chloride-free simulated pore solution is depicted in Fig. 4.3 (Section 4.3.1.1). The OCP response of all sensors in cement extract (CE), containing 20 mM and 260 mM chloride concentration is shown in Figs. 4.4 and 4.5 (Sections 4.3.1.2 and 4.3.1.3).

4.3.1.1 Chloride-free alkaline medium

The OCP response of sensors A to D was monitored during 6 days of immersion in chloride-free simulated pore solution (Fig. 4.3). The initial OCP value for sensors A and B (ca. 150 mV) was more anodic than that for sensors C and D (ca. 120 mV). The sensors' OCP gradually shifted to cathodic potentials and after 6 days of immersion reached 102 mV to 112 mV. In other words, the difference between the OCP response of sensors A and D decreased from 30 mV in the first hours of immersion to 10 mV after 6 days (Fig. 4.3). The OCP variation in time and establishment of a stable OCP value is not only sensor type-dependent but is also due to AgCl de-chlorination and Ag_2O formation at the sensor's surface as previously introduced in Section 4.1. The observed performance of the sensors is governed by an exchange equilibrium (Eq. 4.2), where the expected continuous transformation of AgCl to silver oxide changes the activity of silver ions (Ag^+) near the silver substrate [Suzuki and Taura, 2001]. As a result, a mixed potential develops at the sensors' surface [de Vera et al., 2010; Karthick et al., 2017], shifting the OCP from around 150 mV towards 99 mV (vs SCE) [Svegl, et al., 2006; Duffo et al., 2009; Angst et al., 2010]. The variation between the initial OCP value and that established after 6 days is wider for sensors A and B (40 mV) than for sensors C and D (20 mV). Since the OCP changes would be a result of de-chlorination of the

AgCl layer and the transformation of AgCl to Ag_2O, the wider OCP range from the initial to the stabilized OCP value for sensors A and B (40 mV) most probably reflects a higher amount of purely AgCl at the surface of these sensors. In contrast, the heterogeneous, less adherent and impurities-richer AgCl layer of sensors C and D (Chapter 3) leads to an immediate and enhanced oxidation of the Ag/AgCl interface [Shi et al., 2015]. This explains the smaller difference between the initial, more cathodic OCPs for sensors C and D (ca. 120 mV) and those established at the end of the test (ca. 100 mV), Fig. 4.3.

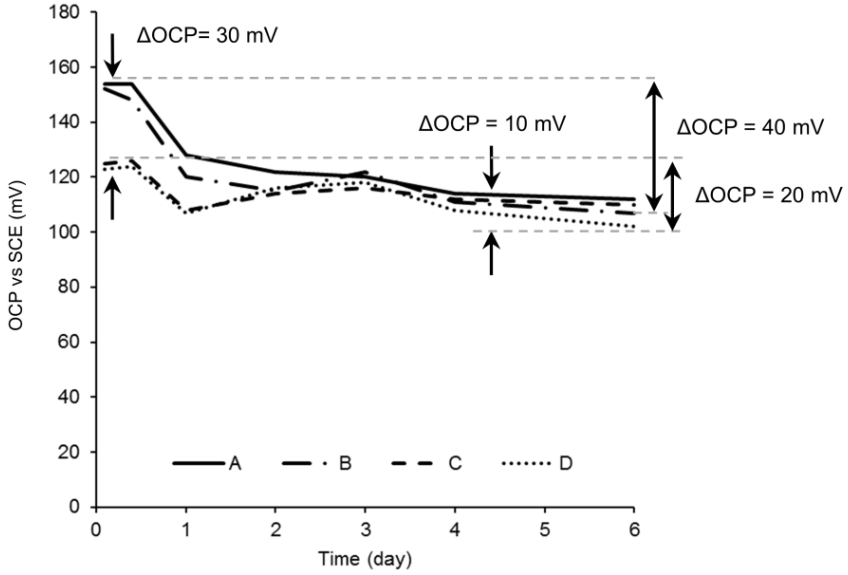

Figure 4.3: Evolution of OCP values of the Ag/AgCl sensors (A, B, C and D) in chloride-free simulated pore solution (SPS).

The properties of the AgCl layer not only affect the sensor's response in chloride-free alkaline medium (as above shown), but would also determine the sensor's response in chloride-containing alkaline medium. This is the subject of discussion in the following.

4.3.1.2 Chloride-containing alkaline medium

The OCP response of the sensors A to D in cement extract (CE) with 20 mM and 260 mM chloride content are presented in Fig. 4.4. Increasing the chloride content from 20 mM (Fig.4.4a) to 260 mM (Fig. 4.4b) results in a cathodic shift of the OCP values for all sensors. For sensors A and B the initial OCP values are between 90 mV (for 20 mM chloride content, Fig. 4.4a) and 25 mV (for 260 mM chloride content, Fig. 4.4b), while the initial values for sensors C and D before stabilization are between 40 mV (for 20 mM chloride content, Fig. 4.4a) and 15 mV (for 260 mM chloride content, Fig. 4.4b). At the end of the test, the final OCPs for all sensors correspond to the chloride content in the medium: for 20 mM chloride content, the adopted values were between 80 and 89 mV; for 260 mM solution, the final values were between 24 and 25 mV. These OCP values reflect the chloride content in the medium. The OCP response of a chloride sensor in 20 mM and 260 mM chloride concentration was previously reported to be 89 mV and 23 mV, respectively [de Vera et al., 2010].

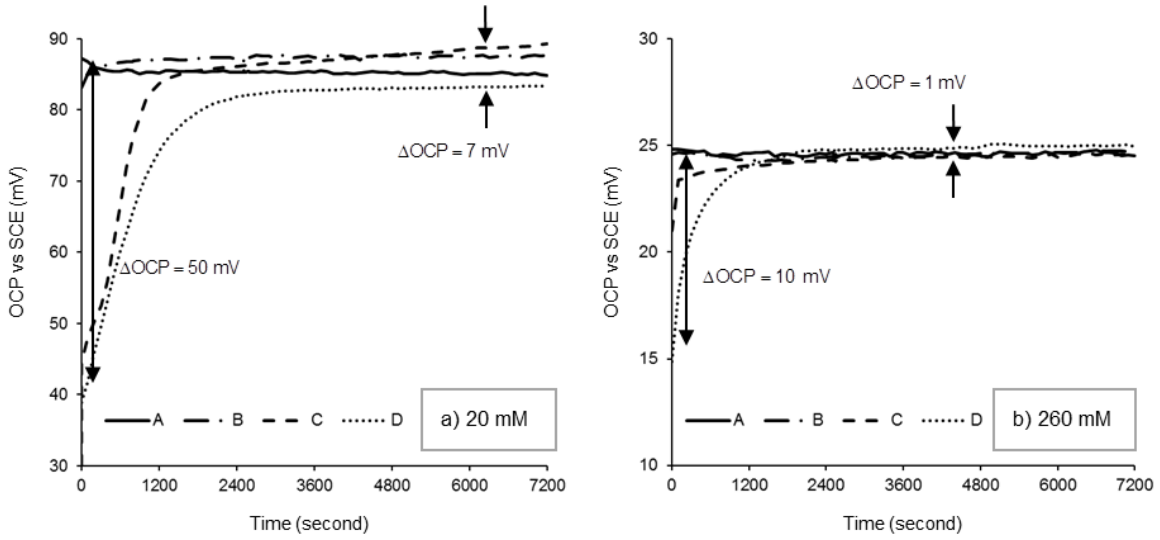

Figure 4.4: Evolution of OCP response of the chloride sensors (A, B, C and D) in chloride-containing cement extract (CE): a) 20 mM chloride content; b) 260 mM chloride content.

To be noted is that the OCP records in cement extract (CE) with 20 mM chloride concentration showed a variation of 50 mV in the beginning of the test, narrowing down to 7 mV after 7200 s (Fig. 4.4a). In 260 mM chloride-containing medium a smaller deviation was observed, i.e. less than 10 mV in the beginning of the test, decreasing to 1 mV after 7200 s (Fig. 4.4b). The results indicate that both OCP variation and the time needed for OCP stabilization are reduced upon increase in chloride concentration from 20 mM to 260 mM. This is irrespective of the sensor type and anodization regime.

Fig. 4.4 also depicts a different performance of the sensors A to D in cement extract solution. The OCP stabilization depends not only on the chloride content in the medium, but also on the properties of the AgCl layer. As can be observed in Fig. 4.4, approximately 60 s were needed for a stable OCP of sensors A and B, prepared at low current densities, while more than 1800 s were required for sensors C and D (with a thicker AgCl layer) to reach a stable value. This observation held for both 20 mM and 260 mM chloride concentrations (Figs. 4.4a and 4.4b). The increase in the AgCl layer thickness from ~8 µm (sensor A) to ~15 µm (sensor B) has a negligible effect on the OCP stabilization time. However, the increase in AgCl layer thickness from 15 µm for sensor B to 20 µm for sensor C and 40 µm for sensor D, has an obvious influence on the OCP stabilization time. Consequently, the observed time difference (1 minute for sensors A and B vs. 30 minutes for sensors C and D) should be attributable to the AgCl layer morphology and microstructure for sensors C and D (Chapter 3), rather than to the AgCl layer thickness alone.

4.3.1.3 Sensors' reliability and reproducibility versus structure of the AgCl layer

The reliability and reproducibility of the sensor's response in chloride containing medium can be affected by the AgCl layer properties. Reproducibility of the sensor's response is specifically important in view of the sensor's performance in alkaline medium [McCarter and Vennesland, 2004; Muralidharan et al., 2008]. In the following, the reproducibility of the OCP response of replicates of sensors A and D in cement extract (CE) with 20 mM and 260 mM chloride content is addressed.

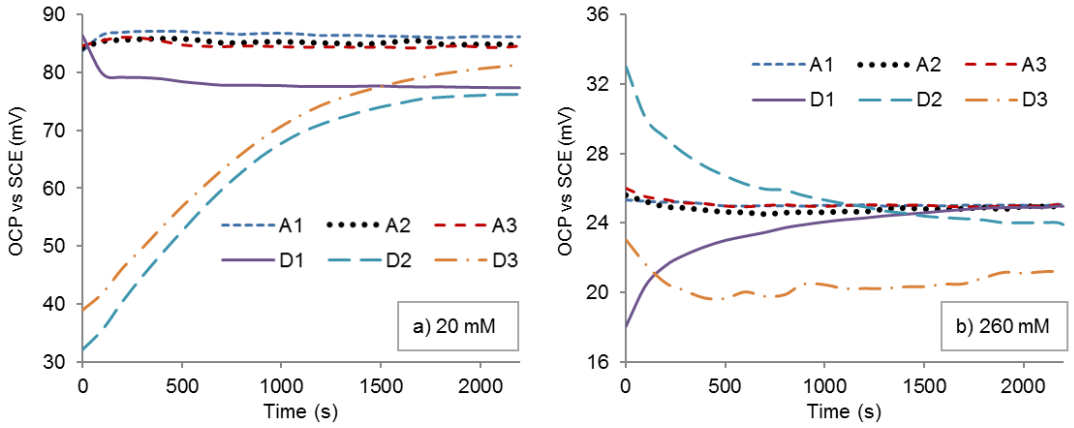

Figure 4.5: OCP response of replicates of sensors A and D in chloride-containing cement extract (CE): a) 20 mM chloride content; b) 260 mM chloride content.

The OCP response of three replicates of sensor A (A1, A2, A3) and sensor D (D1, D2, D3), Fig. 4.5, was monitored for 2200 s. The OCP response of sensors D varied significantly throughout the test, if compared to the relatively stable response of sensors A (Fig. 4.5). In less than a 100 s, sensors A reached to the stable values of 85±1.5 mV and 25±0.2 mV in CE of 20 mM and 260 mM chloride concentrations, respectively. In contrast, a relatively stable OCP for the D sensors was observed after 1800 with a value of 78±3 mV for CE with 20 mM chloride concentration and 23±2 mV for CE with 260 mM chloride concentration. The OCP response of sensors A was reproducible. This is evident from the lower standard deviation of the OCP response of sensors A (0.2-1.5 mV) in comparison to that of sensors D (2-3 mV). The lower reproducibility for sensors D can be attributed to the heterogeneity and multi-layered structure of the AgCl layer for these sensors (discussed in Chapter 3).

Additionally, the following observation is important to be specifically addressed: in the initial period, the higher instability of sensors D, compared to sensors A, was obvious (Fig. 4.5, OCPs prior to 1200 s). This means that sensors D initially "underestimated" or "overestimated" the chloride content, while sensors A present an almost immediate accurate response. The different microstructural properties of the AgCl layer for A versus D sensors (Chapter 3) are supposed to be responsible for the differences in the OCP response. Except the already discussed considerations, the limitation of ion transport of any kind at the sensor/medium interface or limitation of electron transport along the sensors' conductive surface will also be reflected in variation in the time to establish an equilibrium condition. The microstructure, composition, thickness and ionic resistance of the AgCl layer for the different sensors were discussed in Chapter 3. These aspects will be elaborated further below with respect to variation in OCP response.

Consequently, when the sensors are in contact with the chloride-containing alkaline medium, the chloride ions diffusing into the AgCl layer will alter the Ag^+ activity so that a new equilibrium is established on the sensors' surface (Eq. 4.1). A fast equilibrium is achieved in a short period for sensor A, reflected by a stable OCP in the solutions (Figs. 4.4 and 4.5). In the presence of impurities, such as Ag^o in sensors D, a lower concentration of Ag^+ will be available at the surface of the Ag substrate. A lower concentration of Ag^+ subsequently shifts the sensor's OCP towards more negative (cathodic) potentials [Suzuki and Taura, 2001], or determines an erratic response and instability of the sensor, Fig. 4.5. Therefore, a longer time is needed for establishing an equilibrium condition at the Ag/AgCl interface of the sensors with a thicker and more heterogeneous AgCl layer, as in sensor D, compared to that in sensor

A (Fig. 4.5). For all further tests and investigations in this chapter, sensor A was chosen to proceed with.

4.3.2 Sensor's calibration

Calibration of a Ag/AgCl sensor is a necessary step in evaluating its performance, when in contact with external medium. The calibration curve for the chloride sensor is, essentially, the link of the sensor's OCP to the activity of chloride ions in a solution. For this purpose, the OCP of the Ag/AgCl sensor was recorded in demineralized water (DW), simulated pore solution (SPS) and cement extract (CE) of varying chloride content, or in the so-called "calibration" solutions (Table 4.1). The chloride activity was calculated from the chloride concentration by using the activity coefficient (Eq. 2). The mean activity coefficient for NaCl solution in a standard condition was derived from literature [Dobos, 1975; Angst et al., 2010]. Figure 4.6 presents the recorded responses, together with values reported by other researchers for identical or similar conditions.

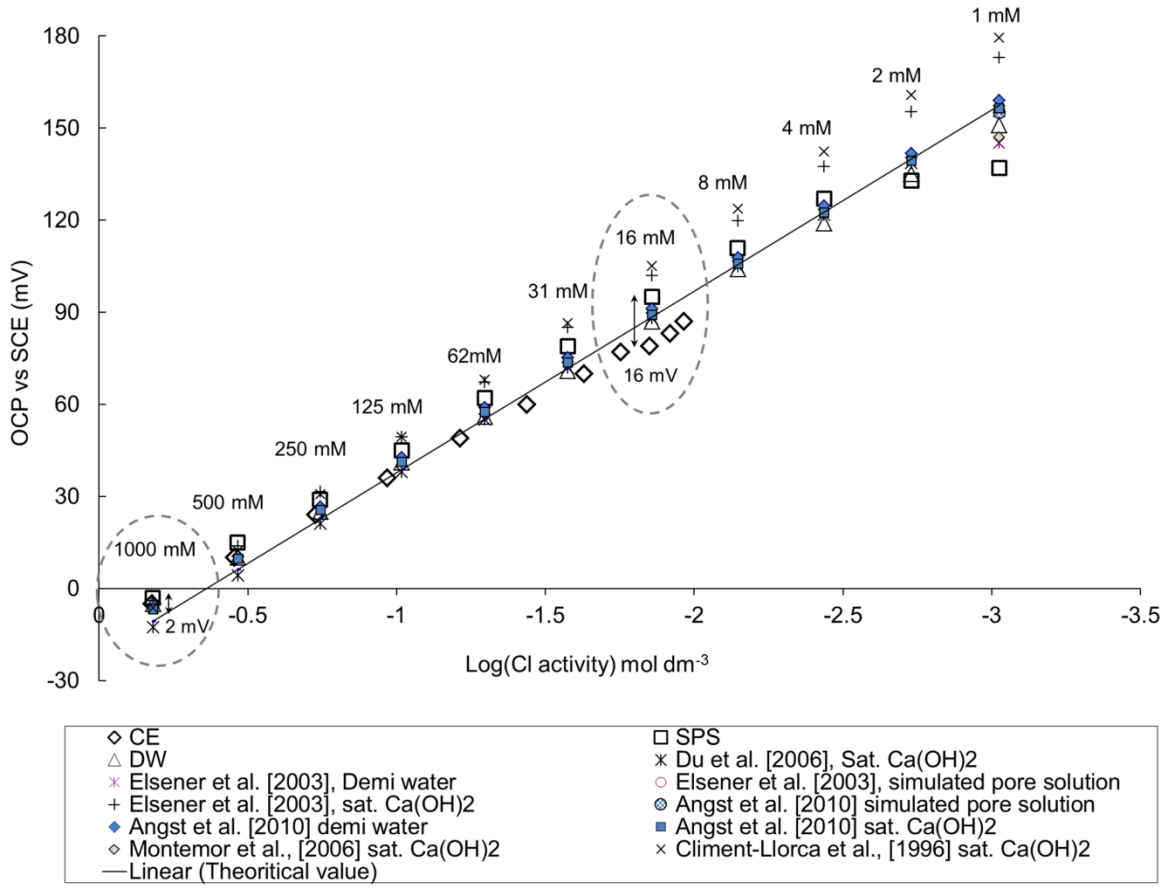

Figure 4.6: OCP response of chloride sensors versus the activity of chloride ions in different solutions.

Linear regression was employed to derive the coefficient of determination (R^2). In DW, the interference of hydroxide ions was negligible. Therefore, the sensor in DW responded accurately to a wide range of chloride concentration (from 2 mM to 1000 mM with an accuracy of R^2=0.999). In the same range of chloride concentration, but in the SPS medium, R^2 equals to 0.985. For increasing the degree of linearity to R^2=0.999, the chloride detection limit in SPS

should be 8 mM. This value is similar to the reported 10 mM detection limit for a Ag/AgCl sensor in alkaline medium (pH 13.7) [de Vera et al., 2010; Angst et al., 2010]. Therefore, the linear regression for the results in SPS was performed for chloride concentration higher than 8 mM. The following Eq. 4.3 was applied for the regression analysis:

$$E\ (mV\ vs\ SCE) = m_0 + m_1 \cdot \lg a_{cl} \qquad (4.3)$$

where m_0 is the potential value at the intersection between the fitting curve and the vertical axis (OCP in Fig. 4.6) and m_1 is the slope of the calibration curve. Table 4.3 summarizes the results of linear regression for all solutions. The slope of the calibration curves varies from -50 mV to -62 mV with an average of -56 mV. Although a good agreement is observed between the results (slope) recorded in this study and the values reported in the literature (Fig. 4.6, Table 4.3), the experimental and theoretical slopes are in fact different, i.e. -50 mV vs. -59 mV, respectively. This deviation from the theoretical value (i.e. from ideal performance) can be related to the chloride ions activity coefficient. While the theoretical slope is based on thermodynamic equilibrium and spontaneity of the reactions at the sensor's surface in standard conditions, the experimental slope is derived in the conditions of the relevant experiments. Changes in the test medium, such as varying alkalinity or ionic strength, resulted in calibration curves with different slopes (Table 4.3). Hence, the difference between the theoretically and experimentally derived slopes of the calibration curves is logic and as expected.

Table 4.3: Slope of the calibration curves and results from the statistical analysis in simulated pore solution (SPS), cement extract solution (CE) and demineralized water (DW).

Solution	This work			Slope from other studies				
	Slope (m_1 in Eq. 4.3)	Axis (m_0 in Eq. 4.3)	R^2	Angst et al., [2010]	Elsener et al., [2003]	Montemor et al., [2006]	Climent-Llorca et al., [1996]	Du et al., [2006]
CE	-49.73	-12.48	0.998	–	–	–	–	–
SPS	-58.11	-13.31	0.999	-57.8	-54	–	–	–
DW	-55.39	-15.69	0.999	-58.3	-50	–	–	–
Sat. $Ca(OH)_2$	–	–	–	-57.6	-59	-53.46	-61.72	-56.02
Theoretical value	-59.16	-21.4	1	–	–	–	–	–

What can be also observed in Fig. 4.6 is that irrespective of the medium and at low chloride concentration, the OCPs of the sensors vary in a wider range. This is valid for both the experimentally derived values and those reported by other researchers. For example, more than 40 mV difference in OCP was observed at 1 mM chloride concentration, while the OCP variation decreased to less than 10 mV at chloride concentration of 1000 mM. This is regardless of the alkalinity and ionic strength of the solution. In this work the difference amongst the sensor's OCP in demineralized water (DW), cement extract (CE) and simulated pore solution (SPS) was 16 mV at 16 mM chloride concentration, decreasing to 2 mV at 1000 mM chloride concentration (Fig. 4.6). The larger scatter at lower chloride content is due to the interference of hydroxide ions, resulting in a limited accuracy of the sensor in determination

of the chloride concentration. Since the hydroxide ions interference would be larger in solutions of higher pH, a chloride content detection limit is determined in view of the practical application of Ag/AgCl sensors in alkaline medium as concrete. This point is discussed in the next section.

4.3.3 Interference and detection limits

As already pointed out, the performance of chloride sensors in alkaline medium is affected by a chloride detection limit. Below this detection limit the sensors respond inaccurately to the chloride content. The reason for the existence of such a limit and imprecise sensors' response is the interference of hydroxide ions, which are readily available in the solution. To further investigate this, the OCP of the chloride sensors was measured in simulated pore solutions (SPS) with different pH (7.0, 9.0, 12.6, 13.6) and varying chloride concentration (1 mM, 2 mM, 4 mM, 16 mM, 62 mM and 250 mM) (Fig. 4.7, Table 4.2 – test series 3). The pH of the solutions was modified by a drop-wise addition of concentrated nitric acid. The OCP in each solution was recorded for 600 s, a sufficient time interval for achieving a stable response, including reflection on the contribution of hydroxide ions interference.

As can be observed in Fig. 4.7, the sensor's OCP shifts to a more cathodic value when the alkalinity of the solution increases from neutral, to pH 9 and pH 13.6. This OCP drift reflects the hydroxide ions interference and is more pronounced at low chloride concentration, i.e. 1 mM and 2 mM (circled region in Fig. 4.7). The observation is in line with the previously discussed results in Fig. 4.6 for the same chloride content, but varying chemical composition and ionic strength of the external medium.

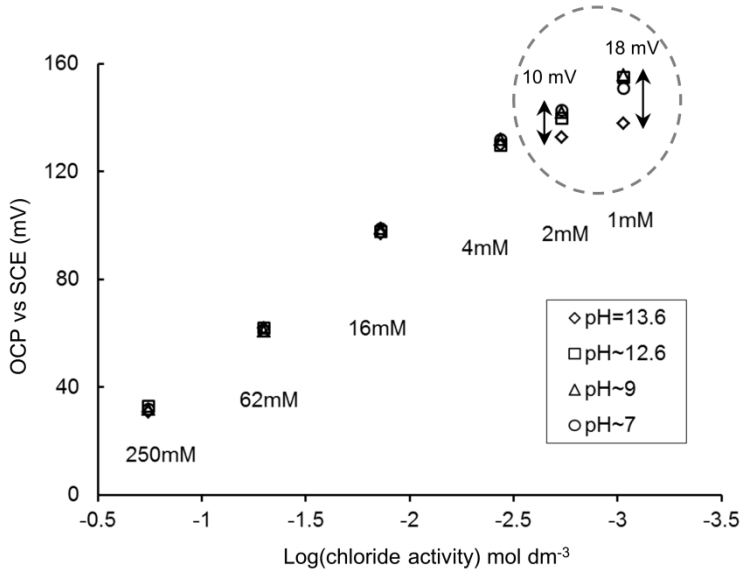

Figure 4.7: The effect of pH on the OCP response of the chloride sensor.

As seen in Fig. 4.7, the difference in OCP response of the sensor in solutions containing 1 mM and 2 mM chloride concentrations is 18 mV and 10 mV, respectively. These OCP differences narrow down to 1-2 mV upon increasing the chloride content to 4 mM. A difference of 1 to 2 mV in OCP values can be considered as negligible [Angst and Vennesland, 2009]. Consequently, the chloride sensors can be used for a relatively accurate determination of the chloride content in alkaline solutions, where the chloride concentration is higher than 4

mM. The reasons behind the higher or lower levels of hydroxide ions interference to the sensors' response in alkaline medium are linked to the transformation of silver chloride to silver oxide on the sensor's surface. This transformation is governed by both the pH and ionic strength of the medium, in addition to the actual chloride content. The transformation of AgCl to silver oxides is confirmed by outcomes from surface XPS analysis of the AgCl layer, presented in Section 4.3.5.

4.3.4 Sensitivity and reversibility of the chloride sensor

The sensitivity of the sensor is reflected by its as expected OCP response to a pre-defined chloride content. Reversibility is the ability of the sensor to return the expected response (Eq. 4.3) upon changing the environment from chloride-free to chloride-containing and vice-versa. Sensitivity was already discussed with relevance to the sensor's response in various solutions (Figs. 4.4 and 4.5). Reversibility is discussed in this section in view of the sensors' response upon changing the medium from chloride-free to chloride-containing.

Both sensitivity and reversibility are illustrated in Fig. 4.8. The figure shows the recorded OCP response of a sensor immersed in alkaline cement extract (CE) in which a continuous change of the chloride content was applied. By increasing the chloride concentration from 12 mM to 1008 mM the OCP changes from anodic to cathodic values. The experimentally derived values are well in line with those derived from the Nernst equation for a Ag/AgCl interface (Chapter 2, Eq. 2.4). For instance, at chloride content in the medium of 20 mM, 77 mM and 513 mM, the sensor's response should be 84 mV, 52 mV and 6 mV, which are well in line with the recorded 79 mV, 50 mV and 10 mV (Fig. 4.8).

In the event of changing the chloride concentration from 1008 mM to 12 mM (i.e. a sharp decrease in chloride content), the sensor's OCP returns in approx. 60 s to the initial, and expected response of 87 mV. This observation demonstrates the good sensitivity and reversibility of the sensor, both of importance for the precision of chloride detection.

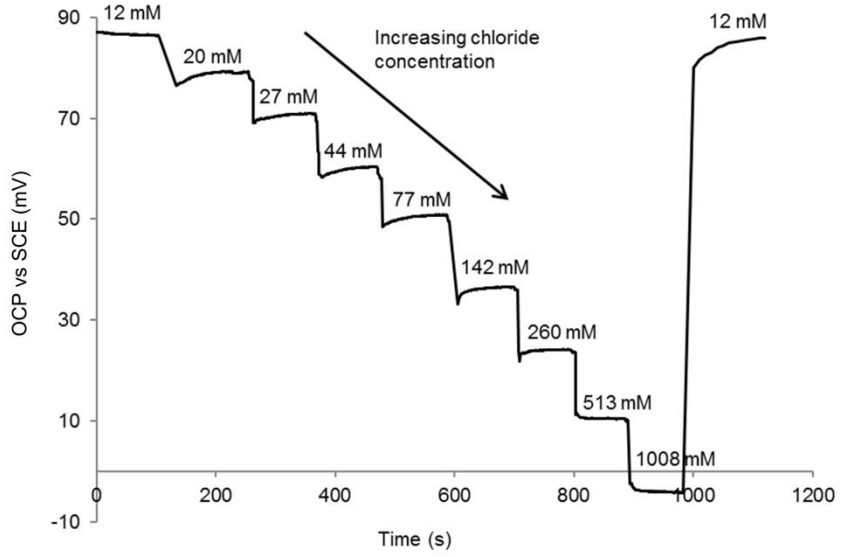

Figure 4.8: Chloride sensor's response in cement extract (CE) at continuously changed chloride concentration.

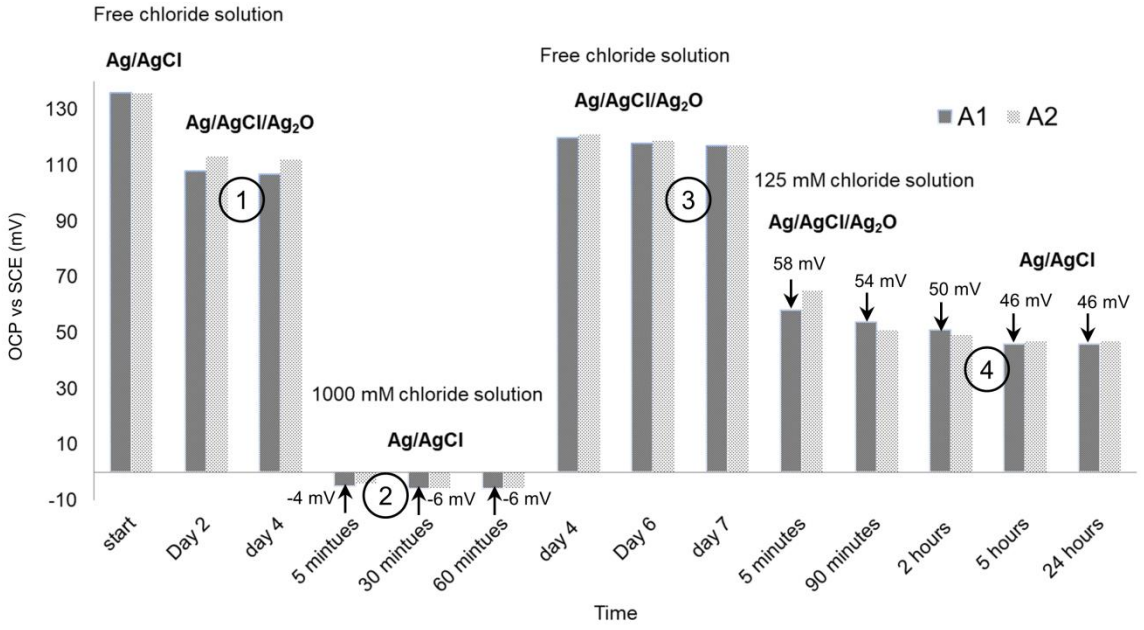

Figure 4.9: Sensor's response in chloride-free and chloride-containing simulated pore solution (SPS).

Reversibility is important in view of the Ag/AgCl sensor's application in cement-based materials. This has a high practical significance for chloride sensors embedded in chloride-free reinforced concrete. In these conditions, the sensor should remain "active" and accurately respond to altered chloride ions concentration in the medium.

The reversibility of the sensor was tested in chloride-free and chloride-containing alkaline simulated pore solution (Table 4.2, test series 5). In the absence of chloride ions the transformation of AgCl to Ag_2O is a preferential reaction, in accordance to Eq. 4.2. The resulting OCP in chloride-free simulated pore solution (SPS) will be anodic (more positive) and will stabilize around values reflecting the equilibrium at a $Ag/AgCl/Ag_2O$ interface. Upon addition and/or increase of the chloride ions concentration the OCP shifts to cathodic (more negative) values, reflecting the equilibrium at a Ag/AgCl interface. The rate at which these OCP changes occur, and/or are reversed, reflect the altered chloride content in the medium, as well as the level of the sensor's reversibility.

The above considerations are illustrated in Fig. 4.9. The sensor (two replicates of sensor A, i.e. A1 and A2) was immersed in chloride-free SPS for four days, followed by addition of chloride at the level of 1000mM. Next, the sensor was transferred to a fresh chloride-free SPS for three subsequent days, after which the chloride content was changed to the level of 125 mM in the solution. The OCP was recorded during all above steps and the established values can be summarized in four main regions – Fig. 4.9. In regions ① and ③, the OCP values were anodic, while in regions ② and ④, a cathodic shift was observed. Region ① presents the point of immersion of the sensors in chloride-free SPS and subsequent treatment, where after four days the OCP stabilizes from the initial ca. 137 mV to around 110 mV. This change reflects the gradual transformation of silver chloride to silver oxide and the establishment of an equilibrium at the $Ag/AgCl/Ag_2O$ interface.

Upon the addition of chlorides in region ② (adjusted to 1000 mM), the sensors react to the chloride ions and the OCP shifts to ca. -6 mV. This corresponds to a change of the $Ag/AgCl/Ag_2O$ interface in region ① to a Ag/AgCl interface, dominant for region ②. The OCP stabilization in region ② was achieved between 30 and 60 min.

In the next step, region ③, the chloride sensor was re-immersed in chloride-free SPS. In region ③ the initial OCP was ca. 120 mV, i.e. more anodic than the final OCP measured in region ① (110 mV) and in the direction of approaching the OCP of a sensor at the beginning of treatment (region ①, ca. 137 mV). This means that the sensor's surface partially recovered the originally present AgCl layer in conditions of sufficient chloride concentration in the medium (region ②,1000 mM in this case), by following a transformation of Ag_2O to AgCl. With prolonged treatment in the chloride-free condition in region ③, the established OCP at ca. 110 mV is again due to Ag_2O formation, similar to that observed at the end of region ①.

Upon the subsequent addition of chlorides in region ④, reaction mechanisms as in region ② were relevant. However, in region ④ the chloride concentration was adjusted to a lower level, i.e. 125 mM. The OCP reached to values of 46 mV and stabilization occurred within 5h of treatment. If the time to establishment of a stable OCP in regions ② and ④ is to be assessed, clearly higher chloride content (1000 mM, region ②) triggers a faster stabilization (30 min) versus the 5h, needed at lower chloride content (region ④). Therefore, the reversibility of the sensor is related to the transformation rate of Ag_2O to AgCl, which is dependent on the chloride concentration in the external medium.

As above mentioned, the transformation of AgCl to Ag_2O is responsible for the deviation of the sensor's response from the expected response (determined by the Eq. 4.2). In the following section the transformation of AgCl to Ag_2O is confirmed by analyzing the sensors' surface chemistry and in-depth composition of the AgCl layer before and after conditioning in alkaline solution.

4.3.5 Composition of the AgCl layer before and after treatment in SPS

The high-resolution spectra from the surface XPS analysis of sensor A are presented in 4.10 and 4.11. Figures 4.10a and 4.11a depict the Ag3d spectra. A similar XPS result as discussed for anodized Ag foil at regime A was observed for anodized Ag foil at regime C, the result of which is presented as additional information in Annex C of this thesis. The characteristic Ag3d states of different Ag compounds and metallic Ag (Ag°) are very close to each other, i.e. within 0.5 eV [Kaushik, 1991; Ferraria et al., 2012]. Hence, the binding energy positions of Ag3d do not unambiguously identify the actual state of Ag. To support the information from binding energy records, the AgMNN Auger peaks were used (Figs. 4.10b 4.11b). For comparative purposes, the AgMNN peak for Ag° is shown in Figs. 4.10b, 4.11b. modified Auger parameter ($\acute{\alpha}$ = KE(AgMNN) + BE($Ag3d_{5/2}$) was used for a more accurate determination of the chemical state of Ag, thus eliminating the surface effects of electrostatic charging [Wagner, 1975]. The KE(AgMNN) represents kinetic energy of the Auger electron and BE($Ag3d_{5/2}$) represents binding energy of the photoelectron. The binding energy for oxygen (O1s) is also presented in Figs. 4.10c and 4.11c. The obtained surface atomic concentrations are given in Table 4.4 (the NIST XPS database was also consulted, [Naumkin al., 2012]). The XPS analysis does not claim absolute values for chemical composition of the AgCl layers, but provides an accurate (quantitative) comparison of equally handled samples, before and after conditioning in alkaline medium. The NIST XPS database was consulted [Naumkin et al., 2012] for the binding and kinetic energies of the elements.

Surface XPS analysis

The $Ag3d_{5/2}$ core level for the sensor's surface before treatment in alkaline medium was measured at 367.9 eV, Fig.4.10a). The $Ag3d_{5/2}$ core level, measured at 367.9 eV can be attributed to more than one compound, e.g. Ag_2CO_3 (367.80 eV), Ag_2O (367.9), AgO (368.0) and AgCl (368.1), [Moulder et al., 1992]. The kinetic energy of the AgMNN peak (Fig.4.10b),

was measured at 356.2 eV, different (with 0.4 eV to 0.8 eV) from the energy corresponding to purely Ag_2O (356.6 eV), AgO (356.9 eV) and AgCl (355.4). The binding energy of the O1s peak, Fig. 4.10c, was measured at 532.2 eV, slightly different from 532.4 eV, attributed to Ag-C-H-O and/or OH^- (or water adsorption) [Weaver and Hoflund, 1994]. Supportive evidence for water adsorption is the recorded shoulder at 533.5 eV in the O1s pattern. Therefore, the binding energy for O1s (532.2 eV), different from the energy of 530.7 eV for O1s in AgO, together with the kinetic energy of 356.2 eV for the AgMNN peak indicate the presence of mainly AgCl on the surface of the untreated sensor. The recorded surface atomic concentration ratio for the untreated sensor was Ag : Cl : O = 10 : 1.6 : 1 (Table 4.4). The chloride/oxygen ratio of 1.6, together with the above observations, confirm the presence of mainly AgCl on the sensor's surface. This is in agreement with the XPS survey scans for untreated sensors as discussed in Chapter 3.

After treatment of the sensor in NaOH solution, the $Ag3d_{5/2}$ peak at 368.1 eV (Fig. 4.10a) cannot be assigned to one compound. The AgMNN peak for the treated sensor (Fig. 4.10b) shows a similar pattern to the untreated sensor, but with a broader high-energy peak (356.2 eV). This broadening is characteristic in situations, where Ag exists in a different state (e.g. Ag°, AgOH, Ag_2O, AgO). The Auger parameter with a value of 724.1 can be equally attributed to AgO (724.2), Ag_2O (724.3) and AgCl (723.5) [Kaushik, 1991]. The surface atomic concentration in Table 4.4 gives a ratio of Ag : Cl : O = 3.3 : 0.2 : 1. Clearly the chloride/oxygen ratio decreases from 1.6 before immersion in NaOH solution to 0.2 after immersion in NaOH solution. Such a decrease in chloride/oxygen ratio is an indication for de-chlorination of the AgCl on the sensor's surface after immersion in NaOH solution.

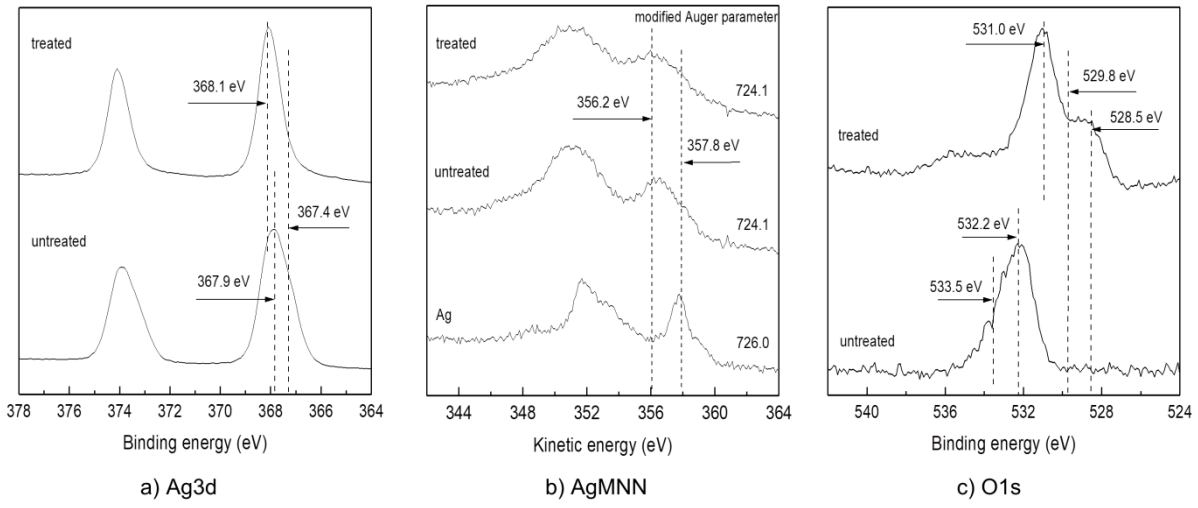

Figure 4.10: High-resolution surface XPS spectra of sensor A before and after conditioning in NaOH solution: a) Ag3d photoelectron lines; b) AgMNN – Auger lines; c) O1s photoelectron lines.

Table 4.4: Atomic concentration (at. %) of elements on the surface and in-depth of the AgCl layer for sensor A before and after conditioning in alkaline medium (C1s (carbon), O1s (oxygen), Ag3d (silver), Cl2p (chloride) and N1s (sodium)).

Sputtering	C1s, carbon (%)	O1s, oxygen (%)	Ag3d, silver (%)	Cl2p, chloride (%)	N1s, sodium (%)	chloride / oxygen
Untreated sensor (before conditioning in NaOH solution)						
0 min	10	7	70	11	2	1.6
5 min (sputtering)	0.7	0.1	92.2	7	-	70
10 min (sputtering)	0.4	0.1	93.5	6	-	60
Treated sensor (after conditioning in NaOH solution)						
0 min	7	17	57	3	15	0.2
5 min (sputtering)	2	17	50	0.3	31	0.02
10 min (sputtering)	1.5	17	50	0.2	31	0.01

The O1s pattern (Fig. 4.10c) for the treated sensor depicts a shift towards lower energies and a characteristic broadening, starting at 528.5 eV. Low energy peaks or low energy broadening in the O1s pattern (from 528.5 eV to 531.0 eV) indicate oxygen in metal oxides. The significantly different O1s patterns for the sensor before and after treatment (Fig. 4.10c) along with the above features clearly show the strong contribution of silver oxides on the sensor's surface after treatment.

In-depth XPS analysis

The Ag3d, AgMNN and O1s patterns in depth of the AgCl layer, before and after treatment in alkaline medium, are presented in Fig. 4.11. As can be seen, the patterns for different elements after 5 minutes and 10 minutes sputtering were similar. The $Ag3d_{5/2}$ peak for untreated and treated sensors was measured at 368.2 eV, Fig. 4.11a. The AgMNN peak and Auger parameter for untreated and treated sensors were measured at ~357.8 eV and 726 eV, respectively, Fig. 4.11b. The $Ag3d_{5/2}$ peak cannot be assigned to just one silver compound, while the AgMNN peak and Auger parameter were attributed to Ag°. The significant contribution of Ag° in depth of the AgCl layer, in both untreated and treated sensors, does not have a straightforward explanation. The detection of Ag° was partly attributed to the sensitivity of AgCl to the test condition [Sharma et al., 1982; Turner et al., 1984]. Despite all the similarities between the XPS spectra for untreated and treated sensors, the secondary AgMNN peak for the untreated sensor at 355.5 eV (Fig. 4.11b) cannot be observed in the treated sensor. This peak is an indication for AgCl (355.4 eV) in the untreated sensor. The absence of such a peak in the treated sensor is due to de-chlorination of the sensor after conditioning in alkaline medium.

The O1s pattern for untreated and treated sensors was significantly different (Fig. 4.11c). The O1s pattern for the untreated sensor is characterized by a flat plateau in all range of binding energies, indicating the absence of oxide compounds in depth of the AgCl layer (Fig. 4.11c). In contrast, the O1s pattern for the treated sensor presents different O1s peaks. The broadening of the O1s pattern at high binding energy (from 536.0 eV to 536.5 eV) indicates the presence of sodium-containing compounds. The O1s peak with binding energy of 532.4 eV is due to the adsorbed H_2O or oxygen-containing contamination, e.g. NaOH. The broadening of the O1s pattern at low binding energy (from 528.0 eV to 529.8 eV) represents the silver oxide compounds (Ag_2O and/or AgO). The atomic concentration for untreated sensor gives a ratio of Ag : Cl : O = 935 : 60 : 1, while for treated sensor this is Ag : Cl : O = 2.9 : 0.008 : 1. The chloride/oxygen ratio decreases from 60-70 to 0.01-0.02 after treatment in alkaline medium. The dechlorination of the AgCl layer and transformation of AgCl to silver oxide compounds are the main cause for such a significant decrease in the chloride content of the layer.

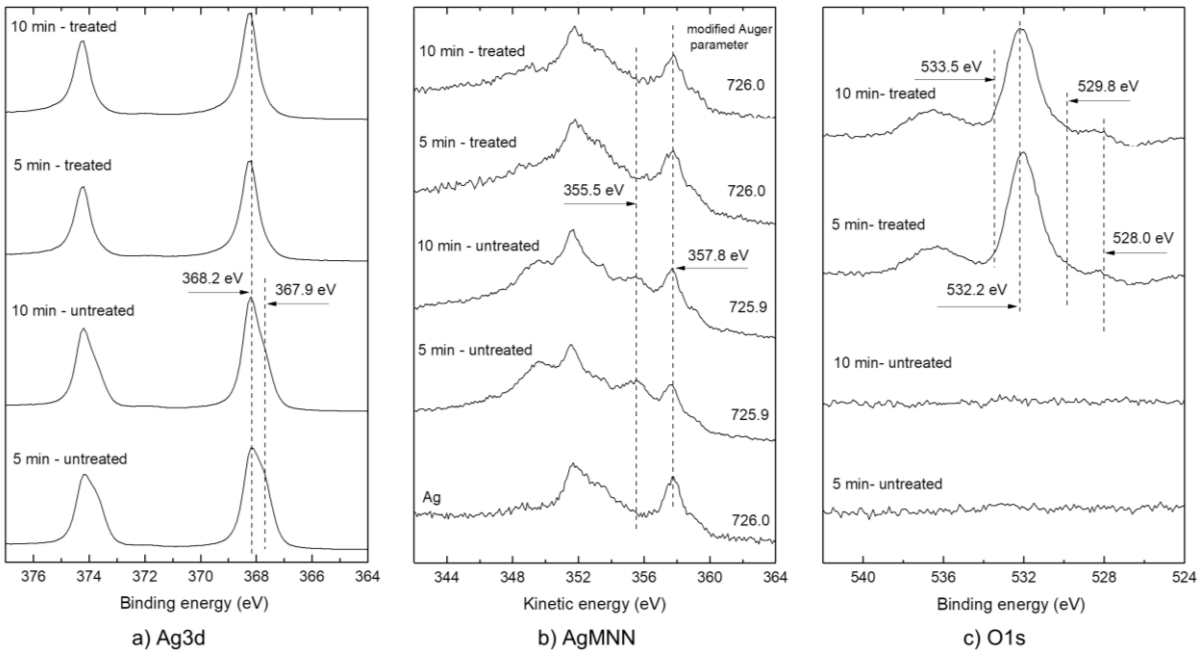

Figure 4.11: High-resolution XPS spectra of AgCl layer of sensor A (5 minutes and 10 minutes sputtering) before and after conditioning in NaOH solution: a) Ag3d photoelectron line; b) AgMNN – Auger lines; c) O1s photoelectron lines.

Based on the XPS-test results AgCl must be the main silver compound that forms during the anodization process of sensor preparation. Conditioning of the sensor in NaOH solution results in de-chlorination of the AgCl layer and formation of silver oxide-rich layer (Ag_2O and AgO). This process subsequently shifts the sensor's OCP towards cathodic values, e.g. 100 mV vs. SCE.

4.4 Conclusions

In this chapter the OCP response of sensors with different thickness, morphology and microstructure of the AgCl layer (sensors A, B, C and D) were monitored in alkaline solution. Considering the criteria of stability and reproducibility of the sensors' response in a chloride-free or chloride-containing medium, a choice was made to study the performance of sensors A only in all subsequent tests in this chapter. Based on the results of the experiments the following conclusions can be drawn:

- The variation in sensors' response in highly alkaline medium depends on the anodization regime used for the sensor's preparation and the chloride concentration in the medium. Sensor A (prepared at a low current density of 0.5 mA/cm^2) was found to be more sensitive, reliable and reproducible than sensors B, C and D (prepared at high current densities of 1, 2 and of 4 mA/cm^2).
- The sensor's calibration curve in alkaline solution represents an excellent linear relationship (R^2=0.999) between the activity of chloride ions and the sensor's OCP at chloride concentration higher than 8 mM.

- The chloride detection limit is alkalinity-dependent. In the pH range of concrete pore solution (12.6-13.6) the detection limit is 4 mM chloride content. Below this limit the hydroxide ions interfere with the sensors' response.
- In chloride-free medium AgCl gradually transforms to silver oxides. The process is reversible, i.e. AgCl will gradually recover upon the addition (or in a subsequent presence) of chloride ions. The time needed for gradual transformation of silver oxides to AgCl and a subsequently stable Ag/AgCl response depends on the chloride concentration in the medium, impeded at lower chloride concentration (e.g. 125 mM) and relatively rapid at high chloride content (e.g. 1 M).
- The instability of a AgCl layer is a major drawback for the application of a Ag/AgCl electrode as chloride sensor in chloride-free alkaline medium. In this condition the sensor's OCP shifts towards more anodic values. This is in line with the transformation of silver chloride to silver oxide. XPS analysis (sensors' surface and in depth of the AgCl layer) confirms that this instability is related to AgCl de-chlorination and transformation of the Ag/AgCl interface to a more complex, Ag/AgCl/Ag_2O interface.

The experimental evidence in this chapter indicates a well-defined feasibility for the application of Ag/AgCl electrodes as chloride sensors in alkaline medium, as concrete. In this regard, the chloride detection limit and reaction constraints at the sensor's surface for the sensitivity and reversibility of the sensors are taken into account.

4.5 References

Angst, U., Elsener, B., Larsen, C. K. and Vennesland, O. (2010). Potentiometric determination of the chloride ion activity in cement-based materials, *Journal of Applied Electrochemistry*, Vol. 40(3), p. 561–573.

Angst, U. and Vennesland, O. (2009), Detecting critical chloride content in concrete using embedded ion selective electrodes–effect of liquid junction and membrane potentials, *Materials and Corrosion*, Vol. 60(8), p. 638-643.

Climent-Llorca, M. A., Viqueira-Perez, E. and Lopez-Atalaya, M.M. (1996), Embeddable Ag/AgCl sensors for in-situ monitoring chloride contents in concrete, *Cement and Concrete Research*, Vol. 26(8), p. 1157–1161.

De Vera, G., Climent, M. A., Anton, C., Hidalgo, A. and Andrade, C. (2010). Determination of the selectivity coefficient of a chloride ion selective electrode in alkaline media simulating the cement paste pore solution, *Journal of Electro analytical Chemistry*, Vol. 639(1-2), p. 43-49.

Dobos, D. (1975). *Electrochemical data: a handbook for electrochemists in industry and universities*, Elsevier Science and Technology.

Du, R. G., Hu, R. G., Huang, R. S. and Lin, C. J. (2006). In Situ Measurement of Cl- Concentrations and pH at the Reinforcing Steel/Concrete Interface by Combination Sensors, *Analytical Chemistry*, Vol. 78 (9), p. 3179-3185.

Duffo, G. S., Farina, S. B. and Giordano, C. M. (2009). Characterization of solid embeddable reference electrodes for corrosion monitoring in reinforced concrete structures, *Electrochimica Acta*, Vol. 54(3), p. 1010-1020.

Elsener, B., Zimmermann, L. and Bohni, H. (2003). Non-destructive determination of the free chloride content in cement-based materials, *Materials and Corrosion*, Vol. 54 (6), p. 440–446.

Femenias, Y. S., Angst, U., Caruso, F. and Elsener, B. (2016). Ag/AgCl ion-selective electrodes in neutral and alkaline environments containing interfering ions, *Materials and Structures*, Vol. 49(7), p. 2637-2651.

Ferraria, A.M., Carapeto, A.P. and Botelho Do Rego, A.M. (2012). X-ray photoelectron spectroscopy:

Silver salts revisited, *Vacuum*, Vol. 86(12), p. 1988-1991.
Jin, M. Xu, J., Jiang, L., Xu, Y. and Chu, H. (2015). Investigation on the performance characteristics of chloride selective electrode in concrete, *Ionics*, Vol. 21(10), p. 2981–2992.
Karthick, S., Kwon, S. J., Lee, H. S., Muralidharan, S., Saraswathy, V. and Natarajan, R. (2017). Fabrication and evaluation of a highly durable and reliable chloride monitoring sensor for civil infrastructure, *RSC Advances*, Vol. 7(50), p. 31252-31263.
Kaushik, V. K. (1991). XPS core level spectra and Auger parameters for some silver compounds, *Journal of Electron Spectroscopy and Related Phenomena*, Vol. 56(3), p. 273-277.
McCarter, W. J. and Vennesland, Ø. (2004). Sensor systems for use in reinforced concrete structures, *Construction and Building Materials*, Vol. 18(6), p. 351-358.
Montemor, M.F., Alves, J.H., Simoes, A.M., Fernandes, J.C.S., Lourenco, Z., Costa, A.J.S., Appleton, A.J. and Ferreira, M.G.S. (2006). Multiprobe chloride sensor for in situ monitoring of reinforced concrete structures, *Cement and Concrete Composites*, Vol. 28(3), p. 233-236.
Moulder, F., Sticke, W. F., Sobol, P. E. and Bombel, K. D. (1992). *Handbook of X-ray Photoelectron Spectroscopy*, Vol. Second edition, J. Castain, Ed., Minnesota, USA: Perkin-Elmer Corporation, Physical Electron Division.
Muralidharan, S., Saraswathy, V., Madhavamayandi, A., Thangavel, K. and Palaniswamy, N. (2008). Evaluation of embeddable potential sensor for corrosion monitoring in concrete structures, *Electrochimica Acta*, Vol. 53(24), p. 7248-7254.
Naumkin, A.V., Kraut-Vass, A., Gaarenstroom, S.W. and Powell, C.J. (2012). *NIST X-ray Photoelectron Spectroscopy Database*, NIST Standard Reference Database 20, Version 4.1. Nat'l Std. Ref. Data Series (NIST NSRDS).
Polk, B. J., Stelzenmuller, A., Mijares, G., MacCrehan, W. and Gaitan, M. (2006). Ag/AgCl microelectrodes with improved stability for microfluidics. *Sensors and Actuators B: Chemical*, Vol. 114(1), p. 239-247.
Scofield, J. H. (1976). Hartree-Slater subshell photoionization cross-sections at 1254 and 1487 eV, *Journal of Electron Spectroscopy and Related Phenomena*, Vol. 8(2), p. 129-137.
Sharma, J., Dibona, P. and Wiegand, D. A. (1982). XPS studies of the photodecomposition of AgCl, *Applications of Surface Science*, Vol. 11, p. 420-424.
Shi, X., Ye, Z., Muthumani, A., Zhang, Y., Dante, J. F. and Yu, H. (2015). *A Corrosion Monitoring System for Existing Reinforced Concrete Structures* (No. FHWA-OR-RD-15-14).
Shirley, D. A. (1972). High-resolution X-ray photoemission spectrum of the valence bands of gold, *Physical Review B*, Vol. 5(12), p. 4709-4714.
Suzuki, H. and Taura, T. (2001). Thin-film Ag/AgCl structure and operational modes to realize long-term storage, *Journal of the Electrochemical Society*, Vol. 148(12), p. E468-E474.
Svegl, F., Kalcher, K., Grosse-Eschedor, Y. J., Balonis, M. and Bobrowski, A. (2006). Detection of Chlorides in Pore Water of Cement-Based Materials by Potentiometric Sensors, *Journal of the Rare Metal Materials and Engineering*, Vol. 35(3), p. 232-237.
Turner, N. H., Dunlap, B. I. and Colton, R. J. (1984). Surface analysis: x-ray photoelectron spectroscopy, Auger electron spectroscopy and secondary ion mass spectrometry, *Analytical Chemistry*, Vol. 56(5), p. 373-416.
Wagner, C.D. (1975). Chemical shifts of Auger lines, and the Auger parameter, *Faraday Discuss. Chem. Soc.*, Vol. 60, p. 291-300.
Weaver, J. F. and Hoflund, G. B. (1994). Surface characterization study of the thermal decomposition of Ag_2O, *Chemistry of materials*, Vol. 6(10), p. 1693-1699.

Chapter 5

Sensor's response in cementitious materials (interpretation of the sensor's response)

Abstract

In Chapter 3, chloride sensors were produced in different anodization regimes. In Chapter 4, the sensors' response in model solutions was assessed. In this chapter the performance of the chloride sensor in cementitious materials with different mix design and cement composition is studied. The chloride sensor's response in a cement matrix depends on the pore solution composition and the distribution of hydration products in the vicinity of the sensor. The chloride sensor is embedded in paste cylinders with different water-to-powder ratio (w/p) and type of cement. The specimens are immersed in alkaline solution with different chloride concentration. The open circuit potential (OCP) of the chloride sensor is discussed with respect to the presence of interfering ions (hydroxide and sulfide ions) in the medium and hydration products around the sensor.

In addition, the chloride content inferred from the sensor's response is compared to the one obtained from destructive water-soluble and acid-soluble chloride methods. The observed difference between the chloride contents, determined by these methods, is discussed.

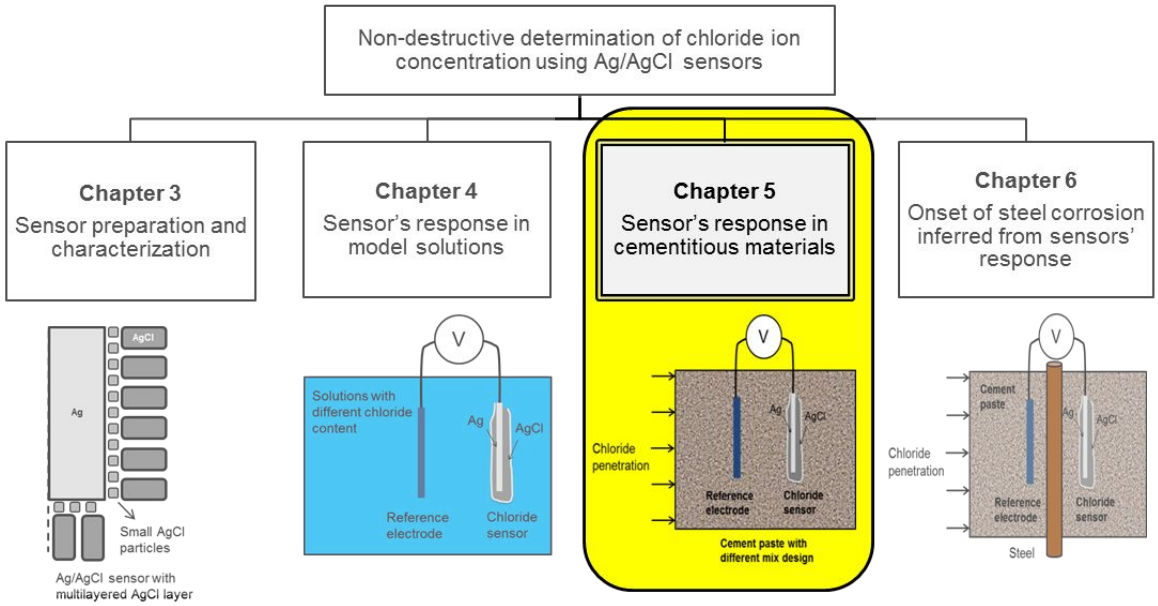

Structure of research process and sequence of chapters in the thesis

---

Part of this chapter is based on the paper:

Pargar, F., Koleva, D. A. & van Breugel, K. (2015). Potentiometric response of chloride sensors in cementitious materials of varying chemical composition and water-to-cement ratio, In proceeding of EUROCORR 2015, Graz, Austria.

5.1 Introduction

The presence of hydration products around the sensor affects the sensor's performance. In this regard, the water-to-cement ratio (w/c), type of cement and pore solution composition play an important role. The cement hydration products cover a certain percentage of the surface of the sensor, preventing a direct contact of the sensor's full active surface with the electrolyte. The lower amount of free chloride in these areas is subsequently reflected in the overall sensor's OCP.

A low w/c ratio (e.g. 0.35) results in a dense interfacial zone between cement paste and aggregate, not much different from the density of the bulk cement matrix [Delagrave et al., 1996]. The interfacial zone between aggregate and cement paste with a high w/c ratio (e.g. 0.5) often has a high content of calcium hydroxide and ettringite, elongated C-S-H particles and fewer unhydrated cement particles, compared to that of the bulk matrix [Brandt, 2009]. A high content of ettringite would result in a more porous interfacial zone [Scrivener et al., 2004]. It was shown that Portlandite, unlike ettringite, effectively fills up the pores at the interface with aggregate or embedded steel [Bentur and Ish-Shalom, 1974; Page et al., 1981; Zimbelmann, 1985; Maso, 2004; Page, 2009]. A similar trend can be expected at the interface between the sensor and cement paste. The formation of Portlandite and ettringite depends on the composition of cementitious materials [van Breugel, 1997; Asbridge et al., 2002]. Consequently, the importance of cementitious mix design and cement composition for the sensor's response needs further investigation. This subject has been rarely discussed in the literature so far.

In this Chapter 5 the influence of water-to-powder ratio (w/p) and type of cement on the sensor's response are studied. The chloride content inferred from the sensor's response is compared to the one obtained by destructive test methods (acid-soluble and water-soluble chlorides). The observed difference between the chloride contents, determined by the aforementioned methods, is discussed with respect to the chloride binding ability of cement hydration products and w/p ratio of the mixture. In other words, Chapter 5 answers the questions: i) how do cementitious mix design and cement composition affect the sensor's response; ii) what is the relation between the chloride content inferred from the sensor's response and the one obtained by destructive test methods.

5.2 Materials and procedures

5.2.1 Specimen preparation and exposure condition

The paste cylinders with cast-in Ag/AgCl sensors were the specimens, subject to investigation in this chapter (Fig. 5.1). Mix design and cement compositions of the specimens are presented in Table 5.1. The chloride sensors were embedded in paste cylinders made of C_3S with and without addition of C_3A and gypsum. Different mixtures were employed to study the influence of calcium aluminum sulfate phases, such as ettringite, on the chloride sensor's response. The performance of the chloride sensor was also assessed in cement pastes made of ordinary Portland cement (CEM I 52.5 N) and blast-furnace slag cement, i.e. CEM III/A 52.5 N with 35-64% of slag [NEN-EN 197-1, 2011]. The pure cement phases were supplied by Mineral Research Processing, France. The cement producer was ENCI cement, The Netherlands.

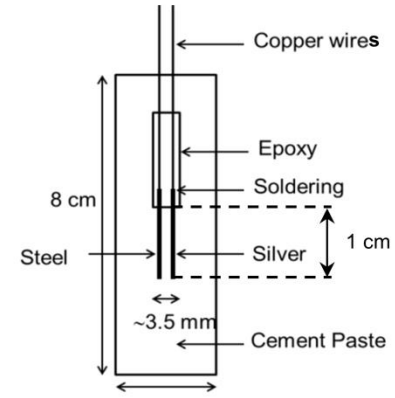

a) Longitudinal section of the specimen

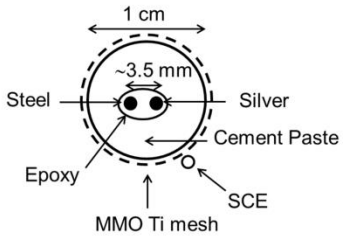

b) Cross section of the specimen

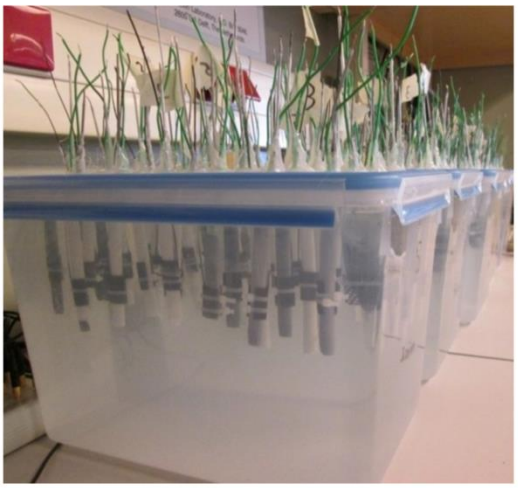

c) Specimens immered in the solution

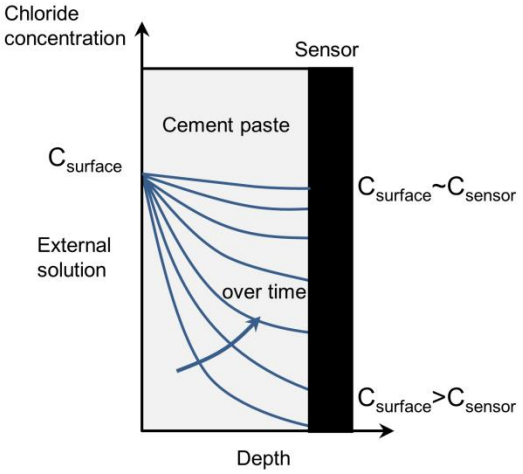

d) Chloride penetration from the outer surface of the specimen towards the sensor

Figure 5.1: (a) schematic representation of a longitudinal section of the specimen; (b) schematic representation of a cross section of the specimen (designed as 3-electrode type cell); (c) specimens immersed in alkaline solution with different chloride concentration; (d) schematic representation of chloride penetration from external solution towards the sensor's surface.

The sensors were prepared at anodization regime A (0.5 mA/cm^2, specified in Chapter 3). The steel wires[1] (1 mm diameter), drawn from low carbon steel, were acetone-cleaned and epoxy-insulated. The sensors and the steel rods were cast-in together in the cylinders in such a manner, that only 1 cm length of both sensor and steel were exposed to the environment (Figs. 5.1a,b), leaving an active surface of 0.39 cm^2 for the steel rods and 0.32 cm^2 for the sensors.

After curing in a sealed condition for 30 days, the specimens were immersed in a simulated pore solution (0.1 M KOH + Sat. $Ca(OH)_2$), pH=13, with different chloride concentrations (10 mM, 100 mM, 500 mM and 1000 mM). A control case, based on chloride-free solution, was also tested. To keep the concentration of chloride ions as constant as possible, the volume ratio of solution to paste was maintained at 40 [Qiang et al., 2011], and the containers were closed to prevent evaporation (Fig. 5.1c). Two replicates per specimen type were immersed in the solutions. The specimens were retained in the solutions for 300 days to reach a state of equilibrium between the chloride ions in the solution and that in the specimens (Fig. 5.1d).

[1] The steel rods are subject to discussion in Chapter 6

Table 5.1: Mix designs of the cementitious materials that were used in this study for preparation of the specimens and the chloride content in the solution that specimens were immersed.

w/p - w/c ratio	Designated code	C_3S	C_3A	Gypsum	CEM I 52.5N	CEM III/A 52.5N	Chloride content in the solution (mM)
0.35	C_3S	100	–	–	–	–	0, 10, 100, 500, 1000
	C_3S+C_3A	87	10	3	–	–	
0.4	C_3S	100	–	–	–	–	
	C_3S+C_3A	87	10	3	–	–	
	CEM I	–	–	–	100	–	
	CEM III	–	–	–	–	100	
0.5	C_3S	100	–	–	–	–	
	C_3S+C_3A	87	10	3	–	–	

5.2.2 Test methods

5.2.2.1 Open circuit potential (OCP) measurement

The cylindrical specimens were immersed in chloride-free and chloride-containing solutions (Table 5.1, last column). The OCP of the sensors versus saturated calomel electrode (SCE) was monitored during 300 days using PGSTAT 302N potentiostat.

5.2.2.2 XRD analysis

The XRD test was carried out on the paste samples after 300-day immersion of the specimens in chloride-free and chloride-containing solutions (Table 5.1, last column). The dried paste samples were grinded until the particle size was smaller than 125 µm. The powdered samples were placed in an aluminum sample holder for XRD analysis. The XRD test was performed using a Philips PW 1830 powder X-ray diffractometer equipped with X'pert High Score Plus software. The scans ranged from 5° to 70° 2θ, with a step size of 0.02° 2θ and a dwell time of 2 seconds per step.

5.2.2.3 Chemical analysis

The acid-soluble and water-soluble chloride contents in the bulk matrix were determined after 300-day immersion of the specimens in chloride containing solutions (Table 5.1). The acid-soluble and water-soluble chlorides were extracted from the dried paste samples following the standard procedures [RILEM TC 178-TMC, 2002; RILEM TC 178-TMC, 2002a; ASTM C1152, 2003; ASTM C1218, 2008], as explained in Chapter 2. The extracted solutions were analyzed for chloride content with Spectroquant ® NOVA 60 photometer and a chloride test set-up (Chloride Cell Test – NO. 114730). The photometer and the chloride test set-up are commercially available from Merck company.

5.3 Results and discussion

5.3.1 OCP measurement of chloride sensor

5.3.1.1 Pure cement phases

The OCP response of the chloride sensor in specimens made of C_3S with and without

addition of C_3A and gypsum was recorded periodically during 300 days (Figs. 5.2 to 5.4). Since the sensor's OCP for two replicates per specimen type followed a similar trend, only the average OCP value is presented in these figures. The alteration in the sensor's OCP was evaluated with respect to the w/p ratio, hydration products and the chloride concentration in the medium (10 mM to 1000 mM). The main features of the OCP response of the sensors in C_3S and C_3S+C_3A specimens with different w/p ratio (0.35, 0.4, 0.5) are discussed in what follows.

w/p=0.35: The OCP response of the chloride sensors over time was arbitrarily divided into three regions: I, II and III (marked regions in Figs. 5.2 to 5.4). From the beginning up to day 80 (region I, Fig. 5.2), the OCP of all sensors (except those in the control case "no Cl") sharply dropped towards cathodic values (e.g. Fig. 5.2). From day 80 to day 140 (region II, Fig. 5.2), OCP stabilization of the sensor was observed. The sensor's OCP has reached a more stable potential after 140 days (region III, Fig. 5.2). The time required for the stable sensor's OCP in C_3S specimens (Fig. 5.2a) is longer than that in C_3S+C_3A specimens (Fig. 5.2b). This trend was mainly observed in the control case (chloride-free) and in the case of 10 mM chloride concentration (Fig. 5.2a). It can be expected that the sensor in C_3S specimens was in contact with the pore solution with higher pH than C_3S+C_3A specimens. The high pH of the pore solution in C_3S is due to the combined effect of low w/p ratio and the absence of C_3A and gypsum in the mixture. It is known that the formation of calcium sulfoaluminate in C_3S+C_3A specimens reduces the alkalinity of the pore solution due to alkali binding by calcium sulfoaluminates [Taylor, 1998; Chappex and Scrivener, 2012]. Therefore, the pH of the pore solution in C_3S+C_3A specimens would be lower than that in C_3S specimens. Moreover, the volume of the pore solution in a matrix with high w/p ratio (e.g. 0.5) would be higher than that in a matrix with low w/p ratio (e.g. 0.35). The reduction in the volume of pore solution increases the concentration of soluble alkalis (NaOH and KOH) and the pH of pore solution [Gascoyne, 2002]. As a result, the pH of the pore solution in C_3S specimens would be highest, due to the synergetic effect of low w/p ratio and less binding of alkalis in this specimen. The pore solution with high pH will lead to de-chlorination of the AgCl layer. That is why a lower stability of the sensor's OCP in C_3S specimens was observed after 140 days of immersion in chloride-free and 10 mM chloride-containing solutions (Fig. 5.2a, region III) in comparison to that in C_3S+C_3A (Fig. 5.2b).

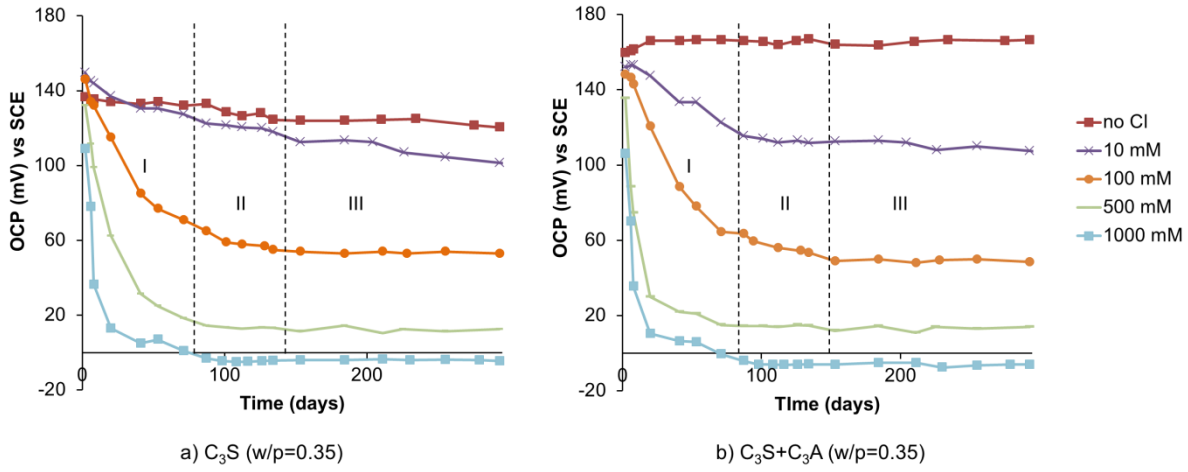

Figure 5.2: The OCP response of chloride sensor in specimens made of cement components, (a) C_3S only and (b) C_3S, C_3A and gypsum, with w/p=0.35 over time.

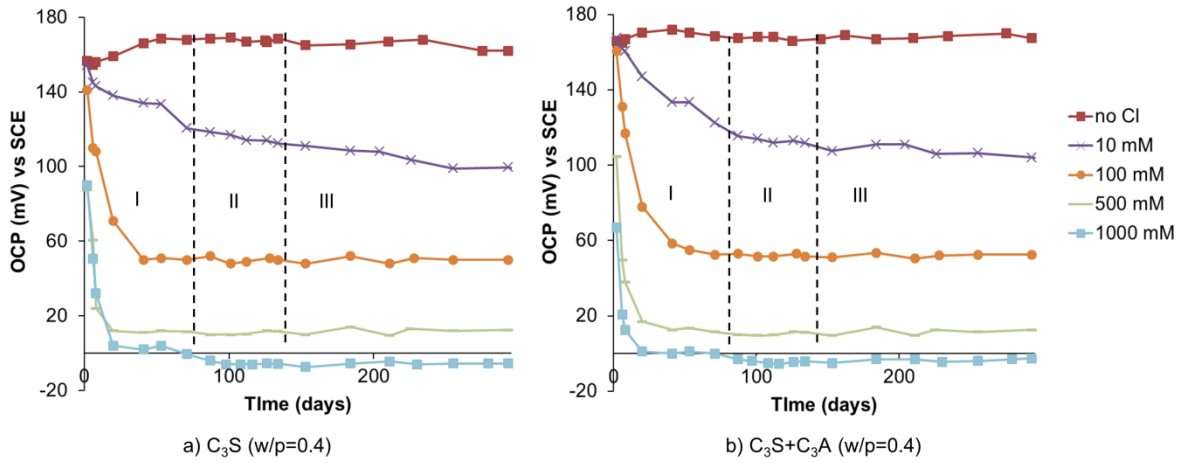

Figure 5.3: The OCP response of chloride sensor in specimens made of cement components, (a) C_3S only and (b) C_3S, C_3A and gypsum, with w/p=0.4 over time.

In the chloride-free solution, the sensor's OCP in C_3S specimen was lower than 140 mV, while the sensor's OCP in C_3S+C_3A specimen was higher than 150 mV. The more cathodic OCP of the sensor in C_3S specimen is another evidence for the influence of high pH of the pore solution and de-chlorination of the AgCl layer on the sensor's response.

w/p=0.4: The sharp decrease in the sensor's OCP towards cathodic values at the beginning of immersion (region I, Fig. 5.3) is followed by a more stable OCP in the later period (regions II and III, Fig. 5.3).

w/p=0.5: In chloride-containing mediums, the sensor's OCP in specimens with w/p=0.5 stabilized earlier than the sensor's OCP in specimens with w/p=0.35 and 0.4 (compare Fig. 5.4 with Figs. 5.3 and 5.2).

In the chloride-free medium (control case), a significant cathodic shift of the sensor's OCP in C_3S+C_3A specimen after 140 days of immersion (region III, Fig. 5.4) is observed. In this case, the sensor's OCP shifted from around 150 mV (regions I and II, Fig. 5.4b) to values between 70-100 mV (region III, Fig. 5.4b) at which the sensor' OCP was unstable and cannot be described by the Nernst equation for a Ag/AgCl interface. It was reported that the sensor's OCP in this condition is dependent on adventitious impurities in the medium [de Vera et al.,

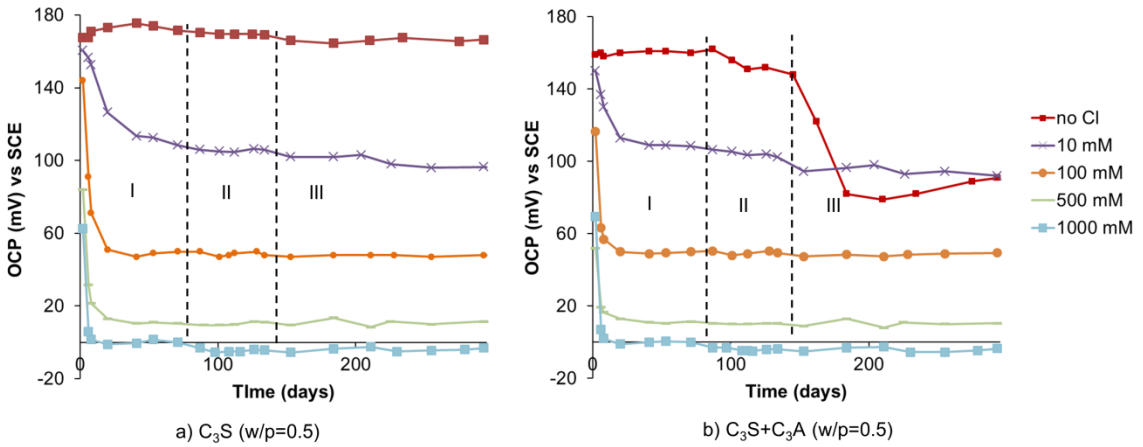

Figure 5.4: The OCP response of chloride sensor in specimens made of cement components, (a) C_3S only and (b) C_3S, C_3A and gypsum, with w/p=0.5 over time.

2010; Suzuki et al., 1998]. This instability of the sensor was not observed in C_3S (w/p=0.5) – control case (Fig. 5.4a), despite the same w/p ratio. The instability of the chloride sensor in C_3S+C_3A (w/p=0.5) is discussed in the following paragraph with respect to the presence of different hydration product at the sensor's surface. ESEM/EDS results at the interface between sensor and paste are presented, for illustrative purposes, in Annex D of this thesis.

In C_3S specimens, the reaction of C_3S with water produces C-S-H and Portlandite. In C_3S+C_3A specimens, the replacement of C_3S by C_3A *and* gypsum (the mix designs were presented in Table 5.1, Section 5.2.1) generates not only C-S-H and Portlandite, but also calcium sulfoaluminate hydrates with different sulfate content, such as monosulfate and ettringite. In C_3S+C_3A specimen the ettringite would at least partly replace the Portlandite at the sensor's surface (Fig. 5.5a). The Portlandite, unlike ettringite, fills up the pores at the paste-sensor interface more effectively (see Fig. 5.5c) [Bentur and Ish-Shalom, 1974; Page et al., 1981; Zimbelmann, 1985; Page, 2009]. Deposition of Portlandite at the sensor/paste interface limits the dissolution of silver compounds into the surrounding medium (Fig. 5.5c). In contrast, the presence of ettringite, i.e. a porous hydration product, facilitates de-chlorination of the AgCl layer, resulting in the presence of metallic silver (Ag°) at the sensor's surface (Fig. 5.5a). The larger amount of Ag° subsequently results in an unstable sensor's OCP. Because of this de-chlorination, the lifetime of the sensor embedded in C_3S+C_3A (w/p=0.5) paste is <150 days (region III, chloride-free in Fig. 5.4) in comparison to that in C_3S (w/p=0.5) paste. Such a trend was not observed at lower w/p ratios (0.4 and 0.35). The dense matrix of cementitious material with low w/p ratio decreases the diffusivity of the matrix and, consequently, the rate of AgCl de-chlorination. Hence, the lifetime of the sensor in a cement-based matrix with low w/p ratio (i.e. 0.4, 0.35) is longer. In addition, in pastes with a low w/p ratio the volume of pore water is also lower, resulting in pore water with higher ionic strength [Flatt and Bowen, 2003]. The activity of chloride ions is lower in a solution with higher ionic strength. The dense matrix of hydration products, together with a reduced chloride ions activity at the sensor's surface, result in a sensor's response different from the one expected for a Ag/AgCl interface. This is further discussed in the next section.

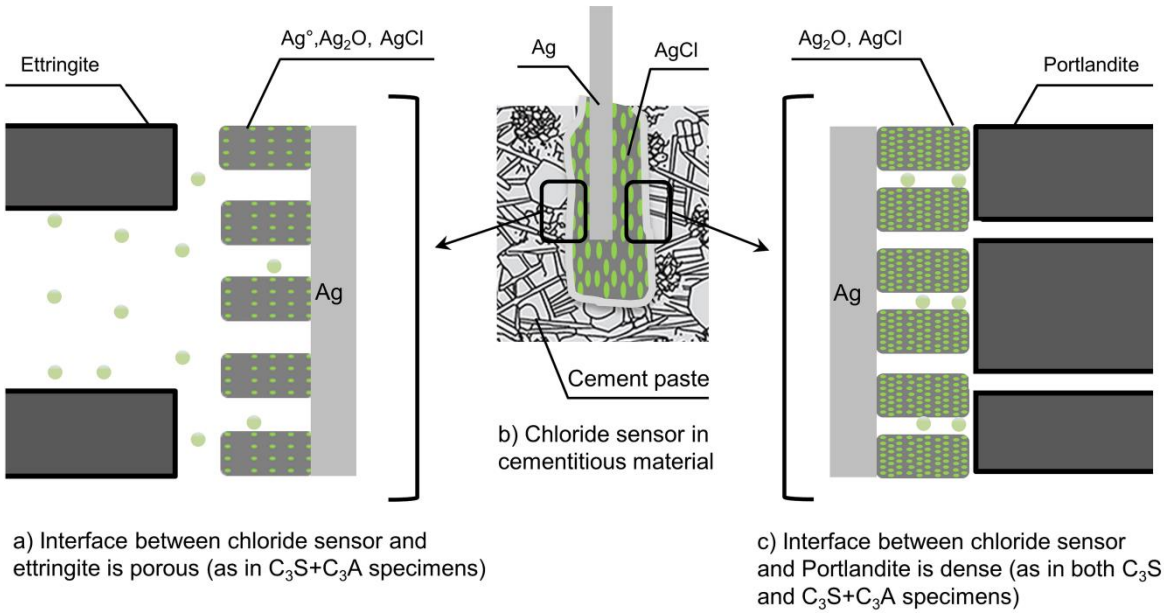

Figure 5.5: Schematic representation of coverage of the chloride sensor's surface by ettringite (a) and Portlandite (c).

5.3.1.2 Discussion on the influence of w/p ratio of the pastes on the sensor's OCP

As discussed above, the presence of cement hydration products around the sensor affects the sensor's OCP response. Figure 5.6 shows the sensor's OCP after 150-day immersion of specimens in solutions with different chloride content, when most of the sensors demonstrate a stable OCP value. The expected response for a Ag/AgCl interface in chloride-containing solutions is also presented in Figs. 5.6a,b. The sensor's OCP in chloride-free solution is above 150 mV. The exception is C_3S (w/p=0.35) (discussed in previous Section 5.3.1.1). In the chloride-containing solutions, the sensor's response depends on the w/p ratio of the mixture. Table 5.2 shows the range of sensor's OCP in C_3S and C_3S+C_3A specimens with different w/p ratio and chloride concentration. It is known that 1 mV difference in the sensor's OCP corresponds to approximately 4% difference in chloride concentration [Angst et al., 2010]. Hence, the OCP difference in Table 5.2 is also presented as percentage difference in chloride concentration. At 10 mM chloride concentration (Table 5.2), the embedded sensors in specimens with w/p=0.35 presented a more anodic OCP (17-23 mV), compared to those in specimens with w/p=0.5. The more anodic OCP of the sensor in pastes with w/p=0.35 (C_3S: 121 mV; C_3S+C_3A: 126 mV in Table 5.2) is an indication for deviation of the sensor's OCP from the expected response for a Ag/AgCl interface (Figs. 5.6a,b). The expected response for a Ag/AgCl interface is 104 mV, which is close to the OCP for specimens with w/p=0.5 (C_3S: 104 mV; C_3S+C_3A: 103 mV in Table 5.2). The dense matrix in specimens with w/p=0.35 together with a lower chloride ions activity at the sensor's surface are the main reasons for the observed deviation. By increasing the chloride concentration to 100 mM and higher, the difference between the sensor's OCP in specimens with w/p ratios of 0.35 and 0.5 decreased to 2-6 mV (Table 5.2). This OCP difference (2-6 mV) is equivalent to 8-24% difference in chloride concentration (Table 5.2). This trend demonstrates the lower importance of the w/p ratio for the sensor's response with increasing chloride concentration.

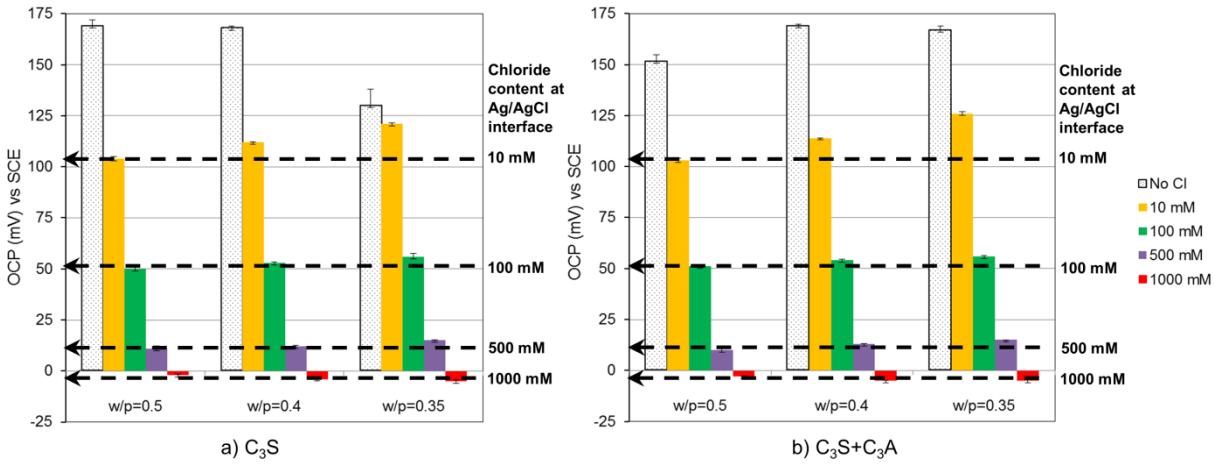

Figure 5.6: The OCP response of chloride sensor after 150-day immersion of (a) C_3S specimens and (b) C_3S+C_3A specimens in solutions with different chloride concentration. The expected response for a A/AgCl interface at different chloride concentration is specified by dashed line.

Table 5.2: The range of sensor's OCP for C_3S and C_3S+C_3A specimens with different w/p ratio and chloride concentration. The OCP difference (mV) was also presented as percentage in terms of chloride concentration.

Chloride concentration in external solution (mM)	Sensor's OCP in C_3S pastes			ΔOCP mV (%*)	Sensor's OCP in C_3S+C_3A pastes			ΔOCP mV (%*)
	w/p				w/p			
	0.5	0.4	0.35		0.5	0.4	0.35	
10	104	112	121	17 (68)	103	114	126	23 (92)
100	50	53	56	6 (24)	51	54	56	5 (20)
500	11	12	15	4 (16)	10	13	15	5 (20)
1000	-2	-4	-5	3 (12)	-3	-5	-5	2 (8)

* OCP difference in mV multiply by 4 equals to percentage (%) difference in chloride concentration.

Additionally and in contrast to expectations, at a chloride concentration of 1000 mM the sensor in specimens with w/p=0.5 was more anodic (2-3 mV, Table 5.2) than that in specimens with w/p=0.35. The more anodic OCP of the sensor in specimens with w/p=0.5 is due to the combined effects of w/p ratio of the mixture and the high chloride concentration (1000 mM). The formation of large crystals of Portlandite is pronounced in the mixture with higher w/p ratio (i.e. 0.5) (discussed in Section 5.3.1.1). The dissolution of Portlandite increases with increasing the chloride concentration beyond 500 mM [Glasser et al., 1999; Galan and Glasser, 2015]. The lower activity of chloride ions in the pore solution with higher ionic strength (i.e. w/p=0.5 in 1000 mM chloride concentration) results in a more anodic OCP of the sensor.

Table 5.2 shows the effect of additions as C_3A and gypsum on the sensor's response in 10 mM chloride concentration. At 10 mM chloride concentration, the difference between the sensor's OCP in C_3S specimens with w/p ratios of 0.5 and 0.35 was 17 mV. This difference in C_3S+C_3A specimens increased to 23 mV. Hence, addition of C_3A and gypsum increased the OCP difference from 17 mV to 23 mV. This is due to the presence of different hydration products that builds up a more complex matrix in the C_3S+C_3A specimens. Consequently, the influence of w/p ratio on the sensor's OCP is larger in a mixture with a more complex matrix and different hydration products.

5.3.1.3 CEM I and CEM III (w/c=0.4)

The OCP response of the chloride sensor in CEM I and CEM III specimens is presented in Fig. 5.7. As previously discussed in Chapter 2 and schematically shown in Figs. 2.10 and 2.11, the sensor's OCP in Portland cement paste and slag cement paste can be different. In the presence of chloride ions in Portland cement paste, AgCl is the dominant reaction product on the sensor's surface. Therefore, the sensor's response in Portland cement paste follows the Nernst equation for a Ag/AgCl interface (Chapter 2, Eq. 2.4), reflecting the chloride ions activity in the medium (Fig. 5.7a). In contrast, the interference of sulfide ions with the sensor in CEM III specimens can limit the reaction of AgCl formation on the sensor's surface. During the hydration of slag cement, Ag_2S forms on the sensor's surface due to the chemical reaction of S^{2-} with the AgCl layer. The rate of Ag_2S formation makes the sensor's OCP deviating from the expected response (compare Fig. 5.7a with Fig. 5.7b).

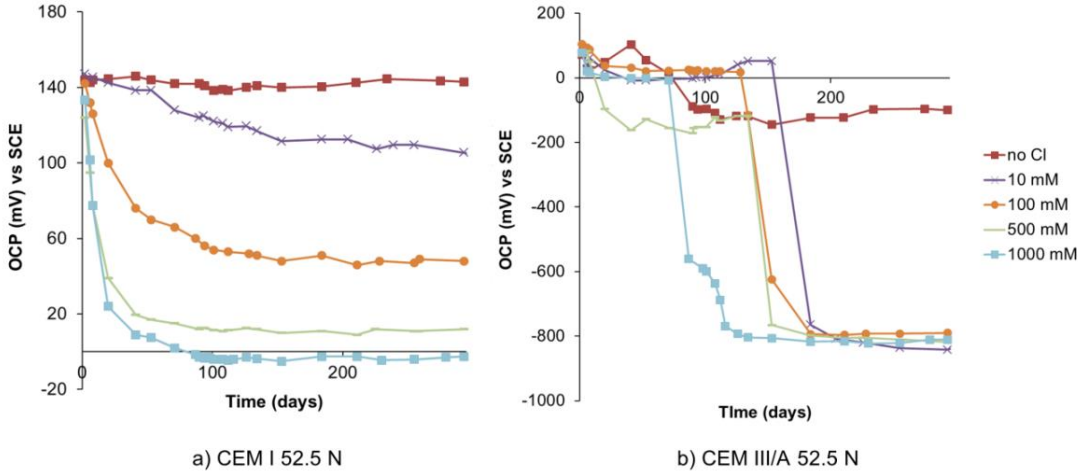

Figure 5.7: The OCP response of chloride sensor in cement paste made of (a) CEM I 52.5 N and (b) CEM III/A 52.5 N with w/c=0.4 over time.

The initially anodic OCP response of the sensor in CEM III specimens (0-120 mV, Fig. 5.7b) was due to the mixed potential of a $AgCl/Ag_2O/Ag_2S$ interface. During immersion in the alkaline solution, the sensor's OCP shifted towards -200 mV in the control case (chloride-free) and -800 mV in chloride-containing solutions. The negative sensor's OCP was the consequence of the high amount of Ag_2S on the sensor's surface. The presence of Ag_2S on the sensor's surface shifts the sensor's OCP towards the standard potential of a Ag/Ag_2S electrode (-935 mV vs. SCE) [Ives and Janz, 1961] and the potential for Ag_2S formation in an alkaline solution (ca. -790 mV) [Conyers and White, 1999; Wan et al., 2015].

For the CEM III specimens, the sensor's OCP in the chloride-containing mediums is more negative than the sensor's OCP in the control case (chloride-free). The concentration of silver ions on the silver substrate increases with increasing the chloride concentration in the medium. Hence, higher amount of Ag_2S can form on the sensor's surface. The increase in the content of Ag_2S on the sensor's surface shifts the sensor's OCP towards negative OCP values (e.g. -800 mV). By increasing the chloride concentration from 10 mM to 1000 mM, the OCP of the sensor shifts to negative potential values after a shorter time interval (Fig. 5.7b). This observation is mainly due to the high tortuosity and low connectivity of the pore network in slag cementitious material, which controls the rate of chloride penetration in CEM III specimens [Ortega et al., 2017]. The rate of chloride penetration is lower for 10 mM chloride concertation. Consequently, chloride ions need longer time to reach the sensor's surface and shift the sensor's OCP towards negative potential. Although the chloride content could not be inferred from the sensor's response, the significant change in the sensor's OCP indicates the presence of free chloride ions at the sensor's surface.

The sensor's OCP in the initial period (10 days) of immersion in the solution is anodic (e.g. 50 to 120 mV) in comparison to the sensor's OCP in the later stage (e.g. -100 to -800 mV after 10 to 150 days). The anodic OCP response indicates the initially lower amount of Ag_2S on the sensor's surface. Therefore, the initial sensor's response is the potential from $AgCl/Ag_2O$ with a slight contribution from Ag_2S. In contrast, the negative OCP of the sensor in the later period of immersion is mainly the potential from Ag_2S with minor impact from AgCl and Ag_2O.

Based on the thermodynamic principles and Gibbs free energy (Chapter 2, Section 2.5.3), the chloride sensor in slag cement paste would recover after immersion in the chloride-containing solution due to transformation of Ag_2S to AgCl. However, the negative sensor's OCP in chloride-containing solution (e.g. -800 mV, Fig. 5.7b) did not indicate the

sensor's recovery. The significantly lower solubility product of Ag_2S ($K_{sp}Ag_2S=1.6\times10^{-49}$ at 25°C) than those of AgCl ($K_{sp}AgCl=1.8\times10^{-10}$ at 25°C) and Ag_2O ($K_{sp}Ag_2O=2\times10^{-8}$) is the main reason for the lack of the sensor's sensitivity to chloride ions [Raynauld and Laviolette, 1987; Graedel, 1992; Payer et al., 1995; Rajbhandari, 2009; Levard et al., 2012]. Moreover, Ag_2S, being the predominant reaction product of silver in CEM III specimens, results in the lack of possibility for the sensor to recover.

In the next section X-ray diffraction (XRD) analysis test results are discussed. XRD was employed to characterize the chloride-containing hydration products in the specimens after 300-day immersion in solutions with different chloride concentration. The obtained information is used in Section 5.3.3 to justify the difference between the chloride content inferred from the sensor's response and the one obtained from destructive test methods, i.e. acid-soluble and water-soluble chlorides.

5.3.2 XRD analysis

The XRD analysis of the paste samples was carried out to characterize the chloride-containing hydration products in the specimens. The XRD test was performed on the paste samples after 300-day immersion in solutions with different chloride concentrations. The diffraction peaks in XRD patterns were analyzed by X'Pert High Score Plus software (Philips, Netherlands) for identification of crystalline phases and in particular the Friedel's salt (Figs. 5.8 to 5.11). A compound is to be detected in a sample, when the 2θ of the main peaks of that compound (derived from X'Pert High Score database) match the XRD pattern.

The XRD patterns of C_3S samples with different chloride concentration are shown in Fig. 5.8. The well-pronounced Portlandite (CH) and anhydrate alite (Ca_3SiO_5, named as CSi) were found in all the samples. The peaks of CH were mainly observed at 2θ of 18°, 34.1°, 47.1°, 50.8°, 54.3°, 62.6° and 64.3°, while the shallow peaks of CSi were detected at 2θ of 29.1°, 32.1°, 33.8°. In the absence of aluminate phases in C_3S samples, the Friedel's salt cannot exist in the samples. Hence, the peak of Friedel's salt was not found in XRD patterns.

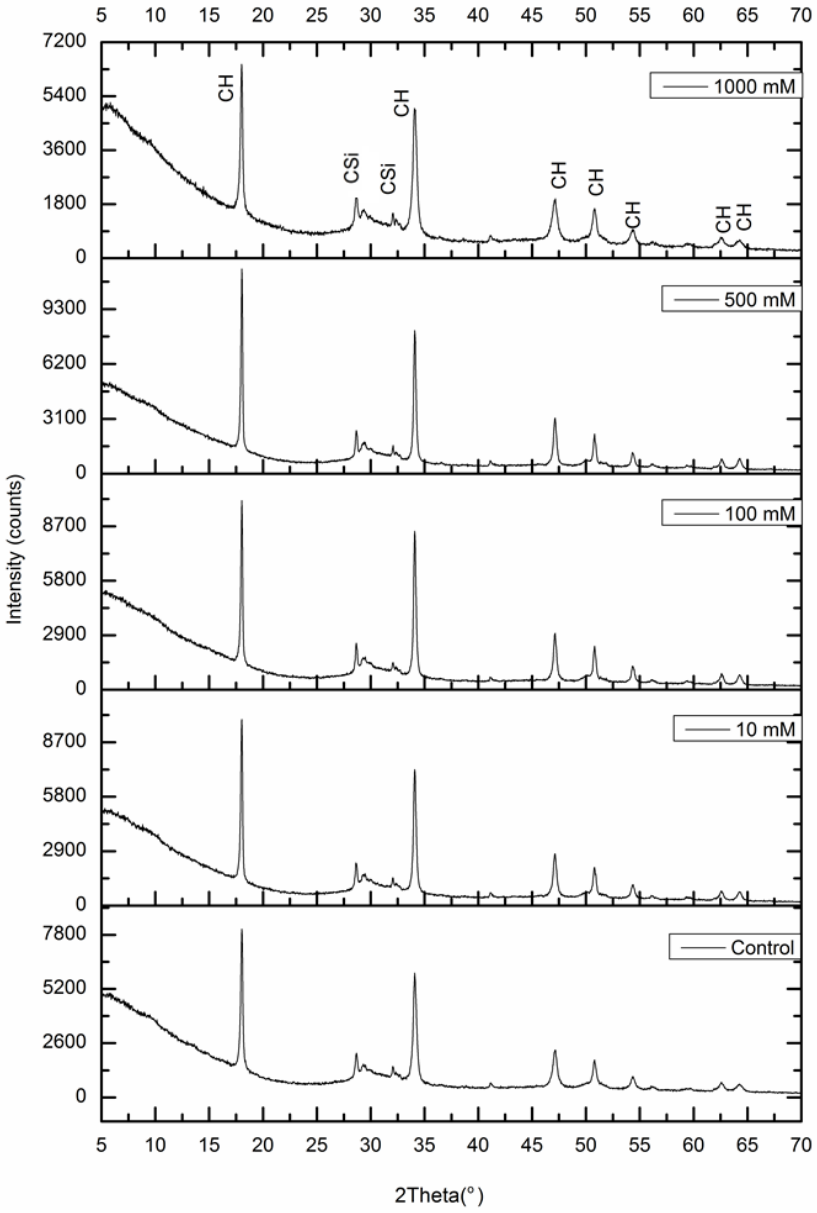

Figure 5.8: XRD pattern of C_3S (w/p=0.4) paste after 300 days of immersion in solutions with different chloride concentration.

The XRD patterns of C_3S+C_3A specimens revealed strong CH peaks (Fig. 5.9). The shallow and multi-peak patterns with lower intensity were for calcium aluminum sulfate phases and chloride-containing compounds. Detection of AFm phases by XRD analysis is not straightforward, as they generally have low crystallinity [Matschei, 2007]. Therefore, the aluminate sulfate and calcium aluminate hydroxide were not pronounced in the XRD patterns with reasonable accuracy and high score. The main chloride-containing compounds were Friedel's salt and hydrocalumite containing chloride ($Ca_2AlClH_{10}O_8$) (2θ =11.2°, 22.5°, 23.1°, 31°, 39°). These compounds were named as FS in Fig. 5.9. Hydrocalumite ($Ca_2AlClH_{10}O_8$) is a Ca–Al phase with a high capacity for chemical binding of chloride ions to its particular structure [Evans and Duan, 2006; Yang et al., 2013; Yoon et al., 2014]. The FS peaks were found at 100, 500 and 1000 mM chloride concentrations with the stronger intensity at higher chloride concentration.

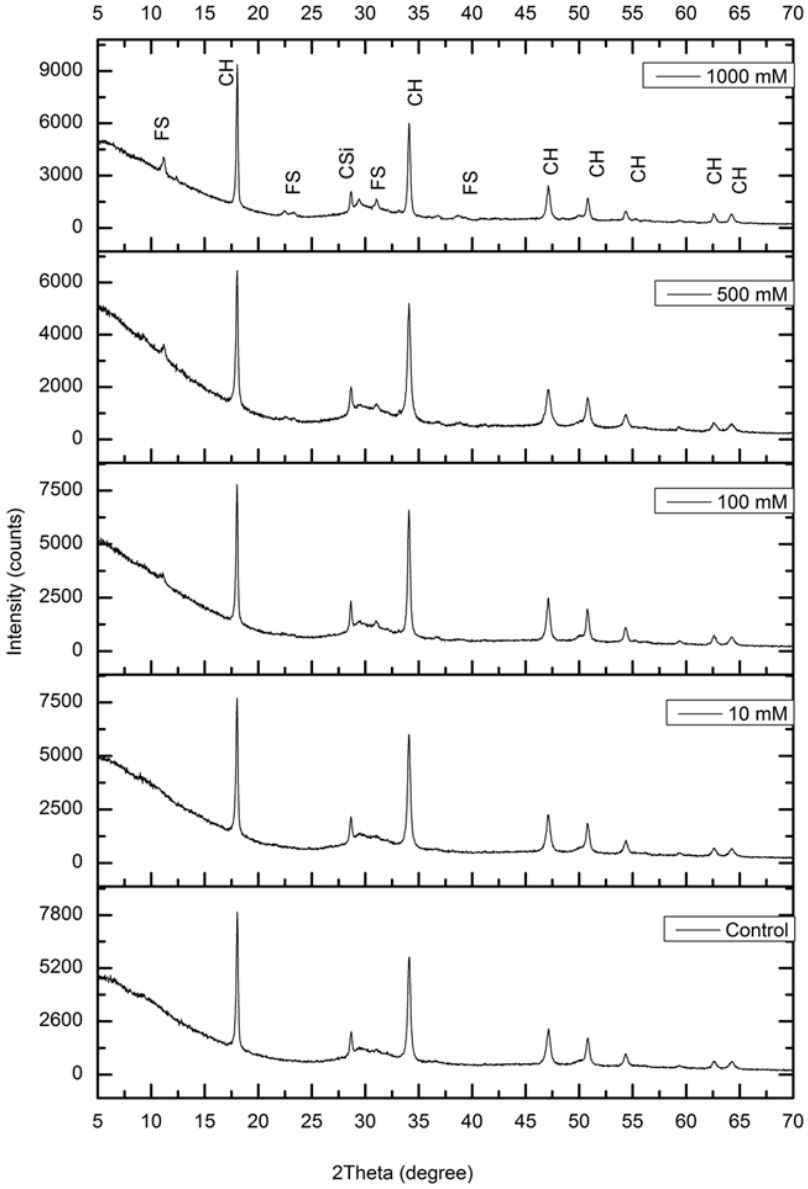

Figure 5.9: XRD pattern of C_3S+C_3A (w/p=0.4) paste after 300 days of immersion in solutions with different chloride concentration.

The sharp peaks in XRD patterns of CEM I specimens were for CH phase (Fig. 5.10). The main shallow peaks were the characteristic of the following phases: unhydrated alite (Ca_3SiO_5, 2θ =29.3°, 32.1°, 51.8°) and belite (Ca_2SiO_4, 2θ =31.2°, 32.5°) named as CSi, $Ca_{54}MgAl_2Si_{16}O_{90}$ (2θ =29.4°, 32.2°, 32.6°, 41.3°) named as CMASi and hydrocalumite containing chloride ($Ca_4Al_2Cl_2H_{20}O_{16}$, 2θ =11.2°, 22.5°) named as FS. The presence of hydrocalumite instead of Friedel's salt was an indication of higher chloride content, entrapped into the bulk matrix of cement paste. The FS phase was detected at chloride concentration of higher than 100 mM, with a stronger peak intensity at higher chloride concentration. The existence of aluminates in the form of CMASi in all samples indicates that this phase can exist without complete transformation to Friedel's salt even at high chloride concentration.

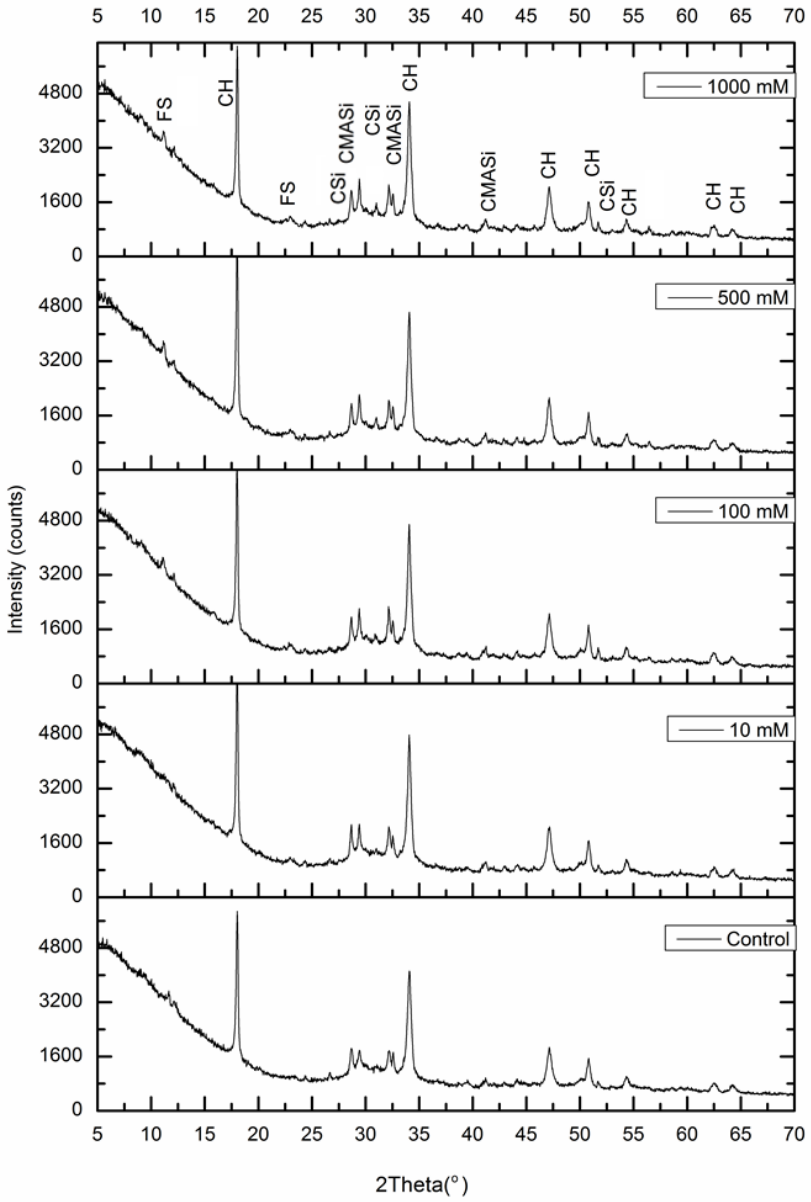

Figure 5.10: XRD pattern of cement paste made of CEM I 52.5N (w/c=0.4) after 300 days of immersion in solutions with different chloride concentration.

The intensity of the CH peak in the CEM III specimen was lower than that in the CEM I specimen (compare Fig. 5.10 and 5.11). The lower intensity of the CH peak in CEM III was mainly due to the reaction of slag with CH to form C-S-H. In addition to the CH peak, the other main peaks in CEM III specimen were: anhydrate alite (Ca_3SiO_5) and belite (Ca_2SiO_4) denoted as CSi, ettringite ($Ca_6Al_2H_{63.5}O_{49.7}S_3$, 2θ=9.1°, 15.8°) (named ET), $Ca_{54}MgAl_2Si_{16}O_{90}$ denoted as CMASi and calcium silicate chloride and calcium aluminate chloride hydrates denoted as FS. Calcium aluminum oxide chloride hydrate is a compound similar to Friedel's salt, but with higher content of chloride. Two main phases of FS with higher intensity were $Ca_4Al_2Cl_2H_{20}O_{16}$ and $Ca_4Al_2Cl_{1.67}H_{0.34}O_{6.34}$ (2θ =11.3°, 22.7°). The peak intensity of these phases increased with increasing chloride concentration. The presence of aluminate containing phases (ET and CMASi) at 1000 mM chloride concentration indicated that these phases can

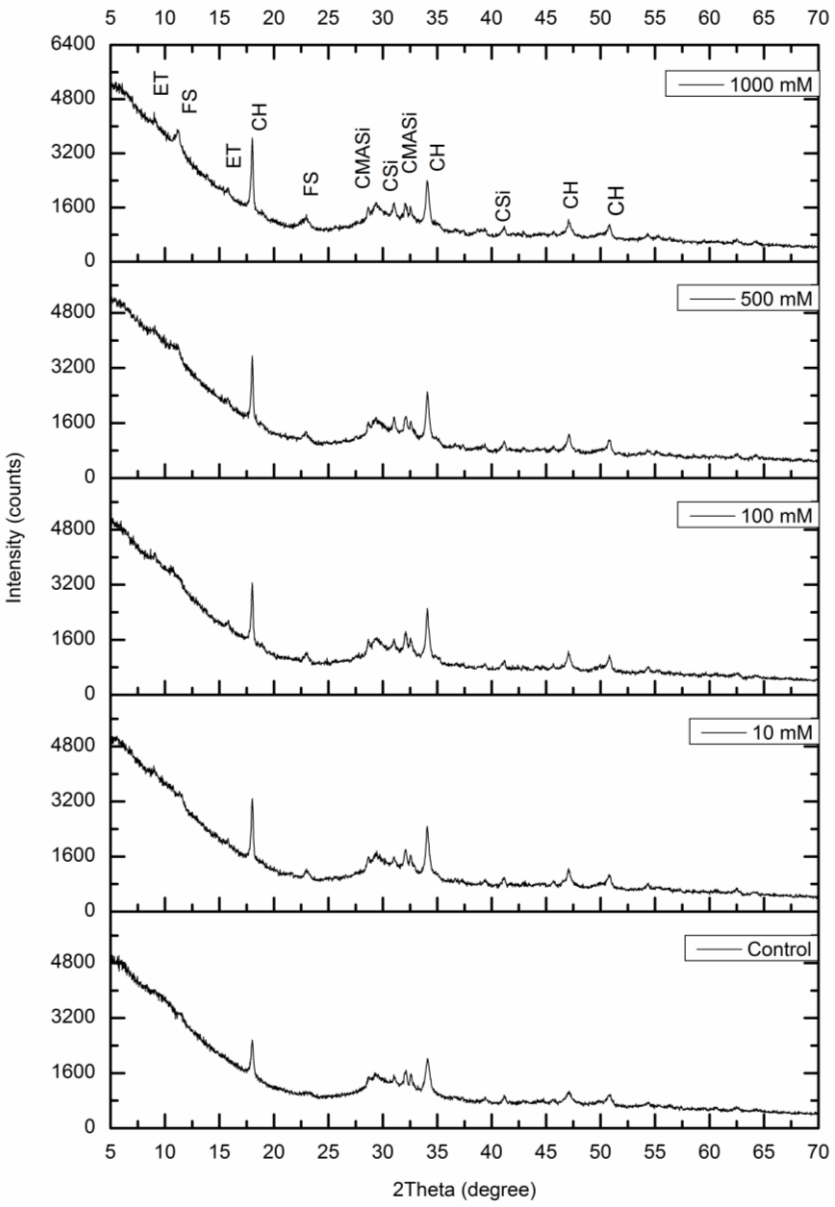

Figure 5.11: XRD pattern of cement paste made of CEM III/A 52.5 N (w/c=0.4) after 300 days of immersion in solutions with different chloride concentration.

exist without complete transformation to Friedel's salt even at such a high chloride concentration.

Based on all above discussions, Friedel's salt was detected in all mixtures, except in C_3S specimens, with the ability to bind chloride ions only *physically*. The chemical binding of chloride (e.g. Friedel's salt) subsequently affects the measured acid-soluble and water-soluble chloride contents. The quantitative information from XRD analysis is used in the next section to describe the difference between acid-soluble and water-soluble chloride contents in the bulk matrix of the specimens and the chloride sensors' readings.

5.3.3 Comparison of chloride contents determined by different methods

A schematic presentation of the potential distribution of free chloride, physically bound chloride and chemically bound chloride in cementitious materials is shown in Fig. 5.12. The influence of free and bound chlorides on the chloride content, determined by different methods, is discussed in this section. Three methods for chloride determination were used: (i) leaching in acid (acid-soluble chloride), (ii) leaching in water (water-soluble chloride) and (iii) potentiometry (chloride sensor's response). The acid-soluble chloride is the total (free+bound) chloride content in cementitious materials. The water-soluble chloride is the free chloride plus *a part* of physically and chemically bound chlorides [RILEM TC 178-TMC, 2002a; Chaussadent and Arliguie, 1999; He et al., 2015]. The sensor can only detect the free chloride content. The distinction of free chloride from water-soluble chloride is difficult [Haque and Kayyali, 1995]. For this reason the measured water-soluble chloride was often considered as the free chloride content [He et al., 2015]. The difference between the water-soluble chloride and the free chloride content inferred from the sensor's response can be significant. This is mainly because the measured water-soluble chloride depends on the amount of bound chlorides released into the water solvent during water-soluble chloride determination. This will be further discussed in this section. The acid-soluble and water-soluble chlorides in the bulk matrix of the specimens are also compared to the free chloride content, inferred from the sensor's response.

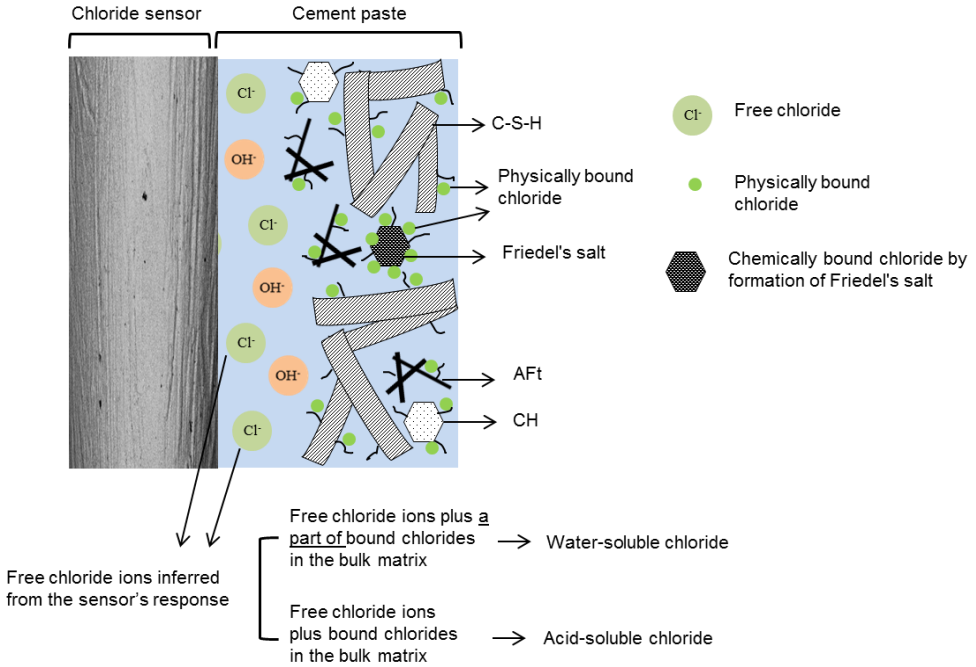

Figure 5.12: The schematic representation of free chloride ions, chemically bound chloride and physically bound chloride in the cement paste. The sensor's response relies on the free chloride content, while acid-soluble and water-soluble chlorides depend on the amount of bound chlorides in the matrix.

5.3.3.1 Acid soluble chloride vs. water soluble chloride

The pastes with various w/p ratio (i.e. 0.35, 0.4, 0.5) (Table 5.1) were immersed in solutions with different chloride concentration for a period of 300 days. The acid-soluble and water-soluble chloride contents in C_3S, C_3S+C_3A, CEM I and CEM III specimens were

determined and results are presented in Figs. 5.13 and 5.14. Below, the results for C_3S and C_3S+C_3A specimens are discussed, followed by the results for CEM I and CEM III specimens.

C_3S specimens: In C_3S specimens chloride ions can only be bound physically. As can be seen in Fig. 5.13, the amount of acid-soluble chloride in C_3S specimens is higher than the amount of water-soluble chloride. The difference between acid and water-soluble chlorides is, in fact, the portion of physically bound chloride not released into the water solvent during water-soluble chloride determination [Yuan et al., 2011; Hu et al., 2015; He et al., 2016]. The mechanism of physical adsorption of chloride ions to the surface of hydration products was explained in Chapter 2, Section 2.3.2.2.

C_3S+C_3A specimens: Similar to C_3S specimens, also in C_3S+C_3A specimens the amount of acid-soluble chloride was higher than the amount of water-soluble chloride (Fig. 5.13). The difference between acid and water-soluble chlorides is due to the portion of bound chlorides (chemically and physically) that was not dissolved into the water solvent during the water-soluble chloride determination. The dissolution of physically bound chloride into the water solvent has a similar explanation as given for C_3S specimens (Chapter 2, Section 2.3.2.2). The release of chemically bound chloride into the water solvent significantly increased the measured water-soluble chloride [Kopecsko and Balazs, 2017]. This is more pronounced in 500 mM and 1000 mM chloride concentrations with higher amount of chemically bound chloride (Section 5.3.2).

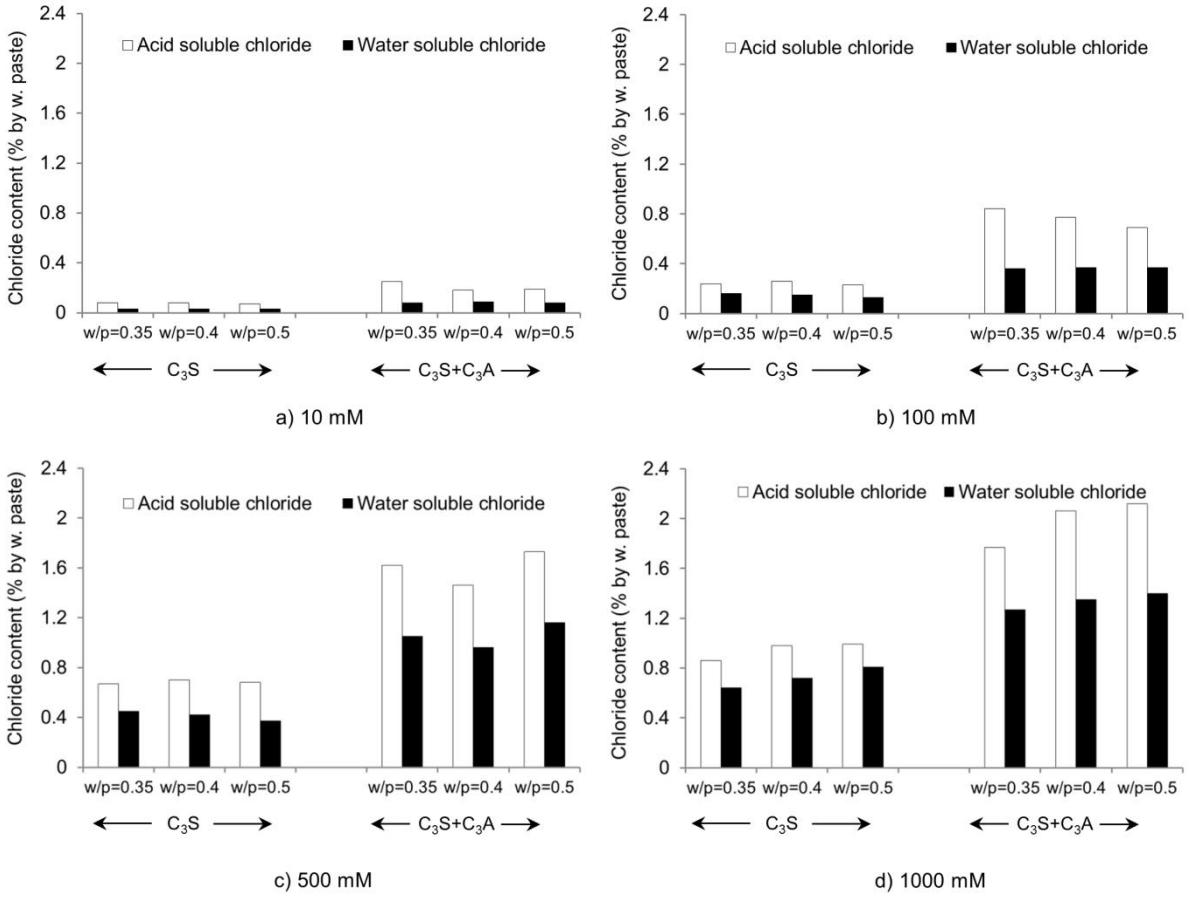

Figure 5.13: The acid-soluble chloride and water-soluble chloride in C_3S and C_3S+C_3A specimens after 300 days of immersion in solutions with different chloride concentration.

The acid and water-soluble chlorides in C_3S specimens were significantly lower than those in C_3S+C_3A specimens (Fig. 5.13). The C_3S specimens have no capacity for chemical binding of chloride ions. The chloride ions can be bound chemically in C_3S+C_3A specimens. The release of chemically bound chloride into the acid and water solvents in C_3S+C_3A specimens is the main reason for the significantly higher acid and water-soluble chlorides.

CEM I specimens: The acid-soluble and water-soluble chloride contents in CEM I specimens, measured after 300 days, are presented in Fig. 5.14a. The amount of acid-soluble chloride was higher than the amount of water-soluble chloride (as expected). This was also observed in C_3S and C_3S+C_3A specimens (Fig. 5.13).

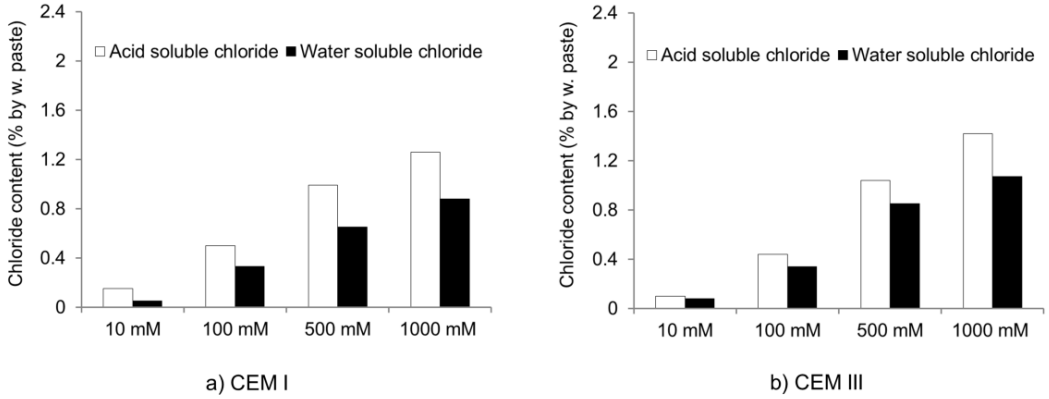

Figure 5.14: The acid-soluble chloride and water-soluble chloride in (a) CEM I and (b) CEM III specimens after 300 days of immersion in solutions with different chloride concentration.

CEM III specimens: Similar to CEM I specimens, after 300 days of immersion in solutions, the acid-soluble chloride in CEM III specimens was higher than the water-soluble chloride (Fig. 5.14b). The slag-containing cementitious materials are known for their ability to bind chloride ions chemically [Dhir et al., 1996; Luo et al. 2003]. Despite this general perception, the water-soluble chloride in CEM III specimens is high compared to that in CEM I specimens. This can be attributed to significant dissolution of chemically bound chlorides into the water solvent, as has been previously reported [Yuan, 2009; Maes et al., 2013]. Moreover, the physical chloride binding ability of CEM III specimens is low [Florea and Brouwers, 2014]. The slag hydration in CEM III specimens consumes calcium hydroxide. Hence, the concentration of calcium ions in the pore solution is reduced. The lower amount of calcium ions decreases the positive surface charge of hydration products (e.g. C-S-H), which can reduce the physical binding of chloride ions [Elakneswaran et al., 2009].

In contrast to what was expected, the acid and water-soluble chloride contents in CEM III specimens are close to those in CEM I specimens (Figs. 5.14a,b). The slag-containing cementitious materials have a tortuous pore network with low pore connectivity [Ortega et al., 2017]. This decreases the chloride penetration in CEM III specimens. Hence, the measured chloride content in CEM III specimens is lower than the maximum chloride content which can be measured in these specimens. That is why acid and water-soluble chlorides in CEM III and CEM I were found almost equal at an age of 300 days.

In the next section the measured water-soluble chloride in C_3S and C_3S+C_3A specimens is compared to the free chloride content inferred from the sensor's response (sensor reading).

5.3.3.2 Water-soluble chloride vs. sensor reading (sensor's response)

C_3S and C_3S+C_3A specimens: The free chloride content inferred from the sensor's response (sensor reading), water-soluble chloride and ratio between these two are shown in Fig. 5.15. In this figure, the left vertical axis is the chloride content and the right vertical axis is the calculated ratio. The ratio of one (right vertical axis in Fig. 5.15) indicates that free chloride content (inferred from the sensor's response) is equal to measured water-soluble chloride. The sensor reading of the chloride content was lower than the measured water-soluble chloride in all chloride concentrations. Hence, the ratio of free chloride content to water-soluble chloride was always significantly less than one (Fig. 5.15). This ratio increased from less than 0.2 in a 10 mM chloride concentration to 0.8 in 500 mM and 1000 mM chloride concentrations. The maximum ratio (>0.8) was observed in C_3S (w/p=0.5) specimens, with only physically bound chlorides, in 500 mM and 1000 mM chloride concentrations. In other words, the ratio was closer to one when cementitious materials with high w/p ratio (e.g. 0.5) and only physical chloride binding ability (e.g. C_3S specimens), were in high chloride concentration (e.g. 500 mM and 1000 mM). These results show that paste composition and w/p ratio, on the one hand, and chloride concentration in the medium, on the other hand, affect the correlation between the free chloride and the water-soluble chloride.

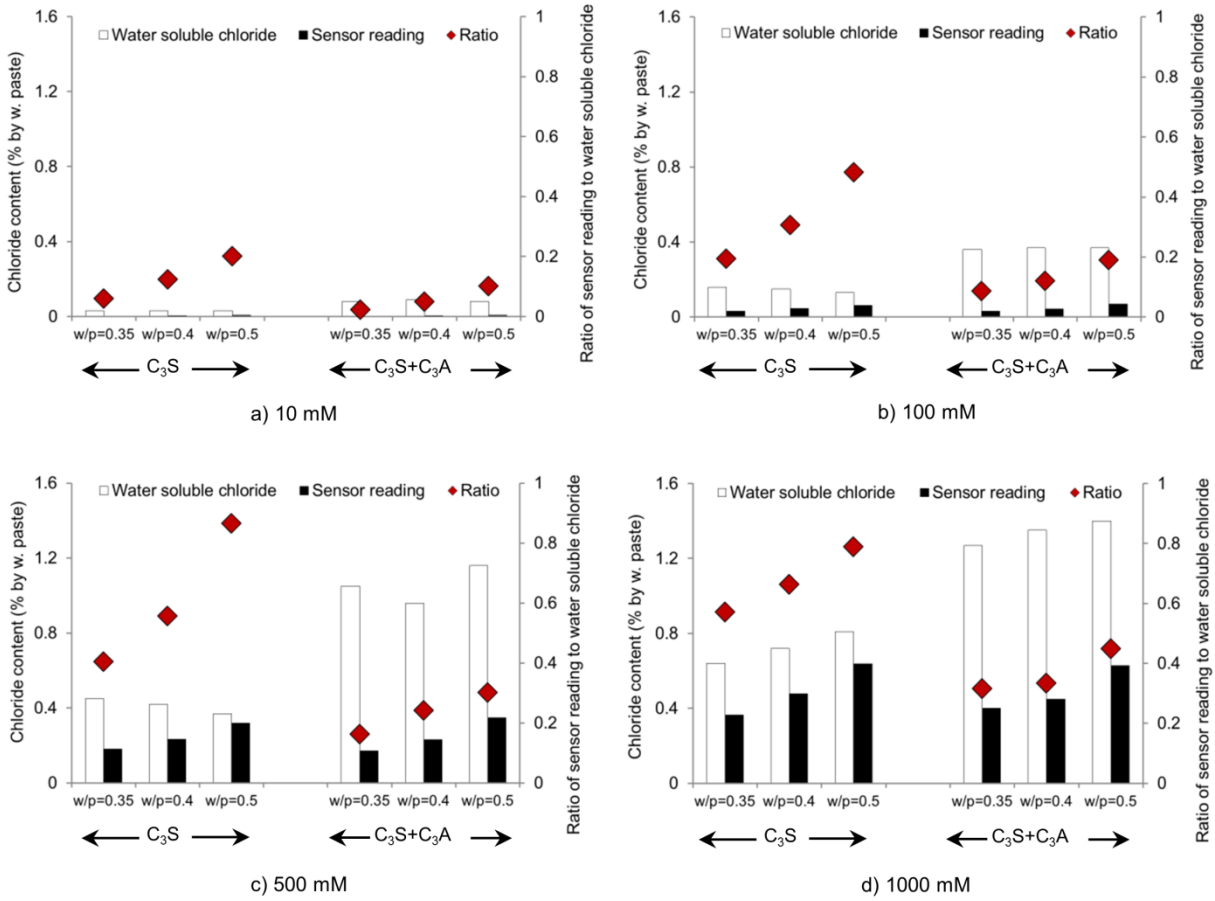

Figure 5.15: The water-soluble chloride, sensor reading of the free chloride content and the ratio of sensor reading to water-soluble chloride for C_3S and C_3S+C_3A specimens after 300 days of immersion in solutions with different chloride concentration.

The difference between the water-soluble chloride and the sensor reading of the chloride content in C_3S specimens is lower than that difference in C_3S+C_3A specimens (Fig. 5.15). As previously mentioned in Section 5.3.3.1, the release of bound chlorides into the water solvent plays a significant role in the measured water-soluble chloride. The release of bound chlorides into the water solvent is larger in C_3S+C_3A specimens (due to the chemical chloride binding ability) than that in C_3S specimens. This results in a larger difference between the water-soluble chloride and the sensor reading of the chloride content in C_3S+C_3A specimens than that in C_3S specimens.

Water-soluble chloride is often considered to be equal to the free chloride content [He et al., 2015]. After 300-day immersion of the specimens in chloride containing solutions, the free chloride content in the pore water of C_3S and C_3S+C_3A specimens would be close to each other (Chapter 2, Section 2.3). In Fig. 5.15, the change in the sensor reading of the chloride content is significantly lower than the change in the measured water-soluble chloride. As mentioned in the previous paragraph, the release of bound chlorides into the water solvent plays a significant role in the measured water-soluble chloride. Consequently, sensor reading of the chloride content is more accurate than water-soluble chloride for determination of the free chloride content in cementitious materials.

5.3.3.3 Relation between free and bound chlorides

C_3S and C_3S+C_3A specimens: Fig. 5.16 shows the share of free and bound chlorides in the total chloride content in C_3S and C_3S+C_3A specimens. This figure represents the acid-soluble, water-soluble and free chloride contents (inferred from the sensor's response) in the specimens at different chloride concentration (Sections 5.3.3.1 and 5.3.3.2). As previously shown in Sections 5.3.3.1 and 5.3.3.2, the measured chloride contents determined with different methods were in the following order: acid-soluble chloride > water-soluble chloride > free chloride. In Fig. 5.16 the acid-soluble chloride (total chloride) was set as 100%. Then the water-soluble chloride and the free chloride (inferred from the sensor's response) were normalized against the total chloride.

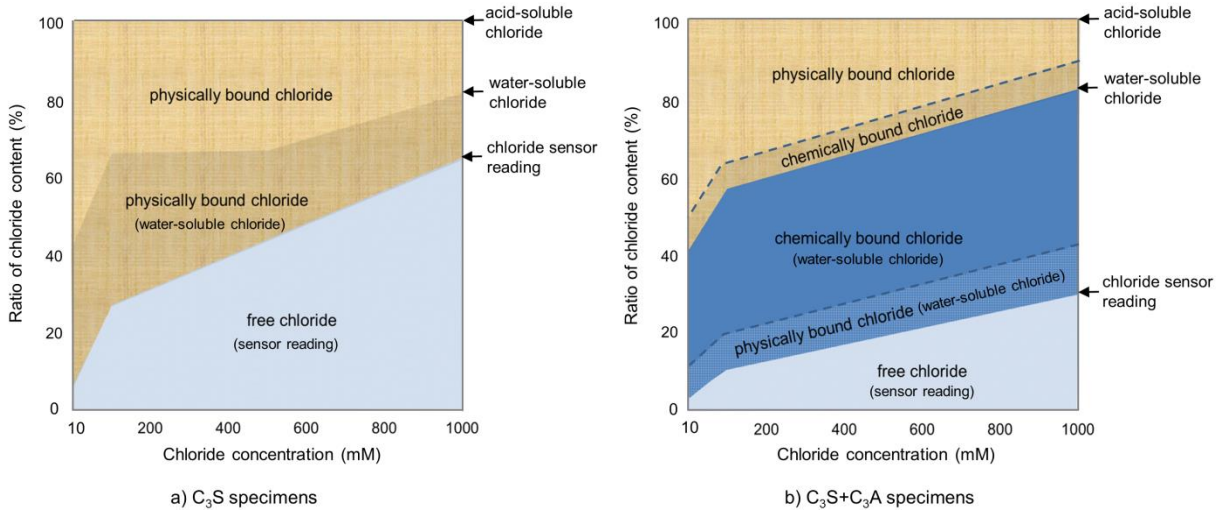

Fig 5.16: The contribution of free chloride, physically bound chloride and chemically bound chloride to the total chloride content in the cementitious materials. The free chloride was measured by chloride sensor.

The chloride in C_3S specimens was present as free and physically bound chlorides (Fig. 5.16a). The free chloride in Fig. 5.16a is the ratio of sensor reading of the chloride content to total chloride content. The subtraction of the free chloride content from the total chloride yields the physically bound chloride (Fig. 5.16a). The difference between the water-soluble chloride and free chloride was also attributed to the physically bound chloride (Fig. 5.16a). The free chloride content increased from about 10% in a 10 mM chloride concentration to 60% in a 1000 mM chloride concentration. The larger free chloride content in higher chloride concentration is the result of a decrease in the physical chloride binding capacity of the hydration products.

The chloride in C_3S+C_3A specimens was present as free chloride, physically bound chloride and chemically bound chloride (Fig. 5.16b). Similar to what has been said about the chloride in the C_3S pastes, the free chloride in Fig. 5.16b was determined from the ratio of sensor reading of the chloride content to total chloride content. However, the borderline between chemically bound chloride and physically bound chloride was assumed. As discussed in Sections 5.3.3.1 and 5.3.3.2, the release of chemically bound chloride into the water solvent is significantly higher than the release of physically bound chloride (Fig. 5.16b). Hence, the difference between the measured water-soluble chloride and the free chloride was attributed to the chemically bound chloride (Fig. 5.16b). For the same reason (i.e. significant release of chemically bound chloride into the water solvent), the difference between the acid and water-soluble chlorides in Fig. 5.16b was attributed to the physically bound chloride.

In the presence of chemically bound chloride, as in the C_3S+C_3A specimen, the free chloride content significantly decreased to about 5% and 30% in 10 mM and 1000 mM chloride concentrations, respectively (Fig. 5.16b). In other words, for the same free chloride concentration, the percentage of bound chloride in C_3S+C_3A specimens was higher than that in C_3S specimens (as expected). This is due to the significant contribution of the chemically bound chloride to the total bound chloride in C_3S+C_3A specimens.

The water-soluble chloride and the free chloride contents in C_3S specimens were closer to each other, compared to those in C_3S+C_3A specimens (compare Figs. 5.16a with 5.16b). This is as expected, since the C_3S has no ability for chemical binding of chloride ions. The chemically bound chloride is responsible for the large difference between the water-soluble chloride and the free chloride content in C_3S+C_3A specimens (Fig. 5.16b).

The results presented in this chapter show that the stability of a Ag/AgCl chloride sensor in cementitious materials is the major challenge for its application. A stable sensor's response depends on the concentrations of chloride, hydroxide and sulfide (as observed in CEM III specimens) ions in the paste. The deposition of hydration products on the sensor's surface influences the stable OCP of the sensor. The extent of this influence depends on the w/p ratio of the paste. The high alkalinity of the pore water in a low w/p ratio (0.35) significantly affects the stable sensor's OCP, especially at low chloride concentration (e.g. 10 mM). The higher accessibility of pore water to the sensor in the mixture with high w/p ratio (0.5) can result in de-chlorination of the AgCl layer and unstable sensor's OCP in chloride-free cementitious materials.

In summary, the free chloride determination in cementitious materials needs knowledge of the surrounding medium. The environment in a C_3S paste is different from that in a C_3S+C_3A paste. In addition to the concerns for lifetime and stability of the chloride sensor in cementitious materials, the application of the potentiometry method is a feasible and reliable approach for a continuous and non-destructive determination of the chloride content.

5.4 Conclusions

In this chapter, the performance of a Ag/AgCl sensor in cementitious materials with different mix design and cement composition was evaluated. Based on the obtained results the following conclusions can be drawn:

- The sensor's OCP in a cement-based matrix with low chloride concentration (e.g. 10 mM) depends on the w/p ratio of the mixture. The sensor's OCP in specimens with low w/p ratio (0.35) is more anodic than the expected response for a Ag/AgCl interface (as observed in specimens with high w/p ratio (0.5)). The more anodic sensor's OCP in specimens with w/p=0.35 indicates the lower accuracy in determination of the free chloride content in mixtures with low w/p ratio. This is the result of a dense matrix of cement hydration products, higher ionic strength and lower activity of chloride ions on the sensor's surface. By increasing the chloride concentration to 100 mM and higher, the dependency of the sensor's OCP on the cementitious mix design decreases.
- The chloride sensor embedded in Portland cement paste (w/c=0.4, CEM I 52.5 N) depicts a stable OCP. In contrast, a significantly different trend in the sensor's OCP in slag cement paste (w/c=0.4, CEM III 52.5 N) is observed. The interference of sulfide ions with the sensor results in Ag_2S formation on the sensor's surface and a shift in the sensor's OCP towards significantly negative potential values (e.g. -800 mV in chloride-containing solution). These cathodic OCP values (although indicative for the presence of free chloride ions on the sensors' surface) cannot reflect an accurate chloride content in this case.
- The free chloride content inferred from the sensor's response (sensor reading) is lower than the measured water-soluble chloride. The free and water-soluble chloride contents are closer to each other in C_3S specimens than those in C_3S+C_3A specimens. This trend is pronounced at higher chloride concentration (e.g. 1000 mM). This observation indicates the importance of cement composition, w/p ratio and chloride concentration in the cement-based matrix for the correlation between the free and water-soluble chlorides.
- On the one hand, a decrease in w/p ratio lowers the content of pore water around the sensor and the rate of AgCl dissolution. This subsequently reduces the reliability of the sensor for determination of chloride ions concentration in the environment. On the other hand, an increase in w/p ratio results in a higher amount of pore water around the sensor. A higher percentage of the sensor's surface can be in direct contact with the pore water. Hence, the sensor can reflect the chloride content in the pore water in a shorter period.

5.5 References

Angst U. and Polder R. (2014). Spatial variability of chloride in concrete within homogeneously exposed areas, *Cement and Concrete Research*, Vol. 56, p. 40-51.

Angst, U., Elsener, B., Larsen, C. K. and Vennesland, O. (2010). Potentiometric determination of the chloride ion activity in cement-based materials, *Journal of Applied Electrochemistry*, Vol. 40(3), p. 561–573.

Asbridge, A. H., Page, C. L. and Page, M. M. (2002). Effects of metakaolin, water/binder ratio and interfacial transition zones on the microhardness of cement mortars, *Cement and Concrete Research*, Vol. 32(9). p. 1365–1369.

ASTM C1152. (2003). *Standard Test Method for Acid-Soluble Chloride in Mortar and Concrete*, American Society for Testing and Materials (ASTM) Philadelphia, PA.

ASTM C1218. (2008). *Standard Test Method for Water-Soluble Chloride in Mortar and Concrete*, American Society for Testing and Materials (ASTM) Philadelphia, PA.

Bentur, A. and Ish-Shalom, M. (1974). Properties of type K expensive cement of pure components II. Proposed mechanism of ettringite formation and expansion in unrestrained paste of pure expansive component, *Cement and Concrete Research*, Vol. 4(5), p. 709-721.

Brandt, A.M. (2009). *Cement-Based Composites: Materials, Mechanical Properties and Performance*, Taylor & Francis.

Chappex, T. and Scrivener, K. (2012). Alkali fixation of C–S–H in blended cement pastes and its relation to alkali-silica reaction, *Cement and Concrete Research*, Vol. 42(8), p. 1049-1054.

Chaussadent, T. and Arliguie, G. (1999). AFREM test procedures concerning chlorides in concrete: extraction and titration methods, *Materials and Structures*, Vol. 32, p. 230-234.

Conyers, J. L. and White, H. S. (1999). Electrochemical growth of Ag_2S on Ag (111) electrodes. Coulometric and X-ray photoelectron spectroscopic analysis of the stepwise formation of the first and second monolayers of Ag_2S. *The Journal of Physical Chemistry B*, Vol. 103(11), p. 1960-1965.

Cwirzen, A. and Penttala, V. (2005). Aggregate–cement paste transition zone properties affecting the salt–frost damage of high-performance concretes, *Cement and Concrete Research*, Vol. 35(4), p. 671-679.

De Vera, G., Climent, M. A., Antón, C., Hidalgo, A., & Andrade, C. (2010). Determination of the selectivity coefficient of a chloride ion selective electrode in alkaline media simulating the cement paste pore solution, *Journal of Electroanalytical Chemistry*, Vol. 639(1), p. 43-49.

Delagrave, A., Pigeon, M., Marchand, J. and Revertegat, E. (1996). Influence of Chloride ions and pH level on the durability of high-performance cement pastes (Part II), *Cement and Concrete Research*, Vol. 26(5), p. 749-760.

Dhir, R. K., El-Mohr, M. A. K. and Dyer, T. D. (1996). Chloride binding in GGBS concrete, *Cement and Concrete Research*, Vol. 26(12), p. 1767-1773.

Elakneswaran, Y., Nawa, T. and Kurumisawa, K. (2009a). Influence of surface charge on ingress of chloride ion in hardened paste, *Materials and Structures*, Vol. 42(1), p. 83-93.

Evans, D. G. and Duan, X. (2006), *layered double hydroxides*, *Structure and Bonding*, Springer book, Vol. 119 (2006), p. 1–87.

Femenias, Y. S., Angst, U., Caruso, F. and Elsener, B. (2016). Ag/AgCl ion-selective electrodes in neutral and alkaline environments containing interfering ions, *Materials and Structures*, Vol. 49(7), p. 2637-2651.

Flatt, R. J. and Bowen, P. (2003). Electrostatic repulsion between particles in cement suspensions: Domain of validity of linearized Poisson–Boltzmann equation for nonideal electrolytes, *Cement and Concrete Research*, Vol. 33(6), p. 781-791.

Florea, M. V. A. and Brouwers, H. J. H. (2014). Modelling of chloride binding related to hydration products in slag-blended cements, *Construction and Building Materials*, Vol. 64, p. 421-430.

Galan, I. and Glasser, F. P. (2015). Chloride in cement, *Advances in Cement Research*, Vol. 27(2), p. 63-97.

Gascoyne, M. (2002). *Influence of grout and cement on groundwater composition*, Possiva, Working Report, 7.

Glasser, F., Tyrer, M. and Quillin, K. (1999). *The chemistry of blended cements and backfills intended for use in radioactive waste disposal*, (No. EA-RD-TR-P--98). Environment Agency.

Graedel, T. E. (1992). Corrosion mechanisms for silver exposed to the atmosphere, *Journal of the Electrochemical Society*, Vol. 139(7), p. 1963-1970.

Haque, M. N. and Kayyali, O. A. (1995). Free and water-soluble chloride in concrete, *Cement and Concrete Research*, Vol. 25(3), p. 531-542.

He, F., Shi, C., Chen, C. and An, X. (2015). Relationship between water-soluble and free chloride concentrations in cement-based materials, *Materials Research Innovations*, Vol. 19(sup8), S8-348.

He, F., Shi, C., Hu, X., Wang, R., Shi, Z., Li, Q. and An, X. (2016). Calculation of chloride ion concentration in expressed pore solution of cement-based materials exposed to a chloride salt solution, *Cement and Concrete Research*, Vol. 89, p. 168-176.

Hewlett, P. C. (2003). *Lea's chemistry of cement and concrete (Fourth Edition)*, Butterworth-Heinemann, Elsevier Ltd.

Hu, X., Shi, C. and De Schutter, G. (2015). Influences of chloride immersion on zeta potential and chloride in concentration of cement-based materials, *14th International Congress on the Chemistry of Cement*, p. 1-15.

Ives, D. J. and Janz, G. J. (1961). *Reference electrodes, theory and practice* (No. 541.3724). Academic Press.

Kopecsko, K. and Balazs, G. L. (2017). Concrete with improved chloride binding and chloride resistivity by blended cement, *Advances in Materials Science and Engineering*, 2017-7940247.

Levard, C., Hotze, E. M., Lowry, G. V. and Brown Jr, G. E. (2012). Environmental transformations of silver nanoparticles: impact on stability and toxicity, *Environ. Sci. Technol*, Vol. 46(13), p. 6900-6914.

Luo, R., Cai, Y., Wang, C. and Huang, X. (2003). Study of chloride binding and diffusion in GGBS concrete, *Cement and Concrete Research*, Vol. 33(1), p. 1-7.

Maes, M., Gruyaert, E. and De Belie, N. (2013). Resistance of concrete with blast-furnace slag against chlorides, investigated by comparing chloride profiles after migration and diffusion, *Materials and structures*, Vol. 46(1-2), p. 89-103.

Mangat, P. S. and Molloy, B. T. (1995). Chloride binding in concrete containing PFA, GBS or silica fume under sea-water exposure, *Magazine of Concrete Research*, Vol. 47(171), p. 129-141.

Maso, J. C. (2004). *Interfaces in cementitious composites*. CRC Press.

Matschei, T., Lothenbach, B. and Glasser, F. (2007). Thermodynamic properties of Portland cement hydrates in the system CaO-Al_2O_3-SiO_2-$CaSO_4$-$CaCO_3$-H_2O, *Cement and Concrete Research*, Vol. 37(10), p. 1379-1410.

NEN-EN 197-1 (2011). *Cement - Part 1: Composition, specifications and conformity criteria for common cements*, European Committee for Standardization.

Ortega, J. M., Sanchez, I., Cabeza, M. and Climent, M. A. (2017). Short-term behavior of slag concretes exposed to a real in situ mediterranean climate environment, *Materials*, Vol. 10(8), p. 915.

Page, C. L. (2009). Initiation of chloride-induced corrosion of steel in concrete: role of the interfacial zone, *Materials and corrosion*, Vol. 60(8), p. 586-592.

Page, C. L., Short, N. R. and El Tarras, A. (1981). Diffusion of chloride ions in hardened cement pastes, *Cement and Concrete Research*, Vol. 11(3), p. 395-406.

Payer, J. H., Ball, G., Rickett, B. I. and Kim, H. S. (1995). Role of transport properties in corrosion product growth, *Materials Science and Engineering: A*, Vol. 198(1-2), p. 91-102.

Qiang, Y., Caijun, S., De Schutter，G., Dehua, D. and Fuqiang, H. (2011). Chloride ion concentration on the surface of cement-based materials in chloride solutions, *Journal of the Chinese ceramic society*, Vol. 39(3), p. 544-549.

Rajbhandari, A., Yadav, A. P., Manandhar, K. and Pradhananga, R. R. (2009). Characterization and applications of silver sulphide based membrane electrodes, *Scientific World*, Vol. 7(7), p. 19-23.

Raynauld, J. P. and Laviolette, J. R. (1987). The silver-silver chloride electrode: a possible generator of offset voltages and currents, *Journal of neuroscience methods*, Vol. 19(3), p. 249-255.

RILEM TC 178-TMC. (2002). Analysis of total chloride in concrete, *Material and Structures*, 35, p. 583-585.

RILEM TC 178-TMC. (2002a). Analysis of water-soluble chloride content in concrete, Recommendation, *Materials and Structures*, Vol. 35, p. 586-588.

Scrivener, K. L., Crumbie, A. K. and Laugesen, P. (2004). The interfacial transition zone (ITZ) between cement paste and aggregate in concrete, *Interface Science*, Vol. 12(4), p. 411-421.

Suzuki, H., Hiratsuka, A., Sasaki, S. and Karube, I. (1998). Problems associated with the thin-film Ag/AgCl reference electrode and a novel structure with improved durability, *Sensors and Actuators B: Chemical*, Vol. 46(2), p. 104-113.

Taylor, H. F. W. (1998). *Cement Chemistry, 2nd Edit*, Thomas Telford Publication.

van Breugel, K. (1991). *Simulation of hydration and formation of structure in hardening cement-based*

materials, Ph.D. Thesis, Delft University of Technology, The Netherlands.

Wan, Y., Wang, X., Wang, X., Li, Y., Sun, H. and Zhang, K. (2015). Determination and generation of the corrosion compounds on silver exposed to the atmospheres, *International Journal of Electrochemical Science*, Vol. 10, p. 2336-2354.

Yang, Z., Fischer, H. and Polder, R. (2013). Modified hydrotalcites as a new emerging class of smart additive of reinforced concrete for anticorrosion applications: a literature review, *Materials Corrosion*, Vol.64(12), p. 1066–1074.

Yoon, S., Moon, J., Bae, S., Duan, X., Giannelis, E. and Monteiro, P. (2014). Chloride adsorption by calcined layered double hydroxides in hardened Portland cement paste, *Materials Chemistry and Physics*, Vol. 145(3), p. 376–386.

Yuan, Q. (2009). *Fundamental studies on test methods for the transport of chloride ions in cementitious materials*, Ph.D. thesis, Ghent University, Belgium.

Yuan, Q., Deng, D., Shi, C. and De Schutter, G. (2013). Chloride binding isotherm from migration and diffusion tests, *Journal of Wuhan University of Technology-Mater. Sci. Ed.*, Vol. 28(3), p. 548-556.

Yuan, Q., Deng, D., Shi, C. and De Schutter, G., Deng, D. and He, F. (2011). Chloride-ion concentration on the surface of cement-based materials in chloride solutions, *Journal of the Chinese ceramic society*, Vol. 39(3), p. 544-549.

Zimbelmann, R. (1985). A contribution to the problem of cement-aggregate bond, *Cement and Concrete Research*, Vol. 15(5), p. 801-808.

Chapter 6

The onset of steel corrosion inferred by sensors' response

Abstract

The determination of the chloride content near the steel reinforcement is important for the assessment of the probability of chloride-induced corrosion in a reinforced concrete structure. The focus of this chapter is to illustrate the sensor's applicability for chloride determination at the time of corrosion initiation on a steel surface. Chloride sensors were embedded together with steel rods in cement paste cylinders. The specimens were immersed in an alkaline solution of pre-defined chloride concentration. Open circuit potential (OCP) and electrochemical impedance spectroscopy (EIS) were employed to continuously monitor the corrosion state of the steel rods. The OCP responses of the embedded sensors were simultaneously recorded, reflecting the chloride content near the steel surface. The OCP values for the sensors were correlated to the time of corrosion initiation at the steel surface, i.e. an attempt for defining the chloride threshold value was made.

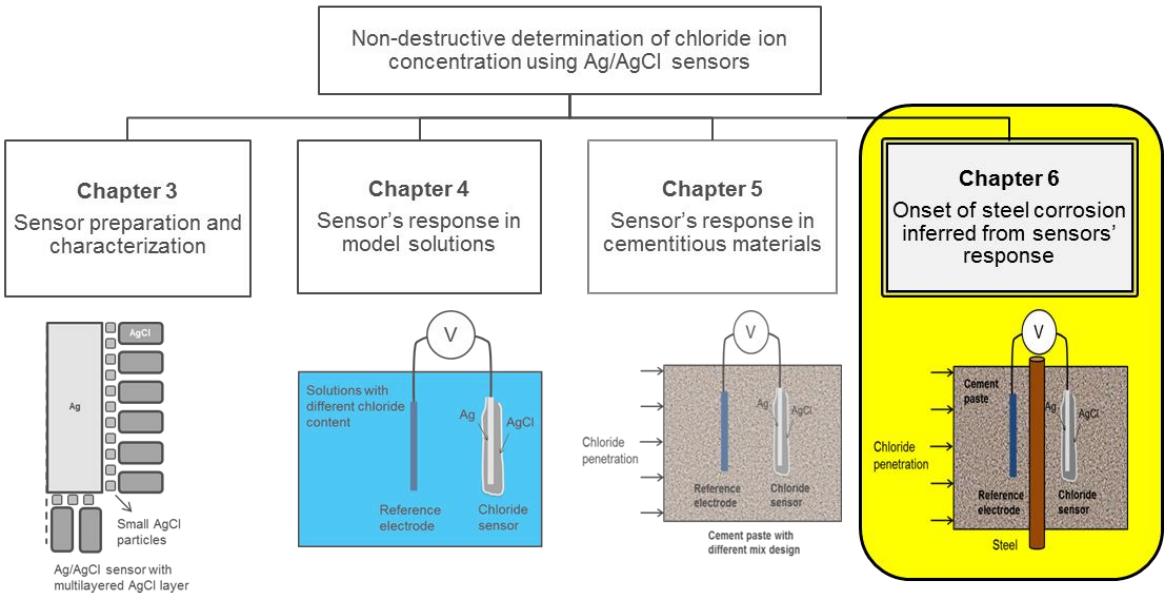

Structure of research process and sequence of chapters in the thesis

---

This Chapter 6 is based on the paper:

Pargar, F., Koleva, D.A., Kolev, H., & van Breugel, K. (2017). The Onset of Chloride-Induced Corrosion in Reinforced Cement-Based Materials as Verified by Embeddable Chloride Sensors. In Concrete Durability – cementitious materials and reinforced concrete properties, behavior and corrosion resistance Eds. R.D. Miron, D.A. Koleva, (pp. 23-55). Springer International Publishing.

6.1 Introduction

As already introduced in Chapter 2 (Fig. 2.6) the steel reinforcement in concrete is in passive state due to a thin iron oxide layer (passive film), which forms on the steel surface in the high pH medium (12.5< pH <13.5) of the concrete pore water. Exposure to a Cl-containing environment and subsequent chloride ions penetration into the hardened concrete would gradually increase the chloride ions concentration in the vicinity of the steel reinforcement. Above a certain threshold value, the chloride ions initiate localized steel corrosion. Well known is that many factors affect the onset of chloride-induced corrosion. Among these, the quality of the steel-concrete interface and the pH of the pore solution are considered as the most influential ones. The level of chloride concentration, prior to or in the event of steel depassivation, is generally used for predictions of the time to corrosion initiation and propagation. The measurement of the relevant chloride concentration, however, is largely affected by the chloride determination methods themselves [Silva, 2013]. The application of Ag/AgCl electrodes as chloride sensors is a promising approach to a continuous and non-destructive determination of the chloride content. Sensors can be used to determine the chloride concentration in both the bulk of the cement paste and/or in the vicinity of the steel reinforcement.

The open circuit potential (OCP) or half-cell potential measurement is a commonly applied non-destructive electrochemical technique for determination of the time to corrosion initiation of reinforcing steel. This technique does not provide any information about the corrosion rate. Additionally, the corrosion rate can vary widely in a narrow range of OCP records [Andrade et al., 2001; Song and Saraswathy, 2007]. Hence, it is accepted that OCP records must be complemented by other (electrochemical) methods. For lab conditions a non-destructive technique, such as electrochemical impedance spectroscopy (EIS), can be used. EIS can simultaneously provide information on both the steel electrochemical behavior and the electrical properties of a cement-based bulk matrix, including properties of the steel/cement paste interface [Andrade et al., 1995; Koleva, 2007]. Additionally, the EIS response can indicate the presence of chloride ions in the vicinity of the steel surface, even prior to corrosion propagation [Andrade et al., 2001]. However, determination of the chloride threshold value through EIS is not possible. The combination of electrochemical techniques with a reliable chloride determination method results in a significantly better detection of the chloride-induced steel corrosion process.

The main focus of this Chapter 6 is the determination of the chloride content (derived from the sensors' OCP response) at the time of steel corrosion initiation (derived from the steel OCP and EIS responses). Monitoring the response of the steel rods aimed to evaluate the corrosion state, whereas monitoring the sensors' response aimed to 'couple' this with the relevant chloride content. The OCP responses of both sensors and steel rods were recorded over 180 days.

This chapter correlates the afforementioned tests and results with the goal of addressing the following research questions: i) what are the important parameters for a reliable sensor's response vs. steel corrosion state; ii) is it possible to determine a chloride threshold value with a sufficient accuracy; iii) is it possible to validate the chloride threshold value by "capturing" the event of corrosion initiation.

6.2 Materials and methods

6.2.1 Materials and test conditions

The specimens, in this chapter, were cement paste cylinders with cast-in steel rods and Ag/AgCl sensors. The cement paste was made using Ordinary Portland Cement, OPC CEM I 42.5 N (ENCI, NL), at a water-to-cement ratio of 0.4. The specimens' geometry, experimental set-up and configuration for electrochemical measurements are identical to those presented in Chapter 5, Figs. 5.1a,b. The sensors were prepared at four different anodization regimes, specified in Chapter 3, i.e. sensor A (regime A, 0.5 mA/cm^2), sensor B (regime B, 1 mA/cm^2), sensor C (regime C, 2 mA/cm^2) and sensor D (regime D, 4 mA/cm^2). After curing in a sealed condition for 30 days the cement paste cylinders (from here onwards referred to as specimens) were immersed in a simulated pore solution (SPS) with the following composition: 0.05 M NaOH + 0.63 M KOH + Sat. $Ca(OH)_2$. The pH of the SPS medium was maintained at 13.6. The desired level of chloride concentration in the solution was adjusted to 870 mM by adding NaCl (as solid). Two replicates per specimen type were monitored during 180-day immersion of specimens in SPS.

6.2.2 Experimental methods

The open circuit potential (OCP) for both sensors and steel rods was monitored over immersion period versus a saturated calomel electrode (SCE). Electrochemical impedance spectroscopy (EIS) was performed for the steel rods at defined time intervals using a three-electrode cell arrangement. EIS was employed in the frequency range of 50 kHz to 10 mHz by using an AC voltage of 10 mV (rms). The equipment was a Metrohm Autolab PGSTAT 302N, combined with a FRA2 module and NOVA software package. A mixed metal oxide (MMO) Ti mesh, positioned around the cement paste cylinder, served as a counter electrode. The steel rods served as a working electrode and a SCE electrode served as a reference electrode (Figure 5.1b – Chapter 5).

6.3 Results and discussion

6.3.1 Open circuit potential (OCP) response of steel rods

6.3.1.1 Overall considerations

Steel embedded in a cement-based material is considered to be active (corroding) when the recorded open-circuit potential (OCP) is more cathodic than -273 mV vs. SCE [ASTM C876, 1991]. A sustained shift to negative (cathodic) OCPs can be linked to the so-called ''chloride threshold". This is because in the presence of a sufficient amount of free chloride ions in the vicinity of the steel surface, a transition from passive to active state would occur. However, OCP is only an indication of the probability of corrosion, while information about the corrosion rate cannot be obtained.

The OCP response of the steel rods can be affected by a number of factors, such as oxygen availability, concrete porosity and the presence of highly resistive layers [Song and Saraswathy, 2007]. For instance, limited oxygen availability can be reflected in a more cathodic OCP value. Hence, the interpretation of OCP values in submerged conditions, as in this work, would be more complex and cathodic OCP would not necessarily indicate enhanced corrosion activity.

The OCP evolution for the steel rods, as embedded in cement paste specimens, is shown in Figs. 6.1 and 6.2. The specimens' designation A, C and D refer to the type of sensor, embedded together with a steel rod. Having two replicates for A, C and D specimens, the designation codes for the steel rods (St) are: $St_{(A1)}$, $St_{(A2)}$, $St_{(C1)}$, $St_{(C2)}$ and $St_{(D1)}$, $St_{(D2)}$. The steel response in B specimens was almost identical to that in C specimens and for simplicity is not presented and discussed.

The time scale in Figs. 6.1 and 6.2 is related to the time of exposure of the cement paste specimens. Time zero (t=0) corresponds to the start of exposure to Cl-containing simulated pore solution (SPS). The specimens are then 30-day old. At that age, a stable product layer (including passive film) will be present on the steel surface in all cases. The variation in the OCP response of the steel rods in the early stage of exposure (from 0 to 30 days, Figs. 6.1) and during prolonged treatment (from 0 to 180 days, Fig. 6.2) are discussed with respect to the time to corrosion initiation on the steel surface. As can be seen in Figs. 6.1 and 6.2 the fluctuation in the initial OCP response (from 0 to 30 days) is more significant. Hence, it is separately and specifically addressed in the following.

6.3.1.2 OCP evolution at early stage (until 30 days of treatment)

The initial OCP for all specimens (t=0 in Fig. 6.1) was between -100 and -280 mV vs. SCE. This range of OCP indicates a passive state [ASTM C876, 1991]. However, with conditioning, a different trend of OCP evolution was observed, despite the otherwise identical environment.

For $St_{(A1)}$ and $St_{(A2)}$, a significant drop in OCP values to ca. -600 mV was observed after 15 days (Fig. 6.1). This can be an indication of steel corrosion initiation. However, corrosion propagation is uncertain, since the cathodic OCP values were not sustained. The OCPs for $St_{(A1)}$ and $St_{(A2)}$ became anodic after 20–25 days (Fig.6.1) with OCP value stabilization above the passivity/activity threshold of -273 mV [ASTM C876, 1991].

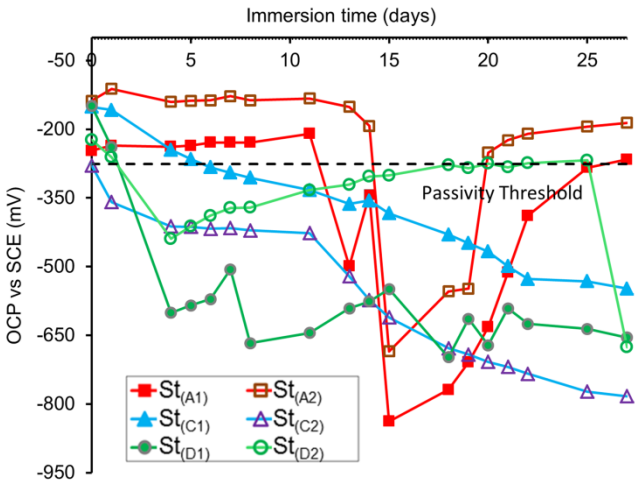

Figure 6.1: OCP response of steel rods cast in cement paste cylinders, during the first 30 days of immersion in Cl-containing simulated pore solution (SPS).

For steel rods in C and D specimens, the OCP evolution depicted either a gradual or an abrupt shift to cathodic values from the beginning of exposure (t=0 to t=5 days in Fig. 6.1). The OCP for $St_{(C1)}$ and $St_{(C2)}$ showed a gradual drop to values more cathodic than -300 mV during 30 days (Fig. 6.1). The initial OCP for $St_{(D1)}$ and $St_{(D2)}$ showed an almost immediate cathodic shift (similar to that in C specimens (Fig. 6.1)). The OCP for $St_{(D1)}$ reached -650 mV after 5 days and remained cathodic until 25 days. The OCP for $St_{(D2)}$ exhibited an anodic shift after 5 days and followed that trend by arriving at OCPs around the threshold of -275 mV after 25 days. A cathodic shift in OCP value for $St_{(D2)}$ was again observed after 25 days (Fig. 6.1).

The penetration of external solution (including chloride ions) into the bulk cement-based matrix determines different levels of oxygen and relative humidity at the steel surface. Balancing of these gradients would be reflected in an OCP stabilization and/or a sustained trend of OCP evolution. This was observed for the steel, embedded in C and D specimens. The cathodic OCP values for $St_{(C1)}$, $St_{(C2)}$, $St_{(D1)}$ and $St_{(D2)}$, immediately after immersion in SPS, could not be due to chloride-induced corrosion initiation only. A cathodic OCP of -600 mV can also indicate both corrosion initiation and limited oxygen availability [Elsener, 2002; Elsener et al., 2003; Bohni, 2005; Silva, 2013]. The same range of cathodic OCPs but with elevated corrosion rates can occur in the case of chloride-induced corrosion [Davis, 2000].

Considering the above-mentioned, the electrochemical state of the steel rods cannot be judged from the OCP values only. The identification of corrosion activity requires an additional electrochemical investigation (Section 6.3.3) which would reflect the corrosion rate of steel rods.

6.3.1.3 OCP evolution with prolonged treatment (full test duration of 180 days)

The passivity breakdown for $St_{(A1)}$ and $St_{(A2)}$ was followed by non-sustained corrosion activity (repassivation) (Fig. 6.2). Repassivation is a sharp decrease in the corrosion current density (discussed in Section 6.3.3) which can be accompanied by a simultaneous shift in the OCP towards anodic values (Fig. 6.2).

The $St_{(C1)}$ and $St_{(C2)}$ depicted active behaviour from the start until the end of the experiment. The initially cathodic OCP values can be attributed to the combined effects of chloride penetration and limited oxygen availability at the steel surface, while a sustained cathodic OCPs can reflect both corrosion initiation and corrosion propagation.

The OCP values for $St_{(D1)}$ and $St_{(D2)}$ stabilized in the region of passivity after 100 and 50 days, respectively (Fig.6.2). Nevertheless, cathodic OCP values for $St_{(D1)}$ and $St_{(D2)}$ were sustained in the period of 25 and 50(100) days of treatment, which can indicate corrosion initiation and propagation in these specimens. Attempts for repassivation were reflected by anodic OCP values after 100 days for $St_{(D1)}$ and after 50 days for $St_{(D2)}$. As mentioned, the OCP response does not provide quantitative information about the corrosion rate of the steel rods. Hence, no further conclusions about the corrosion state of the steel rods can be derived from Fig. 6.2.

A logic question based on the different trend in OCP evolution for steel rods is: if the steel rods and the cement-based specimens were identically prepared, why would the OCP response present such variations? First of all, as already commented, the OCP can only indicate the risk of corrosion. Next to that, a reinforced cement-based specimen is a heterogeneous system [Gu et al., 1994]. This means that even identically prepared specimens are never completely alike. A combination of these parameters is responsible for the different trend in OCP evolution of the steel rods. Further considerations on the recorded OCPs for the steel rods are presented later on with relevance to the OCP records for the sensors.

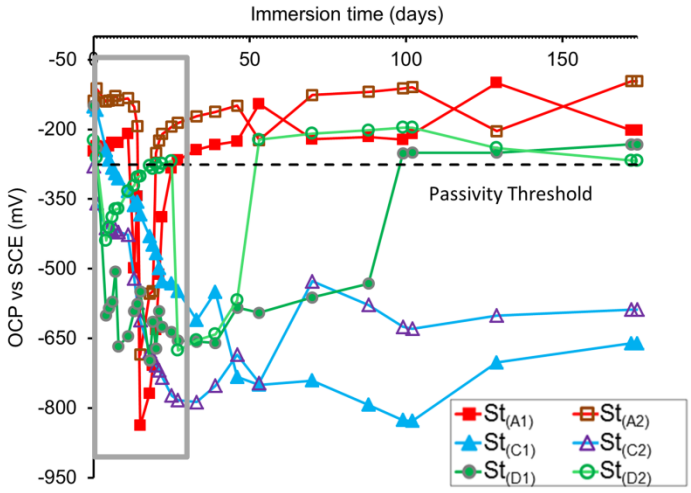

Figure 6.2: OCP response of steel rods cast in cement paste cylinders, during 180-day immersion in Cl-containing simulated pore solution (SPS).

6.3.2 Open circuit potential (OCP) response of chloride sensors

6.3.2.1 Overall considerations

In this chapter, the main concept of defining a chloride threshold value via sensors' application is based on the sensors' OCP at the time of corrosion initiation of the nearby steel rods. The limitations, source of errors and challenges for application of the chloride sensors in cementitious materials were already discussed in Chapter 2. The variation in the OCP response of a chloride sensor is the only criteria for evaluation of the sensor's performance and determination of the chloride content in cementitious materials [Duffo and Farina, 2009; Yu and Caseres, 2012; Femenias et al., 2015].

During the process of chloride penetration in a cement paste, the OCP of a chloride sensor would gradually shift to a more cathodic value (as discussed in Chapter 2). The sensor's OCP stabilizes after reaching an equilibrium with the external medium. The microstructure, morphology and ionic resistivity of the AgCl layer of a sensor determine the sensor's OCP in contact with the relevant environment (discussed in Chapters 3 and 4). Hence, the AgCl layer properties of the sensors need to be considered when their OCP is linked to the critical chloride content for steel corrosion initiation.

The OCP responses of the sensors in A, B, C and D specimens are shown in Figs. 6.3 to 6.6. Having two replicates for A, B, C and D specimens, the designation codes for the sensors are: $Se_{(A1)}$, $Se_{(A2)}$, $Se_{(B2)}$, $Se_{(B2)}$, $Se_{(C1)}$, $Se_{(C2)}$, $Se_{(D1)}$ and $Se_{(D2)}$.

The variation in the initial OCP response of the sensors (first day, Fig. 6.3) is discussed in the following. Next the sensor's OCP during the early stage of exposure (from 0 to 30 days, Fig. 6.4) and after prolonged treatment (180 days, Figs. 6.5 and 6.6) are presented.

6.3.2.2 OCP evolution at early stage

At the beginning of immersion (Fig. 6.3), the OCP of $Se_{(A1,2)}$ and $Se_{(B1,2)}$ was 130-134 mV, while the OCP of $Se_{(C1,2)}$ and $Se_{(D1,2)}$ was 108-122 mV. The difference among the initial readings (26 mV) indicates that within the curing period of the cement paste cylinders (30 days), the surface of the Ag/AgCl sensors was modified. This was as expected and due to the transformation of AgCl to Ag_2O in chloride-free alkaline medium (discussed in Chapters 4). The initially more anodic OCP values for $Se_{(C1,2)}$ and $Se_{(D1,2)}$ are an indication of a higher

amount of Ag_2O-based compounds at the sensor's surface in specimens C and D. The significance of the above considerations is in view of the accuracy in chloride levels determination. For instance, a silver oxide-based sensor surface will react with a delay on the relevant chloride content (phenomena discussed and illustrated in Chapter 4). A larger deviation between the sensors readings is also to be expected for $Se_{(C1,2)}$ and $Se_{(D1,2)}$ (14 mV, Fig. 6.3), where the AgCl layer was originally of a larger thickness (compared to A and B specimens), had higher level of structural heterogeneity and a more significant variation in chemical composition.

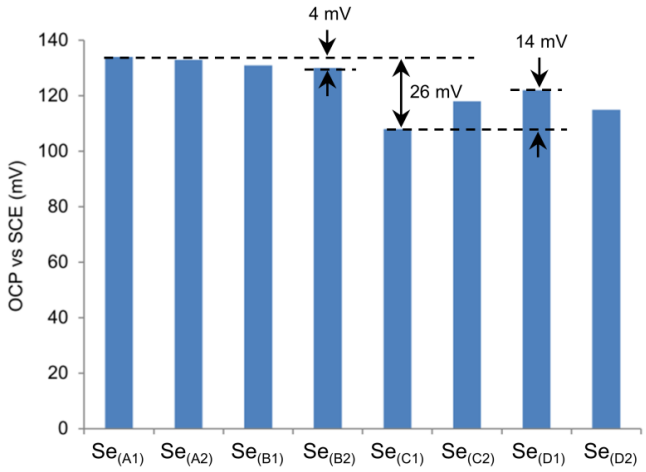

Figure 6.3: OCP response of sensors cast in cement paste cylinders, on the first day of immersion of $Se_{(A1,2)}$ to $Se_{(D1,2)}$ in Cl-containing simulated pore solution (SPS).

6.3.2.3 Initial OCP of the sensors vs initial OCP of the steel rods

The chloride ions gradually penetrate from the external solution into the cement paste. This is illustrated by the initial anodic OCP of the sensors (108 mV to 134 mV, Fig. 6.4), corresponding to a negligible chloride content of lower than 8 mM at the sensors' surface. If the initial OCP response of the steel rods is considered for that same time interval (Fig. 6.1), the sensors' OCP is an additional proof that the cathodic OCP of $Se_{(C1,2)}$ and $Se_{(D1,2)}$ was due to reasons different from chloride-induced corrosion (discussed in Section 6.3.1).

Between 13-15 days the OCP of $Se_{(A1)}$ and $Se_{(A2)}$ was 10-35 mV (Fig. 6.4). This range of OCP values is equivalent to the chloride content of approx. 200-550 mM in the vicinity of the sensor and steel rods, respectively. At the same time interval, a cathodic shift in the OCP of $St_{(A1)}$ and $St_{(A2)}$ can be an indication for corrosion initiation (Fig. 6.1). Considering the reported chloride threshold value (45 mM to 650 mM, Table 2.2 in Chapter 2), the inferred chloride content from the sensor's response is, apparently, large enough to initiate corrosion of the steel rods. These results illustrate the application of the chloride sensor for determination of the chloride content at the time of steel corrosion initiation. However, both the sensor reading and a sustained cathodic OCP for the steel rods would depend on external and internal factors, as already introduced and pointed out in the previous sections.

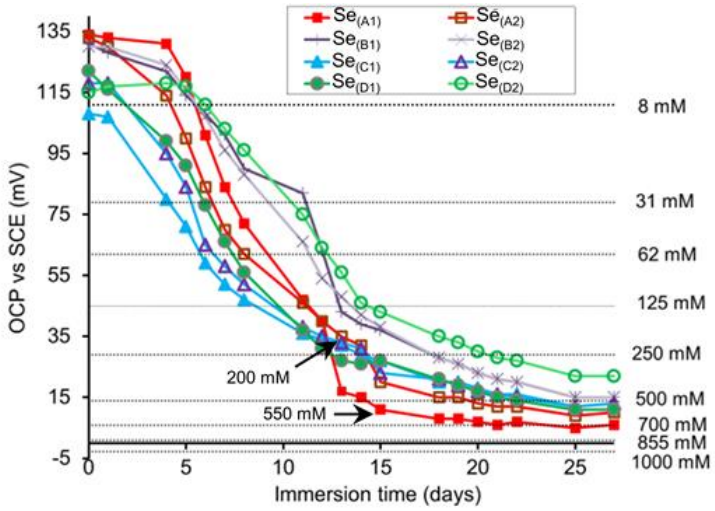

Figure 6.4: OCP response of sensors cast in cement paste cylinders, during the first 30 days of immersion in Cl-containing simulated pore solution (SPS).

6.3.2.4 OCP records for the chloride sensors - full test duration

With the progress of chloride ions penetration into the bulk cementitious matrix, the OCPs of the sensors changed to more cathodic values and after 180 days stabilized at -1 mV to 2 mV (Fig. 6.5).

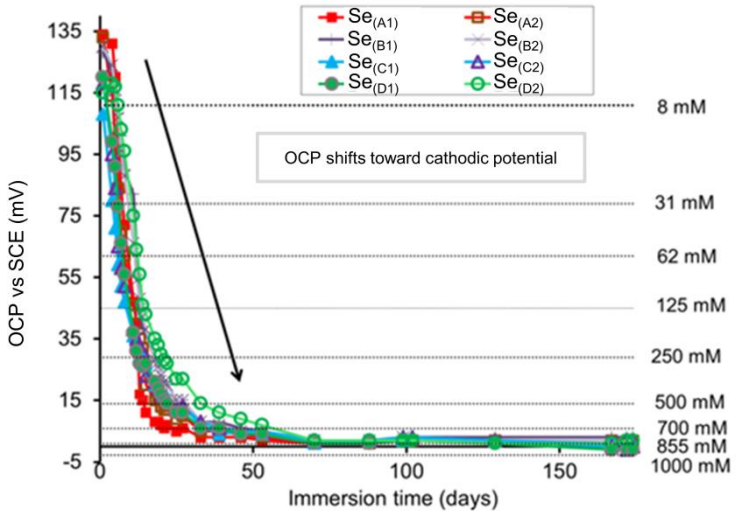

Figure 6.5: OCP response of sensors cast in cement paste cylinders, during 180-day immersion in Cl-containing simulated pore solution (SPS).

Figure 6.6 depicts the sensors' OCP at the stage of 180 days, when a semi-equilibrium was established and a high chloride concentration was already present in the vicinity of the sensors' surface. The stabilized sensors' OCP in A and B specimens was 2±0.5 mV (equivalent to the average chloride concentration of 820 mM), while that in C and D specimens was 0±1.5 mV (equivalent to the chloride concentration of 830-970 mM). The difference between the sensors' OCP is 4 mV (from -1.5 mV to 2.5 mV). Such a difference (4 mV) can be recognized as significant, if the electrochemical response is linked to the actual chloride concentration in the

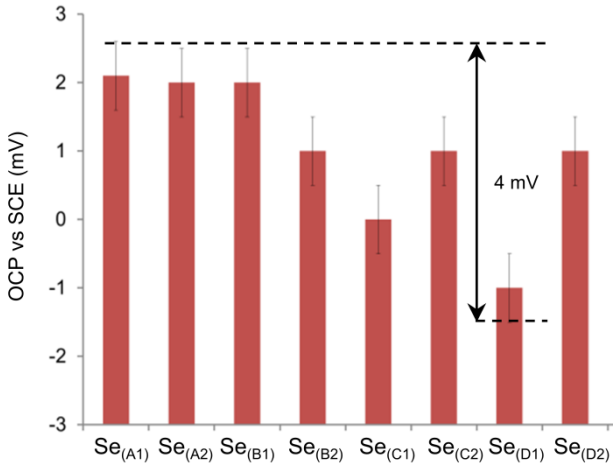

Figure 6.6: OCP response of all sensors after 180-day immersion of specimens in Cl-containing simulated pore solution (SPS).

medium, especially for the range of higher chloride content (considerations already discussed in Chapter 4).

In conclusion, this section discussed the simultaneous monitoring of OCP for both steel and sensors in identical environment. The correlation of results can provide important information on the chloride threshold value for steel corrosion initiation in cement-based materials. However, the accuracy of OCP measurements in view of the time to steel corrosion initiation at the point of derived chloride content (via the sensors readings) needs to be justified. Therefore, electrochemical impedance spectroscopy (EIS) was employed in order to support the above-discussed results.

6.3.3 Electrochemical impedance spectroscopy (EIS) response of steel rods

6.3.3.1 Overall considerations

Electrochemical impedance spectroscopy (EIS) can determine the overall impedance of a system in a certain frequency range. The experimental data is commonly displayed in the format of Nyquist and Bode plots (Fig. 6.7). The high to medium frequency domain (e.g. from 50 kHz and higher to 10 Hz) indicates the contribution of the bulk cement paste matrix (Fig. 6.7) [Andrade et al., 1995; Koleva, 2007]. The low-frequency response (10 Hz to 10 mHz) is related to polarization resistance, including charge transfer phenomena and mass transport or redox processes in the product layer on the steel surface [Andrade et al., 1995; Ford et al., 1998; Andrade et al., 2001; Joiret et al., 2002; Abreu et al., 2006; Subramaniam and Bi, 2009]. In this section, the EIS response in the low-frequency domain was used to evaluate the corrosion state by deriving the corrosion current density (I_{corr}). I_{corr} was calculated by using the well-known Stern-Geary equation, $I_{corr}=B/R_p$, where R_p (polarization resistance) was obtained from the best fit parameters via the EIS response in the low-frequency domain while the B constant was taken as 26 mV, as reported for active steel in cement-based medium [Andrade and Gonzalez, 1978].

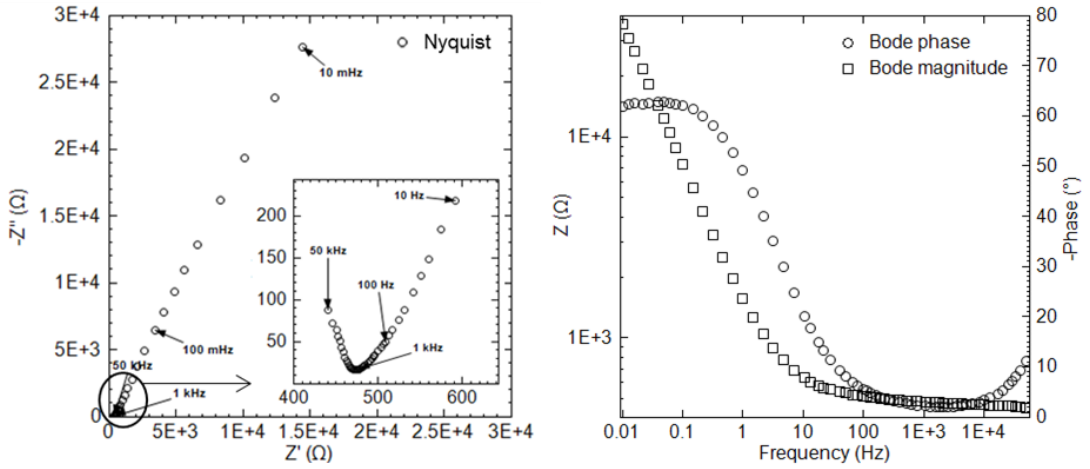

a) Nyquist plot b) Bode plots

Figure 6.7: EIS response of steel rod cast in cement paste cylinder and immersed in Cl-containing simulated pore solution (SPS).

6.3.3.2 Equivalent circuits

Different equivalent circuits can be used for quantitative analysis of the EIS response with equally good fit results. From the mathematical point of view, increasing the complexity of a circuit would decrease the fitting error [Feliu et al., 1998]. The most reliable circuit would be the one with parameters of a clearly defined physical meaning [Subramaniam and Bi, 2009; Koleva et al., 2011]. The electrochemical impedance spectra were recorded in the frequency range of 50 KHz to 10 mHz, while fitting of EIS data for evaluation of the corrosion state was performed in the frequency range of 10 Hz to 10 mHz [Andrade et al., 2001; Joiret et al., 2002; Abreu et al., 2006].

Fig. 6.8 presents EIS responses and best-fit parameters of representative cases at certain time intervals over 180 days of immersion in Cl-containing simulated pore solution (SPS). From the circuit models, as presented in Fig. 6.8, Model (a) (Fig. 6.8a) is commonly used in the literature for fitting of the EIS spectra of steel in cementitious materials [Andrade et al., 2001; Joiret et al., 2002; Abreu et al., 2006]. In this circuit, R_c corresponds to the electrolyte resistance, including the contribution of bulk matrix (cement paste). The first time constant is related to the electrochemical reactions on the steel surface. It comprises double layer capacitance (Q_{dl}) and charge transfer resistance (R_{ct}). Q is a constant phase element (CPE), which is often used instead of an ideal capacitor (C) to represent the non-homogeneity of the system (CPE would be C when n=1).

The second time constant corresponds to the redox or mass transport processes in the passive/oxide layer in which R_f and Q_f are the resistance and pseudo-capacitance, respectively. At certain time intervals, a constant phase element (Q_{pr}) [Wei et al., 2012; Duarte et al., 2014] or a Warburg impedance (W) [Zhao et al., 2007] was added in series with R_f. This changed the circuit from Model (a) to Model (b) or Model (c) (Figs. 6.8b, 6.8c). Hence, Models (b) and (c) are the same as Model (a) with an added element to the second time constant. The added capacitive (Q_{pr}) or diffusive (W) elements in the second time constant can be attributed to a diffusion controlled reaction or re-structuring of the surface film due to the ongoing corrosion processes on the steel surface. The best-fit parameters, after electrochemical fit and simulation, of the relevant system are also included in Fig. 6.8 – inlet in the Bode plots.

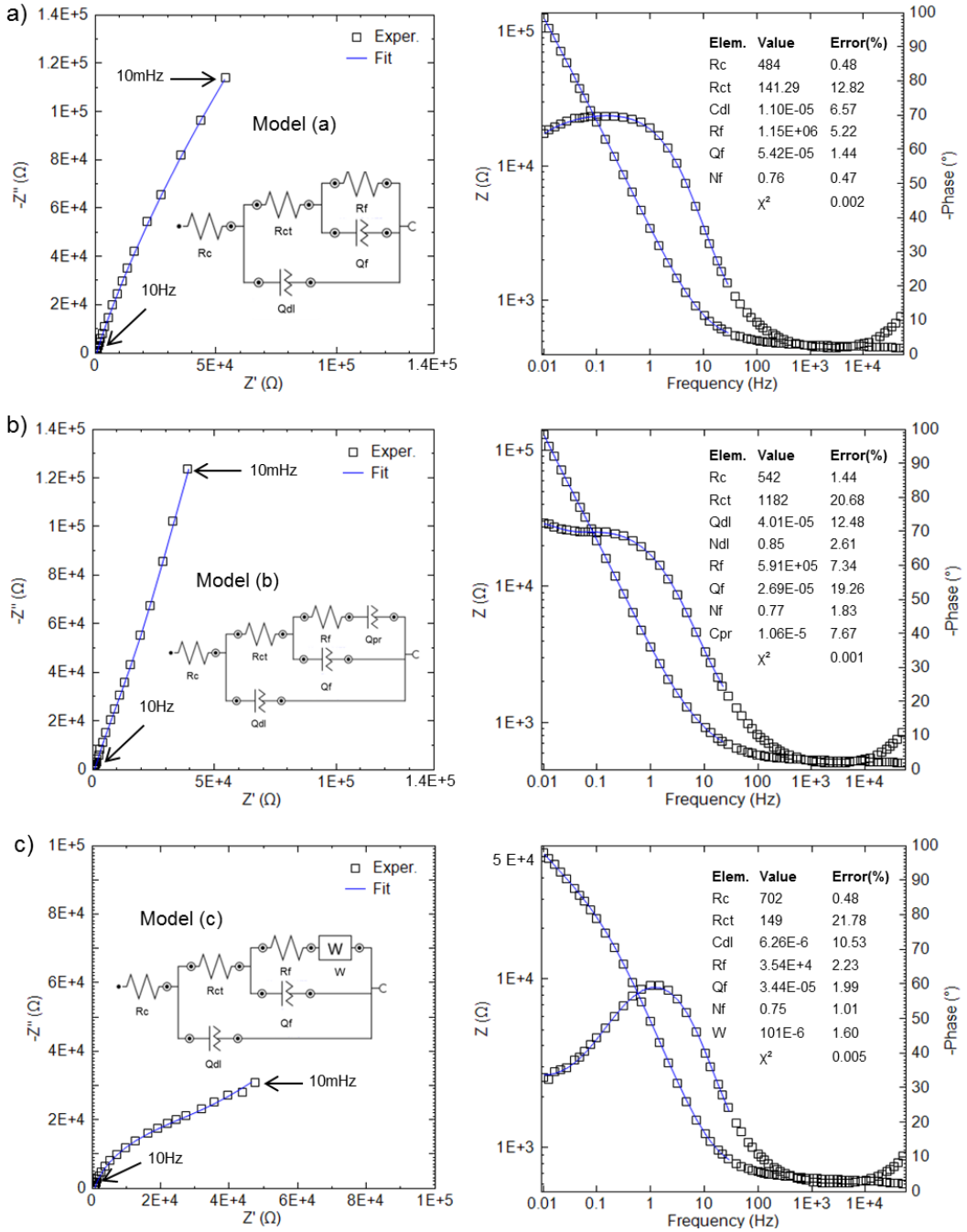

Figure 6.8: Different circuit models for EIS experimental responses (symbols) and fittings (solid lines): a) $St_{(D1)}$ (model (a), 13 days); b) $St_{(C1)}$ (model (b), 11 days); c) $St_{(D1)}$ (model (c), 99 days).

As previously mentioned, the OCP alteration is not sufficient for justification of the corrosion activity on the steel surface over time. Therefore, determination of corrosion initiation and quantification of steel corrosion requires calculation of polarization resistance (R_p) – a parameter linked to the corrosion activity on the steel rods. R_p was determined at certain times over the 180-day of treatment by summing up the best-fit resistance parameters (R_{ct} and R_f). Hence, the obtained R_p values were considered as the global resistance of the embedded steel rods [Jamil et al., 2004; Zheng et al., 2014]. The corrosion current densities were calculated from the R_p values.

6.3.3.3 Quantification of EIS response

As aforementioned, the interpretation of EIS responses can result in quantitative information for the systems under study. If more accuracy within quantification of electrochemical response is to be achieved, the general approach in electrochemistry is to couple at least two types of electrochemical measurements and correlate their outcomes. In this work, EIS mainly was employed as a non-destructive technique to determine the time for steel corrosion initiation in correlation to the chloride sensors' response. Therefore, although corrosion currents for steel during the tests are presented further below, absolute values are not claimed. The figures and discussion are rather presented in the sense of associating this work to reported literature, where corrosion current density is used as a main parameter of discussion. The derived corrosion current densities are also discussed in comparison to the well-accepted threshold values i.e. 0.1 to 0.5 $\mu A/cm^2$ [Castellote et al., 2002], beyond which steel is considered to be in active (corroding) state.

Figures 6.9, 6.10 and 6.11 present the corrosion current density of the steel rods over the immersion period. For comparative purposes, the plots also depict the OCP values of both steel and sensor. A correlation between the measured OCPs for the sensors and the corrosion current density for the nearby steel in each specimen provides information about the chloride concentration at the time of steel corrosion initiation. Depassivation is considered to be a sustained increase in the current density rather than a singular event of an increase in current density [COST 521, 2002; Angst et al., 2011].

It was expected that a passive layer forms on the surface of the embedded steel rods in cementitious materials. In this condition, low corrosion current density and more anodic OCP are generally observed [Gouda, 1970; Li and Sague, 2001; Moreno et al., 2004]. As seen in Fig. 6.9, the $St_{(A1)}$ and $St_{(A2)}$ are in a passive state during the first two weeks of immersion in simulated pore solution (SPS). This is evident from the low corrosion current density (<0.01 $\mu A/cm^2$) and more anodic OCP values (>-273 mV). The onset of steel corrosion is apparent from the simultaneous cathodic drop in OCP (-500 to -800 mV) and the increase in corrosion current density (>0.5 $\mu A/cm^2$) after 13-15 days of immersion. The simultaneously measured OCP of the sensors ($Se_{(A1)}$ and $Se_{(A2)}$) reflects the chloride content in the vicinity of the steel rods. In other words, the sensor's OCP at the time of corrosion initiation of steel can be linked to the chloride threshold value. The chloride threshold value for $St_{(A1)}$ and $St_{(A2)}$ was in the range of 380-440 mM. The chloride concentration at the time of steel corrosion initiation can be sufficiently high to initiate pitting corrosion, but might not necessarily be able to sustain a stable pit growth. The competition between aggressive chloride ions and hydroxide ions (pH=13.6) governs the processes of pitting and repassivation [Li and Sague, 2001; Moreno et al., 2004; Shi et al., 2011]. In the next stage, repassivation of $St_{(A1)}$ and $St_{(A2)}$ was evident from 22 days onwards. In this condition, the OCP of the steel rods shifted towards anodic values (>-273 mV) and the corrosion current density (<0.1 $\mu A/cm^2$) dropped. What can be concluded is that for specimens A, the sensors' response is well in line with the steel response. In other words, the OCP of the sensors reflects the chloride threshold for corrosion initiation, validated through the recorded OCP for the steel rod.

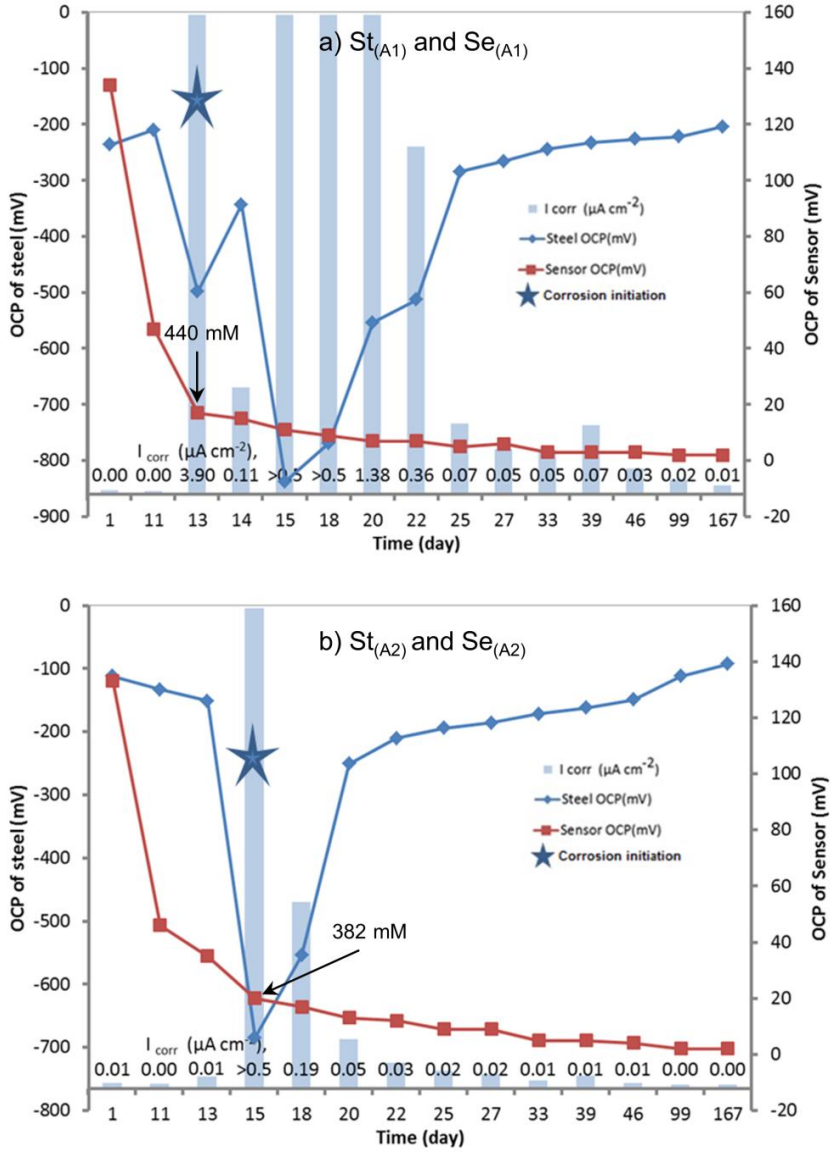

Figure 6.9: Corrosion current density (I_{corr}) of steel rods in addition to the OCP of steel and sensor at a certain time over immersion period: a) $St_{(A1)}$ and $Se_{(A1)}$; b) $St_{(A2)}$ and $Se_{(A2)}$

The electrochemical responses of $St_{(C1,2)}$ and $St_{(D1,2)}$ were different from $St_{(A1,2)}$. Within a few days after immersion, the OCP of $St_{(C1,2)}$ and $St_{(D1,2)}$ dropped to values more cathodic than -273 mV (Fig. 6.10) and the corrosion current density was lower than the threshold value (<~0.1 µA/cm^2) (Figs. 6.10 and 6.11). At the same time, the sensor's response ($Se_{(C1,2)}$ and $Se_{(D1,2)}$) demonstrated a very low chloride concentration (~8 mM) (Fig. 6.10). This amount of chloride ions is much lower than the reported chloride threshold values (45 mM to 650 mM – Table 2.2 in Chapter 2). These results indicate that the sustained cathodic OCP of $St_{(C1,2)}$ and $St_{(D1,2)}$ immediately after immersion in SPS is not due to chloride-induced corrosion initiation. The observed cathodic OCP is related to the limitations of the electrochemical reactions at the steel surface (discussed in Section 6.3.1.1). Corrosion initiation of $St_{(C1,2)}$ and $St_{(D1,2)}$ was evident by a sharp increase in the corrosion current density between 18 to 27 days (Fig. 6.10, 6.11). In these days, the sensor's response ($Se_{(C1,2)}$ and $Se_{(D1.2)}$) indicates a chloride threshold value of 350-480 mM. The corrosion activity for $St_{(C1)}$ and $St_{(D1,2)}$, except for $St_{(C2)}$, was sustained for the remaining period of the test.

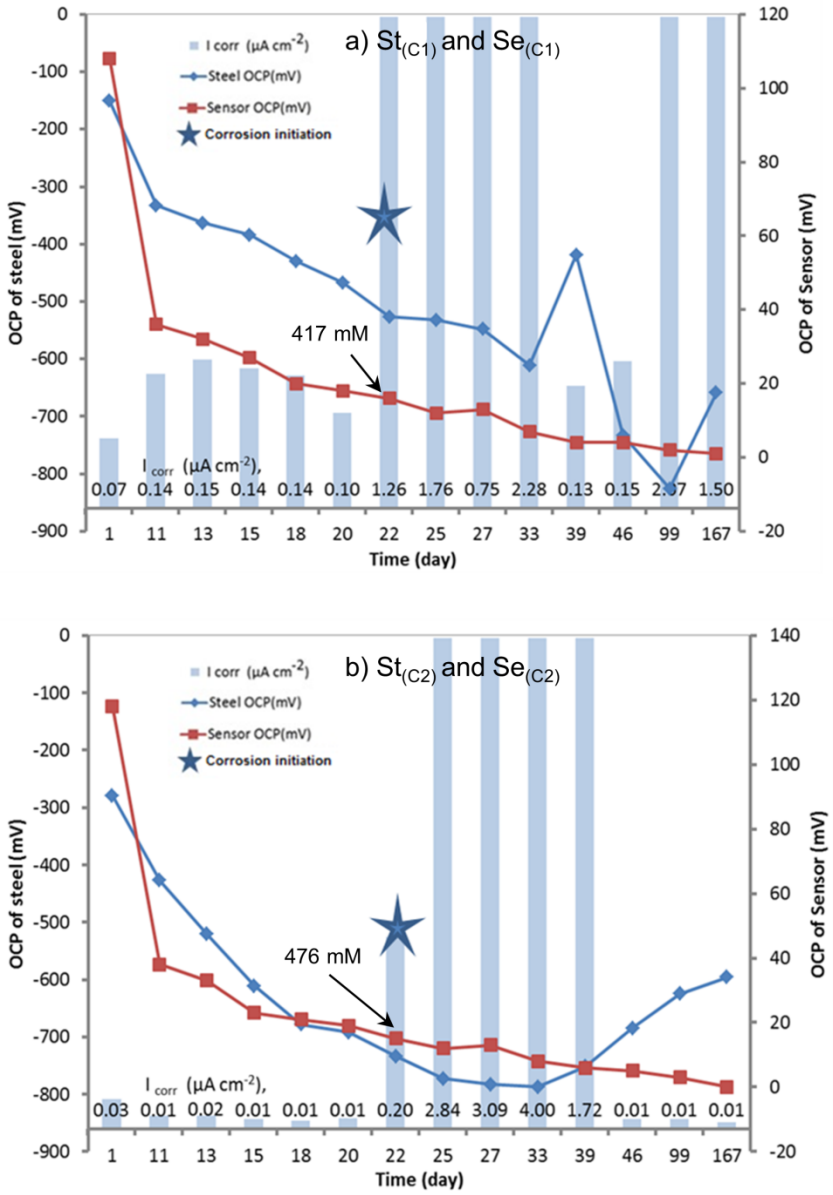

Figure 6.10: Corrosion current density (I_{corr}) of steel rods in addition to the OCP of steel and sensor at a certain time over immersion period: a) $St_{(C1)}$ and $Se_{(C1)}$; b) $St_{(C2)}$ and $Se_{(C2)}$

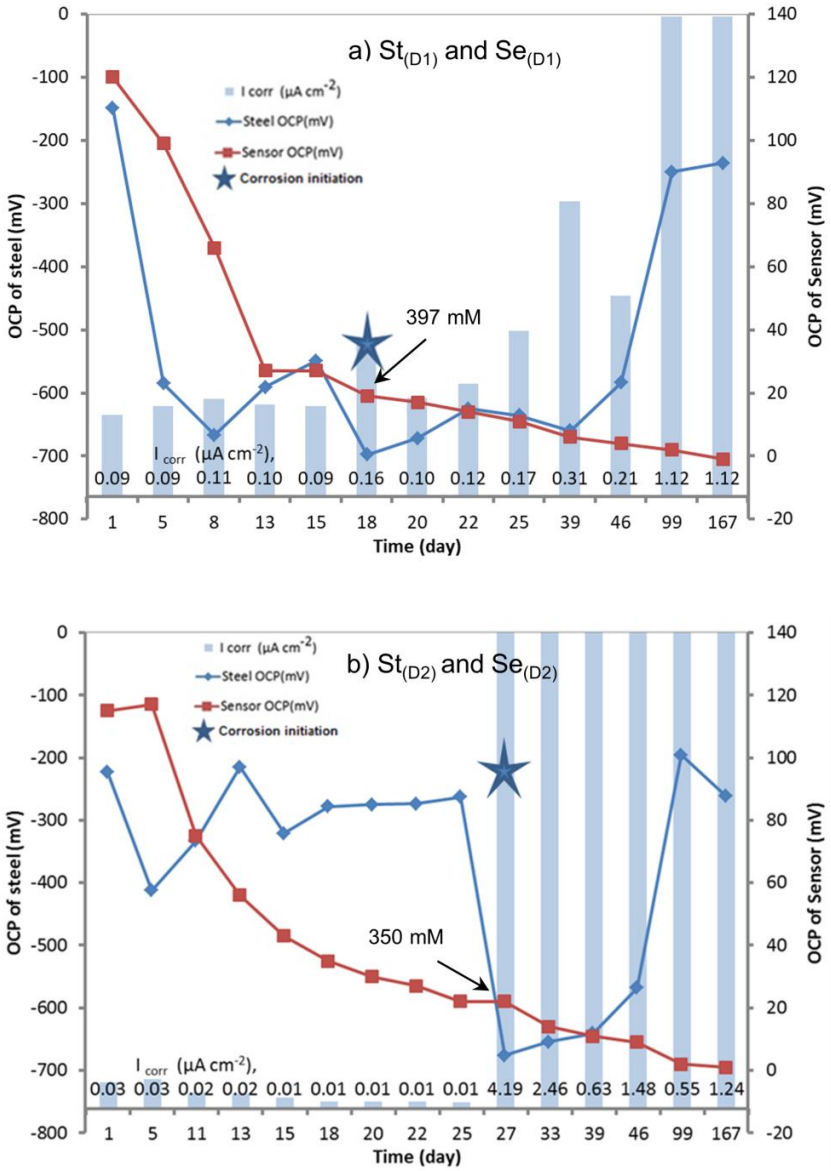

Figure 6.11: Corrosion current density (I_{corr}) of steel rods in addition to the OCP of steel and sensor at a certain time over immersion period: a) $St_{(D1)}$ and $Se_{(D1)}$; b) $St_{(D2)}$ and $Se_{(D2)}$.

With respect to the objective of this chapter, i.e. determination of chloride threshold value, the mathematical calculations show that the time for steel corrosion initiation is at day 19±5, when the sensor's OCP is 19±3 mV (equivalent to the chloride threshold value of 400±50 mM). Hence, 70% difference in the time for corrosion initiation and 30% difference among the chloride threshold values were determined. These variations were mainly attributed to the intrinsic heterogeneity of the cement paste system (including different levels of moisture and oxygen content on the steel surface).

6.4 Conclusions

In this chapter, the chloride sensors' response was linked to the corrosion state of the nearby steel rod. Based on the obtained results, the following conclusions can be drawn:

- Despite the identical experimental conditions (e.g. water to cement ratio, cement type, exposure conditions, pH of the solution, moisture and chloride content as well as steel rods preparation), there was a difference in the observed electrochemical responses of the steel rods and the chloride sensors. In the beginning of immersion, the sensor preparation regime, and therefore AgCl inner/outer morphology was the main cause for the observed variation in the sensor's OCPs, whereas the electrochemical response of the steel rods was similar (OCP>-273 mV and I_{corr}<0.1 µA/cm^2). Within the process of chloride penetration into the specimens, the (high) chloride levels, as determined by the sensors' response (e.g. 400±50 mM at ca. 20 days), did not necessarily correspond to active steel state and vice versa. The primary cause for the observed variability in time to corrosion initiation and in electrochemical response of steel rods appear to be the intrinsic heterogeneity of the cement paste system.
- The influence of the AgCl layer properties on the accuracy of the sensor's response decreases with increasing the chloride concentration in the medium. The chloride threshold value in the test condition of this study was high (i.e. 400 mM). Hence, all chloride sensors accurately determined the chloride concentration close to the steel rods. For a lower chloride threshold value (e.g. <100 mM), a sensor with higher sensitivity, reproducibility and accuracy should be used. These are sensors prepared via anodization regimes at low current densities (e.g. 0.5 mA/cm^2).

6.5 References

Abreu, C.M., Cristobal, M.J., Losada, R., Novoa, X.R., Pena, G. and Perez, M.C., (2006). Long-term behaviour of AISI 304L passive layer in chloride containing medium, *Electrochimica Acta*, Vol. 51(8–9), p. 1881–1890.

Andrade, C. and Gonzalez, J.A. (1978). Quantitative measurements of corrosion rate of reinforcing steels embedded in concrete using polarization resistance measurements, *Materials and Corrosion*, Vol. 29(8), p. 515–519.

Andrade, C., Keddam, M., Novoa, X.R., Perez, M.C., Rangel, C.M. and Takenouti, H. (2001). Electrochemical behaviour of steel rebars in concrete: influence of environmental factors and cement chemistry, *Electrochimica Acta*, Vol. 46(24–25), p. 3905–3912.

Andrade, C., Soler, L. and Novoa, X.R. (1995). Advances in electrochemical impedance measurements in reinforced concrete, *Materials Science Forum*, Vol. (192–194), p. 843 – 856.

Angst, U. M., Elsener, B., Larsen, C. K. and Vennesland, O. (2011). Chloride induced reinforcement corrosion: Electrochemical monitoring of initiation stage and chloride threshold values, *Corrosion Science*, Vol. 53(4), p. 1451–1464.

ASTM C876. (1991). *Standard Test Method for Half-Cell Potentials of Uncoated Reinforcing Steel in Concrete*, American Society for Testing and Materials (ASTM) Philadelphia, PA.

Bohni, H. (2005). *Corrosion in reinforced concrete structures*, CRC, New York.

Castellote, M., Andrade, C. and Alonso, C. (2002). Accelerated simultaneous determination of the chloride depassivation threshold and of the non-stationary diffusion coefficient values, *Corrosion Science*, Vol. 44 (11), p. 2409–2424.

COST 521. (2002). *Final report, Corrosion of steel in reinforced concrete structures*, Luxembourg.

Davis, J. R. (2000). *Corrosion: Understanding the Basics*, ASM International, Materials Park.

Duarte, R.G., Castela, A.S., Neves, R., Freirea, L. and Montemor, M.F. (2014). Corrosion Behavior of

Stainless Steel Rebars Embedded in Concrete: an Electrochemical Impedance Spectroscopy Study, *Electrochimica Acta*, Vol. 124, Volume 124, p. 218–224.

Duffo, G. and Farina, S. B. (2009). Development of an embeddable sensor to monitor the corrosion process of new and existing reinforced concrete structures, *Construction and Building Materials*, Vol. 23(8), p. 2746–2751.

Elsener, B. (2002). Macrocell corrosion of steel in concrete – implications for corrosion monitoring, *Cement and Concrete Composites*, Vol. 24(1), p. 65–72.

Elsener, B., Andrade, C., Gulikers, J., Polder, R. and Raupach, M. (2003). Half-cell potential measurements – Potential mapping on reinforced concrete structures, RILEM TC 154-EMC: Electrochemical Techniques for Measuring Metallic Corrosion, Recommendations, *Materials and Structures*, p. 461-471.

Feliu, V., Gonzalez, J.A., Andrade, C. and Feliu, S. (1998). Equivalent circuit for modelling the steel-concrete interface. I. Experimental Evidence and theoretical predictions, *Corrosion Science*, Vol. 40(6), p. 975-993.

Femenias, Y. S., Angst, U., Caruso, F. and Elsener, B. (2015). Ag/AgCl ion-selective electrodes in neutral and alkaline environments containing interfering ions, *Materials and Structures*, p. 1-15.

Ford, S. J., Shane, J. D. and Mason, T. O. (1998). Assignment of features in impedance spectra of the cement-paste/steel system, *Cement and Concrete Research*, Vol. 28(12), p. 1737-1751.

Gouda, V. K. (1970). Corrosion and Corrosion Inhibition of Reinforcing Steel: I. Immersed in Alkaline Solutions, *Corrosion Journal*, Vol. 5(5), p. 198-203.

Gu, P., Fu, Y., Xie, P. and Beaudoin, J. J. (1994). Effect of uneven porosity distribution in cement paste and mortar on reinforcing steel corrosion. *Cement and Concrete Research*, Vol. 24(6), p. 1055-1064.

Jamil, H.E., Montemor, M.F., Boulif, R., Shriri, A. and Ferreira, M.G.S. (2004). An electrochemical and analytical approach to the inhibition mechanism of an amino-alcohol-based corrosion inhibitor for reinforced concrete, *Electrochimica Acta*, Vol. 49(5), p. 836.

Joiret, S., Keddam, M., Novoa, X.R. N, Perez, M.C. P, Rangel, C. and Takenouti, H. (2002). Use of EIS, ring-disk electrode, EQCM and Raman spectroscopy to study the film of oxides formed on iron in 1M NaOH, *Cement and Concrete Composites*, Vol. 24(1). p. 7–15.

Koleva, (2010). Microstructural Characterization of Reinforced Mortar after Corrosion and Cathodic Prevention in the Presence of Core-shell Micelles, *Corrosion (General)–ECS Transactions, 217th ECS Meeting, The Electrochemical Society*, Vol. 28(24), p. 95-104.

Koleva, D.A. (2007). *Pulse cathodic protection, an improved cost-effective alternative*, PhD Thesis, Delft University Press, Delft, the Netherlands.

Koleva, D.A., de Wit, J.H.W., van Breugel, K., Veleva, L.P., van Westingd, E., Copuroglu, O. and Fraaij, A.L.A. (2008). Correlation of microstructure, electrical properties and electrochemical phenomena in reinforced mortar. Breakdown to multi-phase interface structures. Part II: Pore network, electrical properties and electrochemical response, *Materials Characterization*, Vol. 59(6), p. 801–815.

Li, L. and Sague, A.A. (2001). Chloride corrosion threshold of reinforcing steel in alkaline solutions-open-circuit immersion tests, *Corrosion*, Vol. 57(1), p. 19-28.

Mehta, P.K. and Monteiro, P.J.M. (2006). *Concrete: Microstructure, Properties, and Materials*, McGraw-Hill.

Moreno, M., Morris, W., Alvarez, M.G. and Duffo, G.S. (2004). Corrosion of reinforcing steel in simulated concrete pore solutions: Effect of carbonation and chloride content, *Corrosion Science* Vol. 46(11), p. 2681–2699.

Shi, X., Anh Nguyen, T., Kumar, P., and Liu, Y. (2011). A phenomenological model for the chloride threshold of pitting corrosion of steel in simulated concrete pore solutions, *Anti-Corrosion Methods and Materials*, Vol. 58(4), p. 179-189.

Silva, N. (2013). *Chloride Induced Corrosion of Reinforcement Steel in Concrete - Threshold Values and Ion Distributions at the Concrete-Steel Interface*, Dissertation in Civil Engineering (PhD thesis), Goteborg, Chalmers University of Technology, Sweden.

Song, H.W. and Saraswathy, V. (2007). Corrosion Monitoring of Reinforced Concrete Structures-A

Review, *International Journal of Electrochemical Science*, Vol. 2, p. 1- 28.

Subramaniam, K. V. and Bi., M. (2009). Investigation of the local response of the steel–concrete interface for corrosion measurement, *Corrosion Science*, Vol. 51(9), p. 1976–1984.

Wei, J., Fu, X.X., Dong, J.H. and Ke, W. (2012). Corrosion Evolution of Reinforcing Steel in Concrete under Dry/Wet Cyclic Conditions Contaminated with Chloride, *Journal of Materials Science & Technology*, Vol. 28(10), p. 905–912.

Yu, H. and Caseres, L. (2012). An embedded multi-parameter corrosion sensor for reinforced concrete structures, *Materials and Corrosion*, Vol. 63(1), p. 1011-1016.

Zhao, B., Li, J. H., Hu, R.-G., Du, R. G. and Lin, C.J. (2007). Study on the Corrosion Behavior of Reinforcing Steel in Cement Mortar by Electrochemical Noise Measurements, *Electrochimica Acta*, Vol. 52(12), p. 3976-3984.

Zheng, H., Li, W., Ma, F. and Kong, Q. (2014). The performance of a surface-applied corrosion inhibitor for the carbon steel in saturated $Ca(OH)_2$ solutions, *Cement and Concrete Research*, Vol. 55, p. 102–108.

Chapter 7

Retrospection, conclusions and recommendations

7.1 Retrospection

The Ag/AgCl electrode has been used as chloride sensor for non-destructive and continuous monitoring the content of free chloride ions in cementitious materials. Despite the well-known advantages of using chloride sensors, there are still debates on the performance of these sensors in a cement-based matrix. This strongly limits the application of chloride sensors in real practice. Factors affecting the performance (i.e. stability, reliability, reproducibility and reversibility) of chloride sensors in the alkaline environment of cementitious materials, made of different cement type, are the main concerns of this thesis.

Chapter 1 is an introduction, discussing the necessity of chloride sensors for determination of the chloride content in reinforced concrete structures. In that chapter the background and motivation for the thesis were presented. In Chapter 2 the advantages and drawbacks of available test methods for determination of the chloride content in cementitious materials were explained. The principal factors influencing the performance of the chloride sensor were described. In this regard the importance of the morphology and microstructure of the AgCl layer of the sensor, distribution of cement hydration products around the sensor and pore solution composition of cementitious materials were discussed.

In Chapter 3 the Ag/AgCl chloride sensors were produced in different anodization regimes. The responsible mechanism for AgCl formation during Ag anodization was described. The changes in morphology, microstructure and composition of the AgCl layer were linked to the applied current density and time of anodization. The obtained results gave an insight into how different anodization regimes can affect the properties of the AgCl layer. This chapter provided input to the discussion on different open circuit potential (OCP) response of the Ag/AgCl sensors in otherwise identical alkaline environment.

In Chapter 4 the stability and reproducibility of the prepared chloride sensors were discussed. The calibration curve for chloride sensors in different solution was determined. The interference of hydroxide ions in solutions with different hydroxide and chloride ion contents was assessed. The deviation of the sensor's response from the expected performance was discussed with respect to AgCl de-chlorination and silver oxide formation on the sensor's surface. The electro-chemical transformation of AgCl to silver oxides was confirmed by analysis of the composition of the AgCl layer, before and after conditioning in alkaline solution.

In Chapter 5 the importance of cementitious mix design (water-to-powder ratio – w/p) and cement composition (type of cement) on the OCP response of the chloride sensors were discussed. The sensor's OCP was assessed with respect to the presence of cement hydration products around the sensor and the activity of chloride, hydroxide and sulfide ions in the surrounding cement-based matrix. The chloride content inferred from the sensor's response was compared to the chloride content obtained by destructive water-soluble chloride methods.

The observed difference between the chloride contents determined by these methods was discussed with respect to the cementitious mix design, the chloride binding capacity of cement hydration products and the chloride concentration in the matrix.

In Chapter 6 the chloride sensor was used for determining the chloride content in the vicinity of a steel rod embedded in cement paste cylinders with known mix design. The critical chloride content for corrosion initiation of the steel was inferred from the chloride sensor's response. An attempt for non-destructive determination of the chloride threshold value was made.

7.2 Conclusions

This study deals with the production and performance of the chloride sensor for determination of the free chloride concentration in cementitious materials. The following conclusions are drawn from the obtained results.

Influence of anodization regime used for sensor preparation on the AgCl layer properties

- The anodization regime used for sensor preparation is important for the morphology, microstructure and surface chemistry of the formed AgCl layer. Anodization at low current density (e.g. 0.5 mA/cm^2) results in the formation of "packed-piled" AgCl particles on the Ag substrate. The current density of above 2 mA/cm^2 increases heterogeneity of the AgCl layer. Hence, a bi-layer structure AgCl forms on the Ag substrate. The amounts of silver oxide-based and carbon-based impurities on the sensor's surface are proportional to the thickness and heterogeneity of the AgCl layer. These subsequently result in different OCP response of the chloride sensors in otherwise identical alkaline environment.

Evaluation of the chloride sensors' performance in simulated pore water

- The variation in the OCP response of the chloride sensor in alkaline solution depends on the anodization regime used for sensor preparation and the chloride concentration in the environment. The OCP response of the chloride sensor prepared at low current density regime (e.g. 0.5 mA/cm^2) was found to be more *stable* and *reliable* and *reproducible* than the OCP response of the chloride sensor prepared at high current density regime, e.g. 4 mA/cm^2.
- The response of the sensor in chloride-free alkaline solution is unstable due to the AgCl de-chlorination and transformation of the Ag/AgCl interface to a more complex Ag/AgCl/Ag_2O(AgO) interface. The silver oxides transform again to AgCl (*reversibility*) upon the addition of chloride ions to the solution. The time needed for a sensor's recovery and a stable Ag/AgCl response is chloride-content dependent (see Chapter 4, Section 4.3.4). The transformation of silver oxides to AgCl takes longer time in a solution with a lower chloride concentration (5 hours in 125 mM versus 30 minutes in 1000 mM).

Sensor's response in cementitious materials with different w/p ratio and cement composition

- The sensor's OCP in a cement-based matrix with low chloride concentration (e.g. 10 mM) depends on the cementitious mix design (i.e. w/p ratio). The sensor's OCP in a mixture with low w/p (i.e. 0.35) ratio is more anodic than the expected response for a Ag/AgCl interface (e.g. the sensor's OCP in a mixture with high w/p ratio (i.e. 0.5)). The more anodic OCP indicates the lower accuracy of measuring free chloride content from the

sensor's response in mixtures with low w/p ratio. This is the result of a dense matrix of cement hydration products, higher ionic strength and lower activity of chloride ions on the sensor's surface. By increasing the chloride concentration to values higher than 100 mM [1], the dependency of the sensor's OCP on the w/p ratio of the mixture is decreased.

- The chloride sensor's OCP in Portland cement paste can be described by Nernst equation for a Ag/AgCl interface. However, the sensor's OCP in slag cement paste follows a significantly different trend. The interference of sulfide ions with the sensor results in a Ag_2S formation on the sensor's surface and a shift in the sensor's OCP towards negative potential values (e.g. -800 mV). This shift in the sensor's OCP indicates the presence of free chloride ions on the sensor's surface, but the amount of this chloride ions cannot be determined from the sensor's response.

Evaluation of the chloride sensor's response versus destructive water-soluble chloride

- The free chloride content inferred from the chloride sensor's response is significantly different from the water-soluble chloride measured in cement-based matrix. The cement composition and w/p ratio as well as the chloride concentration in the medium affect the correlation between the free and water-soluble chloride contents. The free chloride and water-soluble chloride contents are close in a cement-based system with low chloride binding ability and high chloride concentration.

Correlation of the sensors' response to the corrosion activity on the steel surface

- The chloride content for corrosion initiation of steel rods was inferred from the response of the nearby sensor in a cement paste. The chloride content for corrosion initiation of steel rods was 400±50 mM [2] and the time to corrosion initiation was in between 19±5 days. The observed variations were attributed to the intrinsic heterogeneity of the cement paste system (e.g. different oxygen content at the steel surface).

Considering all above mentioned, the sensor's response in a medium depends on the alkalinity of the medium, anodization regime used for sensor preparation, type of cement and mix design of cementitious materials. The effect of these parameters on the chloride sensor's response is schematically summarized in Figs. 7.1a to 7.1d. The sensor's response is generally stable in low pH solution (e.g. pH 9) and chloride-containing alkaline solution (Fig. 7.1a). The variation in the OCP response of the chloride sensor in an alkaline solution (e.g. pH > 12.5) depends on the concentration of chloride ions (Fig. 7.1a). The difference between the OCP of the chloride sensor in low pH and high pH solution (Fig. 7.1a) decreases with an increase of chloride concentration.

The anodization regime used for sensor preparation does not affect the stability of the chloride sensor in chloride-free and chloride-containing alkaline solution. The sensor prepared at low/high current density is generally unstable in the chloride-free alkaline solution (Fig. 7.1b), while it is stable in the chloride-containing alkaline solution (Fig. 7.1b). The variation in the OCP of the prepared sensor at high current density (Fig. 7.1b) is chloride content dependent.

[1] It is equivalent to ~0.05% by weight of binder.
[2] In this particular case: 0.22±0.03% by weight of binder.

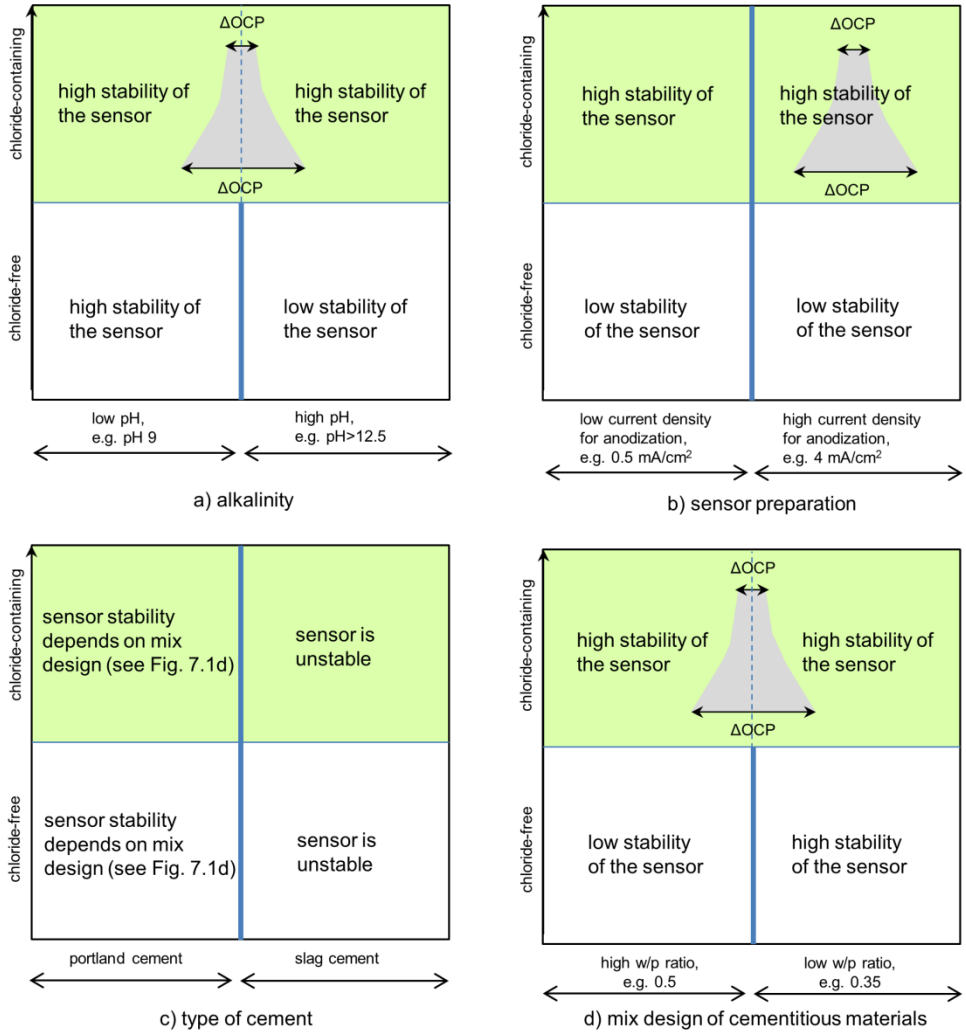

Figure 7.1: Schematic representation of the influence of studied parameters on the performance of the chloride sensor: a) alkalinity of the solution; b) sensor preparation; c) type of cement; d) mix design.

The sensor's response in slag-containing cement paste is potentially unstable (Fig. 7.1c). The stability of the sensor in Portland cement paste depends on the w/p ratio of the paste (Figs. 7.1c and 7.1d). In chloride-free environment (Fig. 7.1d), the lifetime of the chloride sensor in a mixture with high w/p ratio (e.g. 0.5) is shorter than that in a mixture with low w/p ratio (e.g. 0.35). The high accessibility of the pore water to the sensor leads to the gradual dissolution of the AgCl layer and thereby potentially impairs the sensor's stability. Despite the stability of the sensor in chloride-containing cement paste (Fig. 7.1d), the OCP response of the chloride sensor in a mixture with high w/p ratio is different from the one in a mixture with low w/p ratio. The difference between the chloride sensor's OCP in mixtures with high and low w/p ratio decreases for higher chloride concentrations.

In summary, the influence of different parameters on the sensor's response in the alkaline medium of cementitious materials was studied. The interpretation of sensor's response was linked to the knowledge of the surrounding medium. In this regard, the mix design and composition of cementitious materials significantly affects the sensor's response. Despite the limitations of the chloride sensor for application in cementitious materials, the potentiometry method is a feasible and reliable approach for a continuous and non-destructive determination of the chloride content.

7.3 Recommendations for future work

The focus of this thesis was on the performance of the Ag/AgCl sensors in highly alkaline environment, as in reinforced concrete. Further research is recommended on the following aspects:

- The chloride sensor should be robust and durable for application in a concrete structure. Encasing of the sensor in a cementitious material is an approach for use of the chloride sensor in practice. Based on the obtained results, the following mix design for a cement paste is suggested: high w/p ratio (e.g. 0.5), low alkalinity of the pore solution, low chloride binding ability (e.g. sulfate resistance cement) and 10 mM cast-in chloride content.
- For a better interpretation of the sensor's response and evaluation of the risk of corrosion of embedded reinforcement, simultaneous monitoring of chloride and hydroxide ions in the vicinity of reinforcement is necessary. Although coupled chloride-pH sensors have been presented in literature, their performance needs further evaluation. Hence, these aspects require further research.
- For long-term performance of the Ag/AgCl sensor in both Portland and slag cement concrete, the use of two approaches needs be assessed:
  1) the encasing of the chloride sensor in chelating resin or melted AgCl to minimize the interference of hydroxide and sulfide ions (i.e. in CEM III mixtures), but still sensitive to chloride ions.
  2) the application of electrochemical polarization techniques for re-generation of an embedded chloride sensor in cementitious materials, when the deviation in the sensor's OCP from the expected response is significant.
- The performance of the chloride sensor in non-saturated concrete, i.e. splash zone needs to be assessed.

Appendix A:

ESEM observation of Ag/AgCl interface for the produced sensor at 4 mA/cm^2 and varying anodization time

It was revealed in Chapter 3 that, Ag anodization for 1h at 4 mA/cm^2 current density regime (sensors D) causes a high level of complexity, variation in morphological features and a distinct bi-layer structure of the AgCl on the Ag substrate. To support the above discussion, ESEM micrographs of a sensor from type D at 4 mA/cm^2 but with the varying time of anodization (900s, 1500s, 2500s and 3600s) are presented in Fig. A.1. The last time interval (i.e. 3600s) corresponds to the time of 1h anodization used for preparation of sensors A to D (0.5 mA/cm^2 to 4 mA/cm^2) in Chapter 3.

The thickness of the AgCl layer after 900s of anodization (Figs. A.1a,b) was 10 μm. The top surface of the AgCl layer demonstrates the AgCl particles with irregular shapes and small grains appear at the bottom portion of the AgCl layer (Figs. A.1b).

With increase in the anodization time to 1500s, a thicker AgCl layer (15 μm) formed. At this stage, a bi-layer AgCl formation initiates with the contribution of small AgCl grains in both the bulk top layer and on the Ag substrate (Figs. A.1c,d).

After anodization for 2500s and 3600s, the morphology of the top surface of the AgCl layer was highly twisted and irregularly shaped (Figs. A.1e,f). The cross section of the Ag/AgCl interface revealed a bi-layer structure and the presence of small AgCl grains with opened pore space near the Ag substrate (Figs. A.1f,h). These features can be an indication of weak adhesion of the AgCl layer to the Ag substrate.

From the obtained results, it can be concluded that, the complexity and heterogeneity of the AgCl layer depend on the anodization time. The small AgCl grains together with interlayer cavities and irregular empty space were observed at all time intervals. However, a bi-layer AgCl was observed in after a certain time of anodization. The increased heterogeneity and the weak adhesion of the AgCl layer to the Ag substrate subsequently affect the sensors' OCP in an alkaline medium (discussed in Chapter 4).

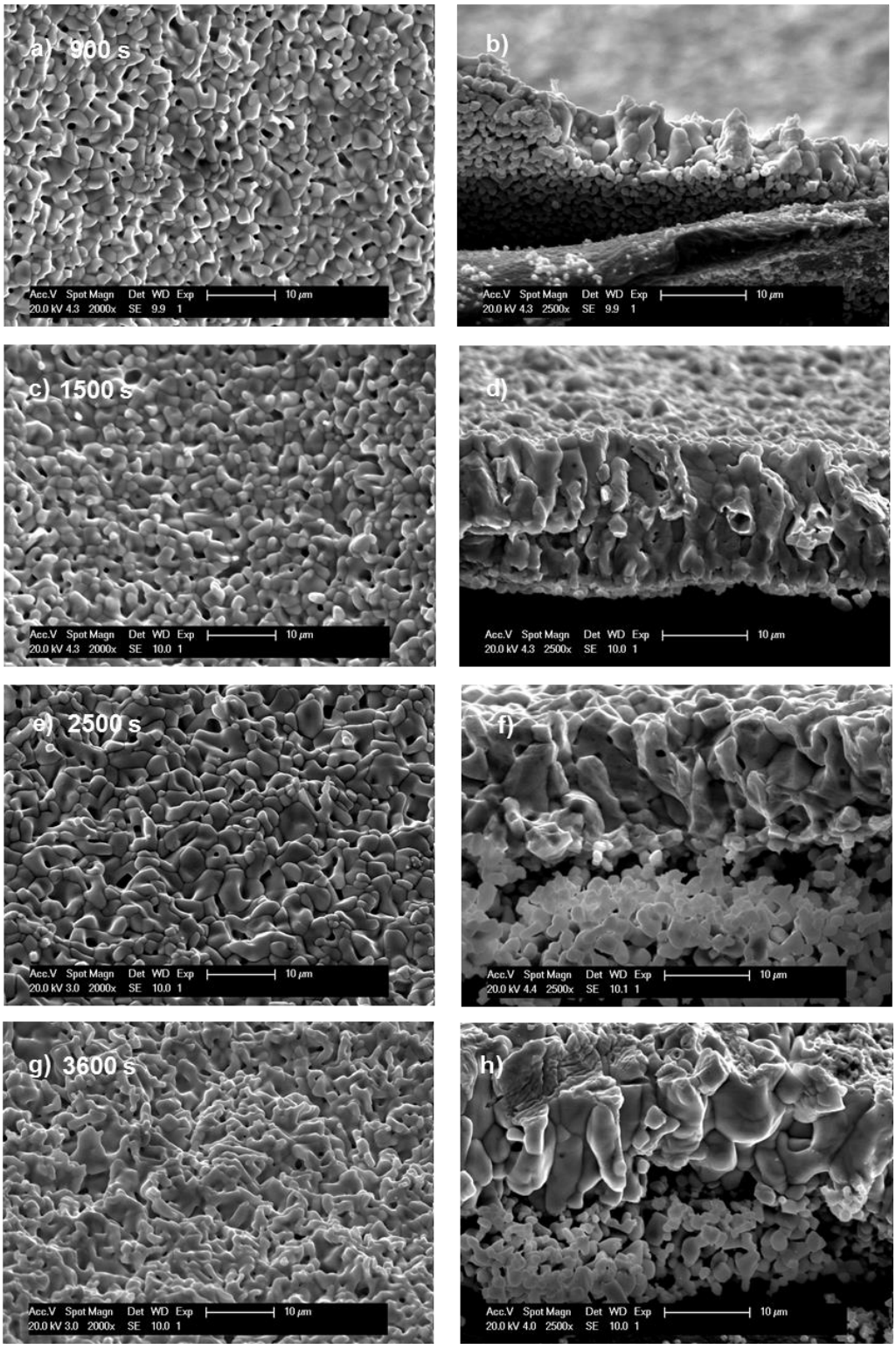

Figure A.1: ESEM images of the surface AgCl layer and cross section of the Ag/AgCl interface for a D-type sensor produced at 4 mA/cm^2 and varying anodization time: (a,b) 900s; (c,d) 1500s; (e,f) 2500s; (h,f) 3600s.

Appendix B:

Surface composition of AgCl layer for produced sensors at different current densities after one hour anodization

The high-resolution XPS spectra for sensor A- 0.5 mA/cm^2, sensor B- 1 mA/cm^2, sensor C- 2 mA/cm^2 and sensor D- 4 mA/cm^2 are presented in Fig. B.1. The Ag3d spectra are presented in Fig. B.1a. The binding energy of Ag3d states of different Ag compounds and metallic silver (Ag°) are very close to each other, i.e. within 0.5 eV [Kaushik, 1991; Ferraria et al., 2012]. For comparative purposes, the AgMNN peak for Ag° is shown in Fig. B.1b. The modified Auger parameter (ά = EK(AgMNN) + EB($Ag3d_{5/2}$) was used for a more accurate determination of the chemical state of Ag by eliminating the surface effects of electrostatic charging [Wagner, 1975]. The binding energy for oxygen (O1s) is also presented in Fig. B.1c. The obtained surface atomic concentrations are given in Table B.1. The XPS analysis does not claim absolute values for chemical composition of the AgCl layers, but provides an accurate (quantitative) comparison of equally handled samples.

Before analysis of the XPS results in Fig. B.1, the following point should be considered. The process of Ag anodization in 0.1 M HCl (pH=1.4) results in electro-formation of a AgCl layer on the Ag substrate. The acidic solution for sensor preparation (0.1 M HCl) limits the formation of Ag_2O and results in AgCl formation (discussed in Chapter 3). Hence, detection of compounds other than AgCl by XPS analysis can be considered as impurities on the sensors' surface. The presence of impurities can be due to the used current density regime for sensor preparation and different thickness, morphology and adhesion of the AgCl layer to the Ag substrate.

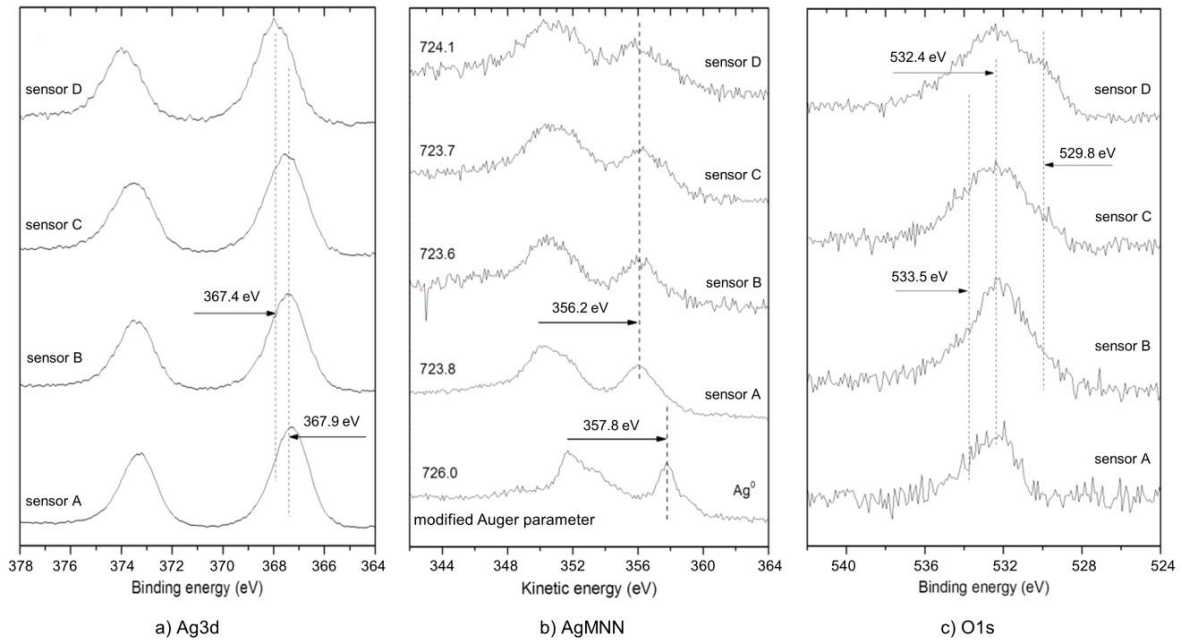

Figure B.1: High resolution XPS spectra for sensors after 1h anodization at 0.5 mA/cm^2 (sensor A), 1 mA/cm^2 (sensor B), 2 mA/cm^2 (sensor C) and 4 mA/cm^2 (sensor D): a) Ag3d photoelectron lines; b) AgMNN – Auger lines and c) O1s photoelectron lines.

Table B.1: Surface atomic concentration (at. %) of the AgCl layer for sensors after 1h anodization at 0.5 mA/cm^2 (sensor A), 1 mA/cm^2 (sensor B), 2 mA/cm^2 (sensor C) and 4 mA/cm^2 (sensor D) – (C1s (carbon), Ag3d (silver), Cl2p (chloride) and O1s (oxygen)).

Sensor	C1s, carbon (%)		Ag3d, silver (%)	Cl2p, chloride (%)	O1s, oxygen (%)
	C-C; C-H	C-O			
A	19	12	27	34	8
B	41	28	8	13	10
C	42	25	10	13	10
D	59	19	3	5	14

B.2.1 XPS analysis for sensors A and B

The $Ag3d_{5/2}$ core level for sensor A at 367.4 eV (Fig. B.1a) is attributed to AgO [Kaushik, 1991]. The kinetic energy of the AgMNN peak at 356.2 eV (Fig. B.1b) slightly differs (0.5 eV) from the corresponding energy for AgO. The binding energy of the O1s peak (Fig. B.1c) at 532.4 eV is attributed to Ag-C-H-O and/or OH^-. Additionally, the modified Auger parameter for sensor A exhibits a value of 723.8. This value is in the range between 723.5 for AgCl and 724.2 for AgO. The recorded atomic concentrations ratio for sensor A (Table B.1) is Ag : Cl : O = 3.4 : 4.2 : 1. These results do not support the presence of AgO on the surface of sensor A.

The binding energies for sensor A and sensor B were similar. The AgMNN peak for the thicker AgCl layer (i.e. in sensor B) was slightly broader, compared to that in sensor A (Fig. B.1b). The Auger parameter for sensor B with a value of 723.6 is closer to that for AgCl (723.5) [Kaushik, 1991]. The surface atomic concentration for sensor B (Table B.1) is Ag : Cl : O = 0.8 : 1.3 : 1. Except the higher amount of carbon impurities for sensor B, the surface composition of sensors A and B is similar.

B.2.2 XPS analysis for sensors C and D

The photoelectron lines and the Auger peaks for sensors C and D are different from those for sensors A and B. Broadening of the Ag3d peak and a shift of the binding energy towards higher values can be observed in Fig. B.1a. The binding energy of 367.5 eV and 367.9 eV was measured for sensors C and D, respectively. The broadening of the Ag3d pattern is related to the presence of sub-peaks for silver in a different state. This is also reflected in the AgMNN peaks (Fig. B.1b), where the kinetic energies of 356.2 eV and 357.8 eV correspond to Ag^{2+} (as source of AgO) and Ag°, respectively. The shape of the AgMNN peak line is similar to that for a mixed silver-silver oxide electrode [Ferraria et al., 2012]. Additionally, several binding energies were obtained from the O1s peaks for sensors C and D (Fig. B.1c). The O1s peak at 532.4 eV corresponds to Ag-C-H-O, whereas the shoulder at 529.8 eV is attributed to Ag_2O and/or AgO. The wide shoulder of the O1s pattern at 533.5 eV corresponds to OH^- or the adsorbed water. The concentration ratio between elements on the surface is Ag : Cl : O = 1 : 1.3 : 1 for sensor C, and Ag: Cl : O = 4.67 : 2.8 : 1 for sensor D.

The surface of the AgCl layer for sensors C and D composed of AgCl together with metallic silver (Ag°), AgO and carbon-based compounds. The presence of Ag° for these sensors is evident in Fig. B.1. The Ag3d peak at 367.9 eV (Fig. B.1b) and the shoulder in the AgMNN Auger line at 357.8 eV are related to Ag° (Fig. B.1b). Broadening of the shoulder in the O1s pattern at 529.8 eV (Fig. B.1c) indicates the presence of AgO on the surface of

sensors C and D. The high atomic concentration of carbon-based compounds (C1s (carbon) in Table B.1) is due to the adsorption of carbon from the air during the anodization process for sensor preparation. The enhanced surface area of the sensors C and D together with the well-known catalytic activity of Ag for CO_2 reduction result in the formation of carbon-based compounds and reduction of Ag^+ to Ag° [Hatsukade et al., 2014].

B.2.3 Correlation of results on surface analysis

Considering the above XPS results, it can be stated that the sensors' surface is mainly composed of AgCl together with impurities such as AgO, Ag_2O and Ag-C-H-O. The concentration of silver oxide and Ag-C-H-O increases with increasing the current density used for sensor preparation. The "purity" of surface AgCl is in the order of: A > B~C > D. Therefore, among all sensors, sensor A contains higher amount of silver chloride at the sensor's surface. The impurities increase in sensors B and C. The highest level of impurities was observed in sensor D. The XPS results confirmed that the presence of impurities on the sensors' surface depends on the anodization regime used for sensor preparation. These results together with the different morphology and microstructure of the AgCl layer (Chapter 3) explain the different OCP response of the sensors in alkaline solution (Chapter 4).

References

Ferraria, A.M., Carapeto, A.P. and Botelho Do Rego, A.M. (2012). X-ray photoelectron spectroscopy: Silver salts revisited, *Vacuum*, Vol. 86(12), p. 1988-1991.

Hatsukade, T., Kuhl, K.P., Cave, E.R., Abram, D.N. and Jaramillo, T.F. (2014). Insights into the electrocatalytic reduction of CO_2 on metallic silver surfaces, *Physical Chemistry Chemical Physics*, Vol. 16(27), p. 13814-13819.

Kaushik, V. K. (1991). XPS core level spectra and Auger parameters for some silver compounds, *Journal of Electron Spectroscopy and Related Phenomena*, Vol. 56(3), p. 273-277.

Wagner, C.D. (1975). Chemical shifts of Auger lines, and the Auger parameter, *Faraday Discuss. Chem. Soc.*, Vol. 60, p. 291-300.

Appendix C:

XPS profile of the AgCl composition for sensor C (2 mA/cm^2) before and after immersion in alkaline solution

Figures C.1 and C.2 depict the high-resolution XPS patterns for the flat Ag/AgCl sensors prepared at 2 mA/cm^2 (i.e. similar to that for preparation of sensor C) before and after immersion in alkaline solution. The atomic concentrations of the different elements were presented in Table C.1.

Surface XPS analysis

For sensor C, binding energy (BE) of $Ag3d_{5/2}$ before and after immersion in alkaline solution is 367.8 eV. This value can be attributed to different silver compounds, but closer to Ag_2O and AgO. The AgMNN peak (Fig. C.1b) with the kinetic energy of 355.7 eV correspond to AgO (355.5 eV) or AgCl (355.4 eV). The Auger parameter for untreated and treated sensors (723.5) is also related to AgO and AgCl (723.5). Considering binding and kinetic energies as well as Auger parameter, the presence of AgO and AgCl on the surface of both untreated and treated sensors is evident.

The broadening of the O1s pattern for the untreated sensor (Fig. C.1c) at a binding energy of 532.4 eV to 533.5 eV is due to the adsorbed H_2O or oxygen-containing contamination (532.4 eV). The main O1s peak (531.0 eV) for the treated sensor is related to Ag_2O (529.2 eV to 530.9 eV) and the shoulder at 529.8 eV is attributed to AgO (528.4 eV to 530.5 eV). The surface atomic concentration ratio (Table C.1) for untreated sensor is Ag : Cl : O = 25 : 4 : 1, and for treated sensor is Ag : Cl : O = 9 : 0.2 : 1. The decrease in chloride to oxygen ratio from 4 for untreated sensor to 0.2 for treated sensor indicates de-chlorination of the sensor after immersion in alkaline medium.

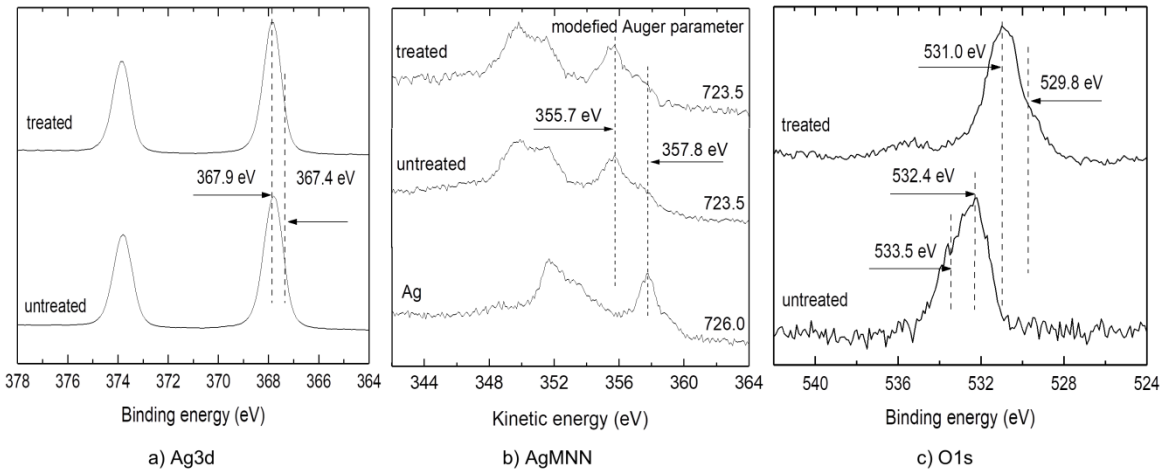

Figure C.1: High-resolution XPS spectra of the A and C sensors (without sputtering) before and after immersion in NaOH solution: a) Ag3d photoelectron line; b) AgMNN – Auger lines and c) O1s photoelectron lines.

Table C.1: Atomic concentration (at. %) of elements on the surface and in-depth of the AgCl layer for sensor A before and after immersion in alkaline medium (C1s (carbon), oxygen (O1s), Ag3d (silver), Cl2p (chloride) and N1s (sodium)).

Sputtering	C1s, carbon (%)	O1s, oxygen (%)	Ag3d, silver (%)	Cl2p, chloride (%)	N1s, sodium (%)	chloride /oxygen
Sensor C – untreated						
0 min	8	3	77	12	-	4
5 min (sputtering)	0.4	0.1	92.5	7	-	70
10 min (sputtering)	0.3	0.1	93.4	6	-	60
Sensor C – treated						
0 min	6	8	78.5	2	4	0.2
5 min (sputtering)	0.4	4	91.0	0.2	4	0.05
10 min (sputtering)	0.3	4	90.5	0.2	4.5	0.05

In-depth XPS analysis:

The Ag3d, AgMNN and O1s patterns in depth of the AgCl layer before and after treatment in alkaline solution are presented in Fig. C.2. The patterns after 5 minutes and 10 minutes sputtering were similar. The $Ag3d_{5/2}$ peak (368.2 eV) for both untreated and treated sensors cannot be attributed to a single silver compound (Fig. C.2a). The AgMNN kinetic energy and Auger parameter (Fig. C.2b) for untreated and treated sensors are close to the one for Ag° with the kinetic energy of 357.8 eV and Auger parameter of 726.0 eV. However, there is a secondary AgMNN peak for the untreated sensor at 355.5 eV which cannot be observed in the pattern for the treated sensor. This peak is related to AgCl (355.4 eV). The absence of this peak in the treated sensor is a strong evidence for the transformation of AgCl to silver oxide compounds after immersion in alkaline solution.

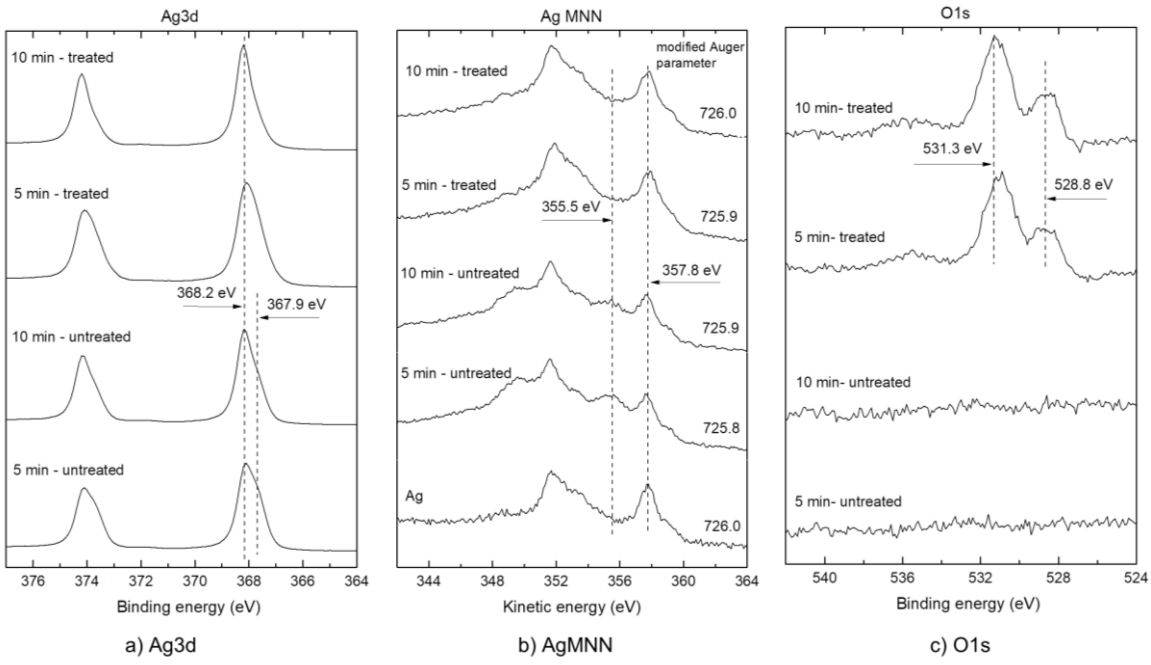

Figure C.2: High-resolution XPS spectra of sensor C (5 minutes and 10 minutes sputtering) before and after immersion in NaOH solution: a) Ag3d photoelectron line; b) AgMNN – Auger lines and c) O1s photoelectron lines.

The O1s patterns (Fig. C.2c) for untreated and treated sensors were different. The O1s pattern for untreated sensor is a flat plateau with low energy peaks. This indicates the absence of oxide compounds in depth of the AgCl layer. However, the pronounced O1s peaks for the treated sensor are related the oxide compounds. The main O1s peak for treated sensor at binding energy of 531.3 eV is related to Ag_2O (529.2 eV to 530.9 eV), while broadening of O1s pattern at 528.8 is due to AgO (528.4 eV to 530.5 eV). The atomic concentration (Table C.1) for untreated sensor is Ag : Cl : O = 934 : 60 : 1, while for treated sensor this is Ag : Cl : O = 21 : 0.05 : 1. The chloride to oxygen ratio decreased from 60-70 to 0.05 after treatment in alkaline medium. The dechlorination of the AgCl layer and formation of silver oxide compounds are the main cause for the significant decrease in the chloride content of the layer.

Appendix D:

ESEM/EDS analysis of the interface between the chloride sensor and the paste in C_3S and C_3S+C_3A specimens after 300-day immersion in chloride-free simulated pore solution

Sample preparation and test method: The C_3S and C_3S+C_3A specimens were impregnated with epoxy resin and cut to reach the tip of the steel and sensor's surfaces. Surface grinding was performed with ≠800, ≠1200 and ≠4000 silicon carbide grinding papers. The specimens were further polished by 6 µm, 3 µm, 1 µm and 0.25 µm diamond paste on a lapping table. Next the specimens were coated with a 10 nm carbon layer in a Leica EM CED030 carbon evaporator. The ESEM/EDS analysis was performed using Philips XL30 scanning electron microscope (ESEM) equipped with an EDAX energy dispersive spectrometer (EDS) in hi-vac mode. The accelerated voltage of 20 kV was used.

Results: The EDS spectra of the cross section of C_3S (w/p=0.5) and C_3S+C_3A (w/p=0.5) specimens show different hydration products (as expected). The large crystals of Portlandite was detected on the surface of the sensor in C_3S (w/p=0.5) specimens (Figs. D.1, D.3a). The formation of large crystals of Portlandite is less pronounced in C_3S+C_3A (w/p=0.5) specimens. The EDS spectra for C_3S+C_3A (w/p=0.5) specimens shows that Portlandite was replaced, at least partly, by sulfide-containing compounds (such as ettringite) on the sensor's surface. These observations indicate the influence of cement composition on the presence of hydration products (such as Portlandite) on the sensor's surface.

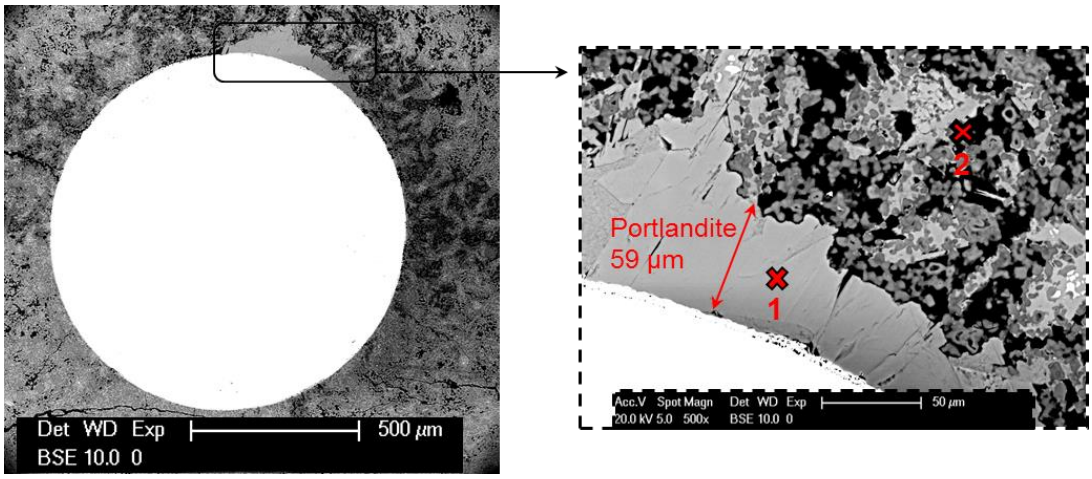

Figure D.1: ESEM images of the cross section of the embedded sensor in C_3S (w/p=0.5) specimen after 300 days of immersion in chloride-free solution. The large crystals of Portlandite can be found occasionally around the sensor. The EDS spectra of the points 1 and 2 are presented in Fig. D.2.

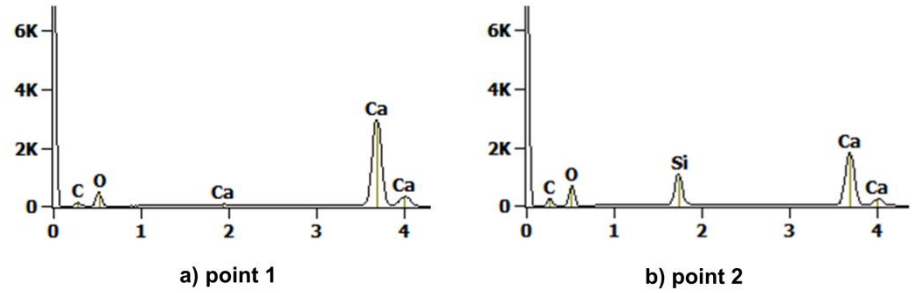

Figure D.2: The EDS spectra of the specified points in Fig. D.1 for C_3S (w/p=0.5) specimen: a) point 1; b) point 2.

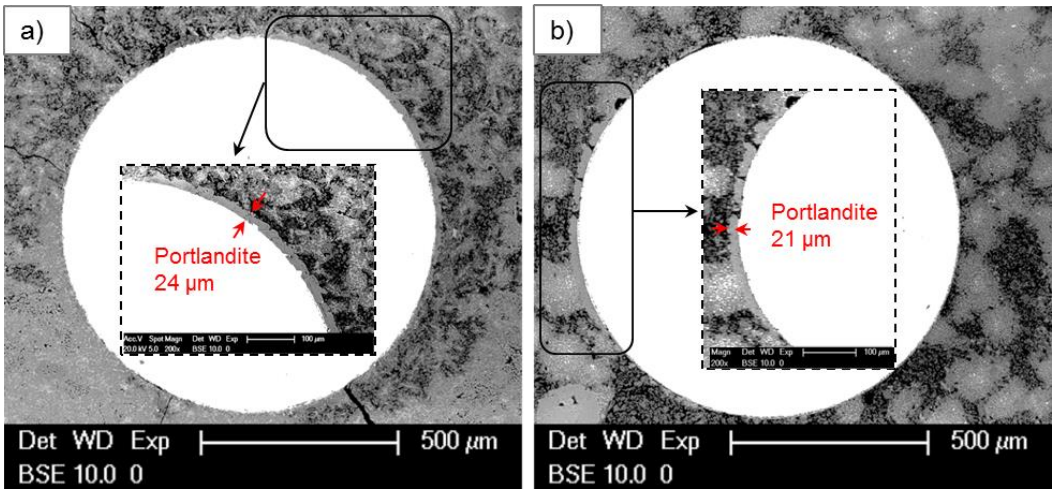

Figure D.3: ESEM images of the cross section of the embedded sensor in a) C_3S (w/p=0.5) specimen and b) C_3S (w/p=0.4) specimen after 300 days of immersion in chloride-free solution. The formation of large crystals of Portlandite occasionally around the sensor is observed.

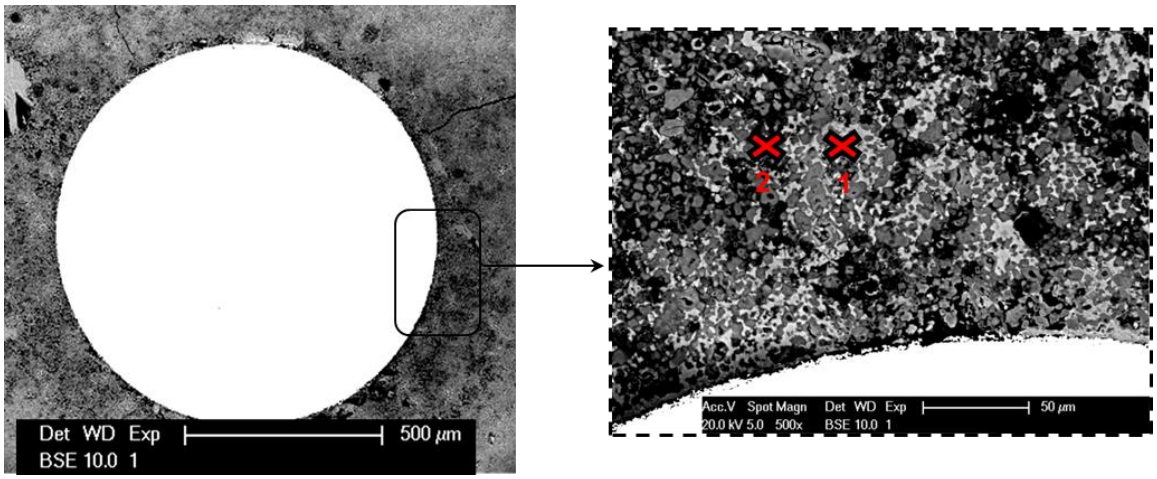

Figure D.4: ESEM images of the cross section of the embedded sensor in C_3S+C_3A (w/p=0.5) specimen after 300 days of immersion in chloride-free solution. The presence of large crystals of Portlandite is not well-pronounced around the sensor. The EDS spectra of points 1 and 2 are depicted in Fig. D.5.

By decreasing the w/p ratio to 0.4 in C_3S (w/p=0.4), Portlandite can still be observed on the sensor's surface (Fig. D.3b). In contrast, for C_3S (w/p=0.35) specimen, Portlandite cannot be observed on the sensor's surface (Fig. D.6). The low w/p ratio (e.g. 0.35) results in a dense cement-based matrix in which the presence of large crystals of Portlandite is less evident.

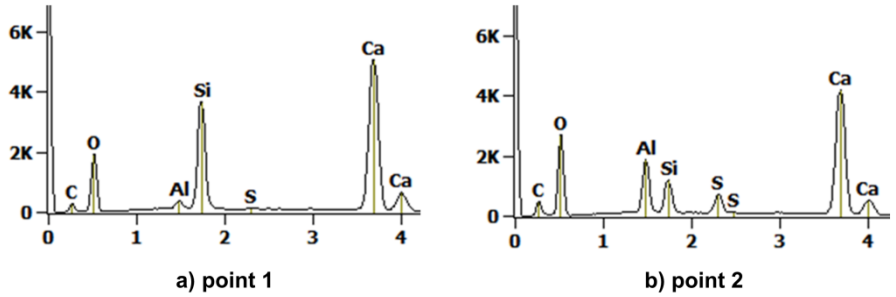

Figure D.5: The EDS spectra of the specified points 1 and 2 in Fig. D.4 for C_3S+C_3A (w/p=0.5) specimen: a) point 1; b) point 2.

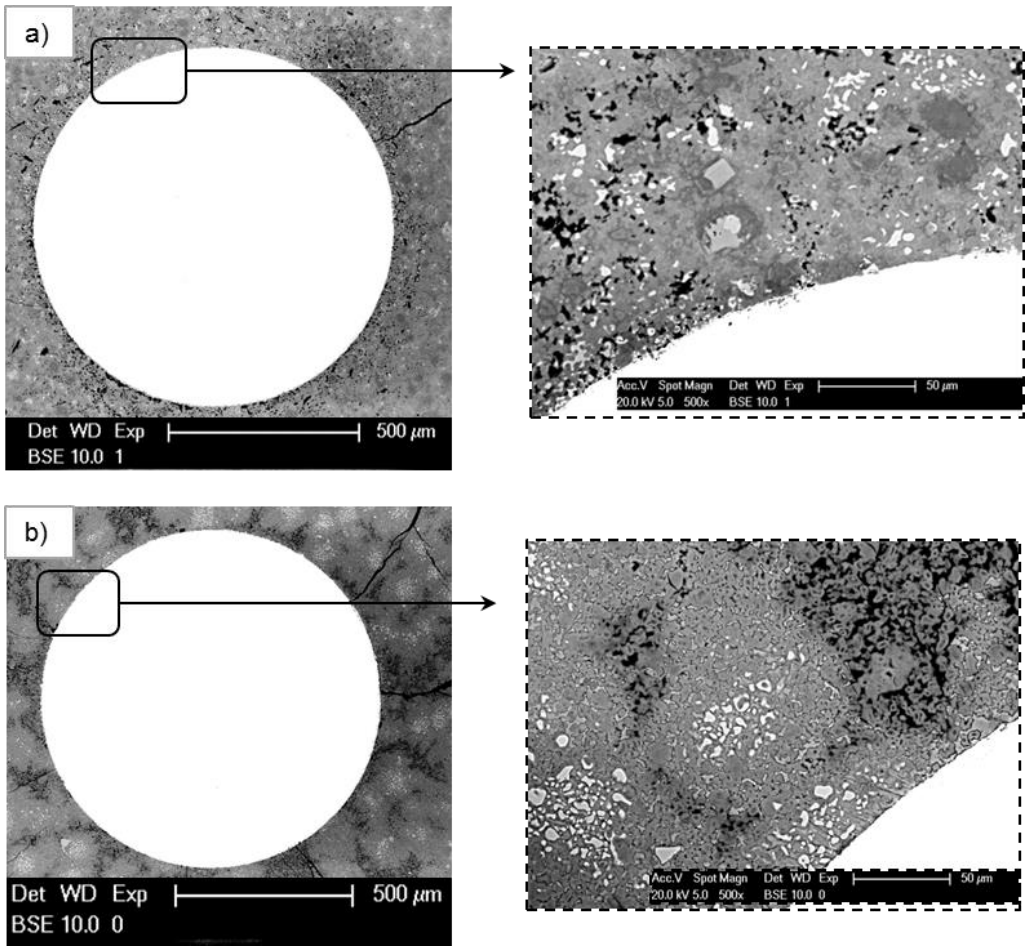

Figure D.6: ESEM images of the cross section of the embedded sensor in a) C_3S+C_3A (w/p=0.35) specimen and b) C_3S (w/p=0.35) specimen after 300 days of immersion in chloride-free solution. The cement matrix in the vicinity of the sensor is denser when compared with the cement matrix in Figs. D.1, D.3 and D.4.

Summary

Determination of the chloride content in a reinforced concrete structure is important for evaluation of the risk of chloride-induced corrosion of reinforcement. The traditional techniques for chloride determination in concrete are laborious, time-consuming and cannot be used for continuous monitoring of the chloride content. The investigation on the use of Ag/AgCl electrodes as chloride sensors in cement-based materials dates back to 1990s. Interpretation of the sensor's response in cementitious materials requires the knowledge of chloride sensor's characteristics and the interaction between the sensor and the surrounding medium. Hence, the stability of the chloride sensor's response in cementitious materials depends on the properties of Ag/AgCl interface, AgCl/cement paste interface and the pore solution composition of cementitious materials. The influence of these factors on the stability of the sensor's response was studied in this thesis.

In Chapter 1 the background and motivation for the thesis were presented. In Chapter 2 the advantages and drawbacks of available test methods for determination of the chloride content in cementitious materials were explained.

Chapter 3: Preparation and characterization of the chloride sensor

In Chapter 3 the Ag/AgCl sensor was produced at different anodization regimes. There was a link between the variation in the morphology of the AgCl layer, the applied current density and the recorded overpotential during the anodization process. The anodization at a high current density (>2 mA/cm^2) increased the thickness, heterogeneity and ionic resistance of the AgCl layer. This resulted in formation of a bi-layer AgCl on the Ag substrate. The top (surface) portion of the AgCl layer was separated by a layer of small (AgCl) grains in the vicinity of the Ag substrate. The presence of a layer of small (AgCl) grains with open inter-grain pore spaces close to the Ag substrate weakened the adhesion of the AgCl layer to the Ag substrate. The number of silver oxide-based or carbon-based impurities on the sensor's surface were proportional to the thickness as well as the morphology and microstructure of the AgCl layer.

Chapter 4: Potentiometric response of the chloride sensor in alkaline solution

In Chapter 4 the variation in the sensors' Open Circuit Potential (OCP) in solution was linked to the anodization regime used for sensor preparation and the chloride and hydroxide ions concentrations. The OCP of sensors prepared at low current densities (e.g. 0.5 mA/cm^2) was more stable and reproducible than the OCP of sensors prepared at high current densities (e.g. 4 mA/cm^2).

The variation in the sensor's OCP in a chloride-free alkaline solution was attributed to de-chlorination of the AgCl layer and transformation of AgCl to silver oxide compounds. The de-chlorination of the AgCl layer was confirmed by X-ray photoelectron spectroscopy (XPS) analysis of the layer before and after treatment in the alkaline chloride-free solution. The already formed silver oxides transformed back to AgCl (reversibility) upon the addition of chloride ions to the solution. The time needed for recovery of the sensor and a stable sensor's OCP was longer in a solution with lower chloride concentration. For instance, recovery takes 5 hours in 125 mM chloride concentration in comparison to 30 minutes in 1000 mM chloride concentration.

Chapter 5: Potentiometric response of the chloride sensor in cementitious materials

In Chapter 5 the chloride sensor's OCP in cementitious materials with different water-to-powder (w/p) ratio, cement composition and chloride concentration was assessed. The chloride sensors were embedded in paste cylinders made of C_3S with and without addition of C_3A and gypsum. The sensor's OCP in the matrix with low chloride concentration (e.g. 10 mM) depends on the w/p ratio of the mixture. The sensor's OCP in the mixture with low w/p ratio (i.e. 0.35) was more anodic than that in the mixture with high w/p ratio (i.e. 0.5). The difference between the sensor's OCP in the mixtures with high and low w/p ratio decreased with increasing the chloride concentration to 100 mM[1] and higher.

The performance of the chloride sensor was also assessed in Portland and slag cement pastes. The response of the chloride sensor in Portland cement paste was different from that in slag cement paste. The chloride sensor's OCP in Portland cement paste was in accordance to the expected response for the Ag/AgCl interface. However, the sensor's OCP in slag cement paste was significantly different. The interference of sulfide ions with the AgCl layer of the sensor was the cause of Ag_2S formation on the sensor's surface and the shift in the sensor's OCP towards negative potential values (e.g. -800 mV in Cl-containing solution). These cathodic OCP values (although indicative for the presence of free chloride ions on the sensors' surface) cannot reflect an accurate chloride content in this case.

The free chloride content in C_3S, C_3S+C_3A and Portland cement pastes inferred from the sensor's OCP was lower than the measured water-soluble chloride content. This trend was observed in all chloride concentrations. The sensor reading of the chloride content and water-soluble chloride were close to each other in the pastes with high w/p ratio, low chloride binding ability and high chloride concentration (e.g. 500 mM and 1000 mM).

Chapter 6: Onset of reinforcing steel corrosion inferred from sensor's response

In Chapter 6 the critical chloride content for the corrosion initiation of the embedded steel rods in cement paste was inferred from the OCP of the nearby chloride sensor. Despite the different trend in OCP response of the steel rods in the specimens, the time to corrosion initiation was in between 19±5 days with only 30% difference among the measured chloride threshold values (400±50 mM)[2]. These variations were attributed to the intrinsic heterogeneity of the cement paste system (e.g. different oxygen content at the steel surface).

Chapter 7: Conclusion and recommendation

In Chapter 7 the conclusions of this study and recommendations for future research were given. The influence of different parameters on the sensor's response in the alkaline medium of cementitious materials was summarized.

To summarize, this thesis investigated the performance of the chloride sensor in alkaline medium of cementitious materials. Based on the study of influencing parameters on the sensor's response, suggestions regarding sensor production and surrounding medium around the sensor have been given for a better performance of the sensor. These give guidance for interpretation of the sensor's response and application of the chloride sensor in cementitious materials.

---

[1] It is equivalent to ~0.05% by weight of binder.
[2] In this particular case: 0.22±0.03% by weight of binder.

Samenvatting

Bepaling van het chloridegehalte in een constructie van gewapend beton is belangrijk voor de beoordeling van het risico op chloride-geïnitieerde corrosie van de wapening. De gangbare methoden voor de bepaling van het chloridegehalte in beton zijn arbeidsintensief en tijdrovend. Daarnaast kunnen deze methoden niet gebruikt worden voor een continue registratie van het chloridegehalte.

Het onderzoek naar het gebruik van Ag/AgCl elektroden als chloridesensor in cementgebonden materialen gaat terug tot de jaren 90 van de vorige eeuw. Interpretatie van de sensorrespons in cementgebonden materialen vereist kennis van de karakteristieken van een chloridesensor en kennis van de interactie tussen de sensor en het omringende medium. De stabiliteit van de respons van de chloridesensor hangt daarbij af van de eigenschappen van de Ag–AgCl interface, de AgCl–cementsteen interface en van de samenstelling van het poriewater. De invloed van elk van deze factoren op de stabiliteit van de sensor respons werd bestudeerd in dit proefschrift.

Hoofdstuk 3: Bereiding en karakterisering van de chloridesensor

In hoofdstuk 3 wordt de productie van de Ag/AgCl sensor beschreven onder verschillende anodiseerregimes. Er is een verband tussen de variatie in de morfologie van de AgCl laag, de toegepaste stroomdichtheid en de geregistreerde overpotentiaal tijdens het anodiseerproces. Het anodiseren bij een hoge stroomdichtheid (> 2 mA/cm^2) verhoogt de dikte, heterogeniteit en ionische weerstand van de AgCl laag. Dit resulteert in de vorming van twee onderscheiden AgCl lagen op het Ag substraat. Het bovenste (oppervlakte) laag is gescheiden van het Ag substraat door een (onderste) grenslaag van kleine (AgCl) korrels. De vorming van kleine (AgCl) korrels op het Ag substraat verzwakt de aanhechting van de AgCl laag aan het Ag-substraat. De hoeveelheden op zilveroxide of zilverkoolstof gebaseerde verstoringen aan het sensoroppervlak zijn evenredig met de dikte, de morfologie en microstructuur van de AgCl laag.

Hoofdstuk 4: Potentiometrische reactie van de chloride sensor in alkalische oplossing

In hoofdstuk 4 wordt de relatie gelegd tussen de variatie in de sensor open circuit potentiaal (OCP) (nullastpotentiaal) van de sensor in een oplossing met het anodiseerregime dat gebruikt wordt voor het vervaardigen van de sensor en met de concentraties chloride en hydroxide ionen. De OCP van de sensor bij lage stroomdichtheden (bijvoorbeeld 0.5 mA/cm^2) is stabieler en beter reproduceerbaard dan de OCP van sensoren die geproduceerd zijn bij hoge stroomdichtheden (bijvoorbeeld 4 mA/cm^2).

De variatie in de OCP van de sensor in een chloride-vrije alkalische oplossing wordt toegeschreven aan dechlorering van de AgCl laag en omzetting van AgCl in zilveroxideverbindingen. De dechlorering van de AgCl laag is bevestigd door middel van röntgenfoto elektronenspectroscopie (XPS) analyse van de laag voor én na behandeling in de chloride-vrije alkalische oplossing. De reeds gevormde zilveroxiden worden ‘terug omgezet’ naar AgCl na toevoeging van chloride-ionen aan de oplossing (reversibiliteit). In een oplossing met een lagere chloride concentratie is de hersteltijd van de sensor naar een stabiele OCP langer. Het herstel in een 125 mM chloride concentratie oplossing duurt bijvoorbeeld 5 uur in vergelijking tot 30 minuten in een1000 mM chloride concentratie oplossing.

Hoofdstuk 5: Potentiometrische respons van de chloridesensor in cementgebonden materialen

In hoofdstuk 5 is de OCP van de chloridesensor in cementgebonden materialen onderzocht voor verschillende water-bindmiddel factor (wbf), cementsamenstelling en chlorideconcentratie. De OCP van de sensor hangt bij lage chlorideconcentratie in de cement matrix (bijvoorbeeld 10 mM) af van de wbf van het mengsel. De OCP van de sensor in het mengsel met lage wbf (0.35) gedraagt zich meer anodisch dan de OCP van de sensor in het mengsel met hoge wbf (0.5). Met het verhogen van de chlorideconcentratie tot 100 mM[1] en hoger neemt het verschil tussen de OCP van de sensor in de mengsels met hoge en lage wbf af.

Het gedrag van de chloridesensor in portlandcementpasta is anders dan in hoogovencementpasta. De OCP van de sensor in portlandcementpasta komt overeen met de verwachte reactie voor de Ag/AgCl interface. De OCP van de sensor in hoogovencementpasta daarentegen is significant anders. De interferentie van sulfide-ionen met de AgCl laag van de sensor veroorzaakt vorming van Ag_2S op het sensoroppervlak en de verschuiving in de OCP in de richting van negatieve potentiaalwaarden (bijv. -800 mV in een chloriden houdende oplossing). Deze kathodische OCP-waarden, hoewel indicatief voor de aanwezigheid van vrije chloride ionen op het sensoroppervlak, kunnen in dit geval geen nauwkeurig chloridegehalte weergeven.

Het vrije chloridegehalte afgeleid van de OCP van de sensor, is lager dan het gemeten in water oplosbare chloridegehalte. Deze trend is waargenomen in alle proefstukken en bij alle chlorideconcentraties. Het chloridegehalte op basis van de OCP van de sensor en het gemeten in water oplosbare chloridegehalte komen het meest overeen in cementpasta's met een hoge wbf, laag chloridebindend vermogen en hoge chlorideconcentratie (bijv. 500 mM en 1000 mM).

Hoofdstuk 6: Begin van wapeningscorrosie afgeleid van de sensor respons

In Hoofdstuk 6 is het kritische chloridegehalte voor de initiatie van corrosie van ingestorte dunne stalen staven in cementpasta bepaald op basis van de OCP van de nabijgelegen chloridesensor. Hoewel de OCP respons van de proefstukken onderling verschilt, ligt de waargenomen tijd tot corrosie initiatie op 19±5 dagen met slechts 30% verschil tussen de gemeten chloridegehalten (400±50 mM)[2]. Deze variaties worden toegeschreven aan de intrinsieke heterogeniteit van de cementpasta (bijv. een verschillend zuurstofgehalte aan het staaloppervlak).

Hoofdstuk 7: Conclusie en aanbeveling

In Hoofdstuk 7 zijn de conclusies van deze studie en aanbevelingen voor toekomstig onderzoek gegeven. De invloed van verschillende parameters op de respons van de sensor in het alkalische milieu van cementgebonden materialen is samengevat.

Tot slot, dit proefschrift onderzocht de prestaties van de chloridesensor in het alkalische milieu van cementgebonden materialen. Op basis van onderzoek naar de invloedparameters op de respons van de sensor zijn suggesties gedaan voor de sensorproductie en voor een betere prestatie van de sensor in relatie tot het milieu waarin de sensor geplaatst wordt. Dit geeft richting aan de interpretatie van de respons van de sensor en de toepassing van de chloride sensor in cementgebonden materialen.

---

[1] Komt overeen met ~ 0.05 gew.% bindmiddel.
[2] In dit specifieke geval: 0.22 ± 0.03 gew.% bindmiddel.

Curriculum Vitae

Farhad Pargar

Date of birth: 22nd April 1981

Place of birth: Astaneh Ashrafieh – Iran

September 1998 to February 2003

BSc student, Faculty of civil engineering, Guilan University, Iran

September 2003 to June 2006

MSc student, Faculty of civil engineering, Tehran University, Iran

April 2004 to August 2011

Construction Materials Institute (CMI) at University of Tehran

September 2011 to November 2018

PhD student, Faculty of Civil Engineering, Delft University of Technology, The Netherlands

E-mails: farhadpargar2000@gmail.com
farhad_pr2000@yahoo.com

List of publications

[1] Pargar, F., Kolev. H., Koleva, D. A. & van Breugel, K. (2018). Potentiometric response of Ag/AgCl chloride sensors in model alkaline medium, *Advances in Materials Science and Engineering*, 8135492.

[2] Pargar, F., Koleva, D. A. & van Breugel, K. (2018). Potentiometric response of Ag/AgCl sensor in Portland and slag cement pastes, *Proceeding of the Workshop on Concrete Modelling and Materials Behaviour in Honor of Professor Klaas van Breugel*, RILEM Publications, Delft, The Netherlands, p. 214-221.

[3] Pargar, F., Kolev. H., Koleva, D. A. & van Breugel, K. (2018). Microstructure, surface chemistry and altered response of Ag|AgCl sensors in alkaline media, *Journal of Materials Science*, Vol. 53(10), p. 7527–7550.

[4] Pargar, F., Koleva, D. A. & van Breugel, K. (2017). Determination of Chloride Content in Cementitious Materials: From Fundamental Aspects to Application of Ag/AgCl Chloride Sensors, *Sensors*, 2482.

[5] Pargar, F. & Koleva, D. A. (2017). Polarization Behaviour of Silver in Model Solutions, *International Journal of Structural and Civil Engineering Research*, Vol. 6(3), p. 172-176.

[6] Pargar, F., Koleva, D. A., Kolev, H. & van Breugel, K. (2017). The Onset of Chloride-Induced Corrosion in Reinforced Cement-Based Materials as Verified by Embeddable Chloride Sensors, *Concrete Durability: Cementitious Materials and Reinforced Concrete Properties, Behavior and Corrosion Resistance*. Rendon Diaz Miron, L. E. & Koleva, D. A. (eds.). Springer, p. 23-55

[7] Pargar, F., Koleva, D. A., Koenders, E. A. B. & van Breugel, K. (2015). Monitoring the electrochemical response of chloride sensors embedded in cement paste, P*roceedings of the 23th international materials research congress 2014 Cambridge: Cambridge University Press*, p. 1-6.

[8] Pargar, F., Koleva, D. A. & van Breugel, K. (2015). Potentiometric response of chloride sensors in cementitious materials of varying chemical composition and water-to-cement ratio, *Proceedings of EUROCORR 2015: Graz, Austria*, p. 877-886.

[9] Pargar, F., Koleva, D. A., Taheri, P., Mol, J. M. C., Koenders, E. A. B. & van Breugel, K. (2014). Chloride threshold for corrosion initiation in reinforced concrete: the applicability of Ag/AgCl sensors revisited, *Proceedings of EUROCORR 2014, Pizza, Italy*, p. 1-10.

[10] Pargar, F., Koleva, D. A., Copuroglu, O., Koenders, E. A. B. & van Breugel, K. (2014). Evaluation of Ag/AgCl sensors for in-situ monitoring of free chloride concentration in reinforced concrete structures, *Young researchers' Forum II: Construction materials. London: University College London*, p. 153-158.

[11] Pargar, F., Koleva, D. A., Koenders, E. & van Breugel, K. (2014). Non-destructive evaluation of chloride-induced corrosion in reinforced concrete: Electrochemical impedance spectroscopy sheds new light on generally applied sensors performance, *6WCSCM*, Barcelona, Spain, p. 1-7.

[12] Pargar, F., Koleva, D. A., Copuroglu, O., Koenders, E. & van Breugel, K. (2014). Nondestructive determination of chloride concentration using Ag|AgCl electrodes produced by electrochemical anodization, *Proceedings of XIII International Conference on Durability of Building Materials and Components: (XIII DBMC)*, p. 561-568.

[13] Pargar, F., Koleva, D. A., Koenders, E. A. B. & van Breugel, K. (2014). The importance of chloride sensors stability in monitoring ageing phenomena in concrete structures: Ag/AgCl electrodes performance in simulated pore-water environment, *Proceedings of the 1st international conference on ageing of materials and structures, AMS'14*, p. 542-547.